UniversitätsSpital Zürich

Direktion Forschung und Lehre

Programm

18th Day of Clinical Research

Georg Friedrich Götz Preisverleihung 2019

Zurich, April 11, 2019

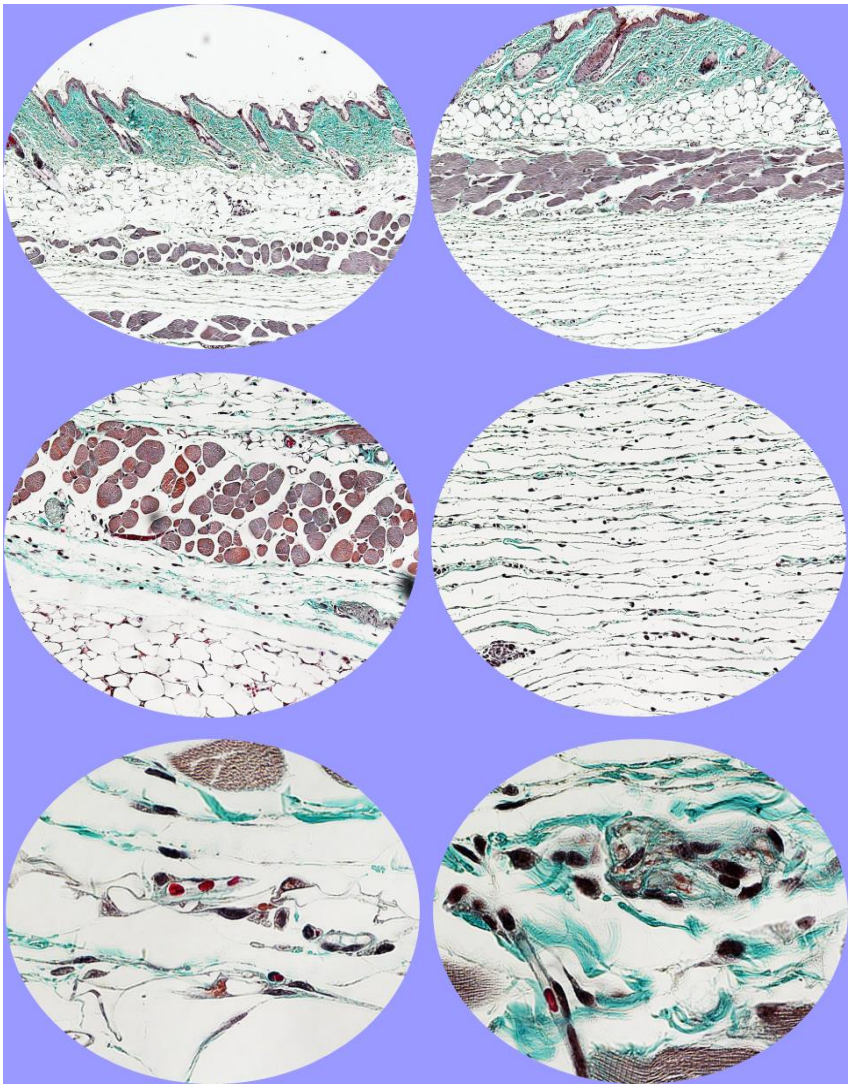

Universität Zürich[UZH]

Assoziierte Kliniken
Universitätsklinik Balgrist
Kinderspital Zürich
Psychiatrische Universitätsklinik Zürich
Zentrum für Zahnmedizin

Committee Day of Clinical Research

Aguzzi Adriano, Prof. Dr.
Cinelli Paolo, PD Dr.
Distler Oliver, Prof. Dr.
Katan Kahles Mira, PD Dr.
Moch Holger, Prof. Dr.
Schneider Robin, MBA
Senti Gabriela, Prof. Dr.
Speck Roberto, Prof. Dr.
von Eckardstein Arnold, Prof. Dr.
Weller Michael, Prof. Dr.

Table of contents

Cover Figure:
Prof. Dr. med. Oliver Distler, Klinikdirektor, Klinik für Rheumatologie, UniversitätsSpital Zürich

The microphotographs of skin specimens from wild-type control mice (left panel, magnifications from up to down pictures: 100, 200, 1000x respectively) and from tight skin mice carrying a mutation in the fibrillin-1 gene (Tsk1+/-; right panel, magnifications from up to down pictures: 100, 200, 1000x respectively) stained with the Masson Trichrome for the collagen deposition in hypodermis.

Programm

Donnerstag, 11. April 2019

Grosser Hörsaal Ost

08.15 **Eröffnung**
Prof. Dr. med. Gabriela Senti
Direktorin Forschung und Lehre, UniversitätsSpital Zürich

08.20 **Begrüssung**
Prof. Dr. med. Gregor Zünd
Vorsitzender der Spitaldirektion, UniversitätsSpital Zürich

08.25 **Begrüssung**
Prof. Dr. med. Rainer Weber
Dekan der Medizinischen Fakultät der Universität Zürich

Session 1: Cardiovascular/Metabolism/Endocrinology
Chairpersons: Prof. Dr. Christian Matter / Prof. Raghvendra Dubey

08.35 Wissenschaftliches Hauptreferat
"Molecular causes and consequences of primary aldosteronism"
Prof. Dr. med. Felix Beuschlein, Klinikdirektor, Klinik Endokrinologie, Diabetologie und Klinische Ernährung, UniversitätsSpital Zürich

08.55 **Endothelial SIRT6 exerts a beneficial role in cerebral ischemia/reperfusion injury by preserving blood-brain barrier integrity**
L. Liberale, A. Akhmedov, V. Nageswaran, S. Costantino, N. Bonetti, J. Pahla, C. Matter, J. Beer, F. Paneni, T. Luscher, G. Camici

09.05 **Effect of daily high-dose vitamin D supplementation on bone micro-architecture as assessed via high resolution peripheral quantitative computed tomography (HR-pQCT) in seniors: a double-blind RCT**
U. Meyer, U. Heilmeier, A. Siegenthaler, R. Theiler, A. Egli, H. Bischoff-Ferrari

09.15 **1-DEOXY-SPHINGOLIPIDS, novel biomarkers of diabetes, are cytotoxic for exocrine pancreatic cells**
R. Chen, T. Hornemann, W. Yu, S. Camargo, R. Graf, S. Sonda

09.25 Coffee Break

Session 2: Hematology/Oncology
Chairpersons: Prof. Dr. Maries van den Broek / Prof. Dr. Mitchell Levesque

09.40 Wissenschaftliches Hauptreferat
"**Novel Therapies for Pediatric Brain Tumors"**
Prof. Dr. med. Michael Grotzer, Ärztlicher Direktor, Kinderspital Zürich

10.00 **Anti-Human CD117 CAR T-Cells Efficiently Eliminate Hematopoietic Stem and CD117-Positive AML Cells**
R. Myburgh, J. Kiefer, N. Russkamp, A. Simonis, S. Pfister, C. Magnani, C. Wilk, A. Müller, M. Van den Broek, B. Becher, D. Neri, M. Manz

10.10 **Supplementation with butyrate producing bacteria reduces tumor load in a mouse model of CRC**
A. Montalban-Arques, I. Olivares-Rivas, E. Katkeviciute, P. Busenhart, K. Bäbler, A. Niechcial, L. Hering, K. Atrott, C. Gottier, S. Lang, G. Leventhal, T. De Wouters, M. Spalinger, M. Scharl

10.20 **Prospective Multicentre Study using High Intensity Focused Ultrasound (HIFU) for the Focal Treatment of Prostate Cancer: Safety Outcomes and Complications**
F. Schmid, A. Mortezavi, J. Sonderer, J. Bruhin, T. Sulser, D. Schindele, D. Eberli, M. Schostak

Session 3: Mixed Topics
Chairpersons: Prof. Dr. med. Dagmar Iris Keller Lang / Prof. Dr. med. Thomas Frauenfelder

10.35 Wissenschaftliches Hauptreferat
"DO-HEALTH 1. Results"
Prof. Dr. med. Heike Bischoff-Ferrari, Klinikdirektorin, Klinik für Geriatrie, UniversitätsSpital Zürich

10.55 **Epigenetic modifications by the methyltransferase SETD7 regulate endothelial cell migration: Insights for personalized therapies in patients with diabetes and peripheral artery disease**
S. Mohammed, S. Costantino, A. Akhmedov, S. Ambrosini, G. Karsay, T. Luscher, F. Paneni

11.05 **Free-breathing dynamic contrast-enhanced Imaging of the upper abdomen using advanced compressed-sensing reconstruction**
D. Hausmann, T. Niemann, D. Kreul, A. Nocito, M. Klarhöfer, D. Nickel, K. Kiefer, S. Bensler, R. Kubik

11.15 **A Bufadienolide-Enriched Fraction of Bryophyllum pinnatum Inhibits Human Myometrial Contractility in Vitro**
S. Santos, C. Haslinger, K. Klaic, M. Faleschini, M. Mennet, O. Potterat, U. von Mandach, M. Hamburger, A.P. Simões-Wüst

11.30 Lunch/Poster Viewing

11.45 Verleihung Georg Friedrich Götz-Preis 2018
mit anschliessendem Apéro Riche

Session 4: Infection/Immunity/Inflammation/Systemic Diseases
Chairpersons: Prof. Dr. med. Onur Boymann / PD Dr. med. Barbara Hasse

13.40 Wissenschaftliches Hauptreferat
"Inflammation hypothesis of depression"
Prof. Dr. med. Roland von Känel, Klinikdirektor, Klinik für Konsiliarpsychiatrie und Psychosomatik, UniversitätsSpital Zürich

14.00 **Determinants of Hematopoietic Stem Cell Aging**
L. Kovtonyuk, M. Manz

14.10 **Combination of high virulence and antibiotic persistence in a Staphylococcus aureus strain resulting in treatment failure**
M. Huemer, S. Mairpady Shambat, S. Söderhom, S. Götschi, M. Boumasmoud, C. Vulin, D. Bumann, R. Schüpbach, A. Zinkernagel

14.20 **Novel tool for PAR1 activation**
Ö. Altintas, A. Franchini, D. Heuberger, R. Schuepbach

Session 5: Head Region/Neuroscience
Chairpersons: PD Dr. Mira Katan Kahles / Prof. Dr. Andreas Luft

14.35 Wissenschaftliches Hauptreferat
"Update: Research Neuroradiology USZ"
Prof. Dr. med. Christoph Stippich, Klinikdirektor, Klinik für Neuroradiologie, UniversitätsSpital Zürich

14.55 **Identifying the determinants of spongiform phenotype in prion infections**
A. Lakkaraju, R. Marpakwar, E. Lemes, U. Herrmann, A. Ballabio, A. Aguzzi

15.05 **Establish Tolerance in MS with myelin-peptide coupled red blood cells - ETIMSred trial**
A. Lutterotti, T. Ludersdorfer, M. Docampo, M. Hohmann, C. Selles Moreno, H. Hayward-Koennecke, I. Jelcic, N. Pfender, TM. Müller, C. Blumer, M. Foege, S. Winklhofer, R. Stenger, M. Kayser, U. Schanz, M. Sospedra, R. Martin

15.15 **Enhancing neuroprotection by CRISPR-mediated activation of LIF expression in Müller cells of the mouse retina**
D. Karademir, F. Storti, C. Grimm

15.30 Coffee Break

Session 6: Career development supported by USZ

15.45 **Präsentation**
“Pancreatic cancer research in Norway - 1 year between polar lights and the summer of the century”
Dr. med. Daniela Lenggenhager, Oberärztin, Institut für Pathologie und Molekularpathologie, UniversitätsSpital Zürich

16.05 **Präsentation**
“Photodynamic Therapy in Maxillofacial Surgery”
Who is the person behind the career? Report of a researcher supported by the USZ
PD Dr. med. Paul Schumann, Leitender Arzt, Klinik für Mund-, Kiefer- und Gesichtschirurgie, UniversitätsSpital Zürich

16.30 Verleihung Day of Clinical Research Preis

16.50 **Apéro**

Cardiovascular / Metabolism / Endocrinology

Basic Research

5381
R. Chen, T. Hornemann, W. Yu, S. Camargo, R. Graf, S. Sonda
1-DEOXY-SPHINGOLIPIDS, novel biomarkers of diabetes, are cytotoxic for exocrine pancreatic cells

5408
M. Luciani, N. Bonetti, A. Akhmedov, L. Liberale, F. Maisano, T. Lüscher, G. Camici
N-Terminal Pro-B-Type Natriuretic Peptide: From Sensor To Effector of Damage?

5409
N. Bonetti, C. Diaz-Canestro, L. Liberale, A. Akhmedov, M. Reiner, M. Merlini, F. Ruschitzka, T. Lüscher, J. Beer, G. Camici
Tumor necrosis factor-Alpha inhibition improves stroke outcome in a mouse model of rheumatoid arthritis

5415
A. Akhmedov, M. Crucet, N R. Bonetti, C. Ospelt, S. Briand, M. Amrollahi-Sharifabadi, A. Ciurea, O. Distler, G. Kollias, B. Simic, F. Ruschitzka, R. Laaksonen, P M. Vanhoutte, T F. Lüscher
Anti TNFα treatment restores endothelial function in rheumatoid arthritis by inhibiting LOX-1 and arginase

5440
A. Akhmedov, F. Montecucco, G. Camici, A. Schaub Clerigue, D. Vdovenko, S. Costantino, N. Bonetti, C. Diaz-Canestro, F. Paneni, F. Mach, T. Lüscher
GDF11 Promotes Increased Sensitivity of the Murine Heart to Ischemic Injury

5441
A. Akhmedov, F. Montecucco, S. Costantino, A. Schaub Clerigue, D. Vdovenko, D. Gaul, F. Carbone, L. Liberale, U. Eriksson, C. Matter, F. Paneni, G. Camici, F. Mach, T. Lüscher
Cardiomyocyte-specific jund regulates infarct size following ischemia/reperfusion cardiac injury by downregulating SIRT3

Translational Research

5371
A. Jomard, O. Chavez-Talavera, A. Tailleux, P. Doytcheva, M. Bueter, A. Taheri, C. Wolfrum, T. Lutz, A. Von Eckardstein, F. Ruschitzka, B. Staels, E. Osto
The Functional Relevance of Bile Acids in the Improvement of HDL-mediated Endothelial Protection After Bariatric Surgery

5380
M. Kirschner, M. Friess, V. Orlowski, B. Gray-Stocker, W. Weder, I. Inci, R. Schüpbach, D. Bettex, S. Ulrich, I. Opitz
Expression of microRNAs in surgical specimens of patients with Chronic Thromboembolic Pulmonary Hypertension

5383
L. Liberale, A. Akhmedov, V. Nageswaran, S. Costantino, N. Bonetti, J. Pahla, C. Matter, J. Beer, F. Paneni, T. Luscher, G. Camici
Endothelial SIRT6 exerts a beneficial role in cerebral ischemia/reperfusion injury by preserving blood-brain barrier integrity

5451
F. Scholkmann, D. Ostojic, H. Isler, D. Bassler, M. Wolf, T. Karen
Mathematical modelling of reference ranges for hemoglobin and hematocrit levels in neonates as a function of gestational age and postnatal age

Clinical Trials

5358
U. Meyer, U. Heilmeier, A. Siegenthaler, R. Theiler, A. Egli, H. Bischoff-Ferrari
Effect of daily high-dose vitamin D supplementation on bone micro-architecture as assessed via high resolution peripheral quantitative computed tomography (HR-pQCT) in seniors: a double-blind RCT

Hematology/Oncology

Basic Research

5318
O. Eichhoff, A. Irmisch, P. Turko, S. Pascoal, N. Zamboni, I. Piazza, P. Cheng, I. Banik, A. Saltari, M. Distel, P. Picotti, R. Dummer, M. Levesque
Metabolic targeting as a strategy to overcome targeted therapy resistance

5327
E. Katkeviciute, L. Hering, M. Scharl, M. Spalinger
Loss of PTPN2 in dendritic or T cells results in reduced tumor burden in the AOM/DSS colon tumour mouse model

5348
M. Meerang, O. Lauk, M. Kirschner, V. Orlowski, V. Cecconi, M. Van den Broek, W. Weder, I. Opitz
Analysis of immune cells in an orthotopic immunocompetent rat model of malignant pleural mesothelioma

5351
J.Schaffenrath, L. Dib, M. Neidert, M. Delorenzi, L. Regli, A. Keller
Transcriptomic profiling of the glioblastoma-BBB

5352
A. Montalban-Arques, C. Gottier, I. Olivares-Rivas, M. Spalinger
Loss of Protein Tyrosine Phosphatase Non-Receptor Type 23 (PTPN23) in intestinal epithelial cells induces inflammation and epithelial hyperproliferation.

5369
M. Wildschut, M. Van Oostrum, P. Schürch, T. Wilhelm, M. Huber, B. Wollscheid, A. Theocharides
The Consequence of CALR Mutations on Proteostasis in Myeloproliferative Neoplasms

5370
R. Myburgh, J. Kiefer, N. Russkamp, A. Simonis, S. Pfister, C. Magnani, C. Wilk, A. Müller, M. Van den Broek, B. Becher, D. Neri, MG. Manz
Anti-Human CD117 CAR T-Cells Efficiently Eliminate Hematopoietic Stem and CD117-Positive AML Cells

5387
S. Salemi, B. Kranzbühler, T. Sulser, D. Eberli
ARN-509 (Apalutamide) combined with autophagy inhibitors: Promising double therapy for advanced prostate cancer

5399
D. Lenggenhager, M. Amrutkar, P. Sántha, M. Aasrum, J. Löhr, I. Gladhaug, C. Verbeke
Comparison of different pancreatic stellate cell cultures currently used for the in vitro study of human pancreatic cancer

5410
S. Steiner, T. Reding, D. Lenggenhager, M. Healy, A. Gupta, G. Wanner-Seleznik, R. Graf
Tumor suppressive mechanisms of Gastrokine 1 in pancreatic carcinogenesis

5412
I. Olivares-Rivas, E. Katkeviciute, P. Busenhart, K. Bäbler, A. Niechcial, L. Hering, K. Atrott, C. Gottier, S. Lang, G. Leventhal, T. De Wouters, M. Spalinger, M. Scharl, A. Montalban-Arques
Supplementation with butyrate producing bacteria reduces tumor load in a mouse model of CRC

5442
P. Schürch, T. Wildschut, L. Malinovska, V. Lysenko, A. Lakkaraju, E. Milani, A. Aguzzi, B. Wollscheid, A. Theocharides
Protein clients are differentially affected by mutations in the endoplasmic reticulum chaperone calreticulin

Translational Research

5170
C. Waschkies, F. Kivrak-Pfiffner, D. Heuberger, P. Wolint, M. Schneider, Y. Tian, M. Calcagni, P. Giovanoli, J. Buschmann
MRI Phenotypization, Vasoreactivity and Hypoxia in MC-38 colon and A549 lung adeno-carcinoma cell grafts grown on the Chorioallantoic Membrane of the Chick Embryo in ovo

5338
N. Enz, F. Janker, S. Andreoli, M. Haberecker, C. Opelz, W. Weder, JH. Jang, W. Jungraithmayr
The co-expression of CD26 and TGF-β1 renders lung cancer targetable to CD26-inhibition

5350
F. Meier-Abt, S. Amon, L. Gillet, W. Wolski, S. Dimitrieva, A. Theocharides, M. Manz, R. Aebersold
Transcriptome-Proteome Correlation in Human Hematopoietic Stem and Progenitor Cells

5388
A. Irmisch, R. Dummer, M. Levesque
In depth molecular profiling of metastatic tissue from melanoma patients- a multi-institutional feasibility study

5398
L. Roth, E. Breuer, R. Graf, P.-A. Clavien, A. Gupta, K. Lehmann
The impact of hyperthermic intraperitoneal chemotherapy (HIPEC) on the anticancer immune response

5400
C. Millan, L. Gstrein, F. Clement, D. Eberli
Developing a liquid biopsy diagnostic for prostate cancer based on extracellular vesicles

5401
S. Deycmar, S. Gruber, W. Dörr, A. Lomax, M. Pruschy
The HSP90 inhibitor ganetespib specifically sensitizes cancer cells for clinical SOBP proton beam irradiation in comparison to photon irradiation.

5405
F. Tschanz, M. Pruschy
ADAM17-Dependent paracrine and intercellular communication in response to irradiation

5406
Y. Nonomura, O. Eichhoff, M. Levesque, R. Dummer
New treatment strategy in melanoma patients with c-kit mutations targeting the tyrosine phosphatase SHP2

5426
V. Waller, M. Pruschy, P. Knobel
Exploring the interactome of ADAM17 in the tumor microenvironment and its role for radiation resistance

5449
C. Pauli, H. Hopkins, M. Rubin, C. Crandori, H. Moch, L. Cantley
A Precision Medicine Approach to Target KRAS mutant Tumors

Clinical Trials

5321
E. Ramelyte, R. Dummer
Intralesional oncolytic virotherapy in cutaneous lymphomas

5391
N. Citak, L. Guglielmetti, Y. Aksoy, O. Isgörücü, M. Metin, A. Sayar, I. Opitz, D. Schneiter, W. Weder, I. Inci
Stage IIIA should be divided in two different subgroups according to T and N status in patients with resected lung cancer: validation with another center database

5392
F. Schmid, A. Mortezavi, J. Sonderer, J. Bruhin, T. Sulser, D. Schindele, D. Eberli, M. Schostak
Prospective Multicentre Study using High Intensity Focused Ultrasound (HIFU) for the Focal Treatment of Prostate Cancer: Safety Outcomes and Complications

5393
F. Schmid, M. Wettstein, T. Thomas, A. Boss, T. Hermanns, D. Eberli
Contrast Media Kinetics in Multiparametric MRI before Radical Prostatectomy Predicts Probability of Postoperative Incontinence

5397
L. Gstrein-Prause, A. Mortezavi, C. Millan, SF. Wyler, T. Sulser, F. Recker, M. Kwiatkowski, D. Eberli
Influence of regular aspirin intake on PSA values, prostate cancer incidence and overall survival in a prospective screening trial cohort (ERSPC Aarau)

5443
D. Hausmann, P. Appenzeller, D. Kreul, C. Caspar, A. Nocito, M. Klarhöfer, B. Kuehn, B. Kiefer, S. Bensler, R. Kubik
Evaluation of an innovative automatized "semi-whole-body" MRI protocol to increase patient comfort and cost-effectiveness of oncologic imaging: initial results

5453
I. Inci, M. Benker, N. Citak, D. Schneiter, C. Caviezel, S. Hillinger, I. Opitz, W. Weder
Extended sleeve lobectomy has same surgical outcome when compared with conventional lobectomy in patients with lung cancer

Mixed Topics

Basic Research

5307
B. Eggerschwiler, D. Canepa, H-C. Pape, E. Casanova, P. Cinelli
Automated digital image quantification of histological staining for the analysis of the trilineage differentiation potential of mesenchymal stem cells

5309
D. Canepa, E. Casanova, E. Arvaniti, B. Eggerschwiler, V. Tosevski, M. Claassen, HC. Pape, P. Cinelli
Comprehensive Mass Cytometry Analysis of Human Adipose Derived Stem Cells for Clinical Applications

5315
S. Erdogan, C. Gonçalves-Moreira, S. Masneuf, C. Baumann, D. Noain
Role of slow-wave sleep delta power on amyloid beta clearance and accumulation in a mouse model of Alzheimer's disease

5322
S. Dudli, D. Hänni, A. Jüngel, M. Betz, J. Spirig, F. Brunner, M. Farshad, O. Distler
Dysregulated bone marrow stromal cells in vertebral bone marrow lesions

5323
E. Lang, O. Pfäffli, S. Koller, W. Berger, C. Gerth-Kahlert
Novel homozygous mutation in the membrane frizzled related protein (MFRP) gene in a family with nanophthalmos

5360
S. Mohammed, S. Costantino, A. Akhmedov, S. Ambrosini, G. Karsay, T. Luscher, F. Paneni
Epigenetic modifications by the methyltransferase SETD7 regulate endothelial cell migration: Insights for personalized therapies in patients with diabetes and peripheral artery disease

5364
P. Helbling, E. Pineiro, R. Gerosa, S. Böttcher, F. Al-Sharour, M. Manz, C. Nombela-Arrieta
Transcriptomic profiling reveals dynamic functional remodeling of the bone marrow microenvironment during postnatal development, aging, and inflammation

5372
I. Iskender, S. Arni, T. Maeyashiki, N. Citak, M. Canic, S. Paal, T. Frauenfelder, I. Schmitt-Opitz, W. Weder, I. Inci
Warm versus cold ischemic donor lung injuries activate distinct pathophysiological responses during ex vivo lung perfusion

5375
D. Kreul, R. Kubik-Huch, J. Froehlich, M. Thali, T. Niemann
Dual energy computed tomography with multiparametric mapping of parenchymatous organs: Normal distribution in a 12-month cohort.

5376
D. Kreul, R. Kubik-Huch, T. Niemann
Influence of CT reconstruction parameters and on image quality and reconstruction efficiency in cinematic reconstructions

5378
S. Hörmann, Z. Gai, G-A. Kullak-Ublick, M. Visentin
Effect of the cellular lipid composition on the transport properties of the organic cation transporter 2 (OCT2)

5379
D. Kreul, D. Gascho, S. Franckenberg, S. Eggert, B. Fliss, R. Kubik-Huch, M. Thali, T. Niemann
Determining postmortal liver steatosis. A retrospective study comparing dual-energy computed tomography to histological graduation

5386
T. Maeyashiki, S. Arni, I. Iskender, W. Weder, I. Inci
Sub-normothermic ex-vivo lung perfusion attenuates ischemia reperfusion injury from donation after circulatory death donors

5422
S. Grossi, H-D. Beer
Exploring the molecular mechanisms of UVB-induced cell death in human keratinocytes

5424
U. Süssbier, HC. Wong, A. Gomariz, S. Isringhausen, P. Helbling, T. Nagazawa, A. Müller, M. Manz, C. Nombela-Arrieta
Functional and structural dynamics of the bone marrow stromal microenvironment after cytoreductive treatments

Translational Research

5168
F. Burgio, N. Rimmer, U. Pieles, J. Buschmann, M. Beaufils-Hugot
Characterization and in ovo vascularisation of a 3D-printed hydroxyapatite scaffold with different extracellular matrix coatings under perfusion culture

5169
L. Otto, P. Wolint, A. Woloszyk, A. Becker, A. Boss, R. Böni, M. Calcagni, P. Giovanoli, M. Emmert, J. Buschmann
Calcification capacity and vascularization of a collagen Matricel® scaffold seeded with human adipose-derived stem cells seeded as single cells or 3D-microtissues on the CAM assay

5171
J. Buschmann, Y. Yamada, K. Schulz-Schönhagen, S. Hess, W. Stark, C. Opelz, G. Meier Bürgisser, W. Weder, W. Jungraithmayr
Stem cell-seeded hybrid nanocomposite for chest wall repair in a murine model

5238
S. Santos, C. Haslinger, K. Klaic, M. Faleschini, M. Mennet, O. Potterat, U. Von Mandach, M. Hamburger, A. Simões-Wüst
A Bufadienolide-Enriched Fraction of Bryophyllum pinnatum Inhibits Human Myometrial Contractility in Vitro

5343
C. Hiller, M. Visentin, Z. Gai, S. Samodelov, N. Perez, S. Häusler, B. Stieger, G-A. Kullak-Ublick
Development of a 3D HuH-7 cell-based system as a model to study drug-induced cholestasis

5365
M. Hohmann, T. Ludersdorfer, P. Englezou, M. Docampo, C. Sellés-Moreno, J. Goede, J. Deuel, F. Guffanti, M. Broggini, E. Scanziani, M. Sospedra, R. Martin, A. Lutterotti
Characterization of Myelin Peptide-Coupled Red Blood Cells

5366
D. Spiess, M. Oufir, O. Potterat, M. Hamburger, A. Simões-Wüst
Optimization of an in vitro model of the placental barrier using BeWo b30 cells for permeability studies

5374
V. Lysenko, N. Wildner, K. Zimmermann, P. Schürch, C. Fritz, R. Flavell, P. Wild, S. Dirnhofer, M. Manz, A. Theocharides
Enhanced support of myelofibrosis stem cells in next generation humanized mice

5396
L. Pasterk, N. Bonetti, S. Gobbato, M. Frick, S. Meier, G. Camici, T. Lüscher, M. Egloff, P. Köpfli, H. Schmid, J. Beer
The effects of PCSK9 inhibitor therapy on platelet structure and function

5402
L. Roth, X. Muller, R. Graf, Y. Tian, B. Imthurn, P. Imesch, N. Ochsenbein-Kölble, P.-A. Clavien, Ph. Dutkowski, O. De Rougemont
Prolonged Cold Preservation Exposes Uterus Grafts to Major Ischemia-Reperfusion Injury

5447
S. Forte, Z. Wang, C. Arboleda, L. Lang, S. Singer, A. Andreas, S. Prevrhal, C. Leo, R. Kubik-Huch, M. Stampanoni
Grating-Based X-Ray Phase-Contrast Mammography: From a research setup to a preclinical system

Clinical Trials

5312
K. Slankamenac, N. Rütsche, D. Keller Lang
Availability of advance directives in the emergency department: a prospective survey

5313
K. Slankamenac, R. Heidelberger, D. Keller Lang
Prediction of Repeated Emergency Department Visits in Patients with Mental Disorders

5320
T. Hamann, S. Hommayda, M. Töteberg-Harms
Focus on refractive predictability and intraocular pressure - iStent Inject alone versus combined phaco

5339
L. Imbach, C. Christian, R. Poryazova, O. Geissler, P. Brugger, I. Mothersill, M. Weller, M. Oertel, L. Stieglitz
Anticonvulsive effect of anterior thalamic deep brain stimulation in super-refractory status epilepticus crucially depends on active stimulation zone – a single case observation

5377
J. Prange, D. Mohr-Haralampieva, R. Alves de Sousa, F. Schmid, D. Eberli
GMP-Verification processes of the final product in a clinical stem cell trial to treat Stress Urinary Incontinence

5385
D. Mohr-Haralampieva, J. Prange, R. Alves de Sousa, F. Schmid, D. Eberli
Towards Implementing a Multisystem Cell Therapy for Improvement of Urinary Continence: MUS.I.C. project

5395
R. Pfeifer, S. Schick, W. Hell, S. Halvachizadeh, K. Sprengel, K. Jensen, H-C. Pape
Analysis of Injury and Mortality Patterns in Deceased Patients with Blunt Trauma: An Autopsy Study

5445
D. Hausmann, T. Niemann, D. Kreul, A. Nocito, M. Klarhöfer, D. Nickel, K. Kiefer, S. Bensler, R. Kubik
Free-breathing dynamic contrast-enhanced Imaging of the upper abdomen using advanced compressed-sensing reconstruction

Infection / Immunity / Inflammation / Systemic Diseases

Basic Research

5165
A. Inderbitzin, Y. Kok, L. Joerimann, A. Kelley, K. Neumann, K. Metzner
CRISPR/Cas9-mediated insertion of HIV-1-based vector into BACH2 does not lead to viral latency in Jurkat T cells

5166
M. Schwarzfischer, L. Hering, E. Katkeviciute, A. Niechcial, K. Atrott, P. Busenhart, K. Bäbler, G. Rogler, M. Scharl, M. Spalinger
TiO2 nanoparticles abrogate the protective effect of the autoimmunity-associated PTPN22 R619W variant during acute DSS colitis

5314
B. Weder, T. Van Haaften, K. Baebler, G. Rogler, G. Dijkstra, P. Imenez Silva, Y. Wang, C. De Vallière, C. Wagner, I. Frey-Wagner, K. Seuwen, P. Ruiz, M. Hausmann
Intestinal acidification sensed by pH-sensing receptor GPR4 contributes to fibrogenesis

5317
L. Hering, E. Katkeviciute, M. Schwarzfischer, D. Mrdjen, J. Komuczki, L. Lang, B. Becher, G. Rogler, M. Scharl, MR. Spalinger
Loss of PTPN2 in dendritic cells promotes increased T cell response and elevated expression of co-stimulatory molecules

5325
M. Gruenbach, E. Schlaepfer, B. Escher, M. Schlapschy, A. Skerra, G. Schreiber, RF. Speck, S. Bredl
Biological activity of different IFN-α subtypes – just an interplay between the dose and affinity?

5336
L. Dubs, F. Janker, C. Opelz, Y. Yamada, W. Weder, JH. Jang, W. Jungraithmayr
CD26/DPP4 is overexpressed in experimental chronic lung allograft rejection and potentially qualifies as a target to reduce chronic rejection

5353
M. Mellett, B. Meier, D. Mohanan, P. Cheng, T. Satoh, J. Danis, S. Nobbe, E. Contassot, L. French
Gain-of-function mutation in the keratinocyte signalling molecule CARD14 drives spontaneous psoriatic skin disease in vivo

5355
J. Danis, L. Kemény, E. Contassot, L. French, M. Széll, M. Mellett
A novel mediator of inflammatory cell death controls Interluekin-36 secretion from keratinocytes – implications for chronic inflammatory skin disease

5363
J. Wang, I. Jelcic, C. Münz, N. Toussaint, Y. Zhao, M. Sospedra, R. Martin
Characterizing Molecular Mimicry in Peripheral Blood-Derived Autoreactive CD4+ T Cells in Multiple Sclerosis

5368
T. Skaria, E. Bachli, G. Schoedon
RSPO3 impairs barrier function of human vascular endothelial monolayers and synergizes with pro-inflammatory IL-1

5390
S. Chaudron, K. Metzner, C. Leemann, K. Kusejko, H. Nguyen, A. Marzel, J. Böni, S. Yerly, T. Klimkait, M. Perreau, R. Kouyos, H. Günthard
A molecular epidemiology method to screen for HIV-1 superinfection in the swiss HIV cohort study

5413
Ö. Altintas, A. Franchini, D. Heuberger, R. Schuepbach
Novel tool for PAR1 activation

5414
M. Reinehr, C. Micheloud, F. Grimm, P. Kronenberg, J. Grimm, A. Beck, J. Nell, E. Furrer, B. Müllhaupt, T. Barth, P. Deplazes, A. Weber
Pathology of echinococcosis - A morphological and immunohistochemical study on 138 cases with focus on the differential diagnosis between cystic versus alveolar echinococcosis

5420
S. Isringhausen, U. Suessbier, L. Kovtonyuk, N. Kräutler, P. Helbling, A. Gomariz, HC. Wong, A. Oxenius, M. Manz, C. Nombela-Arrieta
Chronic viral infections induce persistent loss of hematopoietic stem cell function through disruption of bone marrow stromal cell networks

5435
L. Kovtonyuk, M. Manz
Determinants of Hematopoietic Stem Cell Aging

5436
F. Caiado, L. Kovtonyuk, M. Manz
Role of Inflamm-Ageing of the Hematopoietic Sytem on Clonal Hematopoiesis Progression

5448
I. Jelcic, A. Müller, T. Pokorny, H. Hayward-Koennecke, N. Wolfensberger, J. Ruder, K. Ritter, M. Foege, A. Lutterotti, U. Schanz, R. Martin
Safety and Tolerability of Autologous Hematopoietic Stem Cell Transplantation in Multiple Sclerosis Patients at the USZ

Translational Research

5311
M. Juhas, E. Widlake, J. Teo, D. Huseby, J. Tyrrell, Y. Polikanov, O. Ercan, A. Petersson, S. Cao, A. Aboklaish, A. Rominski, D. Crich, E. Böttger, T. Walsh, D. Hughes, S. Hobbie
In-vitro activity of apramycin against multidrug-, carbapenem-, and aminoglycoside-resistant Enterobacteriaceae and Acinetobacter baumannii

5319
B. Wenk, HA. Mbunkah, N. Ndi, E. Mbu, L. Besong, B. Sama, E. Orock, M. Shilai, C. Leeman, K. Metzner
Prevalence of Integrase Strand Transfer Inhibitors Resistance Mutations in Antiretroviral-Naïve HIV-1 Infected Patients in Cameroon.

5356
S. Samodelov, M. Visentin, Z. Gai, G-A. Kullak-Ublick
Renal glycosuria as a novel early sign of colistin-induced kidney damage in mice

5382
J. Schniering, M. Brunner, O. Distler, M. Guckenberger, M. Bogowicz, D. Vuong, C. Müller, T. Frauenfelder, S. Tanadini-Lang, B. Maurer
Texture-based radiomics features discriminate different stages of experimental interstitial lung disease

5384
I. Jelcic, F. Al Nimer, J. Wang, V. Lentsch, R. Planas, Il. Jelcic, A. Madjovski, S. Ruhrmann, W. Faigle, K. Frauenknecht, C. Pinilla, R. Santos, C. Hammer, Y. Ortiz, L. Opitz, H. Grönlund, G. Rogler, O. Boyman, R. Reynolds, A. Lutterotti, M. Khademi, T. Olsson, F. Piehl, M. Sospedra, R. Martin
Memory B Cells Activate Brain-Homing, Autoreactive CD4+ T Cells in Multiple

5394
M. Huemer, S. Mairpady Shambat, S. Söderhom, S. Götschi, M. Boumasmoud, C. Vulin, D. Bumann, R. Schüpbach, A. Zinkernagel
Combination of high virulence and antibiotic persistence in a Staphylococcus aureus strain resulting in treatment failure

5428
C. Cruciani, W. Faigle, P. Tomas-Ojer, C. Selles Moreno, B. Roschitzki, W. Wolski, N. Schaeren-Wiemers, T. Zeis, R. Reynolds, M. Sospedra, R. Martin
Reactivity of autoreactive T cells against post-translational modifications of brain proteins, specifically citrullinated peptides in MS

5429
M. Puthenparampil, C. Cruciani, P. Tomas-Ojer, M. Hohmann, C. Sellés-Moreno, I. Jelcic, J. Wang, M. Mikolin, R. Martin, M. Sospedra
CSF CD4+ T cells reactivity against auto-antigen in MS patient

5434
M. Boumasmoud, L. Meyer, T. Schweizer, D. Kuehnert, K. Seidl, A. Holzmann-Bürgel, P Schreiber, S. Kuster, R. Kouyos, A. Zinkernagel
Molecular evidence for persistence and adaptation of a vancomycin-resistant Enterococcus faecium ST-203 clone in a central European tertiary care hospital

5446
M. Emmenegger, A. Chincisan, R. Müller, D. Schneider, L. Mottier, J. Domange, A. Rosati, N. Wuillemin, D. Bieli, T. Sonati, A. Barberis, L. Saleh, S. Hornemann, A. Von Eckardstein, A. Aguzzi
Antibody profiling in 20,000 unselected patient samples reveals strong enrichment for anti-peanut IgG antibodies in Cystic Fibrosis patients

Clinical Trials

5337
A. Pregernig, M. Müller, U. Held, B. Beck-Schimmer
Prediction of mortality in adult patients with sepsis, using six novel biomarkers: a systematic review and meta-analysis.

Head Region / Neuroscience

Basic Research

5167
Y. Zarb, S. Nassiri, S. Utz, M. Dilorenzi, M. Colonna, M. Greter, A. Keller
Microglia control vessel-associated calcifications in the mouse model of primary familial brain calcification

5310
D. Karademir, F. Storti, C. Grimm
Enhancing neuroprotection by CRISPR-mediated activation of LIF expression in Müller cells of the mouse retina

5316
M. Morawska, D. Noain, T. Scammell, C. Baumann
Slow-wave enhancement reduces trauma-induced APP overexpression in novel mouse model of traumatic brain injury compatible with EEG/EMG headset.

5324
C. Gonçalves Moreira, M. Scandella, M. Ferster, C. Baumann, D. Noain
Prolonged acoustic modulation of slow-wave sleep alters motor skill learning in rats

5326
E. Kiessling, S. Froese, M. Baumgartner, C. Grimm
Rescue of Vision in cblC Deficiency

5328
Y. Liu, S. Sorce, J. Domange, A. Aguzzi
Prion-induced dopaminergic axon degeneration is independent of cell-autonomous prion protein levels

5329
A. Bentrup, M. Avar, D. Heinzer, S. Hornemann, A. Aguzzi
Tri-part Luciferase-based Homogeneous Immunoassay for Sensitive Detection of the Prion Protein

5330
A. Senatore, G. Horny, R. Reimann, S. Sorce, J. Guo, S. Fels, N. George, T. Pietzonka, S. Hornemann, A. Aguzzi
Novel anti-PrP human antibodies for therapy of prion diseases

5331
A. Senatore, K. Frontzek, M. Bardelli, R. Reimann, S. Hornemann, L. Simonelli, L. Varani, A. Aguzzi
Rational design of neuroprotective antibodies against the prion protein by phage display

5332
M. Avar, D. Heinzer, A. Lakkaraju, A. Chincisan, E. Schaper, M. Emmenegger, S. Hornemann, A. Aguzzi
A whole genome siRNA screen for identification of modulators of prions

5333
A. Lakkaraju, R. Marpakwar, E. Lemes, U. Herrmann, A. Ballabio, A. Aguzzi
Identifying the determinants of spongiform phenotype in prion infections

5334
D. Heinzer, M. Avar, D. Pease, J. Ying, A. Chincisan, E. Schaper, M. Emmenegger, S. Hornemann, A. Aguzzi
Whole genome RNAi screen identifies novel regulators of PrPC as potential therapeutic targets in prion diseases

5341
E. Boran, T. Fedele, P. Klaver, P. Hilfiker, L. Stieglitz, T. Grunwald, J. Sarnthein
Persistent hippocampal neural firing and hippocampal-cortical coupling predict verbal working memory load

5344
O. Török, B. Schreiner, H. C. Tsai, M. Han, M. Greter, B. Becher, A. Keller
Brain pericytes as sentinels controlling leukocyte trafficking in the CNS

5345
E. Lemes, A. Lakkaraju, R. Marpakwar, A. Aguzzi
PIKfyve As a Key Player in Prion-Induced Vacuolation

5346
C. Zhu, P. Schwarz, A. Aguzzi
Deficiency of Progranulin (PGRN) results in accelerated prion diseases

5347
M. Losa, C. Scheckel, K. Frontzek, M. Emmenegger, A. Aguzzi
Characterization, cloning and validation of natively paired human-derived anti-cellular PrP autoantibodies and their germline V-(D)-J segment recombination events using a targeted single cell approach on different patient cohorts

5349
M.-A. Wulf, A. Sattler, K. Frontzek, A. Aguzzi
Acute changes in the cerebellar phosphoproteome induced by neurotoxic antibodies targeting the cellular prion protein

5354
C. Scheckel, M. Mazlami, A. Aguzzi
Systematic Profiling of Molecular Changes during Prion Disease Progression

5357
V. Todorova, M. Barben, M. Samardzija, G. Azarias, B. Weber, C. Grimm
Stabilisation of hypoxia-inducible factor 1-alpha cause mitochondrial dysfunction in photoreceptors

5362
R. Reimann, S. Sorce, A. Chincisan, A. Aguzzi
GPI linked protein overexpression in myoblasts

5373
K. Frauenknecht, M. Emmenegger, A. Chincisan, A. Aguzzi
Incidence of naturally occurring anti-TREM2-antibodies in a large hospital cohort

5389
P. Manogaran, M. Samardzija, A. Schad, C. Wicki, C. Walker-Egger, M. Rudin, C. Grimm, S. Schippling
Longitudinal characterization of optic nerve and retinal pathology in experimental optic neuritis

5403
L. Michels, R. Büchler, K. Kucian
Structural hyperconnectivity in brain regions for number line processing and memory in children with developmental dyscalculia

5407
N. Schneider, M. Ferster, C. Lustenberger, W. Karlen, H. Fehr-Duda, E. Fehr, R. O'Gorman, R. Huber, C. Baumann, A. Maric
Linking the change in decision-making after sleep restriction to the restorative function of sleep

5437
P. Pagella, C. Cantu', M. Schwab, T. Mitsiadis
The neurite outgrowth inhibitor Nogo-A fine-tunes enamel formation

5454
D. Kirschenbaum, F. Voigt, E. Dadgar-Kiani, F. Catto, F. Helmchen, J. Hyung-Lee, A. Aguzzi
Crystal & Hits: quantifying Alzheimer's disease pathology in the whole-mount mouse brain

Translational Research

5335
A. Henzi, A. Senatore, A. Lakkaraju, A. Aguzzi
A Novel Tool for the Treatment of Peripheral Demyelinating Neuropathies

5340
A. Magalhães, A. Chincisan, M. Emmenegger, A. Carrella, A. Aguzzi, S. Hornemann
Unbiased high-throughput microELISA screen for naturally occurring human tauK18 autoantibodies

5367
V. Ginde, A. Ulusoy, C. Conçalves Moreira, L. Jakobi, D. Di Monte, C. Baumann, D. Noain
Effect of slow-wave sleep modulation over α-synuclein spreading in a AAV rat model of spreading of synuclein pathology

5416
J. Bremer, A. Aguzzi
Three-dimensional analysis of skin and peripheral nerve biopsies

5417
A. Reuss, D. Kirschenbaum, P. Nilsson, A. Aguzzi
Establishing a 3D histological grading system for early and late amyloid beta and tau pathology in Alzheimer’s disease patients

5418
M. Carta, C. Scheckel, C. Schiavi, E. Kara, M. Losa, A. Aguzzi
Targeted production of murine antibodies using sorted specific B cells

5421
O. Rus-Oswald, J. Reinhardt, C. Burki, S. Bridenbaugh, C. Stippich, R. Reto, M. Blatow
A clinical fMRI protocol for cognitive-motor dual task

5425

L. Barrios, A. Maeder, P. Oldrati, S. Demirci, S. Santini, A. Lutterotti
Digital Biomarkers for autonomic dysfunction in Multiple Sclerosis

5430
H. Hayward-Koennecke, F. Fuchs, C. Kaiser, F. Von Kaenel, S. Iseli, O. Mujkic, S. Broicher, O. Geisseler, R. Martin, E. Hafen, S. Bignens, A. Lutterotti
The MitrendS App – a new tool to follow MS patients using the citizen controlled MIDATA platform.

5444
M. Emmenegger, E. Capodaglio, A. Chincisan, S. Grathwohl, P. Kumari, D. Schneider, L. Mottier, J. Domange, J. Grimm, R. Riek, A. Aguzzi
Identification and characterisation of patients harbouring anti-ApoE4-specific autoantibodies from an unselected hospital-wide patient cohort

5450
T. Karen, S. Kleiser, D. Ostojic, H. Isler, S. Guglielmini, D. Bassler, M. Wolf, F. Scholkmann
Cerebral hemodynamic responses in preterm neonates to visual stimulation: Classification according to subgroups and analysis of frontotemporal-occipital functional connectivity

Clinical Trials

5215
Y. Valko, E. Werth, L. Imbach, P. Valko, K. Weber
The eyes wake up: Screening for benign paroxysmal positional vertigo with polysomnography

5342
E. Boran, G. Ramantani, K. Krayenbühl, T. Fedele, J. Sarnthein
High Frequency Oscillations in scalp EEG to monitor therapy in the individual patient

5359
M. Haeberlin, G. Narula
Automatic detection of burst-suppression-pattern in neurocritical care patients

5361
C. Brühlmann, T. Honegger, D. Bächinger, E. Michalopoulou, A. Monge Naldi, V. Wettstein, S. Muff, B. Schuknecht, A. Eckhard
Endotype-Phenotype Patterns in Meniere's Disease Based on Gadolinium-Enhanced MRI of the Vestibular Aqueduct

5404
C. Wicki, C. Walker-Egger, T. Simic, J. Hanson, S. Schippling
Repetitive transorbital alternating current stimulation in acute autoimmune optic neuritis: Pathobiological basis and design of a phase I/ IIa pilot study

5411
K. Frontzek, M. Carta, M. Losa, M. Epskamp, G. Meisl, U. Camenisch, S. Hornemann, A. Aguzzi
The presence of autoantibodies against the prion protein is independent of PRNP mutations

5427
M. Docampo, M. Hohmann, C. Sellés-Moreno, C. Cruciani, M. Mikolin, H. Hayward-Koennecke, T. Müller, A. Zaugg, M. Foege, T. Ludersdorfer, A. Lutterotti, R. Martin, M. Sospedra
Immunosafety and Characterization of Tolerance Mechanisms Following Treatment with Myelin Peptide-Pulsed Red Blood Cells (ETIMSred Phase Ib trial)

5431
E. Boran, G. Ramantani, N. Krayenbühl, M. Schreiber, K. König, T. Fedele, J. Sarnthein
High density ECoG improves detection of high frequency oscillations that predict seizure outcome.

5432
A. Lutterotti, W. Faigle, H. Hayward-Koennecke, I. Jelcic, N. Pfender, T. Müller, C. Blumer, M. Foege, S. Schippling, M. Sospedra, M. Sormani, M. Inglese, T. Berger, R. Martin
Treatment of Clinically Isolated Syndrome and Relapsing Remitting Multiple Sclerosis with RNS60 Administered Intravenously – a Phase IIa Clinical Trial

5433
A. Lutterotti, T. Ludersdorfer, M. Docampo, M. Hohmann, C. Selles Moreno, H. Hayward-Koennecke, I. Jelcic, N. Pfender, T. Müller, C. Blumer, M. Foege, S. Winklhofer, R. Stenger, M. Kayser, U. Schanz, M. Sospedra, R. Martin
Establish Tolerance in MS with myelin-peptide coupled red blood cells - ETIMSred trial

5438
M. Sharifshazileh, K. Burelo, J. Sarnthein, G. Indiveri, T. Fedele
A Neuromorphic System-on-a-Chip Approach Towards Detecting High-Frequency Oscillations in Human iEEG

5439
P. Baumgartner, A. Luft, S. Wegener
Optic Nerve Sonography to monitor Intracranial pressure afTer large vessel ischemic strokE – The ONSITE Study

5452
R. Renzel, L. Tschaler, I. Mothersill, LL. Imbach, R. Poryazova
Sensitivity of Long-Term EEG monitoring as second diagnostic step in the initial diagnosis of epilepsy

5165

A. Inderbitzin[1], Y. Kok[1], L. Joerimann[1], A. Kelley[1], K. Neumann[1], K. Metzner[1]

CRISPR/Cas9-mediated insertion of HIV-1-based vector into BACH2 does not lead to viral latency in Jurkat T cells

Infectious Diseases and Hospital Epidemiology, University Hospital Zurich, Zurich[1]

Introduction:
The latent reservoir is a major obstacle to cure HIV-1 infection. HIV-1 integrates into the human genome and can persist for life. Hotspots of HIV-1 integration have been described and some might be associated with clonal expansion of latently HIV-1 infected cells. One such hotspot is the gene *BTB domain and CNC homology 2 (BACH2)*, whose product BACH2 functions as a transcription factor in T cells, B cells, and macrophages.

Methods:
To investigate whether HIV-1 integration into *BACH2* leads to an active or latent viral state, we inserted our dual-fluorescence HIV-1 based vector LTatC[M] (Kok *et al*., 2018) into *BACH2* in Jurkat T cells via CRISPR/Cas9 technology to examine the impact of different loci (introns 2 and 5) and transcriptional orientations on the HIV-1 promoter activity. In LTatC[M], the fluorophore Cerulean reports the activity of the HIV-1 promoter in an HIV-1 Tat-dependent manner whereas the expression of mCherry is kept constitutive upon integration by virtue of an independent constitutive promoter and a pair of flanking genetic insulators. LTatC[M] was also inserted into the safe harbour gene AAVS1.

Results:
Flow cytometric analysis of sorted cell clones showed that a Cerulean and mCherry double positive phenotype was predominant in all loci examined and independent of the transcriptional orientation, and that this phenotype remained unchanged in culture for up to 101 days. Additionally, Western blot analyses confirmed that BACH2 expression levels were not impaired by monoallelic integration of the vector into *BACH2*.

Conclusion:
Our results indicate that integration into *BACH2* does not intrinsically lead to viral latency in the majority of targeted Jurkat T cells up to 3 months of follow up.

5166

M. Schwarzfischer[1], L. Hering[1], E. Katkeviciute[1], A. Niechcial[1], K. Atrott[1], P. Busenhart[1], K. Bäbler[1], G. Rogler[1], M. Scharl[1], M. Spalinger[1]

TiO2 nanoparticles abrogate the protective effect of the autoimmunity-associated PTPN22 R619W variant during acute DSS colitis

Department of Gastroenterology and Hepatology, University Hospital Zurich, University of Zurich, Zurich[1]

Introduction:
Titanium dioxide (TiO_2), commonly used in comestible goods and personal care products, is omnipresent in everyone's daily life. TiO_2 nanoparticles (1-100nm) possess high bioreactivity and aggregate in the human body. We have demonstrated that in patients suffering from inflammatory bowel disease (IBD), defects in the epithelial barrier lead to increased TiO_2 serum concentrations. *In vivo*, oral TiO_2 administration aggravates colitis via activation of the NLRP3 inflammasome. The NLRP3 protein complex is essential for innate immune response and is directly regulated by protein-tyrosine phosphatase 22 (PTPN22). A polymorphism within the *PTPN22* gene locus has been associated with increased risk to develop auto-inflammatory disorders, but protects from Crohn's disease (CD). Since IBD is a complex, multifactorial disease, investigation how genetic risk variants interact with environmental influences is essential to understand the pathogenesis of the disease.

Methods:
To investigate potential interactions between TiO_2 nanoparticles and PTPN22, we induced acute colitis in *Ptpn22* wildtype, *Ptpn22* deficient and *Ptpn22*^{R619W} transgenic mice, which express the murine ortholog to the disease-associated *PTPN22* ^{R620W} variant. Mice (n=8/group) were exposed to 2% dextran sodium sulfate (DSS) in the drinking water with simultaneous TiO_2 administration (500mg/kg BW; 30-50nm rutile) per daily oral gavage.

Results:
As expected *Ptpn22*^{R619W} mice were protected from inflammation in the acute DSS colitis model. TiO_2 application during DSS treatment, however, resulted in strong inflammation within the gastrointestinal tract of *Ptpn22*^{R619W} mice and colonoscopy revealed increased granularity, fibrin deposits and altered vascularization of the colonic wall. Histological analysis confirmed severe colitis and lesions throughout the colon, culminating in immune cell infiltration and epithelial damage. Interestingly, *Ptpn22*^{R619W} transgenic mice, simultaneously exposed to DSS and TiO_2, displayed significantly decreased NQO1 gene and protein expression levels. However, TiO_2 administration did not significantly affect the extent of colitis in the *Ptpn22* deficient mice.

Conclusion:
Our findings indicate that TiO_2 abrogates the protective effect of the CD-associated *Ptpn22*^{R619W} polymorphism during colitis induction. This data demonstrates that consumption of TiO_2 is able to induce colitis in mice carrying the *Ptpn22*^{R619W} variant and therefore to render a protective into a detrimental mechanism. Since TiO_2 nanoparticles are highly abundant in daily life, our findings might contribute to a better understanding of the mechanisms contributing to the onset of IBD. Deciphering how TiO_2 directly targets the mode of action of the *Ptpn22*^{R619W} variant might yield new therapeutic approaches for IBD treatment.

5167

Y. Zarb[1], S. Nassiri[2], S. Utz[3], M. Dilorenzi[2], M. Colonna[4], M. Greter[3], A. Keller[1]

Microglia control vessel-associated calcifications in the mouse model of primary familial brain calcification

Department of Neurosurgery, University Hospital Zurich, Zurich[1], Swiss Institute of Bioinformatics, University of Lausanne[2], Institute of Experimental Immunology, University of Zurich[3], Department of Pathology and Immunology, Washington University School of Medicine, St.Louis, USA[4]

Introduction:
Microglia, the tissue-resident macrophages in brain, regulate development and homeostasis in the central nervous system (CNS). Specifically, microglia are involved in mediating the immune response and clearing cellular debris. In neurodegenerative diseases, the role of microglia is highly debated, especially whether microglial activity are beneficial or detrimental, due to elicited chronic inflammatory response. In this study, we investigated the role of microglia in primary familial brain calcification (PFBC), an autosomal dominant inherited neurodegenerative disease characterized by capillary-associated calcifications in the basal ganglia. Loss-of-function mutations in platelet-derived growth factor B gene (*PDGFB),* one of four causal PFBC genes, also lead to brain calcification in mice. Previously, we have shown that mice hypomorphic for *Pdgfb (Pdgfb*$^{ret/ret}$) develop brain calcifications similar to PFBC patients. In addition, our studies have shown that capillary-calcification in *Pdgfb*$^{ret/ret}$ and PFBC demonstrate an osteogenic environment. Cells surrounding capillary brain calcifications express bone cell markers (i.e., osteoblasts, osteoclasts, osteocytes) and bone proteins. In addition, capillary calcifications, which appear like pearls on a string, are surrounded by CD45^{high}, Iba1^{+} microglia. Microglial dysfunction in patients with Nasu-Hakola disease and neuroinflammation in Type I Interferonopathies are accompanied by basal ganglia calcification. We therefore asked if microglia play a pathophysiologic role in PFBC by controlling vessel-calcification.

Methods:
Microglia in brains of *Pdgfb*$^{ret/ret}$ were characterized using immunohistochemistry, RNAseq and flow cytometry. Lineage tracing studies of microglia in *Pdgfb*$^{ret/ret}$ were performed by crossing microglia-specific Cre lines (Cx3Cr1 Cre^{ERT2} and Sall1 Cre^{ERT2}) with *Pdgfb*$^{ret/ret}$ expressing a reporter Ai14. These mice were used to examine whether microglia surrounding calcifications express osteoclast markers. We crossed *Pdgfb*$^{ret/ret}$ animals with *Trem2* knockout mice and depleted microglia using PLX5622 to study whether there was an increased propensity to develop vessel-calcifications.

Results:
Here, we report that microglia surrounding vessel-calcifications express osteoclast markers, indicating their role in the phagocytosis of brain calcifications. We also observed that genetically impaired microglial function leads to worsening of vessel calcification in *Pdgfb*$^{ret/ret}$;*Trem2*$^{-/-}$ animals compared to *Pdgfb*$^{ret/ret}$;*Trem2*$^{wt/wt}$. Finally, RNAseq analysis on tissue surrounding brain calcifications reveals an enrichment of genes linked to disease-associated microglia. This finding was validated using immunohistochemistry.

Conclusion:
In conclusion, we report that impaired microglial function in PFBC aggravates vessel calcifications. Thus, microglia are critical in controlling the growth of vessel-associated brain calcifications in PFBC. Accordingly, therapeutic targeting of microglia in PBFC might be beneficial for controlling the vessel-calcification.

5168

F. Burgio[2], N. Rimmer[2], U. Pieles[2], J. Buschmann[1], M. Beaufils-Hugot[3]

Characterization and in ovo vascularisation of a 3D-printed hydroxyapatite scaffold with different extracellular matrix coatings under perfusion culture

Plastic Surgery and Hand Surgery, University Hospital Zurich[1], School of Life Sciences, Institute for Chemistry and Bioanalytics (ICB), Basel[2], Novartis Pharma AG, Global Drug Development (GDD), Respiratory Department, Basel[3]

Introduction:
For the fabrication of appropriate bone tissue engineered constructs, several prerequisites should be fulfilled. It should offer long-term stability, allow proper cell attachment and proliferation, furthermore be osteoinductive and easy to be vascularized. Having these requirements as background, we fabricated a novel porous 3D-printed hydroxyapatite (HA) scaffold and treated it with oxygen plasma. To make it less brittle, it was coated with extracellular matrix produced by bone-marrow-derived MSCs in different culture media.

Methods:
The HA scaffolds were seeded with human bone marrow-derived MSCs and cultivated under static or dynamic conditions in a perfusion bioreactor; proliferative culture medium as well as osteogenic culture medium was used. After 4 weeks, elasticity was assessed by nanoindentation, and osteogenic and angiogenic marker genes were analysed using RT-PCR. HA scaffolds with differently fabricated ECM coatings (derived from proliferative or osteogenic culture) were then planted onto the CAM assay after decellularization. Functional perfusion capacity of the vascularized scaffolds after 1 week on the CAM was assessed by MRI in the living chicken embryo in ovo.

Results:
The scaffold had a significantly higher Elastic Modulus with ECM coating compared to ECM-free scaffolds. Higher commitment towards osteoblasts was found under perfusion culture compared to static cultivation. Interestingly, angiogenic markers CD31, eNOS and VEGF were upregulated, especially when osteogenic medium was used compared to proliferative medium. Compared to ECM-free HA scaffolds, *in ovo* vascularization was enhanced by ECM coating; vascularisation induced by ECM from osteogenic medium led to a vessel distribution more homogenously throughout the construct, while ECM from proliferative medium enhanced vessel density at the interface and to a lower extent at the middle and top of the material.

Conclusion:
ECM coating enhances elasticity of otherwise brittle hydroxyapatite and increases the vascularization capacity in ovo compared to ECM-free HA scaffolds. Dynamic cultivation of this novel porous oxygen-plasma treated HA scaffold with human bone marrow-derived MSCs in osteogenic medium and subsequent decellularization provides a promising off-the-shelf bone tissue engineered construct.

5169

L. Otto[1], P. Wolint[1], A. Woloszyk[2], A. Becker[3], A. Boss[3], R. Böni[4], M. Calcagni[1], P. Giovanoli[4], M. Emmert[2], J. Buschmann[1]

Calcification capacity and vascularization of a collagen Matricel® scaffold seeded with human adipose-derived stem cells seeded as single cells or 3D-microtissues on the CAM assay

Plastic Surgery and Hand Surgery, University Hospital Zurich[1], Institute of Regenerative Medicine, University Zurich[2], Institute for Diagnostic and Interventional Radiology, University Hospital Zurich[3], White House Center for Liposuction, Zurich[4]

Introduction:
Bone tissue engineering demands for rapidly calcifying scaffolds, for example by adult stem cells differentiating towards the osteoblastic phenotype. Moreover, they should be well vascularized in order to provide sufficient nutrients and oxygen, especially in critical size grafts. Natural bone is mainly composed of calcified collagen where the microenvironment affects stem cells' fate and differentiation. The calcification capacity as well as the vascularization of collagen seeded with stem cells may depend on the cell format the cells are applied.

Methods:
Human adipose-derived stem cells (ASCs) from two donors were seeded on commercially available collagen scaffold (Matricel®) to study the calcification of collagen. The cells were either seeded as single cells (SCs) or as microtissues (MTs). Moreover, the scaffold was also soaked with the secretome of MTs and SCs, respectively. Finally, in order to address mere chemical calcification (precipitation), the cell-free scaffold was cultivated in culture medium, PBS or water, respectively, before on-plantation on the chorioallantoic membrane of the chicken embryo (CAM assay) for one week. Micro-CT analysis of ex vivo samples was performed to assess micro-calcifications. Histological assessment included Van Kossa staining (extent of calcification), H&E (vascularization), among others.

Results:
There was not only a higher calcification in the case MTs were seeded onto Matricel® scaffolds compared to SCs, but also a higher tissue infiltration from the CAM surface into the collagen scaffold after 1 week of incubation. In addition, vascularization was increased, with more vessels in MT-seeded scaffolds compared to SC-seeded ones.

Conclusion:
Calcification capacity as well as vascularization are influenced by the cell format the seeded stem cells are applied. Three-dimensional MTs favor calcification and lead to a higher vessel density in collagen scaffolds planted onto the CAM assay. It may be worthwhile to apply stem cells as MTs in bone tissue engineering to promote two basic and important processes for functionally adequate bone grafts: calcification and vascularization.

5170

C. Waschkies[3], F. Kivrak-Pfiffner[2], D. Heuberger[5], P. Wolint[1], M. Schneider[4], Y. Tian[4], M. Calcagni[1], P. Giovanoli[1], J. Buschmann[1]

MRI Phenotypization, Vasoreactivity and Hypoxia in MC-38 colon and A549 lung adeno-carcinoma cell grafts grown on the Chorioallantoic Membrane of the Chick Embryo in ovo

Plastic Surgery and Hand Surgery, University Hospital Zurich[1], Institute of Regenerative Medicine, University Zurich[2], Institute for Biomedical Engineering, ETH and University of Zurich[3], Division of Visceral and Transplantation Surgery, University Hospital Zurich[4], Clinic of Intensive Care, University Hospital Zurich[5]

Introduction:
Recently, a tumor model based on the chorioallantoic membrane (CAM) was characterized structurally with MRI [1]. Yet, vascular functional reserve and oxygenation-sensitive MRI measures [2-3] remain largely unexplored in this model. Here, we compare MC-38 colon and A549 adeno-carcinoma cell grafts with regards to their vascular and oxygenation phenotypes. We demonstrate that a functional gas challenge with carbogen is feasible through gas exchange on the CAM, allowing to access vascular function and oxygenation status of the tumor graft in this experimental model.

Methods:
Fertilized Lohman white LSL chick eggs were opened on incubation day (ID) 3.5 and on ID7 5 x 10^5 MC-38 colon or A549 lung adenocarcinoma cells were planted onto the CAM. MRI was performed *in ovo* on ID 14 in 5 samples for each graft type on a 4.7T Bruker PharmaScan system, with chicken embryos sedated (0.3 mg/kg medetomidine). T1w and T2w anatomical reference images obtained and quantitative T1 and T2* maps were compared between periods of air and carbogen (95% O2, 5% CO2). Gases were delivered through a plastic tubing to the CAM. T1w scans were repeated in selected samples after i.v. injection Gd-DOTA (Dotarem®, Guerbet S.A., Switzerland) to study enhancement in the tumor graft. Corroborative histology was be obtained from H&E and Ki-67 staining.

Results:
MC-38 colon and A549 lung adenocarcinoma cell grafts were compared using quantitative T1 and T2* MRI, readouts associated with vascular responsivity and oxygenation status, when compared between periods of air and carbogen. Since the CAM serves as a breathing organ during chick embryo development, these markers might be also applicable for the grafts on the CAM. Our preliminary data show that in A549 lung adenocarcinoma cell grafts T2* values increased upon carbogen exposure, while MC-38 grafts displayed a decreasing trend in T1. Qualitative assessment of Gd-enhancement, suggests that A549 grafts display a more homogeneous enhancement compared to MC-38 grafts that enhance more on the graft border. Furthermore, it will be of interest to explore if such enhancement patterns might be supportive for our vague notion that A549 grafts might display a better vascular response, while only MC-38 show oxygen-induced T1 shortening as observed in normoxia.

Conclusion:
Our experiments show that different tumor grafts planted on the CAM were distinguished non-destructively *in ovo* using MRI. We show that a functional gas challenge is feasible through the CAM, and affects MRI signals associated with vascular reactivity and oxygenation status of the graft. The CAM assay may thus help qualifying such MRI markers to discern distinct vascular functional and oxygenation phenotypes.

References:
[1] Zuo et al. (2014) NMR Biomed 28: 440-447
[2] Baudelet et al. (2006) NMR Biomed 19: 69-76
[3] O'Connor et al. (2015) Cancer Res 76(4) : 787-95

5171

J. Buschmann[1], Y. Yamada[3], K. Schulz-Schönhagen[4], S. Hess[4], W. Stark[4], C. Opelz[2], G. Meier Bürgisser[1], W. Weder[2], W. Jungraithmayr[5]

Stem cell-seeded hybrid nanocomposite for chest wall repair in a murine model

Plastic Surgery and Hand Surgery, University Hospital Zurich[1], Division of Thoracic Surgery, University Hospital Zurich[2], Department of Thoracic Surgery, Kyoto University Hospital, Kyoto, Japan[3], Institute for Chemical and Bioengineering, Department of Chemistry and Applied Biosciences, ETH Zurich[4], Department of Thoracic Surgery, Brandenburg Medical School, Campus Neuruppin, Germany[5]

Introduction:
Resection of the thoracic wall is a common procedure to remove malignant tumours. Usually, Gore-Tex® is used to replace the missing tissue; however, it is inert and not degradable. Novel biodegradable materials are nowadays available that stimulate and guide the regeneration process. Furthermore, stem cell seeding not only reduces inflammatory reaction towards such implants, but also helps to achieve a good integration.

Methods:
A biodegradable bi-layered hybrid nanocomposite material was developed based on poly-lactic-co-glycolic acid and amorphous calcium phosphate nanoparticles (PLGA/aCaP) and pure PLGA. Electrospun meshes were seeded with murine adipose-derived stem cells (ASCs of C57BL/6). Biomechanical tests were performed to assess ultimate failure stress. Using a mouse model (C57BL/LY5.1), ASC-seeded hybrid scaffolds were implanted as a chest wall graft in order to study biointegration and cell-implant interactions. After 4 and 8 weeks, implant integration towards the skin and the lung, cell infiltration into the bi-layered material, inflammatory responses, neo-vascularization, fibrosis and ECM components (collagen I and fibronectin) were determined in six different zones of the graft.

Results:
The bi-layered hybrid nanocomposite was shown to be stable even after a 2-week *in vitro* culture, in contrast to PLGA/aCaP without a PLGA layer. There was a complete biointegration in vivo; with all scaffolds having a good, homogenous vascularization throughout the scaffold. The presence of ASCs induced a higher attraction of $CD45^+$ cells with hematopoietic origin compared to cell-free scaffolds. Inflammatory reaction was slightly enhanced at 4 weeks post-implantation in the presence of ASCs, while it was similar for both groups (± ASCs) at 8 weeks.

Conclusion:
A bi-layered hybrid nanocomposite fabricated of electrospun PLGA/aCaP and a reinforcing layer of pristine PLGA is an ideal scaffold for chest wall reconstruction. It is stable, can easily be seeded with stem cells and allows a proper host tissue integration with a sufficient vascularization. Moreover, it is biodegradable and thus allows a complete substitution of the biomaterial with host tissue.

5215

Y. Valko[1], E. Werth[2], L. Imbach[1], P. Valko[1], K. Weber[3]

The eyes wake up: Screening for benign paroxysmal positional vertigo with polysomnography

Universitätsspital Zürich, Neurology Department[1], Sleep & Health Zurich, University Hospital Zurich[2], Universitätsspital Zürich, Neurology and Ophthalmology Departments[3]

Introduction:
Patients with benign paroxysmal positional vertigo (BPPV) experience attacks of vertigo and nystagmus, typically elicited by nocturnal changes in head position. While positional nystagmus has been shown to be detectable in electrooculography (EOG) tracings of polysomnography (PSG), the frequency of undiagnosed BPPV in patients referred for sleep-wake examination has never been investigated.

Methods:
Prospective evaluation of positional nystagmus in 129 consecutive patients referred to a tertiary neurological sleep laboratory for sleep-wake examination with PSG. Both in the evening and morning, patients had diagnostic positioning maneuvers under ongoing EOG-PSG registration, followed by visual inspection of whole-night EOG for episodes of positional nystagmus.

Results:
In 19 patients (14.7%), we found stereotyped oscillating, crescendo-decrescendo patterns of positional nystagmus, typically appearing few seconds after changes in head position. In 9 of these patients (47%), the nystagmus was also provoked by the positioning maneuvers. Nystagmus only occurred during wakefulness, not during sleep. In a patient with severe cupulolithiasis, we observed a gradual disappearance and reemergence of nystagmus during transitions between wakefulness and N1 sleep stage. In a logistic regression model, positive diagnostic maneuvers, the presence of neurological comorbidity and reduced total sleep times significantly added to the likelihood of nocturnal positional nystagmus occurrence. At the same time, occurrence of nocturnal nystagmus was a strong predictor for positive positioning maneuvers.

Conclusion:
Inspection of EOG-PSG for positional nystagmus is a worthwhile way to detect patients with undiagnosed BPPV. Sleep physician should be aware of this diagnostic opportunity, as BPPV is frequent and cumbersome yet easily treatable.

5238

S. Santos[1,2], C. Haslinger[1], K. Klaic[1], M. Faleschini[2], M. Mennet[3], O. Potterat[2], U. Von Mandach[1], M. Hamburger[2], A.P. Simões-Wüst[1]

A Bufadienolide-Enriched Fraction of Bryophyllum pinnatum Inhibits Human Myometrial Contractility in Vitro

Department of Obstetrics, University Hospital Zurich[1], Division of Pharmaceutical Biology, University of Basel[2], Clinical Research, Weleda AG, Arlesheim[3]

Introduction:
Preterm birth is one of the most common causes of infant morbidity and mortality, and often results from preterm labour. *Bryophyllum pinnatum* is a succulent perennial plant traditionally used since the 1970's in the treatment of premature labour, first in anthroposophic hospitals and, recently, in conventional settings often as an add-on medication. However, it is not known which type of compounds in *B. pinnatum* leaves contribute to the tocolytic effect. The objective of this study was to investigate the effects on human myometrial contractility *in vitro* of *B. pinnatum* leaf press juice (BPJ), and of fractions obtained from the plant, namely a bufadienolide-enriched fraction (BEF), a flavonoid-enriched fraction (FEF), and the corresponding flavonoid aglycon mixture (A-Mix).

Methods:
Myometrial biopsies were collected during elective Caesarean section. Strips of tissue were mounted in an organ bath system (myograph), and spontaneous contractions were recorded. Aliquots of a stock solution of FEF, A-Mix, BEF, BPJ or a vehicle control (Krebs solution or DMSO), were repeatedly added (4 times) in 20 min intervals. The strength (i.e. AUC and amplitude) of contractions were recorded for each 20 min period. After a washout period, vitality of strips was observed for additional 30 min. Cell viability assays were performed with the human myometrium hTERT-C3 and PHM1-41 cell lines.

Results:
Repeated addition of FEF, A-Mix, BEF or BPJ led to a progressive decrease of contraction strength (AUC and amplitude) in a concentration-dependent manner (in all cases, $p<0.05$), without jeopardising the vitality of myometrium strips. BEF was the most active test substance, since 1 µg/mL BEF lowered AUC to 40.1 ± 11.8% of initial, whereas 150 µg/mL FEF, 6.2 µg/mL A-Mix, and 10 µg/mL BPJ (i.e. 1%) were required to achieve comparable inhibition. None of the test substances decreased myometrial cell viability, even at concentrations of 500 µg/ml FEF, 40 µg/ml A-Mix, 3.8 µg/ml BEF and 75 µg/ml BPJ, i.e. higher than those used in the myometrium experiments.

Conclusion:
The data confirm previous observations showing that *in vitro* myometrial contractility can be inhibited by *B. pinnatum* leaf press juice without affecting viability. Given the concentrations of flavonoids in FEF and BPJ, and of bufadienolides in BEF and BPJ, it appears that bufadienolides may be mainly responsible for the relaxant effect.

5307

B. Eggerschwiler[1], D. Canepa[1], H-C. Pape[2], E. Casanova[2], P. Cinelli[2]

Automated digital image quantification of histological staining for the analysis of the trilineage differentiation potential of mesenchymal stem cells

Faculty of Science, University of Zurich, Zurich[1], Department of Trauma Surgery, University Hospital Zurich, Zurich[2]

Introduction:
Multipotent mesenchymal stem cells (MSCs) have the potential to repair and regenerate damaged tissues and are considered as attractive candidates for the development of cell-based regenerative therapies. Currently, there are more than 200 clinical trials involving the use of MSCs for a wide variety of indications. However, variations in their isolation, expansion, and particularly characterization have made the interpretation of study outcomes or the rigorous assessement of therapeutic efficacy difficult. Prediction of the therapeutic abilities of MSCs is of major importance and essential to guaranty that only the most suitable cells will be used. The development of standardized and reproducible assays to predict MSC potency is therefore mandatory. The currently used quantification methodologies for the determination of the trilineage potential of MSCs are usualy based on absorbance measurements which are imprecise and prone to errors. We therefore aimed at developing a methodology offering first a standardized way to objectively quantify the trilineage potential of MSC preparations and second allowing to discriminate functional differences between clonally expanded cell populations. An unbiased and standardized quantification of the differentiation potential of MSCs is of fundamental importance for a therapeutical use of these cells in the clinic.

Methods:
MSCs originating from several patients were differentiated into osteoblasts, adipocytes, and chondroblasts for 14, 17, and 21 days. Differentiated cells were then stained with the classical dyes: Alizarin Red S for osteoblasts, Oli Red O for adipocytes, and Alcian Blue 8GX for chondroblasts. Quantification of differentiation was then performed with our newly developed digital image analysis (DIA) tool followed by the classical absorbance measurement. The results from the two techniques were then compared.

Results:
Quantification based on DIA allowed highly standardized and objective dye quantification with superior sensitivity compared to absorbance measurements. Furthermore, small differences between MSC lines in the differentiation potential were highlighted using DIA whereas no difference was detected using absorbance quantification.

Conclusion:
Our approach represents a novel method that simplifies the laboratory procedures not only for the quantification of histological dyes and the degree of differentiation of MSCs, but due to its color independence, it can be easily adapted for the quantification of a wide range of staining procedures in histology. The method is easily applicable since it is based on open source software and standard light microscopy.

5309

D. Canepa[1], E. Casanova[1], E. Arvaniti[3], B. Eggerschwiler[1], V. Tosevski[2], M. Claassen[3], H-C. Pape[1], P. Cinelli[1]

Comprehensive Mass Cytometry Analysis of Human Adipose Derived Stem Cells for Clinical Applications

Department of Trauma Surgery, University Hospital Zurich, Zurich[1], Mass Cytometry Facility Zurich[2], Institute of Molecular Systems Biology ETH Zurich[3]

Introduction:
Fractures with a critical size bone defect represent a serious issue in orthopaedic surgery because are associated with high rates of delayed and non-union. The standard treatment involve autogenous bone grafts combined with allogenic materials, but this procedure implies different drawbacks. Tissue engineering with mesenchymal stem cells (MSCs), more precisely with adipose derived stem cells (ASCs), represents an interesting alternative to improve the clinical outcomes. MSC *per definition* must (1) adhere to plastic, (2) express CD73, CD90, CD105 and lack the expression of most of the hematopoietic stem cells markers and (3) differentiate toward adipocytes, chondrocytes, and osteocytes. However, MSCs/ASCs consist of a heterogeneous, not yet well-characterized population of different stem/progenitor cells. Understanding the heterogeneous composition of human ASCs is essential not only for understanding the biological properties of MSCs but also in the context of their potential outcomes in cell therapy.

Methods:
To dissect the heterogeneity of 18 human ASC lines we used the novel single cells real-time analysis Cytometry by Time-of-Flight (CyTOF**)**. CyTOF combines both flow cytometry and mass spectrometry and requires individual cells to be labeled with stable heavy metal isotopes. We generated a panel of 31 markers, which includes classical positive and negative MSC markers, epithelial and neural markers, several osteogenic, adipogenic, and chondrogenic markers.

Results:
For assessing the osteogenic differentiation potential of 18 human ASCs, the cells were cultivated over a period of 21 days in osteogenic medium and at different time points real-time quantitative PCR and alizarin red staining were performed. Based on the results, we divided the ASCs in good, intermediate, and bad differentiating cells. In a second step, CyTOF was performed on the first 4 days of differentiation and, by using the T-Stochastic Neighbour Embedding algorithm; we confirmed the phenotypic heterogeneous composition within the ASC lines. Moreover, the analyses given by the CellCNN (convolutional neural network) revealed a subpopulation responding to osteogenic differentiation (Alkaline phosphatase ALP+ and CD73low). This subpopulation is also predictive for the differentiation potential and therefore more present in the good differentiating ASCs compared to the bad ones.

Conclusion:
The data showed fundamental differences between the patient-specific ASC lines and suggest that the heterogeneity observed *in vitro* mirrors the heterogeneity observed in the clinic. Thus, identifying populations with enhanced osteogenic differentiation potential would serve as a diagnostic tool to predict clinical outcomes and would improve the therapeutic approaches.

5310

D. Karademir[1], F. Storti[1], C. Grimm[1]

Enhancing neuroprotection by CRISPR-mediated activation of LIF expression in Müller cells of the mouse retina

Augenklinik, UniversitätsSpital Zürich, Zürich[1]

Introduction:
Müller cells are the principal macroglia of the retina that not only provide crucial homeostatic and metabolic support to retinal neurons, but also promote their survival upon damage through endogenous neuroprotective signalling pathways. We and others have shown that leukemia inhibitory factor (LIF) is key to Müller glia-based neuroprotection. LIF is expressed by a subset of Müller glia in the damaged retina, and is necessary and sufficient to activate a signalling pathway that supports photoreceptor survival in mouse models of both light-induced and inherited retinal degeneration. Despite its striking neuroprotective effects however, high levels of LIF are deleterious to retinal function, preventing its use in humans by cytokine injection or AAV-based delivery of extra copies of the gene.
There is evidence that in healthy Müller cells, *Lif* mRNA is highly unstable unless stabilized by redox signalling factors that are produced during retinal injury. To take advantage of this regulation, which is specific to the endogenous *Lif* transcript, we will test an alternative strategy, where the endogenous *Lif* is upregulated by a non-mutating CRISPR activation system.

Methods:
To target *Lif* in the mouse retina, we utilized a modified CRISPR-SAM strategy involving two AAV constructs. One AAV harbours a ubiquitously-expressed, nuclease-dead Cas9, while the other harbours the transcriptional activator fusion protein MPH (MS2-p65-HSF1) and a modified guide RNA with MS2 hairpins that can recruit the MPH protein to the target locus. Three guide RNAs in a -150 to +100 bp range of the transcriptional start site of the mouse *Lif* gene were chosen based on on- and off-target activity. To test the functionality of the system *in vitro,* the constructs were delivered to mouse N2A cells with Lipofectamine 3000 (medium was changed after 6 hours). After 24, 48 or 72 hours, the upregulation of *Lif* mRNA was assessed with semi-quantitative PCR, relative to *B-actin.*

Results:
The CRISPR-SAM strategy led to a significant upregulation (up to 70-fold) of *Lif* mRNA compared to controls that did not receive a *Lif*-targeting gRNA. The level of upregulation was guide RNA-dependent, and therefore can be tailored to modulate the various effects of LIF.

Conclusion:
Preliminary results show that the CRISPR-SAM strategy is successful for upregulating *Lif in vitro.* Preparations for testing the strategy *in vivo* are underway, and include the usage of a novel synthetic promoter to limit *Lif* activation to Müller cells. *In vivo* assessment of CRISPR activation will include the measurement of *Lif* upregulation in the healthy and damaged retina, whether any neuroprotective or deleterious effects are obtained, and the regulation of activated endogenous *Lif* mRNA.

5311

M. Juhas[1], E. Widlake[2], J. Teo[3], D. Huseby[4], J. Tyrrell[2], Y. Polikanov[5], O. Ercan[4], A. Petersson[4], S. Cao[4], A. Aboklaish[2], A. Rominski[1], D. Crich[6], E. Böttger[1], T. Walsh[2], D. Hughes[4], S. Hobbie[1]

In-vitro activity of apramycin against multidrug-, carbapenem-, and aminoglycoside-resistant Enterobacteriaceae and Acinetobacter baumannii

University of Zurich[1], Cardiff University[2], National University Hospital Singapore[3], Uppsala University[4], University of Illinois at Chicago[5], Wayne State University[6]

Introduction:
Widespread antimicrobial resistance often limits the availability of therapeutic options to only a few last resort drugs which are themselves challenged by emerging resistance and adverse side effects. Apramycin, an aminoglycoside antibiotic, has a unique chemical structure that evades almost all resistance mechanisms including RNA methyltransferases frequently encountered in carbapenemase-producing clinical isolates. This study evaluates the *in-vitro* activity of apramycin against multidrug-, carbapenem-, and aminoglycoside-resistant Enterobacteriaceae and *Acinetobacter baumannii*, and provides a rationale for its superior antibacterial activity in the presence of aminoglycoside resistance determinants.

Methods:
A thorough antibacterial assessment of apramycin with 1,249 clinical isolates from Europe, Asia, Africa, and South America was performed by standard CLSI broth microdilution testing. Whole genome sequencing and susceptibility testing with an engineered panel of aminoglycoside resistance-conferring determinants were used to provide a mechanistic rationale for the breadth of apramycin activity.

Results:
MIC distributions and MIC_{90} values demonstrated broad antibacterial activity of apramycin against *Escherichia coli*, *Klebsiella pneumoniae*, *Enterobacter* spp., *Morganella morganii*, *Citrobacter freundii*, *Providencia* spp., *P. mirabilis*, *S. marcescens*, and *A. baumannii*. Genotypic analysis revealed the variety of aminoglycoside-modifying enzymes and rRNA methyltransferases that rendered a remarkable proportion of clinical isolates resistant to approved benchmark aminoglycosides, but not to apramycin. Screening a panel of engineered strains each with a single well-defined resistance mechanism provided additional evidence and support for superior antibacterial activity of apramycin.

Conclusion:
The superior breadth of activity renders apramycin a promising drug candidate for the treatment of systemic Gram-negative infections that are resistant to treatment with other aminoglycoside antibiotics.

5312

K. Slankamenac[1], N. Rütsche[1], D. Keller Lang[1]

Availability of advance directives in the emergency department: a prospective survey

Institut für Notfallmedizin[1]

Introduction:
Emergency departments (ED) are crowded with critically ill patients, many of whom are not able to communicate with the emergency staff anymore. Substitute decision makers are often not known or reachable in time. Therefore, advance directives (AD) clearly defining patients' values and beliefs regarding end-of-life decisions are urgently required, especially in life-threatening situations. To our knowledge, the prevalence of ADs among Swiss ED patients has not been evaluated yet. The purpose of this prospective survey was to investigate the prevalence of ADs among patients visiting a tertiary care Swiss ED and to identify factors associated with the existence or absence of an AD.

Methods:
In a prospective survey, we enrolled consecutively patients between July 10th to August 6th 2016 who visited a Swiss tertiary care ED one week from 8 am to 6 pm, two weeks from 2 pm to 11 pm and one week from 11 pm to 8 am. The patients completed a written, standardized and self-administrated questionnaire during the waiting time in the ED. The primary endpoint assessed the prevalence of ADs in ED patients. Secondary, we defined predictors associated with the existence or absence of an AD. Descriptive, univariate and multivariable logistic regression models were used.

Results:
Fifty-eight of 292 enrolled ED patients (19.9%) had a completed AD. About half of the survey population (49.3%) was female. Patients having an AD were older (69.5 vs. 39 yrs) and had more co-morbidities (67.2% vs. 38.9%) comparing to patients without ADs. The five leading reasons given for not having an AD were: 33.6% never thought about it, 26% did not know about AD, 14% preferred family to make the decision, and 11.6% too early to make such a decision. Predictors having an AD were older age ($p<0.001$), having a medical specialist ($p=0.050$), being Swiss ($p=0.021$) and with nursing care ($p=0.043$). Almost half of the ED patients (46.6%) who had ADs discussed their AD with the family and in 31% with the general practitioner. Only one patient took the AD along to the ED, whereas 19% would take it along when needing hospital admission.

Conclusion:
Comparing our data with the literature, during the last 20 to 30 years the percentage of patients having an AD did not change. Only every fifth ED patient has a completed AD. Nearly two-thirds of ED patients never thought or did not know about ADs.
Therefore, there is an urgent need to better inform and sensitize the public to timely define legally valid decisions about future medical treatments and wishes by completing ADs.

5313

K. Slankamenac[1], R. Heidelberger[1], D. Keller Lang[1]

Prediction of Repeated Emergency Department Visits in Patients with Mental Disorders

Institut für Notfallmedizin[1]

Introduction:
Patients with mental disorders are more likely to be frequent emergency department (ED) users than patients with medical diseases. There is little information about repeated ED visitors (≥ 4 ED visits/year for the same medical condition) with mental disorders in Switzerland. Therefore, our aim was to investigate the incidence of repeated ED visits due to mental disorders and to determine which mental disorders and risk factors were associated with repeated ED visits.

Methods:
In a retrospective analysis, we enrolled consecutively patients with mental disorders between January and December 2015 who presented more than once in the ED of a Swiss tertiary care hospital. ED patients presenting due to mental disorders were grouped in a repeated group with at least four ED visits or in a control group visiting the ED twice or three times within a year. The first endpoint was to assess the incidence of repeated ED patients due to mental disorders. As secondary endpoints, we investigated which mental disorders and risk factors were associated with repeated ED visits. Descriptive, univariate and multivariable logistic regression models were used.

Results:
Of 33,335 primary ED visits, 642 ED visits (1.9%) were performed by 177 visitors suffering from mental disorders. Forty-five (25.4%) of those 177 patients were repeated ED visitors; 132 (74.6%) frequently visited the ED twice or three times (control). Patients with personality and behavior disorders had a four times higher risk (95% CI 1.4 – 11.8, p=0.011) to be a repeated ED visitor compared to the control group. Repeated ED visitors with mental disorder had significantly higher number of in-house admissions (adjusted difference 1.6, 95% CI 1.1 – 2.0, p<0.001), suicide attempts (adjusted difference 0.4, 95% CI 0.1 – 0.8, p=0.004), accidents (adjusted difference 0.3, 95% CI 0.1 – 0.5, p=0.013) and were more often singles (adjusted OR 2.2, 95% CI 1.1 – 4.8, p=0.045). Although repeated ED visitors had more often an outpatient general physician or psychiatrist, they visited the ED more often within office hours (adjusted difference 1.5, 95% CI, 1.1 – 1.9, p<0.001) than the control group.

Conclusion:
A quarter of frequent ED users due to mental disorders are repeated ED visitors and were more likely to suffer from personality and behavior disorders. Repeated ED visits are associated with higher rate of suicide attempts and accidents as well as more in-house admissions that cause higher in-hospital costs and stress to the health care system. Therefore, a case management for repeated ED patients with mental disorders is needed to optimize the patient-centered care and to reduce the ED visit frequency.

5314

B. Weder[1], T. Van Haaften[2], K. Baebler[1], G. Rogler[1], G. Dijkstra[2], P. Imenez Silva[3], Y. Wang[3], C. De Vallière[1], C. Wagner[3], I. Frey-Wagner[1], K. Seuwen[4], P. Ruiz[1], M. Hausmann[1]

Intestinal acidification sensed by pH-sensing receptor GPR4 contributes to fibrogenesis

Department of Gastroenterology and Hepatology, University Hospital Zurich[1], Department of Gastroenterology and Hepatology, University Medical Center Groningen, University of Groningen, Netherlands[2], Institute of Physiology, University of Zurich[3], Novartis Institutes for Biomedical Research, Basel[4]

Introduction:
During active inflammation, intraluminal intestinal pH is decreased in patients with inflammatory bowel disease (IBD). Acidic pH may play a role in IBD pathophysiology. pH-sensing G-protein-coupled receptor (GPR) 4 is regulated by key inflammatory cytokines. Patients suffering from IBD express increased mucosal levels of GPR4 compared to non-IBD controls. pH-sensing may be relevant for progression of fibrosis, as extra-cellular acidification leads to fibroblast activation and extracellular matrix remodeling. We aimed to determine *GPR4* expression in fibrotic lesions in the intestine of Crohn's disease (CD) patients, and the effect of *Gpr4* deficiency in fibrogenesis.

Methods:
Human fibrotic and non-fibrotic terminal ileum was obtained from CD patients undergoing ileocecal resection due to stenosis. Gene expression of fibrosis markers and pH-sensing receptors was analyzed. The *in vivo* murine model of DSS-induced chronic colitis and the heterotopic transplantation model of intestinal fibrosis were used. Collagen layer thickness and hydroxyproline content were determined. Primary human fibroblast cultures were obtained from surgical specimens taken from healthy areas of the mucosa of a patient undergoing surgery for colorectal carcinoma. Fibroblasts were exposed to pH 6.4, 7.4 and 7.8 for 3h and 24h, respectively, and additionally stimulated with recombinant TGF.

Results:
Increased expression of fibrosis markers was accompanied by an increase of *GPR4* in fibrosis-affected human terminal ileum, compared to the non-fibrotic resection margin (3.07±1.03 vs. 0.80±0.12*, P*=0.035). Positive correlation between *GPR4* expression and pro-fibrotic cytokines (*TGF* and *CTGF*) or collagens was observed. *Gpr4*$^{-/-}$ mice from both the DSS-induced chronic colitis model and the heterotopic transplantation animal model for intestinal fibrosis showed a significant decrease in mRNA expression of fibrosis markers as well as a decrease in collagen layer thickness and hydroxyproline, compared to wildtype mice. *In vitro*, *GPR4* expression in both human and murine primary intestinal fibroblasts was increased at low pH (6.4) compared to normal pH (7.4). Furthermore, expression of pro-fibrotic *TGF* and collagen was increased at low pH. p-SMAD2 and P-SMAD3 were translocated into the nucleus upon exposure to low pH, pointing to the activation of the pro-fibrotic TGF signalling pathway.

Conclusion:
In patients suffering from CD, *GPR4* expression correlates with the expression of pro-fibrotic genes, and increased levels of collagen deposition. *Gpr4* deficiency is associated with a decrease in fibrosis formation in two models of fibrosis. Targeting GPR4 may be a new and promising potential therapeutic target for IBD-associated fibrosis

5315

S. Erdogan[1], C. Gonçalves-Moreira[1], S. Masneuf[1], C. Baumann[1], D. Noain[1]

Role of slow-wave sleep delta power on amyloid beta clearance and accumulation in a mouse model of Alzheimer's disease

Neurology Department, University Hospital Zürich, Zurich[1]

Introduction:
Despite being seemingly crucial both in health and disease, little is known about the effects of sleep on behavioral outcomes of AD in relation to reduced amyloid deposition. In this study, we explore effects of enhanced delta power during SWS on cognitive performance of a mouse model of AD by utilizing a clinically relevant sleep enhancer drug (Xyrem®). We hypothesize that Aβ accumulation will be reduced in the mouse model of AD by SWS delta power-dependent increased clearance from the brain and therefore, the Xyrem treated mice will perform better in cognitive tasks compare to the placebo treated mice.

Methods:
We use the well-established tg2576 mutant mice as model of AD and their wild type siblings as a control. We keep the animals in individually ventilated cages with constant temperature and humidity conditions. The room holds a 12 h dark-light cycle, and the mice have access to food and water *ad libitum*. We carry all experimental procedures according to local and federal Swiss regulations and with specific approval and supervision of the veterinary office of the Canton Zurich (License: ZH210/17).

We implant EEG/EMG headsets in adult Tg2576 mice (5.5 months of age for early- and 10.5 months of age for late- interventions) for periodic electrophysiological monitoring of vigilance states. After 14 days of recovery, we examined cognitive performance (episodic memory by novel object recognition test and spatial and working memory by T-maze test) of the mice to determine baseline. After the behavior tests, we administer animals with pharmacological SWS enhancer (Xyrem®, 300mg/kg, p.o.) and placebo twice daily for a period of two weeks. We record 24 hours sleep/wake activity of mice before (baseline) and during the treatment (first and the last day of treatments). We repeat the behavioral tests after the treatments end and use Congo red staining for the visual detection of amyloid plaques in the brains of both transgenic and wild type mice.

Results:
We will show preliminary results on t-maze behavior tests and sleep/wake activity in both early and late interventions before and after treatment.

Conclusion:
To make confident conclusion, we intend to have significantly increased the number of animals in our experimental groups by the time of poster presentation.

5316

M. Morawska[1], D. Noain[1], T. Scammell[2], C. Baumann[1]

Slow-wave enhancement reduces trauma-induced APP overexpression in novel mouse model of traumatic brain injury compatible with EEG/EMG headset.

Department of Neurology, University Hospital of Zurich, Zurich[1], Department of Neurology, Beth Israel Deaconess Medical Centre, Harvard Medical School, Boston[2]

Introduction:
Traumatic brain injury (TBI) is one of the leading causes of death and disability worldwide, with cognitive impairment being the most prevalent symptom. We recently showed that slow-wave modulation could be used as a potential therapeutic option for protein overexpression/accumulation in TBI. Here, we present further evidence supporting the role of slow-wave oscillations in the delta frequency band in decreasing protein burden following TBI in mice.

Methods:
We adapted a classical weight-drop diffuse mouse TBI model for use in animals preinstrumented with EEG/EMG headset by applying a 70° angle for a 115g impactor falling from 1m distance. We then characterized posttraumatic neurological function, cognition and assessed overexpression of amyloid precursor protein (APP) as a histological trauma indicator. We tested the effect of 3 doses of sodium oxybate (*per os*; 100, 200, and 400mg/kg) on NREM duration and EEG spectral power during NREM sleep. Finally, we tested the effect of 3 day, 2xday 400mg/kg sodium oxybate treatment regime on trauma-induced APP overexpression.

Results:
Our results show that sodium oxybate had dose-dependent effect on the NREM duration (dark phase: repeated measures ANOVA, $p<0.01$, light phase: repeated measures ANOVA, $p<0.05$, n=5/group) and increased EEG power in the delta band (Dunett's multiple comparisons (compared to vehicle): 100mg/kg: 1.5Hz $p<0.05$, 2-2.5Hz $p<0.001$; 200mg/kg: 0.5Hz-3Hz $p<0.001$; 400 mg/kg: 0.5-2.5Hz $p<0.001$, 3.5Hz $p<0.05$, 4Hz: $p<0.01$; n=4) in the first 2 hours post-injection. The TBI animals showed no neurological impairment (n=5/group), decreased power in ultra-slow component of delta frequency band (n=4/group, two-way ANOVA $F(1, 768)= 6.5$, $p<0.05$, Tukey posthoc: 0.25-1.5Hz &3.25-3.5Hz) and impaired object recognition 5 days after trauma (t-test, compared to chance level (0.5), SHAM: $p<0.05$, TBI: ns, n=8/group). What is more the TBI animals show APP overexpression in perikarya, dendrites and axons (two-way ANOVA, $p<0.01$, n=4/group), while twice daily administration of sodium oxybate during 3 days after trauma significantly reduced trauma-induced APP overexpression in the cortex (two-way ANOVA, $p<0.01$, n=4/group).

Conclusion:
In summary, our murine model shows high degree of construct, face and predictive validity, reflected by replicability of histological trauma marker and cognitive impairment, compared to other rodent models. Further experiments aimed at decreasing delta power following TBI are needed to fully establish the role of slow-wave oscillatory activity in posttraumatic recovery.

5317

L. Hering[1], E. Katkeviciute[1], M. Schwarzfischer[1], D. Mrdjen[2], J. Komuczki[2], L. Lang[1], B. Becher[2], G. Rogler[1], M. Scharl[1], MR. Spalinger[1]

Loss of PTPN2 in dendritic cells promotes increased T cell response and elevated expression of co-stimulatory molecules

Department of Gastroenterology and Hepatology, University Hospital Zurich[1], Institute of Experimental Immunology, University Hospital of Zurich[2]

Introduction:
Variants within the gene locus encoding protein tyrosine phosphatase non-receptor type 2 (PTPN2) are associated with the development of inflammatory disorders. The role of PTPN2 in T cells has been investigated in depth, but its role in dendritic cells (DCs) remains unclear. Here, we addressed whether loss of PTPN2 in DCs affects the expression of co-stimulatory molecules and subsequently activation of T cells.

Methods:
We generated mice lacking PTPN2 specifically in DCs (PTPN2-CD11cCre mice). Using multicolour flow cytometry, we analyzed different organs in PTPN2-CD11cCre mice and their wildtype controls.

Results:
PTPN2-CD11cCre mice exhibit splenomegaly, dermatitis, inflammatory infiltrations in the liver and even liver cell damage in some mice. Severity of the inflammation varies between individuals, resulting in spontaneous death in some mice but only mild inflammation in others. At the age of 5 weeks, PTPN2-CD11cCre mice show increased infiltration of neutrophils and monocytes in skin, liver, spleen and lung. Consistent with increased expression of the co-stimulatory molecules CD80 and CD86, we observed increased numbers of CD44+ effector/memory CD4+ and CD8+ T cells, indicating an enhanced T cell activation capacity of PTPN2-deficient DCs. Further, the ratio between CD11b+ cDC2 and CD24+ cDC1 is increased in skin of young mice. However, at the age of 22 weeks, we observed comparable levels of DC activation markers and reduced infiltration of CD44+ effector/memory T cells in the skin compared to wildtype controls, while in liver, lung and kidney, old PTPN2-CD11cCre do not differ in terms of CD44+ effector/memory T cells.

Conclusion:
In conclusion, our results show that PTPN2 is important to maintain anti-inflammatory functions of DCs. Loss of PTPN2 in DCs promotes expression of co-stimulatory molecules and subsequently aberrant T cell activation in young mice, leading to severe systemic inflammation later in life. In older mice, however, T cell activation is reduced and DC activation markers are downregulated, possibly due to compensatory mechanisms or exhaustion of inflammatory cells.

5318

O. Eichhoff[1], A. Irmisch[1], P. Turko[1], S. Pascoal[2], N. Zamboni[3], I. Piazza[3], P. Cheng[1], I. Banik[1], A. Saltari[1], M. Distel[2], P. Picotti[3], R. Dummer[1], M. Levesque[1]

Metabolic targeting as a strategy to overcome targeted therapy resistance

Department of Dermatology, University Hospital Zurich, Zurich[1], Children's Cancer Research Institute, Vienna[2], Institute of Molecular Systems Biology, ETH Zürich, Zurich[3]

Introduction:
MAPK inhibitors have shown outstanding clinical responses for melanoma patients with BRAF mutations. Unfortunately, this success could not be repeated for melanoma patient with NRAS mutations were treatment with MEK inhibitors (MEKi) showed only partial clinical responses thus leaving this patient cohort with limited treatment option. Cancer cell heterogeneity poses a major challenge in the treatment of metastatic melanoma. Targetable driver mutations are well characterized, but phenotype switching provides plasticity to melanoma cells to escape treatment. We have shown that melanoma cells in a melanocytic expression state (MelanA, Mitf positive) are sensitive to targeted therapies, invasive signature cells (e.g. high TGFbeta signalling, WNT5a and AXL) are treatment resistant. Therefore, new small molecule inhibitors targeting treatment resistant and NRAS mutated melanoma cells are urgently needed.

Methods:
We performed a high-throughput screening (HTS) composed of 960 small molecules on a cohort of NRAS-mutated primary human melanoma cell cultures including those derived from targeted therapy resistant tumors. One compound (STO) specifically targeted cell viability in melanoma cells resistant to MEK inhibition. We confirmed the compound's selectivity on a larger patient cohort which we also conducted transcriptome analysis by RNA sequencing and metabolomics via mass spectrometry. Metabolic changes were validated with Seahorse technology and FACS. We also evaluated the effects of STO in a 3D spheroid assay, an in vivo Zebrafish metastasis model as well as on patient-derived tumor slice cultures.

Results:
HTS revealed compound STO to be specific for MEKi resistant melanomas. Transcriptome analysis of a larger melanoma cohort showed that melanoma cell cultures do cluster in two distinct transcriptional phenotypes. One signature is composed of melanocytic gene expression, and genes known to be involved in invasiveness dictate the other one. MEKi resistant cell cultures do all cluster within the second signature where sensitivity to compound STO is associated. Metabolomics revealed that melanocytic melanomas upregulated several pathways e.g. glycolysis. We found significantly more lactate being produced by MEKi sensitive melanomas compared to MEKi resistant ones where intra-cellular reactive oxygen species (ROS) are significantly elevated. ROS levels increased upon STO treatment only in resistant cultures and STO-induced melanoma cell death was only detected in 3D spheroids derived from these resistant cultures. We confirmed in vivo efficacy of STO in an in vivo Zebrafish model were STO decreased metastasis formation only in the therapy-resistant melanomas. Patient-derived tumor slice cultures confirmed the in vivo effects of STO also on patient material.

Conclusion:
HTS led to the discovery of the small molecule compound STO, which reduces the viability of NRAS-mutated and MEKi resistant melanoma cell cultures by ROS induction. Consistent with the Warburg hypothesis in which tumors produce a large proportion of energy through glycolysis, melanocytic and treatment sensitive melanoma cells have elevated glucose metabolism. In contrast, MEKi resistant cells are high in cytosolic ROS levels, lacking the antioxidative benefits of glucose uptake. Our results revealed a tight link between transcriptional state, metabolic cell activity and drug sensitivity, which suggests metabolic targeting as a treatment strategy for patients with NRAS mutated and MEKi resistant tumors.

5319

B. Wenk[1], H. Mbunkah[1], N. Ndi[2], E. Mbu[2], L. Besong[3], B. Sama[4], E. Orock[5], M. Shilai[1], C. Leeman[1], K. Metzner[1]

Prevalence of Integrase Strand Transfer Inhibitors Resistance Mutations in Antiretroviral-Naïve HIV-1 Infected Patients in Cameroon.

Department of Medicine, Division of Infectious Diseases and Hospital Epidemiology, University Hospital Zurich, University of Zurich[1], Regional Hospital Bamenda, Cameroon[2], District Hospital Kumba, Cameroon[3], District Hospital Ndop, Cameroon[4], Regional Hospital Ngaoundere, Cameroon[5]

Introduction:
Antiretroviral therapy (ART) of the Protease Inhibitor, Nucleoside and Non-Nucleoside Reverse Transcriptase Inhibitor (NRTI/NNRTI) classes have been available in Cameroon for a while. Recently, the Integrase Strand Transfer Inhibitors (INSTIs) were introduced to be administered alongside two NRTIs. Since routine genotypic resistance tests are still uncommon in the country, there is very limited data on INSTI resistance patterns. We therefore determined the prevalence and types of INSTI resistance-associated mutations in newly diagnosed patients in three regions of the country, using next-generation sequencing.

Methods:
We designed universal primers targeting the HIV-1 integrase region of the *pol* gene and used them to modify our previously established protease and reverse transcriptase genotypic resistance assay. Our INSTI resistance assay is applicable to dried blood spot (DBS) samples and also universal - genotyping HIV-1 groups M, N, and O. DBS samples were collected from 339 newly diagnosed HIV-1 patients between 2015 and 2016 in four hospitals in areas with some of the highest HIV-1 prevalence rates in Cameroon. RNA extracted from DBS samples was used to amplify the integrase region from amino acid position 1 to 276, in a nested RT-PCR. The first 160 successful amplicons were sequenced with Illumina next-generation sequencing. Sequences were analyzed with the Polymorphism Analysis Sequencing (PASEQ) platform and the Stanford HIV Sequence Database was used to interpret resistance mutations.

Results:
All 160 patients had no viral load records but a median (range) CD4 T-cell count of 276 (4 - 892) cells/µl. The PCR amplification success rate of the assay is 77.6% so far. Unsuccessful samples had been previously shown to have low cDNA copy numbers. Subtype diversity among patients was high, with the commonest subtypes being: CRF02_AG (68.8%), A (10%), and CRF01_AE (7.5%). At nucleotide frequencies >15%, only one individual (0.6%) with major resistance-associated mutations to INSTIs was detected. However, expanding the analysis to low-abundance drug resistance mutations, 3/160 individuals (1.9%) were identified. The mutations Y143C, T66I and S147G were found in these persons at nucleotide frequencies of 9%, 1.5% and 1.5% respectively. These individuals were previously known to harbor no PI and/or NRTI/NNRTI mutations. The polymorphic accessory resistance mutations E157Q and T97A were found in 13.8% and 5.6% of patients respectively, but had very little or no effects on INSTI susceptibility, evidenced by the mutation scores.

Conclusion:
Pre-treatment HIV-1 drug resistance to INSTIs in Cameroon is very low in the study sites. The absence of drug resistance mutations to Dolutegravir (DTG) supports its use in Cameroon.

5320

T. Hamann[1], S. Hommayda[1], M. Töteberg-Harms[1]

Focus on refractive predictability and intraocular pressure - iStent Inject alone versus combined phaco

University Hospital Zurich, Clinic for Ophthalmology, University of Zurich[1]

Introduction:
Glaucoma is one of the leading causes of visual impairment and blindness. In this retrospective study we investigated the efficacy and safety of a newly available micro-invasive glaucoma surgery (MIGS) procedure - the iStent Inject - as a stand-alone procedure and combined with phacoemulsification and artificial lens implantation (phaco). The second aim was to evaluate predictability in refractive outcomes when combined with phaco.

Methods:
Cases after iStent Inject implantation alone (n=12) and combined phaco (n=15) were included. Intraocular pressure (IOP) and hypotensive, topical medication (AGD), was recorded at baseline and postoperatively. Change in IOP was computed. Furthermore, (1) refractive stability was calculated as change in target refraction between month 1 and 3 and (2) predictability as variation between planned target refraction and manifest refraction at 1 month in the combined group.

Results:
Three months after surgery the mean IOP in the iStent Inject group (n=12) decreased from 20.0 to 17.0 mmHg (-15% compared to baseline, $p<0.05$) and in the combined group (n=15) from 17.7 to 12.4 mmHg (-30% compared to baseline, $p<0.05$). AGD were reduced but not statistically significant. Refraction did not change significantly between month 1 and 3 (+0.25 change in refraction in both groups). Target refraction in the combined group was -0.33D, while manifest refraction was -0.25D at 1 month. No serious complications occurred in both groups. Data collection of a larger sample size and longer follow-up is ongoing.

Conclusion:
Predictability of target refraction was not negatively influenced when cataract surgery was combined with iStent Inject implantation. iStent Inject alone or combined with phaco lowered IOP. The iStent Inject is a promising MIGS procedure as stand-alone surgery and in conjunction with cataract surgery.

5321

E. Ramelyte[1], R. Dummer[1]

Intralesional oncolytic virotherapy in cutaneous lymphomas

Dermatologische Klinik, Universitätsspital Zürich, Zürich[1]

Introduction:
The therapy options for early and localized skin cancer lesions comprise of surgery, topical therapy with immune stimulating or antiproliferative agents, and radiotherapy. For melanoma, intralesional oncolytic virus, Talimogene laherparepvec (T-VEC), has been approved in 2015. However, in cases of non-melanoma skin cancers (NMSC), where above mentioned therapies cannot be implemented, the only other treatment options are systemic agents, which are associated with considerable toxicity. There is an unmet medical need for new therapies in patients with locally advanced tumours, which do not qualify for standard of care.
T-VEC is a genetically engineered herpes simplex virus, which selectively replicates in tumour tissue and carries the gene for human granulocyte macrophage colony-stimulating factor (GM-CSF). Injected directly in the tumour, it replicates in the malignant cells and leads to local and distant tumor response in melanoma, proposedly mediated by $CD8^+$ cytotoxic T cells.
As treatment with oncolytic virotherapy was successfully implemented in cancers other than melanoma, we initiated a trial with TVEC in NMSC and will concentrate on CTCL and CBCL.

Methods:
Patients with histologically confirmed cutaneous lymphoma, non-suitable for surgery or radiotherapy, without extracutaneous involvement were treated with intralesional T-VEC. The treatment was continued until patients received 8 injections, showed complete response or developed serious adverse events (AE). From the injected lesions, we took punch biopsies at baseline, 2 weeks after the 2nd injection and 2 weeks after the 5th injection, in case the lesions were still present. In addition to CD8 and HSV1 immunohistochemical staining, the samples were stained for CD4 in patients with CTCL and CD20 for patients with CBCL. To assess the tumor response, the size of injected and non-injected lesions was measured at each visit.

Results:
5 patients (3 with CTCL and 2 with CTCL) have received 3 or more intralesional T-VEC injections so far. 2 of them (both with CBCL) have finished the treatment plan. The median age was 61.8 years (54-70), 3 of the 5 patients were females. Before starting the intralesional T-VEC, 4 patients have been treated with systemic therapies. Four out of five patients have developed at least one adverse event, one of them developed a serious adverse event (not treatment related).
At baseline, CTCL patients showed a prominent infiltration with $CD4^+$ T-cells and less pronounced $CD8^+$ T cell infiltration. CBCL patients showed a prominent infiltration with $CD20^+$ B cells and less pronounced infiltration with $CD8^+$ T cells. In the follow up biopsies taken at 6 weeks after the first injection, a marked reduction of lymphocytic infiltration was seen. The proportion of $CD4^+$ and $CD20^+$ cells in CTCL and CBCL, respectively, was markedly reduced, whereas $CD8^+$ T cell infiltration was increased.

Conclusion:
Intralesional T-VEC is a well tolerated therapy, that leads to tumor response and increased infiltration with $CD8^+$cytotoxic T cells in both CTCL and CBCL lesions as early as after 2 injections. Furhter tissue analysis is needed to allow the characterisation of immune cells in the lymphoma infiltrates and for evaluation the mechanism of action of T-VEC.

5322

S. Dudli[1], D. Hänni[2], A. Jüngel[1], M. Betz[3], J. Spirig[3], F. Brunner[1], M. Farshad[3], O. Distler[1]

Dysregulated bone marrow stromal cells in vertebral bone marrow lesions

University Clinic of Rheumatology, University Hospital Zurich and Balgrist University Hospital, Zurich[1], Center for Microscopy and Image Analysis, University of Zurich, Zurich[2], Department of Orthopedic Surgery, Balgrist University Hospital, Zurich[3]

Introduction:
Modic type 1 changes (MC1) are fibrotic-inflammatory vertebral bone marrow lesions adjacent to degenerating discs and are specific for axial low back pain. In MC1, extra-cellular collagen is deposited, myelopoiesis is dysregulated, and bone is rapidly remodeled. These are signs of a chronic inflammation. The cellular mechanism is unknown, yet bone marrow stromal cells (BMSC) are key regulators of myelopoiesis, can differentiate into collagen-producing cells, and modulate inflammation. The objective of this study was to link BMSC phenotype and function to molecular changes in MC1.

Methods:
From patients undergoing lumbar spondylodesis, bone marrow aspirates (n=5 MC1+5 control, adjacent level healthy bone marrow (Ctrl)) or biopsies (n=2 MC1+2 Ctrl) were taken through pedicle screw trajectory before screw insertion.
Biopsies: fixed, dehydrated, imaged with multiphoton fluorescence microscopy (MPE). Second-harmonics-generation of collagen (SHG) and tissue auto-fluorescence were recorded of full-length biopsies (<200 µm penetration depth) and qualitatively evaluated. Spectrally selective fluorescence-life-time-imaging-microscopy (FLIM) of the auto-fluorescence signal was performed in key areas of biopsies and single-photon-counting histograms were fitted with a triple-exponential decay function.
Aspirates: BMSC were isolated by plastic adherence and characterized (passage 2): CD14/16/19/34/45/73/90/105/284 expression (FACS, t-test), proliferation rate (CellTrace™, t-test), differentiation capacity (histology, wilcoxon test), RNA sequencing (Illumina Novaseq).

Results:
Biopsies: Collagen was more abundant in MC1 than in Ctrl bone marrow, particularly in areas of adipocyte clusters and around adipocytes. FLIM revealed different auto-fluorescent life-times for adipocytes (τ=2.1-2.7ns), leukocytes (τ=0.4-0.8ns), erythrocytes (τ=0.2-0.4ns), and for SHG of collagen (τ<0.15ns).
Aspirates (MC1 vs Ctrl BMSC): no difference in expression of surface markers; reduced proliferation rate (29.3±1.7 vs. 26.2±1.0 hours, p=0.07); reduced adipogenic differentiation (67%, p=0.03), no change in osteogenic (144%, p=0.31 wilcoxon) and chondrogenic differentiation (69%, p=0.18 wilcox). Most overrepresented gene ontology categories in significantly dysregulated genes (p<0.01, n=154) were ‘cell adhesion’ (p<9.3e-13) and ‘extracellular matrix organization’ (1.8e-7). Aggrecan (fold change=0.25, p<1e-7) and osteopontin (fold change=5.26, p<1e-5) were the first and third top-most differentially regulated genes.

Conclusion:
MPE imaging of full-mount biopsies in combination with FLIM revealed unprecedented insight into MC1 pathomechanism. It allowed to distinguish and investigate the 3D-organization of bone marrow elements with minimal processing of the delicate biopsies. MPE is a prime technology to investigate fibrotic pathologies and allows to morphologically study the importance of BMSCs in MC1.
Together, these data suggest a dysregulation of bone marrow mesenchymal cells in MC1 (BMSC, adipocytes, osteoblasts) that helps explaining molecular changes in MC1. MC1 BMSCs proliferate slower and their differentiation capacity is shifted away from chondrogenesis/adipogenesis towards osteogenesis. The inflammatory milieu is known to disturb anabolic/catabolic balance of matrix-producing cells and to suppress chondrogenic differentiation. The BMSC/adipocyte axis seem to play a pivotal role in the fibrotic pathomechanism. Adipocytes have not been regarded as pathomechanistically relevant yet and hence open novel targets for therapeutics.

5323

E. Lang[1], O. Pfäffli[1], S. Koller[2], W. Berger[2], C. Gerth-Kahlert[1]

Novel homozygous mutation in the membrane frizzled related protein (MFRP) gene in a family with nanophthalmos

Department of Ophthalmology, University Hospital Zurich[1], Institute of Medical Molecular Genetics, University of Zurich, Schlieren[2]

Introduction:
Nanophthalmos is a rare usually binocular condition with shortened axial length resulting in high hyperopia ranging from +8.00 to +25.00 diopters. Nanophthalmos may be associated with additional pathological ocular findings or may be part of a syndrome including abnormalities of other organs. Inheritance follows an autosomal dominant or recessive pattern or appearance may be sporadic. Mutations in the MFRP gene on chromosome 11q23 account for recessively inherited nanophthalmos cases. The gene encodes a transmembrane protein mainly expressed in the retinal pigment epithelium and ciliary body. It is involved in a regulatory network of ocular growth during childhood and retinal maintenance in the adult.

Methods:
For assessment of the phenotype a comprehensive ophthalmologic examination was performed. Genetic analysis based on whole-exome-sequencing (WES) using next generation sequencing (NGS) platform was performed for both affected siblings. Sanger sequencing of the target genes in the clinically non-affected mother and sibling 3 enabled segregation analysis. The patients or guardians of the patients gave their consent.

Results:
Phenotype of affected sibling 1 (age 14): nanophthalmos was clinical diagnosed through the following measures: hyperopic spherical equivalent, axial length and anterior chamber depth in the right (OD)/ left (OS) eye, respectively: 15.25/ 15.0 diopter, 15.65/ 15.56mm, 3.09/ 3.11mm. Best-corrected visual acuity (BCVA) was of 0.6 (OD) and 0.4 (OS). Fundus examination revealed enhanced macular lutein deposits and macular folds. Optical spectral domain coherence tomography showed diminished foveal depression, enhancement of ellipsoid zone. Clinical findings of affected sibling 2 (age 30) were sinmilar. Both parents and sibling 3 had no history of hypermetropic refractive errors or other ophthalmological abnormalities.
Genotype: Genetic analysis revealed a homozygous missense mutation in Exon 5 (c.497C>T) in both affected siblings. The non-affected mother and sibling 3 were found heterozygous at position c.497 by Sanger sequencing analysis. The resulting amino-acid substitution of prolin166-to-leucin (P166L) of the MFRP was predicted as deleterious by the prediction algorithm SIFT.

Conclusion:
The clinical and genetic findings suggest the mutation at c.497 to be causative for the nanophthalmic phenotype in the two siblings. In what extent the amino acid substitution, situated in the extracellular cubilin domain 1 (CUB1), affects protein function, needs to be determined by functional assays. Previously reported mutations of the MFRP gene cause truncation of the protein or amino acid substitution at highly conserved sites, often correlating with complex forms of nanophthalmos.The phenotype found in the two affected siblings might indicate correlation to a mild mutation, referring to a residual function of the protein. However, more cases are necessary for a better understanding of the clinical phenotypes (and their clinical progression) associated with mutations in the MFRP gene.

5324

C. Moreira[1], M. Scandella[1], M. Ferster[2], C. Baumann[1], D. Noain[1]

Prolonged acoustic modulation of slow-wave sleep alters motor skill learning in rats

Animal Sleep Laboratory, Neurology Department, University Hospital Zurich[1], Mobile Health Systems Laboratory, D-HEST, ETH Zurich[2]

Introduction:
Slow oscillations (SOs), the hallmark of slow-save sleep (SWS), play a major role in sleep-dependent memory formation, including learned motor tasks. SOs consist of an upstate where neurons have an increased excitability, followed by a downstate where neurons are silenced. Previous studies in humans established that targeting auditory pulses to SOs' upstate constitutes a privileged time window for improvement in memory reactivation, whereas intervening SOs' downstate seems to disrupt slow oscillatory patterns and ultimately diminish recall performance. We hypothesize that upstate acoustic stimulation in healthy rats during single pellet reaching test (SPRT), a fine motor skill learning task, increases slow-wave activity, which translates into enhanced learning; whereas downstate stimulation offers the opposite effect.

Methods:
A new acoustic stimulation protocol was established in a closed-loop with electroencephalography/electromyography (EEG/EEMG) in rodents. Briefly, clicks of pink-noise (30 ms, 40 dB) are delivered within 8 ms in two conditions: to enhance - SOs' upstate at 60 ° phase - or to disrupt - SOs' downstate at 270 ° phase - oscillatory activity. No noise is presented in a third condition as control. For that, a real-time NREM detection feature (RMS [δ-band (0.1-2 Hz)⁄β-band (20-30 Hz)] ⊥ RMS [EMG (10-1000 Hz)]) runs alongside the 1-Hz EEG component as a derivative sinusoidal of the endogenous signal for phase targeting. To assess the progressive learning of a fine skill, we trained the animals during 12 consecutive days to the SPRT, in which the rats reach for, grasp, and eat food pellets in a stereotyped sequence. This task was performed during the first hour of the light period, or until the animal attempts 100 pellets, further moving to their own stimulation chamber until the following day.

Results:
Upstate closed-loop acoustic stimulation increases slow-wave activity to a median of 18% (IQR = 10% to 27%) whereas downstate stimulation decreases it to a median of -10% (IQR = -7% to -23%), both without altering total amount of sleep per 24h. Subjects undergoing upstate stimulation performed overall 7% more successfully and 30% faster than control animals, with a collective 1-fold improvement over the last 4 days of training. Symmetrically, downstate stimulated animals were 14% slower than control animals, accomplishing a residual success-rate improvement during the same 4 days of training. To assess long-term memory, we kept the animals under uninterrupted acoustic stimulation and without motor assessment during 4 days following the last training day. On the 5th day, slow-wave enhanced animals and mock animals scored near their last success rate (0% to 8% less successful), while slow-wave disrupted subjects performed moderately worse (27% less successful).

Conclusion:
Improving or disturbing slow oscillatory activity by prolonged and uninterrupted acoustic stimulation after daily training seems to influence motor skill learning and maintenance in the SPRT. Our results reveal an increase in successful attempts and overall speed in animals subjected to constant enhancement of slow-wave activity, without altering sleep amount. On the other hand, animals undergoing disruptive modulation of slow-wave sleep appear to have a worsened learning rate over all training days. More in-depth EEG analysis will reveal whether spindles, a sleep feature intrinsically related to procedural motor learning, play a role on the observed changes in performance, whereas histological examination might reveal altered brain processes, such as increased markers of plasticity or pruning of dendritic spines in the motor cortex, well characterized structural adaptations in the brain after repetitive motor learning.

5325

M. Gruenbach[1], E. Schlaepfer[1], B. Escher[2], M. Schlapschy[2], A. Skerra[2], G. Schreiber[3], R. Speck[1], S. Bredl[1]

Biological activity of different IFN-α subtypes – just an interplay between the dose and affinity?

Department of Infectious Diseases, University Hospital Zurich, University of Zurich[1], Chair of Biological Chemistry, Technical University of Munich, Munich, Germany[2], Department of Biomolecular Sciences, Weizmann Institute of Science, Rehovot, Israel[3]

Introduction:
While there is an ongoing debate about the biological activity of IFN-α subtypes, we found only quantitative differences in their ability to block HIV *ex vivo*. Currently, we study PASylated (PAS) IFN subtypes with distinct IFNAR affinity in humanized mice for their biological effects and ability to block HIV. Notably, PASylation increases their half-lives 10x.

Methods:
First, we compared the activity of the PAS IFNs to the wild-type IFNs by using RPE-ISRE reporter cells. We then evaluated the PAS IFN's anti-HIV activities in ex vivo HIV-infected human PBMCs. We are currently determining the optimal dose/schedule for the PAS IFN treatment in humanized mice.

Results:
We found that PAS IFNs induce luciferase expression to a lesser extent than their WT counterparts. Similarly, PAS IFNs were less effective against HIV than the WT IFNs. The high affinity PAS IFN-α14 and YNS blocked HIV replication more efficiently than IFN-α2. *In vivo* data showed a dose-dependent stimulation of ISGs and a shift of the naïve T cell population towards an effector phenotype with IFN-α2 being equally potent as IFN-α14.

Conclusion:
High affinity IFNs are more potent at an equimolar dose in our ex vivo cellular assays. PASylation appears to decrease IFNs' potency, which we believe may be due to steric hindrance of the long tail. Strikingly, PAS IFN-α2 and IFN–α14 resulted in similar upregulations of ISGs in humanized mice treated three times a week. This dose schedule, however, appears to be too frequent as the ISGs prior to the next dose are still increased, which might result in immune exhaustion.
We are currently working on refining the dosing schedule in vivo. We will then compare WT with PAS IFNs and explore their effects on HIV-infection in humanized mice.

5326

E. Kiessling[1], S. Froese[2], M. Baumgartner[2], C. Grimm[1]

Rescue of Vision in cblC Deficiency

Ophthalmology Department, University Hospital Zurich[1], Children's Research Center, University Children's Hospital of Zurich[2]

Introduction:
Methylmalonic aciduria with homocystinuria (cobalamin deficiency cblC type) is a rare disease, caused by mutations in the *MMACHC* gene. This disorder is accountable for a vast number of symptoms, including neurological, ophthalmological, cardiovascular and respiratory abnormalities. Especially patients with early-onset disease frequently show a number of ophthalmic manifestations such as macular degeneration, optic nerve pallor and vascular changes, which, if left untreated, progress to complete blindness. The MMACHC protein is responsible for the correct transport and processing of vitamin B_{12} (cobalamin, Cbl) within the cell. This step is required for the functional catabolism of branched-chain amino and odd-chain fatty acids, as well as the production of methionine and methyl group donors. Parenteral cobalamin supplementation has so far improved some of the systemic impairments in these patients, but the ocular phenotype remains progressive. We hypothesize that the eye phenotype might result from a local dysfunction of MMACHC in the retina or the retinal pigment epithelium (RPE) causing oxidative stress and thus a degeneration of the ocular cells. We aim at the characterization of the function and regulation of MMACHC in the retina and the establishment of a local treatment to alleviate the ocular symptoms.

Methods:
Mmachc$^{flox/flox}$ mice were generated at PolyGene©, Switzerland. Pax6-Cre mice have been described by Marquart *et al*. (Marquart, T. *et al*., *Pax6 Is Required for the Multipotent State of Retinal Progenitor Cells.* Cell, 2001. **105**: 43–55). Hypoxic exposure of mice took place at 7% O_2 for 6 hours. Light microscopy was used to investigate retinal morphology. Retinal function was measured by scotopic and photopic electroretinography (ERG). Semi-qualitative real-time PCR was used to determine gene expression in the retina and eyecups (representing primary the RPE) of mice and human donor eyes. To knock down HIF1A and/or HIF2A, the human RPE cell line ARPE19 was transfected using siRNAs. To investigate hypoxic regulation ARPE19 cells were exposed to 0.2% O_2.

Results:
Expression of MMACHC in healthy human retinas and eyecups was not significantly impaired during ageing (17 – 96 years). Similarly, in wild-type mouse eyes *Mmachc* gene expression in the retina and RPE reached steady-state levels after completion of post-natal retinal development.
Since Pax6-Cre mice express Cre in most retinal cells of the peripheral but not central retina (Marquart *et al*., 2001) the generation of *Mmachc$^{flox/flox}$;Pax6-Cre* mice resulted in an incomplete knockout of *Mmachc* in the retina. Nevertheless, expression of *Mmachc* in retina$^{\Delta Mmachc}$ mice was reduced by 70%. Despite the lack of *Mmachc* in most cells of the retinal periphery, retinal morphology and function was normal up to 8 months of age.
Hypoxic exposure down-regulated *Mmachc* expression in the mouse retina by 40%, a result corroborated by *MMACHC* expression analysis in hypoxic ARPE19 cells. *MMACHC* reduction was HIF-dependent since siRNA mediated knockdown of HIF1A and/or HIF2A resulted in increased *MMACHC* mRNA expression levels under hypoxia. Host Cell Factor C1 (*HCFC1*) - one of the enhancing transcription factors of *MMACHC* - was upregulated 120-fold by hypoxia. This upregulation was HIF-independent since knockdown of HIF1A and/or HIF2A did not affect the upregulation of *HCFC1* mRNA.

Conclusion:
Preliminary data indicate that *Mmachc* expression is repressed by HIF transcription factors in a hypoxic environment, suggesting a connection between *Mmachc* gene regulation and oxidative stress. Furthermore, we aim at discovering the function of *Mmachc* in the mouse retina in order to rescue the eye phenotype observed in humans by a gene-therapy approach.

5327

E. Katkeviciute[1], L. Hering[1], M. Scharl[1], M. Spalinger[1]

Loss of PTPN2 in dendritic or T cells results in reduced tumor burden in the AOM/DSS colon tumour mouse model

Gastroenterology and Hepatology, University Hospital Zurich[1]

Introduction:
Protein tyrosine phoshatase non-receptor type 2 (PTPN2) has been identified as a potential cancer immunotherapy target. However, the mechanism of how PTPN2 is involved in colorectal carcinoma (CRC) pathogenesis has not yet been determined. Our recent data demonstrate that loss of PTPN2 in myeloid cells results in reduced tumour burden in the azoxymethane (AOM)-dextran sodium sulphate (DSS) induced model of CRC. Here, we show that specific loss of PTPN2 in dendritic cells (DC) or T-cells results in reduced tumour load in the AOM/DSS model.

Methods:
We generated two mouse lines lacking PTPN2 in either DC (PTPN2fl/fl-CD11cCre) or T- cells (PTPN2fl/fl-CD4Cre). Colon tumours were induced using AOM/DSS protocol and immune cells from spleen, mesenteric lymph nodes (mLN) and lamina propria (LPL) were analysed using flow cytometry.

Results:
Tumour burden was significantly reduced in PTPN2fl/f-CD4Cre and PTPN2fl/f-CD11cCre mice compared to their WT littermate controls. PTPN2-deficient mice exhibited significantly increased levels of CD44+ CD4+ and CD8+ T-cells in spleen, mLN and LPL, indicating enhanced T-cell activation. Additionally, we observed higher expression levels of interferon gamma in all analysed organs and increased abundance of granzyme B in the LPL from AOM/DSS treated PTPN2fl/fl-CD4Cre mice compared to their littermate controls, suggesting increased cytotoxic activity of PTPN2-deficient CD8+ T-cells. Finally, PTPN2-deficient mice presented increased levels of the exhaustion markers PD-1 on T-cells and PD-L1 on antigen presenting cells, supporting the anti-tumour response.

Conclusion:
This demonstrates an *in vivo* role of PTPN2 in the pathogenesis of CRC. Loss of PTPN2 in DC or T-cells exerts anti-tumour effects and results in lower tumour burden in the AOM/DSS model of CRC. This effect is likely mediated via promoting immune responses by modulating T-cell activation, cytotoxicity and immune checkpoint protein expression.

5328

Y. Liu[1], S. Sorce[1], J. Domange[1], A. Aguzzi[1]

Prion-induced dopaminergic axon degeneration is independent of cell-autonomous prion protein levels

Institute of Neuropathology, University of Zurich[1]

Introduction:
Cellular prion protein (PrP^C) is believed to be essential for the initiation of the degenerative signaling in neurons affected by prions. However, many neurons do not degenerate after prion infection although they express similar levels of PrP^C compared with the degenerated ones and prion deposition is clearly present in the brain regions harboring them. In another scenario, mice expressing PrP^C exclusively in astrocytes developed prion disease after prion infection. These observations raise the question that whether neuronal death induced by prions is truly determined by the cell-autonomous PrP^C expression levels. Here we test this rigorously by selective deletion or overexpression of PrP^C in dopaminergic (DA) neurons.

Methods:
Prion infection was performed on mice with DA neuron selective PrP^C deletion or overexpression. The survival, behavioral decline and degeneration of DA system were examined after prion infection.

Results:
We found that there was extensive degeneration of DA axons in the striatum but not the DA somata in the ventral midbrain after prion infection, suggesting a retrograde neurodegenerative mechanism playing in prion diseases. Surprisingly, we found that neither loss nor overexpression of PrP^C in DA neurons affected the survival, behavioral decline or DA axon degeneration of the prion-infected mice.

Conclusion:
Our results suggest that DA axon degeneration in prion diseases is independent of PrP^C expression levels in DA neurons, challenging the dogma that cell-autonomously expressed PrP^C is essential for the initiation of the death signaling in all the neurons that are affected in prion diseases.

5329

A. Bentrup[1], M. Avar[1], D. Heinzer[1], S. Hornemann[1], A. Aguzzi[1]

Tri-part Luciferase-based Homogeneous Immunoassay for Sensitive Detection of the Prion Protein

Institute of Neuropathology, University Hospital Zürich[1]

Introduction:
Quantitative assessment of protein levels in a sample is a ubiquitous requirement in biology. The reliable detection of proteins of very low abundance is still a challenge, as the commonly used methods are not sensitive enough. A second limitation in ultra-sensitive protein quantification is the number of working steps needed for existing assays, as this makes them not only time-intensive, but also error-prone.

Methods:
Here, a 384 well homogenous phase immunoassay is established to sensitively detect and quantify the murine cellular prion protein ($mPrP^C$) in biological samples such as protein extracts from cells or brain homogenate. The assay is based on the complementation of the NanoLuc luciferase enzyme from three constituents. Due to the coupling of two 11-residue NanoLuc fragments to the PrP-specific antibodies POM1 and POM19, the functional NanoLuc can only form and convert its substrate in presence of PrP. Luminescence intensity is therefore indicative of PrP levels.

Results:
The workflow for ultra-sensitive protein-detection was reduced to three steps in this assay: mixing the assay components, adding them to the sample, and reading the chemiluminescent signal after four hours of incubation at room temperature. The assay was capable of detecting recombinant PrP^C as little as 13.7 pg, which is comparable to the sensitivity of a sandwich ELISA and superior to FRET when using the same antibody pair. When challenged with complex matrices such as brain homogenate and cell lysate, the lower sensitivity limit was 1.5 ng of PrP^C-containing protein in brain homogenate, and 123 ng of PrP^C-containing protein cell lysate, making this assay up to two logs more sensitive than the aforementioned methods. Moreover, the need for sequential immobilization, blocking and washing before reading the assay as well as performance of complex calculations afterwards are eliminated.

Conclusion:
The developed method is not only a sensitive, but also an easy and fast alternative to the established methods FRET and ELISA for detection of minute amounts of PrP^C in biological samples, using almost exclusively reagents that can be straightforwardly produced in-house.

5330

A. Senatore[1], G. Horny[2], R. Reimann[1], S. Sorce[1], J. Guo[1], S. Fels[2], N. George[2], T. Pietzonka[2], S. Hornemann[1], A. Aguzzi[1]

Novel anti-PrP human antibodies for therapy of prion diseases

Institute of Neuropathology, University Hospital Zürich[1], Novartis Institutes for BioMedical Research, Novartis Pharma, Basel[2]

Introduction:
Prion diseases are fatal neurodegenerative disorders of sporadic, genetic or infectious origin. They are caused by the conformational conversion of the cellular prion protein (PrP^{C}) into the misfolded scrapie form (PrP^{Sc}), which is neurotoxic and able to self-replicate. PrP^{C} is a cell membrane protein, highly abundant in the nervous system, consisting of a C-terminal structured globular domain (GD) and a N-terminal flexible tail (FT) including the octapeptide repeat region (OR). PrP^{C} function in the central nervous system is dispensable while its presence on the neurons is essential for prion pathogenesis. Thus, targeting PrP^{C} represents a rational approach for treatment. Whether antibody-based therapy for prion diseases is a valuable strategy has been highly debated. Since the biological effect of anti-PrP antibodies depends on the targeted PrP epitope, we executed a high-throughput screen for antibody generation by phage display to identify PrP epitopes that can be pursued for immunotherapy.

Methods:
We selected a synthetic human Fab (hFab) phage library against PrP and we identified a panel of anti-PrP hFabs with definite binding profile

Results:
A panel of 49 hFabs were characterized biochemically and tested for their ability to prevent neuronal loss *ex vivo* in prion infected cerebellar organotypic cultured slices (COCS). Different OR binders blocked prion induced neurodegeneration in COCS. We now plan to use murine models of prion infection to test if OR binding Fabs prolong survival of inoculated mice and rescues prion-induced neuropathological changes.

Conclusion:
As genetic prion diseases exist that are caused by insertion mutations in the OR of PrP (OPRI-mutations), we will assess also if the OR binder Fabs revert the OPRI-associated pathology in vitro and *in vivo*, using newly generated transgenic mouse models of OPRI-linked prion diseases.

5331

A. Senatore[1], K. Frontzek[1], M. Bardelli[2], R. Reimann[1], S. Hornemann[2], L. Simonelli[2], L. Varani[2], A. Aguzzi[1]

Rational design of neuroprotective antibodies against the prion protein by phage display

Institute of Neuropathology, University Hospital Zürich[1], Institute for Research in Biomedicine, Bellinzona[2]

Introduction:
Immunotherapies against neurodegenerative diseases represent a valuable therapeutic strategy, yet antibodies targeting certain epitopes of the prion protein PrP^C exert neurotoxicity closely mimicking prion infection. Analysis of binding of toxic antibody POM1 to PrP^C by molecular dynamics simulations showed a decreased rigidity of the β2α2 loop of PrP^C and the formation an R208-H140 hydrogen bond within PrP^C that is not found in the unbound protein. We hypothesized that the R208-H140 interaction might play a role in $POM1^{WT}$-induced toxicity. If both POM1 and prions switche PrP^C into similar toxic conformers, antibodies that selectively target PrP^C but not its conformers could prevent prion neurotoxicity.

Methods:
To test this hypothesis, we engineered a double mutation (R208C/I139C) that mimics the formation of the R208-H140 hydrogen bond while rigidifying the POM1 epitope through a disulfide bridge. We then used phage display technology to generate antibodies (Fab fragments) that bind PrP^C preferentially over $PrP^C_{R207C\text{-}I138C}$ mutant mimicking the POM1-induced toxic conformation. For the in vitro antibody selection, we designed two strategies setting selective pressure for PrP^C over $PrP^C_{R207C\text{-}I138C}$ mutant. In the subtractive panning strategy, the Fab phage library was first exposed to $PrP^C_{R207C\text{-}I138C}$ mutant coated plates and then the unbound fraction was used for selection of PrP^C binders. In the panning strategy using depletion by competition, we used avi-tag biotinylated PrP^C in the presence of 3-fold molar excess of $PrP^C_{R207C\text{-}I138C}$ mutant in solution followed by capturing of the PrP^C binders on streptavidin-coated surface.

Results:
By ELISA screening of the panning output pools, we identified a panel of Fabs that bound bound PrP^C preferentially over $PrP_{R207C/I138C.}$ We then tested whether these anti-PrP^C Fabs were able to prevent neurodegeneration in prion infected COCS. None of the tested Fabs were intrinsically toxic. Fab 10 and FabD9, which preferentially bound PrP^C prevented prion neurotoxicity whereas FabE2 binding PrPC and $PrP_{R207C/I138C}$ with similar affinity, had no beneficial effect.

Conclusion:
These findings point to specific rearrangements within PrPC as the cause of prion toxicity. The structural clarification of anti-PrP^C neuroprotection enables the rational design of efficacious antiprion drugs.

5332

M. Avar[1], D. Heinzer[1], A. Lakkaraju[1], A. Chincisan[1], E. Schaper[1], M. Emmenegger[1], S. Hornemann[1], A. Aguzzi[1]

A whole genome siRNA screen for identification of modulators of prions

Institute of Neuropathology, University Hospital Zürich[1]

Introduction:
Misfolding of the cellular prion protein (PrP^{C}) results in the well-characterized scrapie isoform (PrP^{Sc}) which is hypothesized to be the underlying cause of prion diseases. However, events leading up to the formation of PrP^{Sc} or downstream events, resulting in neurodegeneration, astrogliosis and spongiform change, are poorly understood. An arrayed whole genome RNAi screen will enable us to identify genetic players in clearance of prions and modulators of PrP^{Sc} formation. This approach bears the potential to shed light on possible pathways that may offer opportunities in prevention of prion diseases.

Methods:
In the context of this project, we aim to do a cell-based high throughput screen to determine PrP levels upon silencing each gene. In a 384-well plate format, chronically infected mouse hypothalamic neuronal cell line, scGT1-7, will be subjected to a pooled set of three siRNAs targeting the same gene, incubated for 72h and treated with phosphoinositide phospholipase C (PI-PLC) to remove surface PrP^{C}. Following treatment, a FRET based readout using two antibodies, targeting different epitopes of PrP^{C} will be used. Genes that effect levels of intracellular and/or extracellular PrP^{Sc}, as well as intracellular PrP^{C}, will yield a stronger or a weaker FRET signal depending on direction of regulation. With this current setup we were able to achieve a Z`factor of > 0.5, which suggests the screen to be highly robust.

Results:
In the context of this project, we aim to do a cell-based high throughput screen to determine PrP levels upon silencing each gene. In a 384-well plate format, chronically infected mouse hypothalamic neuronal cell line, scGT1-7, will be subjected to a pooled set of three siRNAs targeting the same gene, incubated for 72h and treated with phosphoinositide phospholipase C (PI-PLC) to remove surface PrP^{C}. Following treatment, a FRET based readout using two antibodies, targeting different epitopes of PrP^{C} will be used. Genes that effect levels of intracellular and/or extracellular PrP^{Sc}, as well as intracellular PrP^{C}, will yield a stronger or a weaker FRET signal depending on direction of regulation. With this current setup we were able to achieve a Z`factor of > 0.5, which suggests the screen to be highly robust.

Conclusion:
Through downregulation of every single gene in the genome, we propose to identify genes that modulate prion replication and clearance. Furthermore, we seek to pinpoint novel interactors of prions, which may be liable for transmission of neurotoxic signals. The identification of such interactors carries the potential to identify therapeutic targets in prion disease and possibly other neurodegenerative diseases.

5333

A. Lakkaraju[1], R. Marpakwar[1], E. Lemes[1], U. Herrmann[1], A. Ballabio[2], A. Aguzzi[1]

Identifying the determinants of spongiform phenotype in prion infections

Neuropathology, University Hospital of Zurich, Zurich[1], Telethon Institute of Genetics and Medicine (TIGEM), Via Campi Flegrei 34, 80078 Pozzuoli, Naples, Italy[2]

Introduction:
Prion diseases are protein misfolding and aggregating disorders (PMA) implicated in Creutzfeldt-Jakob disease (CJD) and several transmissible spongiform encephalopathies of humans and animals. It is characterized by the accumulation and deposition of an abnormal conformer (PrP^{Sc}) of the endogenous prion protein (PrP^{C}). In addition to generic neuropathological changes (astrogliosis, neuronal loss, deposition of amyloid plaques), prion-infected brains feature a characteristic "spongiosis" which is caused by the accumulation of intraneuronal/intraneuritic vacuoles containing membrane fragments and, sometimes, degenerating organelles which are of uncertain biogenesis and content. Previous studies have documented the accumulation of PrP^{Sc} in multivesicular bodies after prion infection, suggesting impairment of the endo/lysosomal machinery. Depletion of PIKfyve and/or FIG4, which are involved in synthesis of phospholipid PI(3,5)P2 a key cog of endo/lysosomal machinery, induces vacuolation similar to spongiosis. We therefore decided to investigate whether the breakdown of the endolysosomal fusion machinery is the cause of spongiosis in prion infections.

Methods:
To address the mechanistic details of spongiosis, we use animal models (mice), organotypic slice cultures and cell lines. Techniques such as immunohiostochemistry, electron microscopy and *in vitro* biochemical assays were utilized in all these model systems, to identify determinants of vacuolation. Rescue experiments have been performed by treating the cell lines and mouse organotypic cultured slices with a water -soluble version of PI(3,5)P2. Mice models were used to assess time course of events preceding the generation of vacuoles and the downstream effects of vacuolation.

Results:
We monitored the protein levels of PIKfyve and FIG4 in the brains of prion-infected *tga20* mice (overexpressing PrP^{C}) infected with the Rocky Mountain Laboratory strain 6 (RML6) of prions. PIKfyve was significantly downregulated at 90 days post-infection and profoundly depleted in terminally sick mice. The mRNA levels of PIKfyve was unaltered, suggesting that posttranslational events led to destabilization. ER stress plays an important role in the toxicity in prion infections and time course analyses in prion-infected mice revealed PIKfyve depletion post ER stress induction. Interestingly PIKfyve was deacylated in prion infection, which further led to its ubiquitination and degradation. Loss of PIKfyve was associated with upregulation of lysosomal genes in a Transcription factor EB dependent manner, mimicking a lysosomal storage disease. Treatment with GSK2606414, which alleviates the ER stress induced by PERK pathway, restored acylation and steady state PIKfyve levels. Restoration of PI(3,5)P2 levels in cell culture models and cultured organotypic slices by treating them with a water soluble analog of PI(3,5)P2 rescued vacuolation and lysosomal defects.

Conclusion:
Our data suggests that spongiform change in prion infections may directly result from the suppression of the PIKfyve kinase, resulting in the impairment of endolysosomal machinery and formation of progressively larger vacuoles. In our study, activation of chronic ER stress preceded the depletion of PIKfyve, We observed that ER stress induces deacylation of PIKfyve thereby destabilizing it and promoting its degradation. Furthermore vacuolation and lysosomal defects could be rescued in our *in vitro* and *ex vivo* model systems using water soluble analog of PI(3,5)P2.

5334

D. Heinzer[1], M. Avar[1], D. Pease[1], J. Ying[1], A. Chincisan[1], E. Schaper[1], M. Emmenegger[1], S. Hornemann[1], A. Aguzzi[1]

Whole genome RNAi screen identifies novel regulators of PrPC as potential therapeutic targets in prion diseases

Institute of Neuropathology, University Hospital Zurich[1]

Introduction:
Although the physiological role of the cellular prion protein (PrP^C) remains controversial, its involvement in prion diseases is indisputable. During the progression of prion diseases, PrP^C serves as an essential substrate for its misfolded isoform PrP^{Sc} to maintain propagation. Additionally, PrPC itself is shown to be indispensable in mediation of neurotoxic signaling. Therefore, reduction of PrP^C alone can provide a viable therapeutic approach to combat prion diseases. This has also been convincingly demonstrated in $Prnp^{-/+}$ mice, which show a significant delay in the manifestation and progression of prion disease when compared to wild type mice. Hence, uncovering regulators of PrP^C could provide novel therapeutic targets against these invariably fatal disorders.

Methods:
We established a cell-based high-throughput platform to determine PrP^C levels after downregulation of each individual gene of the human genome. In a 384-well plate format, U-251 MG cells are be treated with siRNAs, incubated for 72h and a FRET-based readout is be performed using two antibodies coupled to a FRET-pair and targeting different epitopes of PrP^C. This method represents a one-pot reaction with no further sample preparation or washing steps to detect genes, which upon downregulation, lead to enhanced or decreased PrP^C expression. Candidates, which significantly regulate expression levels, have been further challenged by means of a secondary screen to determine high-confidence hits.

Results:
In a primary screen using a set of three pooled siRNAs targeting the same transcript, we could identify 583 genes that efficiently regulate PrP^C levels. An overall z'-factor of 0.55 over 166 plates demonstrated the robustness of the approach. The 583 genes from the primary screen were further challenged in a secondary screen with the individual siRNAs uncovering 45 high-confidence hits, which upon downregulation with at least 2 out of 3 distinct siRNAs regulated PrP^C levels.

Conclusion:
The high-confidence hits will be further validated using orthogonal methods such as CRISPRa, CRISPRi and CRISPR knockout and the mechanistic of PrP^C regulation will be investigated. Additionally, out of 45 hits in the human screen, we could identify 38 mouse homologs, which will be assessed in their capability to reduce PrP^{Sc} by means of a cell-based scrapie assay. Thereby, we aim to exploit these novel regulators of PrP^C as possible targets for therapeutic intervention in prion disease.

5335

A. Henzi[1], A. Senatore[1], A. Lakkaraju[1], A. Aguzzi[1]

A Novel Tool for the Treatment of Peripheral Demyelinating Neuropathies

Neuropathology, University Hospital of Zurich, Zurich[1]

Introduction:
Peripheral demyelinating diseases like Guillain-Barré Syndrome (GBS) or chronic inflammatory demyelinating polyneuropathy (CIDP) are diseases of the peripheral nervous system, in which the myelin sheath is the main site of damage. The treatment options for these diseases are currently unsatisfying, with a substantial number of patients showing no good recovery or remaining severely disabled. The adhesion-G-protein coupled receptor Gpr126 is essential for initiation and maintenance of the myelin sheath. A peptide derived from the N terminal flexible tail region (FT-peptide) of the normal cellular prion protein (PrP^C) was previously described as an activating ligand of Gpr126, increasing the expression of myelination related genes in Schwann cells in vitro and in vivo. A common strategy to prolong the half-life of peptides in the circulation is the fusion to crystallisable fragment (Fc-γ) of antibodies. We aim to exploit the pro-myelinating properties of PrP^C by coupling the flexible tail of PrP^C to an Fc-γ antibody fragment, resulting in the FT_2Fc-fusion protein. This fusion protein might be applied to treat demyelinating diseases of the peripheral nervous system. Here, we show that FT_2Fc retains the properties of the FT-peptide and activates Schwann cells in a Gpr126 specific manner.

Methods:
Wild type SW10 cells ($SW10^{WT}$) and SW10 cells devoid of Gpr126 ($SW10^{\Delta Gpr126}$) were treated with purified FT_2Fc or, as a positive control, FT-peptide. For negative controls, cells were treated with diluent. Unless otherwise noted, cells were lysed after 20min. The lysate was used to perform a direct cAMP ELISA assay (Enzo) or for western blotting. For western blotting, primary antibodies were used at a dilution of 1:1000 (pAKT, AKT) or 1:10’000 (Actin).

Results:
When treated with FT_2Fc, $SW10^{WT}$ but no $SW10^{\Delta Gpr126}$ react with increased cAMP levels. The increase is concentration dependent and similar to the increase elicited by FT-peptide treatment. Also, FT_2Fc leads to a Gpr126 dependent increase in AKT phosphorylation in a time course experiment.

Conclusion:
The promyelinating property of PrP^C might be exploited to treat demyelinating diseases of the peripheral nervous system. We have developed a FT_2Fc-fusion protein which activating Gpr126 similarly to the FT-peptide. We aim to apply FT_2Fc in vivo by treating mice with the purified protein. Our goal is to understand whether this protein can rescue the PrP^C-ablation related peripheral demyelination, and to test whether it can support the maintenance of the myelin sheath in demyelinating diseases like CIDP, GBS or Charcot Marie Tooth disease.

5336

L. Dubs[1], F. Janker[1], C. Opelz[1], Y. Yamada[1], W. Weder[1], J. Jang[1], W. Jungraithmayr[1]

CD26/DPP4 is overexpressed in experimental chronic lung allograft rejection and potentially qualifies as a target to reduce chronic rejection

University Hospital Zurich, Department of Thoracic Surgery[1]

Introduction:
Chronic lung allograft dysfunction (CLAD) is the major obstacle for long term survival in lung transplant recipients. The transmembrane molecule CD26/dipeptidyl peptidase 4 (CD26) is known to be a surface marker of fibrogenic stroma formation. We observed that CD26 is co-expressed with TGF-β1 within the fibrotic stroma compartment of lung tumors. We therefore hypothesize here if CD26 is expressed in a CLAD mouse lung transplant model which would render CD26-inhibition as a therapy against fibrosis.

Methods:
We previously developed CLAD lesions in mouse lungs eight weeks after lung transplantation using BALB/c (donors) and C57BL/6 (recipients) under mild immunosuppression. Pro-fibrotic genes including IGF1, MMP9, CXCL9, IL6, and IL13 were analyzed by RT-qPCR. Protein levels of EMT-related genes including Vimentin, N-cadherin, E-cadherin, Slug, and Hif1α were measured by western blotting, and immunohistochemistry (IHC) was employed to assess CD26 in transplants.

Results:
The development of CLAD lesions in mouse lungs was confirmed by a significantly higher expression of the EMT proteins Vimentin, N-cadherin, Slug, and Hif1α vs. normal lungs ($p<0.05$). Also, gene expression levels of IGF1, MMP9, and CXCL9 where significantly higher expressed in CLAD-developing lungs vs. normal lungs ($p<0.05$). In these CLAD lesions, the transmembrane molecule CD26 was significantly higher expressed in IHC vs. normal lungs ($p=0.0003$). In contrast, gene expression levels of IL6 and IL13 were significantly decreased vs. normal lungs ($p<0.0001$).

Conclusion:
The increased expression of CD26 in chronically rejected lung allografts suggests that CD26 is a potential target to attenuate the development of CLAD lesions after transplantation.

5337

A. Pregernig[1], M. Müller[1], U. Held[2], B. Beck-Schimmer[1]

Prediction of mortality in adult patients with sepsis, using six novel biomarkers: a systematic review and meta-analysis.

Institute of Anesthesiology, University Hospital Zurich[1], Epidemiology, Biostatistics and Prevention Institute, Department of Biostatistics, University of Zurich[2]

Introduction:
Sepsis requires rapid recognition and urgent treatment. But at the same time, the use of biomarkers to help identify patients with a high risk of mortality is appealing. The aim of our systematic review and meta-analysis was to assess the prognostic value of angiopoietin-1 (Ang-1) and 2 (Ang-2), high mobility group box 1 (HMGB1), soluble receptor for advanced glycation endproducts (sRAGE), soluble triggering receptor expressed on myeloid cells 1 (sTREM1), and soluble urokinase-type plasminogen activator receptor (suPAR) for all-cause mortality in adult patients with sepsis.

Methods:
The systematic review focused exclusively on observational studies of adult patients with sepsis, any randomized trials were excluded. For the meta-analysis, only studies which provide biomarker concentrations within 24h of admission in sepsis survivors and non-survivors were included. For pooling of the results, reported means with standard deviations (SD) were used for calculations. Results are presented as forest plots of pooled mean differences (MD) between non-survivors and survivors with 95% confidence interval for each of the six biomarkers. Studies not included in the quantitative analysis are narratively summarized.

Results:
The qualitative analysis was performed with 44 studies of which 28 were part of the meta-analysis. The pooled mean differences in biomarker concentration (non-survivors – survivors), measured at onset of sepsis, are listed as follows:

1. Ang-1: −2.9 ng/ml (95%CI: −4.1 to −1.7, p<0.01)
2. Ang-2: 4.9 ng/ml (95%CI: 2.6 to 7.1, p<0.01)
3. HMGB1: 1.2 ng/ml (95%CI: 0.0 to 2.4, p=0.05)
4. sRAGE: 1002.8 pg/ml (95%CI: 628.2 to 1377.3, p<0.01)
5. sTREM-1: 86.8 pg/ml (95%CI: 2.4 to 171.1, p=0.04)
6. suPAR: 5.2 ng/ml (95%CI: 4.5 to 6.0, p<0.01)

ROC analyses for the prediction of mortality according to baseline (≤24h of admission) biomarker concentration further support the utility of Ang-1, Ang-2, and suPAR, with AUCs of 0.620 to 0.778, 0.632 to 0.960, and 0.670 to 0.788, respectively. The other biomarkers had lower AUCs: 0.570 to 0.610 for HMGB1, and 0.444 to 0.827 for sTREM-1. For sRAGE, we found a single AUC of 0.660.

Conclusion:
Ang-1, Ang-2, and suPAR provide beneficial prognostic information about mortality in adult patients with sepsis. The further development of standardized assays and the assessment of their performance when included in panels with other biomarkers may be recommended.

5338

N. Enz[2], F. Janker[1], S. Andreoli[1], M. Haberecker[3], C. Opelz[1], W. Weder[1], JH. Jang[1], W. Jungraithmayr[1]

The co-expression of CD26 and TGF-β1 renders lung cancer targetable to CD26-inhibition

University Hospital Zurich, Department of Thoracic Surgery[1], University Hospital Rostock, Department of Thoracic Surgery[2], University Hospital Zurich, Department of Pathology, Zurich[3]

Introduction:
CD26/dipeptidyl peptidase 4 (CD26) is a transmembrane multifunctional molecule present on various haematopoetic and somatic cells. We showed previously that lung cancer growth is decreased upon CD26-inhibition. Also, we could demonstrate that CD26 is highly expressed in human lung adenocarcinoma. We here extended our analysis on the expression of CD26 within the lung tumor microenvironment.

Methods:
Samples from patients with lung malignancies (n=103) including adenocarcinoma (n=38), squamous carcinoma (n=26), lung metastases (n=14), and others (n=25) were analyzed against normal lung on a gene level for CD26, TGF-β1, TGF-R1, TGF-R2 and CCL2 by RT-qPCR, on a protein level for CD26 and TGF-β1 by ELISA, and by immunohistochemistry (IHC) for CD26 (n=80). The expression of CD26 on tumor cells was graded from 0 to 3.

Results:
Adenocarcinoma expressed significantly more CD26 than other thoracic malignancies (n=80, $p=0.0001$). While stage IA adenocarcinoma expresses significantly higher amounts of CD26 compared to stage IIIA ($p=0.0019$), levels of CD26 raised in stage IIIB and IV, however, without significance. Furthermore, we found a significant correlation between the gene expression of CD26 on tumors for TGF-β1 ($p<0.0001$), TGF-R1 ($p=0.0004$), and TGF-R2 ($p<0.0001$). Also, the pro-inflammatory chemokine ligand CCL2 was significantly correlated with CD26 ($p=0.0011$). The co-expression of CD26 and TGF-β1 could be additionally confirmed on a protein level.

Conclusion:
We could confirm that CD26 is highly expressed in lung adenocarcinomas and that CD26 is co-expressed with pro-fibrotic proteins relevant to tumor microenvironment formation. This co-expression supports the potential for the treatment of lung cancer with CD26-inhibitors.

5339

L. Imbach[1], C. Christian[1], R. Poryazova[1], O. Geissler[1], P. Brugger[1], I. Mothersill[3], M. Weller[1], M. Oertel[2], L. Stieglitz[2]

Anticonvulsive effect of anterior thalamic deep brain stimulation in super-refractory status epilepticus crucially depends on active stimulation zone – a single case observation

Departement of Neurology, University Hopsital Zurich[1], Departement of Neurosurgery, University Hospital, CHUV Lausanne[2], Swiss Epilepsy Centre, Zurich[3]

Introduction:
Super-refractory status epilepticus is a neurological emergency with high mortality and its treatment poses significant clinical challenges.

Methods:
We report the case of a 65-year old woman suffering from pharmacotherapy-resistant epilepsy, who was successfully treated with deep brain stimulation (DBS) for status epilepticus.

Results:
On admission, the EEG showed bilateral diffuse epileptiform potentials consistent with non-convulsive status epilepticus. Anticonvulsive treatment was extended with midazolam, phenytoin, phenobarbital and brivaracetam. Due to ongoing status epilepticus, we initiated deep burst suppression anesthesia with thiopental for 72h without effect on the continuous epileptic activity. Due to failure of pharmacotherapy, DBS was considered as an alternative.
Bilateral DBS leads were implanted in the anterior nucleus of the thalamus. Stimulation was initiated intraoperatively (contacts 2/10). However, one day after implantation, the patient suffered from recurrent bilateral tonic-clonic seizures and the EEG showed ongoing status epilepticus. After adaptation of the stimulation to more cranial electrode contacts (contacts 3/11), the status epilepticus was resolved and the patient remained seizure-free.

Conclusion:
This case underlines the feasibility and efficacy of thalamic DBS for the treatment of status epilepticus. Furthermore, we report the remarkable finding that changing the active DBS contacts within the target region had an immediate and long-term anticonvulsive effect.

5340

A. Magalhães[1], A. Chincisan[1], M. Emmenegger[1], A. Carrella[1], A. Aguzzi[1], S. Hornemann[1]

Unbiased high-throughput microELISA screen for naturally occurring human tauK18 autoantibodies

Institute of Neuropathology, University Hospital Zürich[1]

Introduction:
Pathologically phosphorylated tau aggregates are a major component of neurofibrillary tangles in tauopathies including Alzheimer's disease. Currently, treatment strategies for tauopathies are scarce and there is a need for specific treatment options. Studies in mice expressing mutant tau protein that were vaccinated with phospho-tau peptides demonstrated the generation of anti-tau antibodies that were able to reduce tau pathology and to rescue behavior. This is in line with a new approach striving towards the development of novel disease-modifying strategies for neurodegenerative diseases that use naturally occurring monoclonal antibodies as therapy. To interrogate the human immune repertoire, a high-throughput screen for naturally occurring tauK18 antibodies was performed to explore the potential value of those as diagnostic biomarkers and therapeutics.

Methods:
The screen was performed as part of the automated microELISA screening platform established at the Institute of Neuropathology. Residual heparin plasma samples from the Institute of Clinical Chemistry were tested in the microELISA format using recombinant monomeric tauK18 as antigen. Natural antibodies from reactive patients' samples were purified using epoxy-coated tauK18 resin and eluted with glycine buffer. Purified autoantibodies were used for validation assays; specifically, natural antibodies were tested in competitive ELISAs and compared to commercially available antibodies using Western Blot and immunofluorescence stainings.

Results:
Preliminary epidemiological data from the automated microELISA screen showed 2% of distinctly reactive patients (-logEC50 >= 2) for tauK18 monomers, which is higher than the general reactivity against other targets. Purified natural antibodies were successfully competed in a competition ELISA with soluble recombinant tau compared to a negative recombinant control. For Western Blot assays, HEK293 cell lysate was loaded onto a SDS-PAGE and stained after immunoblotting with commercially available tau HT7 antibody and purified natural antibodies. Both antibodies stained bands of similar size, matching the size of soluble tau. Purified antibodies were also able to immunofluorescence stain SH-SY5Y_tau441P301LS320F cells, overexpressing a mutant form of tau, but not SH-SY5Y WT cells as did commercially available tau RD4 antibodies.

Conclusion:
The validation assays were able to show that the anti-tauK18 antibodies detected in reactive patients' plasma were indeed specific and sensitive for the detection of tau using distinct techniques such as Western Blot and immunofluorescence. We will complement our study with isotype determination and epitope mapping experiments. We aim to screen >20,000 patients and perform an epidemiological study of tau autoantibodies correlating patient reactivity with clinical data (e.g. age, gender, ICD-10 codes). This study will enable us to explore the potential of tau autoantibodies as diagnostic biomarkers of tauopathies and further elucidate on the current controversy about the occurrence of anti-tau autoantibodies in healthy vs. diseased subjects.

5341

E. Boran[1], T. Fedele[1], P. Klaver[1], P. Hilfiker[2], L. Stieglitz[1], T. Grunwald[2], J. Sarnthein[1]

Persistent hippocampal neural firing and hippocampal-cortical coupling predict verbal working memory load

USZ Neurochirurgie[1], Epiklinik[2]

Introduction:
The maintenance of items in working memory relies on persistent neural activity in a widespread network of brain areas. It remains, however, unclear how load on working memory influences persistent neural activity, particularly in the hippocampus and in its functional connections.

Methods:
To address these issues, we asked human subjects to maintain sets of letters in memory while we recorded single neurons and intracranial EEG in the medial temporal lobe and EEG from their scalp.

Results:
Hippocampal neural firing distinguished between the periods of a trial and increased with the number of letters to be memorized. Along the periods of a trial, hippocampal firing differentiated between success and error trials during stimulus encoding, predicted workload during memory maintenance, and predicted the subjects' behavior during retrieval. During maintenance, neuronal firing was synchronized with intracranial hippocampal EEG. On the network level, synchronization between hippocampal and scalp EEG in the theta-alpha frequency range increased with the number of letters and thereby showed workload dependent oscillatory coupling between hippocampus and cortex.

Conclusion:
Thus, we found that persistent neural activity in the hippocampus participates in a process of working memory that is load sensitive and specific to memory maintenance. Local hippocampal activity is synchronized to cortex by a long-range theta-alpha oscillatory network for working memory.

5342

E. Boran[1], G. Ramantani[2], K. Krayenbühl[1], T. Fedele[1], J. Sarnthein[1]

High Frequency Oscillations in scalp EEG to monitor therapy in the individual patient

USZ Neurochirurgie[1], Kinderspital[2]

Introduction:
High frequency oscillations (HFO) are promising biomarkers of epileptogenicity. The evidence supporting their significance derives mainly from invasive EEG. Since invasive EEG recordings entail a risk of morbidity that is only justified for selected epilepsy surgery candidates, Therefore, HFO in the readily accessible scalp EEG are desirable. Here, we investigated whether scalp HFO are related to invasive HFO and if they are affected by surgical therapy.

Methods:
In 10 children with refractory focal epilepsy, we recorded pre- and/or post-operative scalp EEG with a custom-made low-noise amplifier (LNA) in addition to a commercial device (CD). We recorded intraoperative ECoG during epilepsy surgery in five of these children, and invasive EEG in one. We then apply a previously validated automated detector in the time-frequency domain to provide a prospective definition of clinically relevant HFO.

Results:
Across the patient group, the scalp HFO rate correlated with seizure frequency ($R^2 = 0.83$, $p < 0.0001$). In the individual patient, scalp HFO rates were higher in patients with severe epilepsy (14/14 recordings, PPV = 100%, NPV = 100%, accuracy = 100% CI [77% 100%]). Scalp HFO were detected in the ripple band (80-250 Hz). Higher HFO rates were detected with the LNA in scalp EEG than with the CD (8.20 vs. 5.15 HFO/min, $p < 0.0001$). The location of scalp HFO matched the location of HFO in invasive recordings. HFO in scalp EEG decreased after successful epilepsy surgery.

Conclusion:
HFO in scalp EEG mirrors the state of disease in pediatric focal epilepsy. The automated detector ensures a prospective, bias-free definition of a clinically relevant HFO in a scalp EEG. This is the first step towards using scalp HFO to monitor therapy in the individual patient.

5343

C. Hiller[1], M. Visentin[1], Z. Gai[1], S. Samodelov[1], N. Perez[1], S. Häusler[1], B. Stieger[1], G. Kullak-Ublick[1]

Development of a 3D HuH-7 cell-based system as a model to study drug-induced cholestasis

Klinische Pharmakologie und Toxikologie, UniSpital, Zürich[1]

Introduction:
Bile acids are produced in the hepatocytes from cholesterol and excreted into the canaliculi by the bile salt export pump (BSEP). Bile acids travel throughout the biliary tree and are emptied into the small intestine where they are reabsorbed by the apical Na^+-dependent bile acid transporter (ASBT) and the basolateral organic solute and steroid transporter (OSTα-OSTβ). Finally, the hepatic uptake of bile acids at the sinusoidal level is mediated by the Na^+-taurocholate cotransporting polypeptide (NTCP) and by the organic anion transporting polypeptides (OATPs). This enterohepatic circulation of bile acids allows the recycling of more than 90% of the bile acid pool. A reduced elimination of bile acids from the hepatocytes is a major cause of primary cholestasis and is the result of an impaired BSEP activity. Due to their detergent properties, accumulation of bile acids is detrimental and can cause severe damage to the liver. Several widely prescribed drugs can reduce BSEP activity, causing liver damage. Drug-induced cholestasis is one of the mechanisms of drug-induced liver injury (DILI), a major cause of severe liver damage, drug attrition, withdrawals and restrictions. Assessment of drug-BSEP interaction is a preclinical requirement of the European medical agency (EMA). Among the existing methods to study drug-BSEP interaction, the most used in preclinical safety is the assessment of *cis*-inhibition by monitoring transport of BSEP substrates in isolated membrane vesicles overexpressing the transporter. While practical, relatively inexpensive, and suitable for high throughput screening, this assay carries a relatively high rate of false positives and, in turn, leads to unnecessary drug attrition. To increase the accuracy in preclinical drug assessment, a 3D cell system based on overconfluent hepatocellular carcinoma cells (HuH-7) was developed.

Methods:
Cellular polarization was induced by growing HuH-7 cells on 3-µm pore size membranes in a Transwell® system for 21-24 days exchanging medium every 2 to 3 days. Gene expression was assessed by RT-qPCR. Cell polarity was investigated by immunostainings of membrane proteins and markers, analyzed with confocal microscopy. Integrity of the cell monolayer was evaluated using the cell-impermeable fluorophore Lucifer yellow and by transepithelial electrical resistance (TEER) measurements. The effect of thirteen selected compounds on the transport of [^{3}H]taurocholic acid was assessed in overconfluent HuH-7 cells on Transwell and in inside-out membrane vesicles prepared from Sf21 insect cells overexpressing BSEP.

Results:
Overconfluent HuH-7 cells upregulated the mRNA expression of the main bile acid transporters as compared to normal HuH-7 cells. On Transwell® membranes overconfluent HuH-7 cells displayed minimal paracellular solute movement (leakage). BSEP and Na^+/K^+ ATPase localized at the apical and the basolateral membranes, respectively. The two compartments were physically separated by tight junctions, indicating a hepatocyte-like polarization of the cells. The increase in taurocholate in the compartment opposed to that of the injection site as a function of time was linear, and reflects the unidirectional transcellular flux of [^{3}H]taurocholate. Notably, the transport rate of taurcholate was ~3 fold greater from basolateral to apical than from apical to basolateral, in line with the apical localization of BSEP (slope, 0.008 ± 0.0002 vs 0.003 ± 0.0001 pmol μg^{-1} h^{-1}). The 3D HuH-7 cell-based system was less sensitive (67% vs 100%) but more specific (60% vs 90%) than the membrane vesicle assay in flagging compounds that induce primary cholestasis.

Conclusion:
The 3D HuH-7 system is functional and suitable for predicting drug-induced cholestasis. Based on the results obtained using a selected group of compounds, it appears that, in combination with the standard vesicle assay, our model can improve the current preclinical safety strategy with regard to drug-induced cholestasis.

5344

O. Török[1], B. Schreiner[2], H. Tsai[3], M. Han[3], M. Greter[2], B. Becher[2], A. Keller[1]

Brain pericytes as sentinels controlling leukocyte trafficking in the CNS

Department of Neurosurgery, Clinical Neuroscience Center, University Hospital Zurich and University of Zurich[1], Institute of Experimental Immunology, University of Zurich[2], Department of Neurology and Neurological Sciences, Stanford University, CA, USA[3]

Introduction:
Under homeostasis lymphocyte trafficking into the central nervous system (CNS) is tightly controlled by the blood–brain barrier (BBB). In multiple sclerosis (MS) autoreactive leukocytes enter the CNS and cause demyelinating pathology. Although vast effort is made to understand the pathophysiology of autoimmunity in MS, knowledge about pathological changes of the CNS vasculature that permit the extravasation of autoimmune leukocytes is still limited. Additionally, it has been demonstrated that pericytes play an important role in the development of the BBB but further studies are needed to better define the role of pericytes in regulating immune cell trafficking in the CNS.

Methods:
As an animal model of pericyte-deficiency we use *Pdgfb-ret* (*Pdgfb*$^{tm3.1Cbet}$) mice. These animals show approximately 85% reduction of pericyte coverage in the CNS vasculature. We use an animal model of MS-experimental autoimmune encephalomyelitis (EAE) to investigate the role of pericytes in neuroinflammation and a myelin oligodendrocyte glycoprotein (MOG) specific T cell receptor transgenic mouse line (2D2). The following techniques are used: immunohistochemistry, histochemistry, confocal microscopy and flow cytometry.

Results:
The analysis of brains of adult *Pdgfb*$^{ret/ret}$ mice showed increased extravasation of leukocytes. An increased number of CD45^{hi} leukocytes was detected in the brain parenchyma in pericyte-deficient mice compared to controls, with a significant increase in the CD11b^{+}, Ly6C^{hi} and CD11c^{+} populations. The endothelium of *Pdgfb*$^{ret/ret}$ mice showed higher expression of certain leukocyte adhesion molecules (LAMs), i.e. VCAM-1 and ICAM-1. Immunization of *Pdgfb*$^{ret/ret}$ mice with MOG peptide led to increased mortality and an early, atypical EAE phenotype which is accompanies by an increased infiltration of CD45^{hi} cells into brains of *Pdgfb*$^{ret/ret}$ mice compared to controls but not in the spinal cord. Fingolimod (FTY-720) treatment rescued the atypical EAE phenotype of pericyte-deficient mice. *Pdgfb*$^{ret/ret}$*; 2D2*^{tg} mice present an early onset of atypical EAE symptoms compared to control mice and show an infiltration of T-cells into the brain parenchyma.

Conclusion:
Our data suggest that pericytes regulate leukocyte extravasation into the CNS parenchyma by contributing to the non-permissive properties of the endothelium during homeostasis, and thus, restricting immune cell transmigration into the CNS. Pericyte-deficiency changes the clinical phenotype in EAE and accelerates spontaneous activation of self-reactive T-cells.

5345

E. Lemes[1], A. Lakkaraju[1], R. Marpakwar[1], A. Aguzzi[1]

PIKfyve As a Key Player in Prion-Induced Vacuolation

Universitätsspital Zürich, Institute for Neuropathology, Zürich[1]

Introduction:
Prion diseases are inevitably lethal protein misfolding disorders mainly defined by the accumulation of abnormal aggregates (Prp^{Sc}) of the cellular Prion protein (Prp^{C}), astrocytosis, intraneuronal vacuolation and neuronal degeneration leading to spongiform change in the central nervous system. Loss of PIKfyve, a lipid kinase acting on phospholipids in late endosomal and lysosomal membranes, was previously shown to lead to the generation of large intracellular vacuoles. Interestingly, loss of PIKfyve protein was also observed in prion-infected mouse brains, suggesting a key role of PIKfyve in prion-induced vacuolation and neurotoxicity. Further results obtained within our lab suggested that in prion disease PIKfyve is degraded after ER stress and subsequent alternative splicing. However, exact mechanisms responsible for loss of PIKfyve and pathways downstream of PIKfyve-deficiency that ultimately lead to vacuolation in prion disease are not identified yet. Since vacuolation is believed to be a key event in prion-induced pathology experiments were conducted with the general aim to characterize the mechanisms that lead to vacuolation in prion disease.

Methods:
In order to obtain mechanistic insights into vacuolation we use cell culture systems (GT1-7, N2a, HEK293 cell lines) and animal models (prion-infected mice). Levels of PIKfyve and its complex proteins Fig4 and VAC14 were altered in the cell lines via transfection of shRNA targeting PIKfyve or overexpression of the complex proteins. Brains of mice infected with prions (RML6) or normal brain homogenate (NBH) were analyzed for alternative splicing by reverse transcription of RNA and amplification of the suspected exons. Additionally techniques like immunochemistry, (Phospho-) Western Blot, ER-stress induction assay, fluorescence microscopy, pH-sensor dyes and co-immunoprecipitation were used.

Results:
Here, we established a model system for studying vacuolation in which shRNA-mediated PIKfyve knockdown caused severe vacuolation. Using this system together with prion-infected mouse brain samples we show that degradation of PIKfyve is most likely ER stress-independent and not caused by alternative splicing of PIKfyve. Furthermore, lysosomal markers were found to accumulate around vacuoles, suggesting fusion defects between lysosomal and vacuolar membranes to be causative of large vacuole formation. Lastly, three potential protein substrates of PIKfyve were found in the phosphoproteomics analysis.

Conclusion:
Our data suggests that spongiform change may directly result from the suppression of the PIKfyve kinase, resulting in the impairment of endolysosomal machinery and formation of progressively larger vacuoles. We introduced a new model system for studying vacuolation and dismissed alternative splicing of PIKfyve as the main event leading to its degradation. The compelling discovery of three potential PIKfyve protein-substrates proposes that there might be an alternative pathway, besides lipid phosphorylation, contributing to vacuolation and cell death in prion disease. In order to obtain more unbiased information about PIKfyve and its downstream interactors we plan to perform a synthetic viability screen using a whole genome sgRNA library and the CRISPR/Cas9 system. Lastly, the possibility that PIKfyve-dependent events may play a causative role in other neurodegenerative disorders exhibiting vacuolation will be investigated.

5346

C. Zhu[1], P. Schwarz[1], A. Aguzzi[1]

Deficiency of Progranulin (PGRN) results in accelerated prion diseases

Institute of Neuropathology, University Hospital of Zurich[1]

Introduction:
Progranulin (PGRN) is a secreted glycoprotein expressed mainly by microglia and neurons in in the central nervous system. Mutations in PGRN encoding gene GRN that result in haploinsufficiency lead to frontotemporal lobar degeneration and Alzheimer's diseases. However, the underlying molecular mechanisms remain largely unknown. To determine whether PGRN is involved in a broad spectrum of neurodegenerative conditions including prion disease, we aimed to delineate the role of PGRN in prion pathogenesis.

Methods:
We intracerebrally infected $GRN^{-/-}$mice and their $GRN^{+/-}$and wild type littermates with RML6 prions. Survival curves determined by the time lapse between the prion inoculation and end stage of disease were compared between the three genotypes. Vacuolation, lesion pattern, PrP^{Sc}deposition, astrogliosis and microglial activation in RML6-infected $GRN^{-/-}$ mice and their $GRN^{+/-}$and wild type littermates were characterized by histology and biochemistry.

Results:
We found that $GRN^{-/-}$mice showed accelerated prion progression in comparison to $GRN^{+/-}$and wild type littermates. Histology revealed that $GRN^{-/-}$microglia were aberrantly activated, resulting in amoeboid morphology and altered cytokine profiles. Biochemical analysis demonstrated that at 120 days post prion inoculation, $GRN^{-/-}$microglia were more activated and competent to clear prions, resulted in decreased prion deposition. Whereas at 150dpi, over-activation of $GRN^{-/-}$microglia led to excessive complement activation and insufficiency of prion clearance, resulting in similar level of $PrP^{Sc}$to that of $GRN^{+/-}$and wild type littermates. These results suggest that Progranulin modulates prion-induced microglial activation and protects prion diseases by suppressing excessive activation of complement cascade.

Conclusion:
Microglial activation by prion infection is a stepwise process. Progranulin is an important negative regulator of prion-induced microglial activation. Depletion of PGRN resulted in aberrant microglial activation and accelerated prion disease, suggesting that Progranulin could be a potential target for prion therapeutics.

5347

M. Losa[1], C. Scheckel[1], K. Frontzek[1], M. Emmenegger[1], A. Aguzzi[1]

Characterization, cloning and validation of natively paired human-derived anti-cellular PrP autoantibodies and their germline V-(D)-J segment recombination events using a targeted single cell approach on different patient cohorts

Neuropathology, University Hospital of Zurich, Zurich[1]

Introduction:
Prion diseases (PrD), which are also termed 'transmissible spongiform encephalopathies' are rapidly progressive, incurable and lethal neurodegenerative diseases which attack the central nervous system. Their incubation period ranges from years to decades. Typical hallmarks of these diseases are vacuolation, neuronal loss and microglia activation. Despite decades of research, no therapies for these devastating diseases are currently available.
Prions consist of scrapie PrP (PrP^{Sc}), an aggregated form of cellular PrP (PrP^{C}) and replicate by changing the conformation of PrP^{C}. Targeting PrPc with antibodies as immunotherapeutics may inhibit the spread of prions by depleting the substrate or by stabilizing the native conformation of PrP^{C}. This approach may be a game changer in the therapy of these dramatic diseases.

Methods:
After the identification of high antibody titer patients using a high-throughput approach and a well-established enzyme-linked immunosorbent assay (ELISA) at the University Hospital of Zurich, the specific anti- PrP^{C} antibody producing memory B-cells from high titer patients are isolated from blood samples with a bait-gated FACS approach. We aim to establish a single-cell-based antibody-cloning pipeline, which will enable us to characterise, clone and validate human-derived and natively paired (heavy and light chain) anti-PrP^{C} autoantibodies and analyse their germline V-(D)-J segment recombination events from memory B-cells. These antibodies may then be used for i*n vitro* and *in vivo* studies and may serve as immunotherapeutic drugs in patients suffering from these diseases.

Results:
We have successfully established an optimized MACS protocol to enrich for B cells, a bait-gated FACS protocol for the sorting of PrP^{C} reactive memory B cells as well as a single cell PCR assay to amplify heavy and light chains. To date, the single-cell RT/PCR analysis of a total of 15 PrP^{C} reactive memory B cells has yielded one variable heavy and two variable light chains from different cells.

Conclusion:
These human-derived antibodies may recognize diverse epitopes of the PrP^{C} and may elicit different and so far unknown effects a phenomenon our group has observed with mouse antibodies against PrP. The human-derived antibodies might serve as valuable immunotherapeutic approach in these dramatic neurodegenerative diseases.

5348

M. Meerang[1], O. Lauk[1], M. Kirschner[1], V. Orlowski[1], V. Cecconi[2], M. Van den Broek[2], W. Weder[1], I. Opitz[1]

Analysis of immune cells in an orthotopic immunocompetent rat model of malignant pleural mesothelioma

Department of Thoracic Surgery, University Hospital Zurich[1], Institute of Experimental Immunology, University of Zurich[2]

Introduction:
An immunocompetent rat model of malignant pleural mesothelioma (MPM) allows studying a clinically relevant tumor microenvironment. To explore a rationale for applying this model to test the efficacy of immunotherapy, we have analyzed tumor-infiltrating immune cells. Because T-cells are the major mediators of protective anti-cancer immunity, we focused on T-cells.

Methods:
We implanted 10^6 luciferase-expressing IL45 rat mesothelioma cells underneath parietal pleura of immunocompetent F344 rats (n=4). As soon as the animal wellbeing was compromised as a result of MPM, we harvested tumor tissues and processed these into single-cell suspensions. We incubated cells for 5 h with PMA/ionomycin in the presence of brefeldin A, stained for surface CD45, CD11b, TCR, CD4 and CD8, for dead cells, and for intracellular interferon-gamma (IFNg) followed by flow cytometry. We analyzed samples with FlowJo software.

Results:
All tumor samples contained leukocytes ($CD45^+$) with a median of 5.1% of all live cells. Within live $CD45^+$ cells, myeloid cells ($CD45^+CD11b^+$) were the most abundant population, whereas T-cells ($CD45^+$, $TCRa/b^+$) accounted for a median of 35%. The ratio $CD4^+/CD8^+$ was approximately 1 in all samples. A minority of T-cells produced IFNg (5.6 % of $CD4^+$ and 8.6 % of $CD8^+$ T-cells), suggesting that tumor-infiltrating T-cells are functionally compromised in this rat MPM model.

Conclusion:
We propose that the IL45 orthotopic model for MPM in rats is a useful tool for developing novel immunotherapies for MPM as monotherapy or in combination with standard treatments.

5349

M. Wulf[1], A. Sattler[1], K. Frontzek[2], A. Aguzzi[1]

Acute changes in the cerebellar phosphoproteome induced by neurotoxic antibodies targeting the cellular prion protein

Institute of Neuropathology, University Hospital Zürich[1], Institute of Surgical Pathology, Department of Pathology, University Hospital Zurich[2]

Introduction:
Prion diseases are inevitably fatal neurodegenerative diseases induced by misfolding of cellular prion protein (PrPC) into a toxic conformer (PrPSc). PrPC resides on the cell surface of neurons and glial cells and its expression is necessary for the manifestation of toxic effects induced by misfolded PrPSc. Most of these toxic cacades can be replicared using prion mimetic antibodies that target the C terminal domain of PrPC. As with many gpi-anchored proteins, PrPC resides in detergent resistant membranes and interacts with a plethora of other proteins in the vicinity. The early events in prion induced toxicity are thought to happen on the cell surface and it is hypothesized that generation of prions lead to a toxic gain of function which includes dysregulation of several of these interaction partners and their signaling cascades. Currently very little is known about these events and we posit to identify sub set of these events using a phosphoproteomic approach. Since most signaling events are associated with phosphorylation, we plan to identify differentially phosphorylated proteins upon treatment with prion mimetics.

Methods:
Acute cerebellar slices from wild type mice (C57BL6/J) were incubated with 500nm toxic POM1 (prion mimetic) or a non-toxic mutant of POM1 (POM1Y104A) at a concentration of 500nM for 0, 5, 15 or 30min. Slices were then subjected to the phosphoproteome analysis at the Functional Genomics Center Zurich. All samples were digested using trypsin and a small aliquot was used for the quantification at the proteome level, while most part of the digested samples were used for phosphopeptide enrichment using Ti (IV)- immobilized metal ion affinity chromatography and label-free quantification. Phosphopeptides were classified as differentially regulated applying a threshold of q mod < 0.05 and a log2 fold change ≥ 1 and log2 fold change ≤ -1.

Results:
In total, proteome analysis identified approximately 4900 proteins in our samples and phosphopeptide enrichment identified 8600 phosphopeptides in each condition. Applying above thresholds, no significant changes were detected at the proteome level. Phosphopeptide analysis however revealed that phosphorylation of Claudin11 was significantly increased after 30 min of POM1 treatment compared to control (log2FC = 3.2396424, q mod = 0.0001639).

Conclusion:
We performed an unbiased approach to detect phosphorylation changes on the proteome level in a model of acute prion toxicity. We found one differentially phosphorylated protein after 30 min of POM1 treatment, namely Claudin11. Claudin11 is a cell surface protein involved in tight junction formation. In the central nervous system (CNS) it is predominantly expressed in oligodendrocytes and is a major component of CNS myelin. Future work aims at validating this result and further investigating a putative role of Claudin11 in prion toxicity.

5350

F. Meier-Abt[1], S. Amon[4], L. Gillet[4], W. Wolski[3], S. Dimitrieva[3], A. Theocharides[2], M. Manz[2], R. Aebersold[5]

Transcriptome-Proteome Correlation in Human Hematopoietic Stem and Progenitor Cells

*Hematology, University and University Hospital Zurich, and Department of Biology, Institute of Molecular Systems Biology (IMSB), ETH Zurich, *These authors contributed equally to this work[1], Hematology, University and University Hospital Zurich[2], Functional Genomics Center Zurich (FGCZ), University of Zurich, ETH Zurich[3], Department of Biology, Institute of Molecular Systems Biology (IMSB), ETH Zurich[4], Department of Biology, Institute of Molecular Systems Biology (IMSB), ETH Zurich and Faculty of Science, University of Zurich[5]*

Introduction:
Hematopoietic stem cells (HSCs) can self-renew and/or differentiate into various functionally divergent progenitor cell types, such as common myeloid progenitors (CMPs), megakaryocyte-erythrocyte progenitors (MEPs) or granulocyte-macrophage progenitors (GMPs). When the process of self-renewal and differentiation is altered, e.g. upon genetic or epigenetic changes in HSCs, abnormal (pre)leukemic stem cell subpopulations may form, eventually resulting in the onset of hematopoietic malignancies. To gain insight into the physiology and subsequent patho-physiology of self-renewal and differentiation, highly refined analyses of HSCs and downstream progenitor cells are needed.

Methods:
We developed an ultra-sensitive mass spectrometric method for robust quantitative proteomic analysis of highly purified FACS-isolated cell populations and applied this method to quantify the proteome of 25’000 human hematopoietic stem and progenitor cell subpopulations isolated from five healthy donors. The proteomic analyses were complemented by transcriptomic analyses.

Results:
A comparison of proteomic and transcriptomic profiles of the respective cell types indicated hematopoietic stem/multipotent progenitor cell-specific divergent regulation of biochemical processes essential for maintaining stemness at the proteome rather than transcriptome level. Specifically, several telomerase maintenance proteins and quiescence-inducing isocitrate dehydrogenase proteins, both assumed to be essential for long-lived stem cells, were found to be upregulated in HSCs on the protein but not on the mRNA level when compared to myeloid progenitor cell subpopulations (CMPs, MEPs, GMPs).

Conclusion:
The divergent mRNA/protein regulation of telomerase maintenance and quiescence-inducing isocitrate dehydrogenase proteins in HSCs illustrates the relevance of generating high quality proteomic data for well-defined cell subpopulations with the goal to identify biological processes that are insufficiently determined by genomic or transcriptomic analyses. The presented approach paves the way for proteomic profiling of relevant disease sample sub-fractions such as (pre)leukemic stem cells in hematopoietic malignancies as well as cancer stem cells from solid tumors and, ultimately, may allow to find therapeutic targets in (pre)leukemic/cancer stem cells.

5351

J. Schaffenrath[1], L. Dib[2], M. Neidert[1], M. Delorenzi[2], L. Regli[1], A. Keller[1]

Transcriptomic profiling of the glioblastoma-BBB

Department of Neurosurgery, University Hospital Zürich, Zürich[1], Swiss Institute of Bioinformatics, Université de Lausanne, Lausanne[2]

Introduction:
Glioblastoma multiforme (GBM) is the most common primary brain tumor with high severity and low therapeutic success. Although GBM is the most sequenced of human tumors today, currently available therapies are not effective and life expectancy does not exceed 12-15 month after diagnosis. GBM vasculature received attention in context of anti-angiogenic therapy development, however specific molecular changes in GBM vasculature have not been studied extensively. Vasculature is the main interface for drug delivery and therefore we decided to study molecular changes of GBM vasculature. Successful delivery of drugs into tumor site is limited by the special protecting properties of brain vasculature – the blood brain barrier (BBB). The BBB is a multicomponent system consisting of several components e.g. tight endothelial cells (EC), astrocyte end feet and pericytes. Most of prescribed drugs are small lipid soluble molecules, which are effectively removed from the brain by transporters expressed in these special BBB-ECs (ABC transporters). Extending the knowledge about the molecular composition of the GBM BBB-ECs will hopefully bring insights into biology of GBM vasculature, and help to design better treatment strategies with elevated delivery efficiency.

Methods:
In this study, we aim to characterize the transcriptome of the human BBB in health and GBM. Human ECs are isolated from GBM and normal human brain tissue. As a control, we use autopsy material with a maximum post mortem interval of 20 hours or brain tissue removed during epilepsy surgery. For both tissues, normal and GBM, the isolation of ECs include enzymatic tissue dissociation followed by negative selection with anti-CD15 and anti-CD45 antibodies coupled to magnetic beads to exclude leukocytes and circulating progenitor cells. ECs are isolated using anti-human CD31 antibody. After enrichment for ECs, RNA is isolated and subjected to RNA sequencing.

Results:
Analysis of RNA sequencing data from 5 GBM and 6 control cases enriched for ECs was performed. An unsupervised hierarchical clustering analysis using Euclidian distance measurement showed similarity of samples according to their origin - GBM or control tissue. Bioinformatics analysis of differentially expressed genes (DEG) in our dataset revealed deregulation of EC`s SLC transporters in GBM ECs compared to controls. Interestingly, the expression of several ABC transporters – with the exception of P-glycoprotein – remains unaltered, or is upregulated in GBM ECs. This highlights that delivery of lipid soluble drugs is an obstacle in GBM treatment. Furthermore, some genes involved in BBB`s characteristic closed cell-cell junctions are downregulated (OCLN, JAM2). In addition, our data indicates a different composition of GBM vascular cells (e.g. smooth muscle cells, pericytes, fibroblasts) compared to the normal tissue. This may have consequences on the function of GBM endothelium and might serve as therapeutic target.

Conclusion:
RNA sequencing analysis suggests deregulation of several transporters (e.g. SLC & ABC transporters) in GBM ECs, which may occur due to loss of BBB characteristics upon GBM formation. Several SLC transporters, but only one ABC transporter (ABCB1) are downregulated in GBM compared to control samples. This situation could underlie the low therapeutic success of GBM chemotherapy, where efflux (ABC) of the drugs remain unaltered, but influx (SLC) is reduced.

5352

A. Montalban-Arques[1], C. Gottier[1], I. Olivares-Rivas[1], M. Spalinger[1]

Loss of Protein Tyrosine Phosphatase Non-Receptor Type 23 (PTPN23) in intestinal epithelial cells induces inflammation and epithelial hyperproliferation.

Department of Gastroenterology and Hepatology, University Hospital Zurich, University of Zurich[1]

Introduction:
Colorectal carcinoma (CRC) is still a mayor complication in patients with inflammatory bowel disease (IBD) with colonic involvement. Colitis-associated cancer patients have a worse prognosis than those with spontaneous CRC, and are frequently diagnosed at an advance stage. Protein tyrosine phosphatase non-receptor type 23 (PTPN23) regulates signal transduction events involved in cell differentiation, proliferation, apoptosis, migration and invasion. Although PTPN23 is involved in some epithelial cancers, it is unknown whether PTPN23 affects intestinal epithelial cells (IEC) homeostasis and/or malignant transformation. Here we aim to identify a role for PTPN23 in the pathogenesis of IBD and CRC.

Methods:
To investigate the role of PTPN23 in IBD and CRC, we generated mice specifically lacking PTPN23 in IEC. For this aim, mice homozygous for a LoxP flanked PTPN23 gene ($PTPN23^{fl/fl}$), were crossed with mice heterozygous for the $PTPN23^{fl}$ gene expressing Cre under the Villin Promoter ($PTPN23^{fl/WT}$ $VillinCre^{+/-}$ mice). $PTPN23^{fl/fl}$ $VillinCre^{+/-}$ (KO) and control littermates were analysed at the age of 6 weeks. Additionally, PTPN23 expression was examined in patients with IBD and CRC by immunohistochemistry.

Results:
PTPN23 KO mice were born at a reduced frequency. Those that were born and did survive until weaning, were significantly smaller, featured less weight and developed severe diarrhoea. Kaplan Meier survival curve demonstrated that all of them died spontaneously within 140 days after birth. Interestingly, PTPN23 KO mice presented severe splenomegaly, but elongated small intestine and colon compared to their WT littermates. Histologically, PTPN23 KO mice showed epithelial cell hyperplasia, with an increase of Ki67+ epithelial and immune cells through the epithelium. In human, PTPN23 was highly expressed in colon tissue derived from patients with IBD and CRC primary tumours compared to healthy regions from the same patients. Aside from high expression in cancerous epithelial cells, we also observed high PTPN23 staining in immune cells within the lamina propria, indicating an important role for PTPN23 in hematopoietic cells as well. In contrast to primary CRC tissue, PTPN23 expression was almost completely lost in liver and lung metastases of the same CRC patients.

Conclusion:
Our results suggest that PTPN23 plays an important role in IEC proliferation and inflammation. The development of this novel mouse model lacking PTPN23 specifically in IEC will allow unravelling mechanism involved in intestinal inflammation and cancer. Given the strong inflammatory phenotype observed in mice lacking PTPN23 in IEC, PTPN23 represents an interesting target in the treatment of IBD and CRC.

5353

M. Mellett[1], B. Meier[1], D. Mohanan[1], P. Cheng[1], T. Satoh[1], J. Danis[2], S. Nobbe[1], E. Contassot[1], L. French[1]

Gain-of-function mutation in the keratinocyte signalling molecule CARD14 drives spontaneous psoriatic skin disease in vivo

Dermatology Dept. University Hospital Zurich, Zurich[1], MTA-SZTE Dermatological Research Group, University of Szeged, Szeged, Hungary[2]

Introduction:
Rare missense mutations in the gene encoding the keratinocyte signalling molecule, Caspase Recruitment Domain-Containing Protein 14 (CARD14), have been associated with an increased susceptibility to chronic inflammatory skin diseases, including psoriasis and the rare skin disorder pityriasis rubra pilaris (PRP). CARD14 is predominantly expressed in keratinocytes and upon activation, recruits interacting partners BCL10 and the paracaspase, MALT1 to a signalling complex (termed the CBM complex) that initiates NF-κB and MAPK activation. Gain-of-function mutation of CARD14 is believed to lead to spontaneous NF-κB activation, leading to the upregulation of pro-inflammatory and pro-survival genes.
Despite recent advances, however, the physiological impact of CARD14 gain-of-function mutations as drivers of disease pathogenesis remains to be fully determined *in vivo*. Furthermore, a number of critical questions regarding CARD14 biology remain unanswered. It is unknown how CARD14 is activated, in homeostatic conditions and also in a chronic inflammatory setting. It also remains unclear why clinically distinct disease entities are associated with different CARD14 variants.

Methods:
To determine the physiological role of CARD14, mice harbouring a gain-of-function mutation (*Card14*Δ*E138*) were generated using CRSPR/Cas9 genome editing. The phenotype of transgenic mice was characterized using immunohistochemistry, flow cytometry and RNA-seq transcriptome analysis. Additionally, primary keratinocytes were isolated from wild-type and transgenic mice and cultured *ex vivo* and subject to quantitative PCR and confocal microscopy. Human primary keratinocytes were used, in parallel, to assess the effect of human CARD14 variants *in vitro*. To determine the role of CARD14 in psoriasis pathogenesis development, mice lacking full-length CARD14 were subjected to the Imiquimod-induced psoriasiform disease.

Results:
Heterozygous mice harbouring a gain-of-function mutation in *Card14 (Card14ΔE138$^{+/-}$)* spontaneously develop a chronic psoriatic phenotype with characteristic skin lesions, epidermal thickening, keratinocyte hyperproliferation and immune cell infiltration mirroring human disease. Affected skin shows elevated expression of anti-microbial peptides, chemokines and cytokines (including IL-1β, IL-36γ, IL-19, IL-23p19, IL-22 and IL-17 cytokines) as measured by RNA-seq transcriptome analysis, qPCR and ELISA. Flow cytometry analysis shows an immune infiltrate rich in neutrophils, myeloid cells and T-cells, reminiscent of human psoriatic skin, and neutralization of IL-23p19 significantly reduced skin lesions and the expression of pro-inflammatory molecules. Contrastingly, mice lacking full-length CARD14 are protected against Imiquimod-induced psoriasiform disease compared to wild-type counterparts. Epidermal tissue from *Card14ΔE138$^{+/-}$* transgenic mice displayed increased CARD14 activity and keratinocytes from *Card14ΔE138$^{+/-}$* skin shows spontaneous CBM complex formation unlike control cells.

Conclusion:
Gain-of-function mutation of the keratinocyte signalling molecule, CARD14 causes spontaneous signalosome assembly in human and murine keratinocytes and is sufficient to orchestrate the complex immunopathogenesis that drives psoriatic skin disease *in vivo*.

5354

C. Scheckel[1], M. Mazlami[1], A. Aguzzi[1]

Systematic Profiling of Molecular Changes during Prion Disease Progression

Neuropathology, University Hospital of Zurich, Zurich[1]

Introduction:
Prion diseases are fatal neurodegenerative diseases and are caused by proteinaceous infectious particles termed prions. While the infectious agent of prion disease has been identified decades ago, the actual cellular processes that subsequently cause neurons to degenerate remain poorly understood. Importantly, different cell types show remarkable differences in their susceptibility to prion clearance, replication and toxicity, yet what determines these differences is entirely unknown. This highlights the importance of studying individual cell types rather than entire tissues. Of particular interest to prion disease are microglia and astrocytes, which are activated during prion disease progression, as well as neurons, which are especially vulnerable to prions.

Methods:
Prion diseases are fatal neurodegenerative diseases and are caused by proteinaceous infectious particles termed prions. While the infectious agent of prion disease has been identified decades ago, the actual cellular processes that subsequently cause neurons to degenerate remain poorly understood. Importantly, different cell types show remarkable differences in their susceptibility to prion clearance, replication and toxicity, yet what determines these differences is entirely unknown.
This highlights the importance of studying individual cell types rather than entire tissues. Of particular interest to prion disease are microglia and astrocytes, which are activated during prion disease progression, as well as neurons, which are especially vulnerable to prions.

Results:
We have generated mice that express GFP-tagged ribosomes specifically in either excitatory or inhibitory neurons, microglia, or astrocytes. These mice were subjected to prion injection, and, at the specified time points post prion infection, brain samples were frozen for cell-type specific ribosome profiling and immunohistochemistry. Cell-type specific ribosome profiling libraries were generated, submitted for high-throughput sequencing, and were bioinformatically analyzed to identify cell-type specific changes in protein synthesis rates during prion disease progression. The approach identified ~150 genes that are differentially translated in neurons, as well as > 2000 genes that are differentially translated in microglia and astrocytes.

Conclusion:
The outlined approach yielded a comprehensive list of genes that are differentially regulated during the progression of prion disease and that are important for different aspects of disease pathogenesis. Importantly, the investigation of specific cell types identified numerous differentially translated genes that were not identified in previous studies, which applied a more general approach such as RNA sequencing of brain regions. This project yields novel and important insights into prion disease pathophysiology by shedding light on the role and interplay of different cell types in pathophysiologyand contributes to our understanding of other neurodegenerative diseases.

5355

J. Danis[1], L. Kemény[2], E. Contassot[1], L. French[3], M. Széll[2], M. Mellett[1]

A novel mediator of inflammatory cell death controls Interluekin-36 secretion from keratinocytes – implications for chronic inflammatory skin disease

Dermatology Dept. University Hospital Zurich[1], MTA-SZTE Dermatological Research Group, University of Szeged, Szeged, Hungary[2], Department of Dermatology and Allergology, Ludwig-Maximilian-University of Munich, Germany[3]

Introduction:
Psoriatic skin disease is characterised by scaly lesions on the skin of sufferers, which is partially caused by the hyperproliferation of keratinocytes in the epidermis. Mice harbouring a gain-of-function mutation in a keratinocyte signalling molecule Caspase Recruitment Domain-Containing Protein 14 (CARD14), synonymous to human disease, display spontaneous epidermal thickening and keratinocyte hyperproliferation, defining features of human psoriatic skin disease. Interestingly, RNAseq analysis of psoriatic tissue from *Card14ΔE138*$^{+/-}$ transgenic mice show an increase in expression of genes encoding novel members of the gasdermin family, a protein family that mediate pyroptosis or inflammatory cell death by forming pores in the membrane of cells. Furthermore, we find that keratinocytes from *Card14ΔE138*$^{+/-}$ transgenic mice display high expression of some gasdermin family members compared to wild-type cells. Gasdermin-driven pyroptosis is typically associated with the release of mature Interleukin (IL)-1β from macrophages, subsequent to inflammasome activation, but a role for gasdermin proteins in epidermal keratinocytes and in psoriatic skin disease is unknown.

Methods:
Previously, the synthetic analogue of double-stranded RNA, Poly(I:C), was shown to cause pyroptosis in primary keratinocytes *in vitro* and resulted in subsequent release of IL-36γ. To determine the role of gasdermin proteins in mediating pyroptosis in response to Poly(I:C), CRISPR/Cas9 technology was used to generate clonal knockout cells of gasdermin proteins. Lactate dehydrogenase assay was used to assess cell death and ELISA and immunoblotting techniques were used to assess IL-36γ release in response to transfected Poly(I:C), which was performed to mimic viral infection.

Results:
In response to transfected Poly(I:C), cells deficient in a gasdermin family member was protective against Poly(I:C)-induced cell death compared to control cells. Additionally, IL-36γ secretion was diminished in these cells. Rescue of the phenotype was achieved by reintroducing expression of our Gasdermin protein *via* lentivirus transduction. Clonal knockout keratinocyte cell-lines for MAVS, the adaptor protein of cytosolic dsRNA detecting pattern-recognition receptors Mda5 and RIG–I, and Caspase–8 were also protected against Poly(I:C)-induced cell death.

Conclusion:
Gasdermin family members have been previously associated with mediating pore formation in cell membranes that allows release of IL-1β subsequent to inflammasome activation and prior to pyroptosis. We have identified a novel role for a gasdermin family member in primary keratinocytes that modulates IL-36γ release. The role of pyroptotic proteins in the epidermis and particular in psoriatic skin disease is unknown and warrants further investigation.

5356

S. Samodelov[1], M. Visentin[1], Z. Gai[1], G-A. Kullak-Ublick[1]

Renal glycosuria as a novel early sign of colistin-induced kidney damage in mice

Department of Clinical Pharmacology and Toxicology, University Hospital of Zurich, Zurich[1]

Introduction:
Colistin, a polymixin antibiotic, is used as a last resort treatment for multidrug resistant infections (MDR). Made available in 1959, colistin became largely obsolete by the 80's due to a high incidence of acute kidney injury (AKI) and the development of less nephrotoxic drugs. With the rise in nosocomial MDR over the last decades, it has again become clinically relevant, with research on its undesired nephrotoxic effects lagging behind. Colistin leads to AKI after a few days treatment, as measured by the diagnostic markers of serum creatinine and golmerular filtration rates (GFR), although reversible through treatment termination. Severe MDR require treatment until infection clearance, with the risk of recurrence or increased resistance when treatment is terminated preterm. For these reasons, it is essential to understand colistin nephrotoxicity to optimize dosing and monitoring of kidney function during the course of treatment. Our study aimed at identifying the early effects of colistin on mice for understanding the nephrotoxic mechanism and evaluating the earliest markers of AKI for this drug.

Methods:
Female C57/BJ mice were treated daily with 20 mg/kg colistin sulfate or PBS via *i.p.* injection for 7 days. Urine was collected via micturition at various time points. After the last injection, mice were starved overnight and a glucose tolerance test (GTT, *i.p.* 1 g/kg D-glucose) was performed the following morning using a glucometer (mylife Unio^{TM}), before sacrificing the mice via CO_2 and harvesting kidneys and serum. Kidney tissue was either fixed in paraformaldehyde for pathology and histochemical analyses, snap frozen for protein and mRNA quantification, and/or used for assessing the uptake of [^{3}H]D-glucose in brush border membrane vesicles (BBMV) isolated by Mg^{2+} precipitation.

Results:
Mice treated with colistin showed varying degrees of kidney damage upon histological examination, with dilated proximal tubules, protein cast formation, and loss of brush border membranes. Serum and urine cystatin C, creatinine, and albumin were not homogenously nor significantly increased in the colistin-treated group. Histochemical analyses of additional markers of kidney injury, kidney injury marker 1 (Kim-1) and neutrophil gelatinase-associated lipocalin (Ngal), also showed varying results, with increased staining intensities and areas in some but not all kidney slices from the colistin-treated group. However, a significant increase in urinary glucose was observed in these mice at the end of the experiment. GTTs were similar for both groups, indicating euglycemic glycosuria. Because glucose is primarily reabsorbed in the proximal tubules by the sodium/glucose cotransporter 2 (Sglt2), mRNA and protein amounts were quantified. Immunohistochemical stainings of kidney slices showed reduced levels of Sglt2 in colistin-treated mice, corroborated by western blot, with no change in mRNA levels in whole kidney tissue homogenates. BBMV isolated from colistin-treated mice also showed a reduction in glucose uptake in comparison to the control group.

Conclusion:
Markers of kidney damage monitored in a clinical setting include serum creatinine, cystatin C, and GFR. Newly arising suggested markers for AKI include Kim-1 and Ngal, although not routinely implemented clinically as diagnostic markers. Histological analysis remains the most sensitive means of assessing the presence and severity of AKI, although not a diagnostic possibility in patient treatment and care. Our results and the need for early indicators of kidney damage, especially in the case of the last resort antibiotic colistin, prompts the question of whether urinary glucose could be used as a simple, inexpensive marker to monitor colistin-induced kidney damage at the site of the proximal tubules. Our results indicate that colistin leads to a reduction in glucose resorption, possibly through the loss of Sglt2 in the proximal tubules, at an earlier stage of AKI than standard clinical diagnostic markers.

5357

V. Todorova[1], M. Barben[1], M. Samardzija[1], G. Azarias[2], B. Weber[2], C. Grimm[1]

Stabilisation of hypoxia-inducible factor 1-alpha cause mitochondrial dysfunction in photoreceptors

Dept. Ophthalmology, University Hospital Zurich[1], Institute of Pharmacology and Toxicology, University of Zurich[2]

Introduction:
The retina is one of the metabolically most active tissues of the body. It requires large amounts of oxygen for energy production, especially in photoreceptor cells. Several ophthalmic diseases, including age-related macular degeneration, diabetic retinopathy and glaucoma are increasingly recognized to be linked to mitochondrial function deficiencies, probably leading to impaired energy metabolism. Interestingly, all of these diseases also feature a possible hypoxic component, linking the molecular hypoxic response to energy production, and thus potentially to disease onset and progression. In cancer cells, hypoxia and abnormal stabilization of hypoxia-inducible factor 1α (HIF1α) are associated with a metabolic shift from oxidative phosphorylation towards glycolysis. Even though the metabolic shift is widely studied in cancer cells, little is known about its occurrence and consequences in other cell types. Here, we study the influence of chronic HIF1α stabilisation and activation on mitochondrial function in photoreceptors.

Methods:
To study the influence of the chronic hypoxic response on mitochondrial function in photoreceptors, we used the rod (*rod$^{\Delta Vhl}$*) and cone (*all-cone$^{\Delta Vhl}$*) -specific von Hippel–Lindau (*Vhl*) knockdown mice. The absence of VHL leads to long-lasting stabilisation of the HIFα subunits and progressive retinal degeneration in both mouse models. We examined the activity of respiratory enzymes by enzyme histochemistry for mitochondrial complex II (succinate dehydrogenase - SDH) and IV (cytochrome c oxidase - COX) on retinal sections from *rod$^{\Delta Vhl}$* and *all-cone$^{\Delta Vhl}$* mice at different ages. Immunohistochemical staining of mitochondrial proteins was performed to visualise and analyse mitochondria.

Results:
In wild-type retinas, COX and SDH activity localised to the photoreceptors' inner segments, the outer plexiform layer, and the inner retina. In *all-cone* control retinas, COX activity was also visible in the perinuclear mitochondria of the cone photoreceptors. The complexes' activity in control mice did not differ between time points tested. In *rod$^{\Delta Vhl}$* and *all-cone$^{\Delta Vhl}$* retinas, COX and SDH activity were impaired in the photoreceptors' inner segments. Furthermore, impaired COX activity was observed also in the cone perinuclear mitochondria of *all-cone$^{\Delta Vhl}$* mice. The impairment of the COX and SDH respiratory enzymes was observed already at a time point when retinal morphology was still intact. Interestingly, COX and SDH enzyme activity was restored in mice that lacked *Hif1a* in addition to *Vhl* (*rod$^{\Delta VhlHif1a}$* and *all-cone$^{\Delta VhlHif1a}$*). Additional deletion of *Hif2a* was without effect. Immunofluorescence stainings for the mitochondrial marker VDAC1 reveal areas of mitochondrial network disorganisation within the photoreceptors inner segments. However, the signal localisation does not differ between our hypoxic models and their controls, suggesting conserved number of mitochondria in the hypoxia mouse models. Furthermore, immunofluorescence stainings for mitochondrial transcription factor A (TFAM) show altered signal distribution in the outer nuclear layer of *rod$^{\Delta Vhl}$* and *all-cone$^{\Delta Vhl}$* retinas compared to their controls.

Conclusion:
Our results suggest that a chronic molecular response to hypoxia leads to impaired mitochondrial function and thus reduced respiration in rod and cone photoreceptors prior to their degeneration. However, further analyses are required in order to gain a better understanding about the energy metabolism processes during chronic hypoxia and their potential connection to photoreceptor degeneration.

5358

U. Meyer[2], U. Heilmeier[2], A. Siegenthaler[2], R. Theiler[1], A. Egli[2], H. Bischoff-Ferrari[3]

Effect of daily high-dose vitamin D supplementation on bone micro-architecture as assessed via high resolution peripheral quantitative computed tomography (HR-pQCT) in seniors: a double-blind RCT

Department of Geriatrics, University Hospital Zurich[1], Centre on Aging and Mobility, University Hospital Zurich, Waid City Hospital, and University of Zurich[2], Department of Geriatrics, University Hospital Zurich; University Clinic for Acute Geriatric Care, Waid City Hospital; Centre on Aging and Mobility, University Hospital Zurich, Waid City Hospital, and University of Zurich[3]

Introduction:
Vitamin D (VitD) is a well-recognized key player in bone and mineral metabolism and VitD supplementation has been widely attributed beneficial effects on musculoskeletal health. However, to date, the optimal supplemental dose remains controversial. In addition, the detailed effect of VitD on bone microarchitecture in humans is still largely unknown as most clinical trials use DXA to assess bone outcomes, a 2D technique that cannot resolve bone microstructure. With the advent of HR-pQCT, a promising, non-invasive imaging tool has emerged which allows for in vivo 3D characterization of human bone microstructure at a spatial resolution of 82 µm.
Therefore, the purpose of this study was to evaluate the effect of two different dosages of daily, 2-year long VitD supplementation (800 IU vs. 2000 IU) on bone microarchitecture using HR-pQCT in seniors with a special focus on seniors starting with deficient VitD levels.

Methods:
This was a 2-year randomized, double-blind clinical trial. 273 seniors aged ≥ 60 y were randomized to receive daily doses of either 2000 IU VitD (HD-group) or the standard-dose of 800 IU VitD (SD-group), and all received 500 mg calcium supplement per day. At baseline and 24 months, bone microarchitecture of the distal radius and tibia was imaged by HR-pQCT. Bone structural parameters (0m, 24m, Δ) were computed. General linear models adjusted for age, sex, BMI, baseline bone parameters, and osteoporosis category (DXA-based T-score ≥ -1 vs. DXA-based T-score < -1.0) were employed to compare bone changes over time between treatment groups. A subgroup analysis was performed in seniors starting with serum 25-hydroxycholecalciferol (25(OH)D) levels < 20 ng/ml.

Results:
195 (71%) participants (70.3±6.3 years, 51% women) had HR-pQCT parameters at baseline and 24 months and could be included into analyses. At baseline, both groups were similar with respect to mean age, sex, BMI, and serum 25(OH)D levels. After 2 years, higher 25(OH)D levels were observed in the HD-group compared to the SD-group (46.2 (standard error 0.84) vs. 37.7 (SE 0.82) ng/ml; $p \leq 0.001$). While there was no clear signal for VitD supplementation in the whole sample, we noted a beneficial effect of HD versus SD in the subgroup starting with 25(OH)D levels <20 ng/ml: Compared to the SD-group, HD-group showed a significant increase in trabecular number (ΔTb.N 0.07 (SE 0.03) vs. -0.03 (SE 0.03) 1/mm, p = 0.006) and a significant decrease in trabecular thickness (ΔTb.Th -2.3 (SE 1.08) vs. 0.77 (SE 1.17) µm, p = 0.019) and separation (ΔTb.Sp -16.7 (SE 7.29) vs. 4.9 (SE 8.14) µm, p = 0.012) at the tibia, but not at the radius. This translated into a significant increase in trabecular density (ΔTb.BMD 0.81 (SE 1.26) vs. -2.23 (SE 1.40) mg/cm^3, p = 0.048). No statistical significant differences were found in cortical parameters and total volumetric BMDs at both sites.

Conclusion:
We conclude that a high dose VitD supplementation of 2000 IU daily for 2 years compared to the standard dose might have a beneficial effect on bone microarchitecture in seniors starting with 25(OH)D levels below 20 ng/ml by enhancing the trabecular structure of the tibia. Further microfinite element analyses are necessary to determine if this translates into improved biomechanical bone properties.

5359

M. Haeberlin[1], G. Narula[2]

Automatic detection of burst-suppression-pattern in neurocritical care patients

Department of Neurology, University Hospital and University of Zurich[1], Neurointensive Care Unit, Department of Neurosurgery, University Hospital and University of Zurich[2]

Introduction:
Monitoring of a burst-suppression-pattern (BSP) in electroencephalography (EEG) is relevant to control barbiturate-induced coma. Currently, the assessment of BSP bases on continuous observation of the multi-channel EEG with manual counting of diffuse bursts per minute (BPM) by experts, which is prone to inter-rater variability.

Methods:
We evaluated the reliability of a new algorithm for automatic BSP-detection compared to manual assessment in a Thiopental-induced burst-suppressed patient for 28 hours. A bipolar 8-channel EEG-montage was recorded (256 KHz). After bandpass filtering (0.3 and 40 Hz) data was segmented into 2 secs epochs (0.1 secs overlap). For each epoch, we computed temporal covariance matrices. By the Foerstner-Moonen metric a normalized distance matrix between all epochs in the first hour was generated for conversion into a similarity matrix. Spectral Clustering allowed to cluster this matrix into 3 clusters and identified the burst cluster in one minute of training data. We labelled the rest of the (test) data with a kNN (k-nearest neighbors) classifier learned from the labels produced by clustering. The EEG was scored by a neurologist to get 38 ground truth BPM ranges (min, max for intervals of 10 minutes to 1 hour). Estimated ranges of BPM for these intervals were computed.

Results:
The pilot data shows a high correlation of automatic burst counts compared to the manual counting. We found a significant regression coefficient between estimated and ground truth BPM ranges (negative binomial regression, coefficient: 0.19, $p<0.001$). We found no significant difference between estimated and ground truth BPM ranges at a 5% level (Wilcoxon rank sum: $z = -1.595$, $p=0.11$).

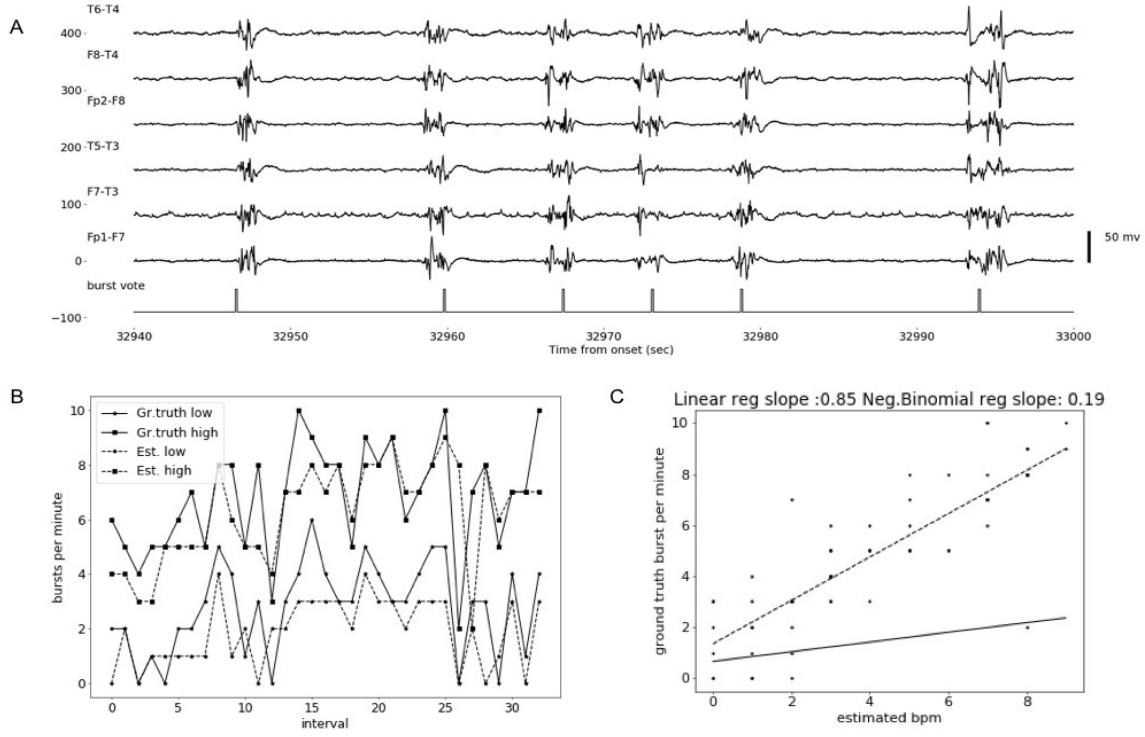

Fig 1. (A) An example EEG trace of 1 minute duration containing bursts and suppression phases. Our algorithm's vote for burst (high values) is the bottom row. (B) Low and High range values of bursts per minute in 38 different intervals of recording as scored by the physician (solid lines) and as estimated by the algorithm (dashed lines). (C) Scatter plot of the same values in one plot with linear (dashed, slope: 0.85) and negative binomial (solid, slope: 0.19) regression lines.

Conclusion:
The automatic detection of the bursts provides an objective and fast assessment of BSP. The algorithm showed a slightly lower sensitivity due to the missing detection of very short or low bursts.

5360

S. Mohammed[1], S. Costantino[1], A. Akhmedov[1], S. Ambrosini[1], G. Karsay[2], T. Luscher[3], F. Paneni[4]

Epigenetic modifications by the methyltransferase SETD7 regulate endothelial cell migration: Insights for personalized therapies in patients with diabetes and peripheral artery disease

Centre for Molecular Cardiology, University of Zurich, Zurich[1], Institute for Clinical Chemistry, University Hospital Zurich[2], Development, Royal Brompton and Harefield Hospital trust, London, Uk [3], University Heart Center, Cardiology, University Hospital Zurich, Zurich[4]

Introduction:
Peripheral artery disease (PAD) is highly prevalent in people with diabetes (DM), and associates with a high rate of limb amputation and poor prognosis. Surgical and catheter-based revascularization have failed to improve outcome in DM patients with PAD. Hence, a need exists to develop new treatment strategies able to promote blood vessel growth in the ischemic limb of DM patients. Epigenetic changes – namely DNA methylation and histone modifications - have recently shown to regulate the expression of genes involved in angiogenesis. Mono-methylation of histone 3 at lysine 4 (H3K4m1) - a specific epigenetic signature induced by the methyltransferase SETD7 – favors a chromatin conformation which enables the transcription of genes involved in endothelial inflammation and oxidative stress. The present study was designed to investigate whether SETD7-dependent epigenetic changes modulate angiogenesis in the setting of hyperglycaemia.

Methods:
Primary human aortic endothelial cells (HAECs) were exposed to normal glucose (NG, 5 mM) or high glucose (HG, 20 mM) concentrations for 48 hours. Mannitol (20 mM) was used as an osmotic control. SETD7 protein and H3K4me1 levels were investigated by Western blot and Chromatin immunoprecipitation (ChIP). Knockdown of SETD7 was achieved by small interfering RNA (siRNA) and scrambled-siRNA was used as a negative control. Pharmacological blockade of SETD7 was performed by using the highly selective inhibitor *(R)*-PFI-2, while its inactive enantiomer, *(S)*-PFI-2, was used as a control. Scratch and tube formation assays were performed to investigate the impact of SETD7 on angiogenic properties of HAECs. RNA sequencing (RNA-seq) and Ingenuity Pathway Analysis (IPA) were employed to unveil putative genes regulated by SETD7 in HAECs exposed to NG and HG. SETD7 expression was also investigated in adductor muscle specimens isolated from diabetic (*db/db*) and non-diabetic mice undergoing hindlimb ischemia for 21 days.

Results:
HG exposure in HAECs led to a time-dependent increase of both SETD7 gene and protein expression, as compared to NG. SETD7 upregulation in HG-treated HAECs was associated with an increase of H3K4me1 levels as well as with impaired endothelial cell migration and tube formation. Of interest, both gene silencing and pharmacological blockade of SETD7 rescued hyperglycemia-induced impairment of angiogenic properties in HAECs. RNA-seq in HG-treated HAECs with and without SETD7 depletion unveiled an array of differentially expressed genes, which were mainly involved in blood vessel growth and angiogenic response, as shown by IPA analysis. Among dysregulated genes, ChIP assays showed that SETD7 specifically mono-methylates H3K4m1 in proximity of Semaphorin-3G (SEMA-3G) promoter, thus regulating its expression. Finally, we show that SETD7 signaling was activated in *db/db* mice with chronic hindlimb ischemia as compared to non-diabetic animals.

Conclusion:
Our study suggests that SET7 may act as a regulator of angiogenesis in the setting of experimental diabetes. Taken together, these results may provide insights for novel epigenetic therapies to boost neovascularization in diabetic patients with PAD.

5361

C. Brühlmann[1], T. Honegger[1], D. Bächinger[1], E. Michalopoulou[2], A. Monge Naldi[1], V. Wettstein[1], S. Muff[2], B. Schuknecht[3], A. Eckhard[1]

Endotype-Phenotype Patterns in Meniere's Disease Based on Gadolinium-Enhanced MRI of the Vestibular Aqueduct

Department of Otorhinolaryngology and Head and Neck Surgery, University Hospital Zurich[1], Institute of Epidemiology, Biostatistics and Prevention, Department of Biostatistics, University of Zurich[2], Medical Radiological Institute MRI, Zurich[3]

Introduction:
Meniere's disease (MD) is a chronic inner ear disease of unknown aetiology. To date, the clinical variability of patients with MD is a major diagnostic and therapeutic challenge. In this study we established clinical imaging-based criteria to distinguish homogeneous subgroups based on two MD-specific inner ear pathologies – degeneration and hypoplasticity – of the endolymphatic sac (ES). Clinical features with special regard to audiological and vestibular function as well as anamnestic data were collected and compared. The aim was to evaluate how and to what extent these parameters correlate with the two subgroups.

Methods:
In this retrospective study, we used Gadolinium-enhanced MRI data of temporal bones of MD patients with the diagnosis of «definite Meniere's disease» (n=72) to determine the angle of the vestibular aqueduct (VA). This served as a a radiographically distinguishing marker for either ES degeneration (<120°, n=55) or hypoplasticity (>140°, n=17). Audiological, vestibular and anamnestic data were collected and statistically compared between the subgroups.

Results:
Statistical analysis of phenotypic patient subgroup characteristics revealed evidence for differences in radiographic (temporal bone abnormalities), clinical (disease laterality, average vertigo frequency, vestibular function) and epidemiological (sex distribution, family history) parameters.

Conclusion:
With this study, we set the first step to a clinical classification of patients suffering from Meniere's disease. The results showed that certain vestibular parameters as well as the gender are more common in patients with either a hypoplasticity or a degradation of the endolymphatic sac. Audiological parameter did not seem to correlate with either pathomorphological subtype. This proposed subgroup classification for MD harbors the potential for a more personalized and precise MD diagnosis, and may lead to a more individualized patient management.

5362

R. Reimann[1], S. Sorce[1], A. Chincisan[1], A. Aguzzi[1]

GPI linked protein overexpression in myoblasts

Universitätsspital Zürich[1]

Introduction:
Among the diseases of inflammatory myopathy, inclusion body myopathy (IBM) resembles a degenerative disease of skeletal muscle with the accumulation of pathological protein aggregates such as the cellular prion protein (PrP^C) or Amyloid beta. In contrast to other myopathies with T-cell rich inflammation IBM is largely unresponsive to immunotherapeutic agents and no other curative treatment exists, predisposing patients to relentlessly progressive loss of muscle strength. Insufficient understanding of the underlying pathogenesis impedes the development of effective therapeutic strategies. Towards the understanding of the degenerative pathogenesis of IBM, protein overexpression strategies of amyloidogenic proteins in transgenic animals, like amyloid-beta or the prion protein, and in transfected myocytes, have been undertaken beside genetic approaches. These model systems recapitulate some aspects of IBM, like mitochondrial dysfunction, calcium dyshomeostasis and impaired innervation by cocultured neurons.

Methods:
DNA construct of either the full-length murine Prnp gene, mCherry, NeonGreen (NG) or GFP linked to a glycosylphosphatidylinositol (GPI) anchor, where cloned into a pCAG plasmid. Murine C2C12 myoblast or CAD5 cells were co-transfected with mCherry together with one of the other plasmids. A time-course analysis was performed with the IncuCyte® live cell analysis platform at 12, 18, 24 and 30 hours after transfection. Subsequently the morphology of the cells was analysed with an in house developed MATLAB quantification tool. Additionally, cells were grown on cover-slips followed by an in-vivo staining with Annexin V.

Results:
Towards the morphological analysis of mCherry expressing myoblast we developed a MATLAB quantification tool. In order to model protein dysregulation in skeletal muscle, we transiently co-transfected C2C12 myoblast with plasmids allowing for the expression of mCherry together with either PrP^C, NeonGreen or glycosylphosphatidylinositol anchored GFP (GPI-GFP). Thereafter we performed a time-course analysis with the IncuCyte® live cell analysis platform at 12, 18, 24 and 30 hours after transfection. Upon quantification of these images, cells overexpressing PrP^C displayed decreased cell size and were significantly rounder compared to those with NG overexpression. Additionally, we found a high number of mCherry positive fragments upon PrP^C overexpression, suggestive for cellular debris. Overexpression of GPI-GFP, initially used as a control, led to a similar phenotype. Morphologically we recognized an increased number of apoptotic bodies upon PrP^C and GPI-GFP overexpression. We confirmed induction of cell death by utilizing Annexin V assay. Performing the same analysis with the murine neuroblastoma cell line CAD5, we could not observe an increase in Annexin V positive apoptotic figures open overexpression of GPI-GFP nor PrP^C.

Conclusion:
Analogous to cellular AβPP overexpression models, we performed a transient overexpression study with the GPI anchored protein PrP^C in myoblasts. We observed induction of cell death, not seen upon artificial cytoplasmatic overexpression of the protein NeonGreen. Crucial a similar overexpression of PrP^C does not have a comparable effect on the neuroblastoma cell line CAD5. In order to test if the phenotype is specific for PrP^C we additionally overexpressed GPI-GFP and recognised the same phenotype. We concluded that likely any GPI linked protein overexpressed at the cell surface of myoblast is inducing apoptosis.

5363

J. Wang[1], I. Jelcic[1], C. Münz[2], N. Toussaint[3], Y. Zhao[4], M. Sospedra[1], R. Martin[1]

Characterizing Molecular Mimicry in Peripheral Blood-Derived Autoreactive CD4+ T Cells in Multiple Sclerosis

Neuroimmunology and MS Research, Neurology Clinic, University Hospital Zurich, University Zurich[1], Institute for Experimental Immunology, University Zurich[2], NEXUS Personalized Health Technologies[3], Biometric Research Program, Division of Cancer Treatment and Diagnosis, NCI, NIH, Rockville, Maryland[4]

Introduction:
Autoreactive $CD4^+$ T cells are considered critical for the pathogenesis of multiple sclerosis (MS), and molecular mimicry between foreign and self-antigens is considered one main mechanism for their activation. However, the foreign agent/s, which may activate autoreactive T cells in MS, are not well defined, although EBV and Akkermensia have been suggested as important environmental pathogens.

Methods:
Autoreactive $CD4^+$ T cell clones (TCC) from peripheral blood of patients with MS were established by limiting dilution. TCR Vβ sequences of TCC was analyzed by DNA sequencing. An unbiased and systematic antigen search strategy, which combines testing the clone with combinatorial peptide libraries and subsequent bioinformatics analyses, was used to search target autoantigens and antigens from foreign pathogens.

Results:
In this study, we successfully generated a HLA-DR2b-restricted $CD4^+$ T cell clone (TCC), TCC14, from peripheral blood of a patient with MS. Analysis of TCR Vβ sequences of TCC14 and comparison with TCR Vβ sequences found in brain lesions of the same MS patient showed that TCC14 clonally expanded in MS brain lesions. Using the unbiased and systematic antigen search strategy, we identified RAS guanyl-releasing protein-2 (RASGRP2) as target autoantigen of TCC14. Proteomics analysis demonstrated high abundance of RASGRP2 in both proinflammatory B cells and brain. Next, the scoring matrix of TCC14 was used to score contiguous decapeptides contained in public protein database of EBV and Akkermensia. Candidate peptides were selected and synthesized. Proliferative response testing showed that TCC14 responded to both EBV- and Akkermensia-derived peptides, but their stimulatory potency is lower than $RASGRP2_{(78\text{-}87)}$.

Conclusion:
Our study supports that molecular mimicry derived from suggested environmental triggers of MS, i.e. EBV and Akkermansia, can stimulate a brain-infiltrating autoreactive $CD4^+$ T cell clone in MS.
Acknowledgements: The project is supported by ERC Advanced Grant N°340733–HLA-DR15 in MS and by the Clinical Research Priority Program MS of the University Zurich

5364

P. Helbling[1], E. Pineiro[2], R. Gerosa[1], S. Böttcher[1], F. Al-Sharour[2], M. Manz[1], C. Nombela-Arrieta[1]

Transcriptomic profiling reveals dynamic functional remodeling of the bone marrow microenvironment during postnatal development, aging, and inflammation

Department of Medical Oncology and Hematology, University of Zurich and University Hospital Zürich[1], Bioinformatics Unit, Spanish National Cancer Research Center, Madrid (Spain)[2]

Introduction:
Stromal components are not only fundamental structural constituents of the bone marrow (BM), but they also provide extrinsic cues to critically regulate the hematopoietic system and support its maintenance and adaptation to external stress. Vital stromal-hematopoietic interactions in defined niches regulate many levels of hematopoiesis, from hematopoietic stem cell (HSC) maintenance, to lineage differentiation and maturation. The identity and function of hematopoiesis-regulating BM stromal cells has been best studied in homeostasis. Nonetheless, the dynamic changes in composition, function, and molecular identity that BM stromal cells undergo during homeostatic aging as well as in inflammatory settings, and how these relate to alterations in hematopoietic output, are poorly understood.

Methods:
We performed a transcriptome-wide gene expression analysis (RNA-seq) of four murine mesenchymal and vascular BM cell populations, which together comprise the majority of the known medullary stroma, namely CXCL12-abundant reticular cells (CARc), PαS cells, sinusoidal endothelial cells (SECs), and arterial endothelial cells (AECs).

Results:
To obtain a comprehensive view of stromal adaptations during the normal life span and during inflammation, we profiled cells isolated from 2 weeks, 2 months and 2 years old mice, as well as mice stimulated with bacterial and viral infection-mimicking agents (LPS and poly I:C). Using this global dataset, we report that: i) molecular fingerprints inform on potentially novel stromal cell-specific functional features and define identity markers for the investigation of topographical distribution and cellular interactions *in situ* ii) major remodeling of the transcriptional landscape occurs in the transition from post-natal to adult period, when HSC proliferation is known to drop sharply iii) aging leads to a predominant upregulation of pro-inflammatory gene expression iv) inflammatory stimuli trigger massive and pathogen-specific adaptations in the transcriptome of all cell types analyzed v) convergent gene-expression programs exist in aging and inflammation, which partially explain aging-driven alterations in BM hematopoietic function.

Conclusion:
In summary, we characterized in depth the molecular profiles of four critical BM stromal cell types at various developmental stages and in inflammatory conditions on the population level.

5365

M. Hohmann[2], T. Ludersdorfer[2], P. Englezou[3], M. Docampo[2], C. Sellés-Moreno[2], J. Goede[4], J. Deuel[5], F. Guffanti[6], M. Broggini[6], E. Scanziani[7], M. Sospedra[1], R. Martin[1], A. Lutterotti[1]

Characterization of Myelin Peptide-Coupled Red Blood Cells

Department of Neurology, University Hospital Zurich[1], Wyss Zurich, University of Zurich / ETH Zurich[2], Division of Molecular Hematology, Lund University, Lund, Sweden[3], Department of Haematology, Kantonsspital Winterthur[4], Division of Hematology, University of Zurich[5], Department of Oncology, IRCCS-Istituto di Ricerche Farmacologiche "Mario Negri", Milano, Italy[6], Department of Veterinary Medicine, University of Milano, Italy[7]

Introduction:
The development of safer and more efficient immune therapies remains an important unmet medical need in patients with autoimmune diseases. Induction of antigen-specific immune tolerance can be achieved via injection of cells chemically coupled with target antigens. Preclinical studies with peptide-coupled splenocytes have suggested „cross-tolerance" as the main mechanism of action for inducing tolerance (1), whereby peptide-coupled cells undergo apoptosis and are processed by macrophages in the spleen to represent the antigens in a tolerogenic way. Much less is known using peptide-coupled red blood cells (RBCs) instead of peptide coupled splenocytes.
Objectives of this project are to analyze the effects of the coupling procedure on RBCs *in vitro* and investigate the biodistribution of peptide-coupled RBCs *in vivo*.

Methods:
To determine the coupling effiency of the coupling agent ethylcarbodiimide (EDC) a fluorescently labelled peptide was coupled on the cell surface of RBCs and detected via fluorescence-activated cell sorting (FACS) as well as fluorescence microscopy analysis. Ektacytometry and electron microscopy analysis of the EDC-treated RBCs were performed to analyze potential EDC induced morphological changes. Finally, we injected RBCs coupled with fluorescently labelled peptides intravenously into BALB/c mice to analyze the biodistribution by bioluminiscence imaging.

Results:
Treatment with the cross-linker ethylcarbodiimide (EDC) led to a reduced deformability of peptide-coupled RBCs as observed by ektacytometry. Electron microscopy analysis revealed only minor morphological changes following treatment with EDC.
In addition, coupling of RBCs initiates physiological changes such as a rapid influx of cytosolic calcium and phosphatidylserine exposure, both hallmarks of programmed cell death in RBCs, called eryptosis.
Both deformability and morphological changes of peptide-coupled RBCs appear to influence the *in vivo* biodistribution and direct these cells to specific organs. To identify the cellular origin involved in the uptake of peptide-coupled RBCs, we injected fluorescently-labelled peptides coupled to RBCs intravenously in BALB/c mice and analysed the biodistribution, both *in vivo* and *ex vivo*.
Bioluminiscence imaging data indicates the liver as one of the major organs involved in the uptake of peptide-coupled RBCs. Histological analysis confirmed the aforementioned findings, demonstrating uptake of peptide-coupled RBCs by liver macrophages/Kupffer cells.

Conclusion:
RBCs exhibit hallmark characteristics of eryptosis following peptide coupling and these are efficiently taken up by macrophages/Kupffer cells in the liver following their intravenous administration.

1: Miller SD et al, Nat Rev Immunol 2007.

5366

D. Spiess[1], M. Oufir[2], O. Potterat[2], M. Hamburger[2], A.P. Simões-Wüst[1]

Optimization of an in vitro model of the placental barrier using BeWo b30 cells for permeability studies

Department of Obstetrics, University Hospital Zurich[1],
Division of Pharmaceutical Biology, University of Basel, Basel[2]

Introduction:
Knowledge of fetal exposure to exogenous compounds is crucial for the fetal risk assessment. Since clinical trials in pregnant women are challenging due to obvious ethical reasons, transplacental transport of compounds has to be studied in different models. *In vivo* models with pregnant animals are available, but extrapolation of results to humans is difficult because of large interspecies differences. A non-invasive *ex vivo* model, such as the human placental perfusion, is an alternative for such validation and is currently in use at the University Hospital Zurich. This model mimics the *in vivo* conditions the best. However, a full-term placenta is used, which is not fully representative of the situation during the first trimester. To better understand how substances are being transported across the placenta the *ex vivo* placental perfusion model should be complemented with *in vitro* studies. A cell-based *in vitro* permeability model, using the Transwell system was therefore optimized. The major aim of this optimization was to find a commercially available insert that allows obtaining the highest transepithelial electrical resistance (TEER) values stable enough to perform permeability experiments in the shortest period of time.

Methods:
The BeWo (clone b30) choriocarcinoma cell line, whose morphology and biochemistry is similar to those of human trophoblasts, was used for all experiments. The cells were cultured on permeable tissue culture inserts (24-well format). Cell culture medium (0.3 mL apical compartment, 1.0 mL basolateral compartment) was replaced until the cells were confluent to form a monolayer. Formation of a monolayer with tight junctions was verified by recording TEER and cell layer capacitance (C_{CI}) using a cellZscope+®. TEER values were considered stable if they did not vary more than 1% during 2 h. For the optimization of the Transwell system, tissue culture inserts from several manufacturers (Corning Transwell, Corning Falcon, Greiner Bio-One and Millipore) with different properties (optics, material, pore size) were screened. Additionally, the influence of coating (human placental collagen type 4) and cell seeding density was investigated.

Results:
The tested inserts behaved very different regarding their maximal TEER value. In general, translucent inserts were not able to reach as high stable TEER values as the transparent ones. The most suitable insert for permeability studies with BeWo b30 cell line were from Greiner Bio-One (0.336 cm^2 insert growth area, transparent PET membrane, 0.4 µm pore size) that enabled attaining a mean stable TEER value of 86.31± 12.61 $\Omega \cdot cm^2$ in 90.4 ± 18.8 hours (~4 days). Preliminary experiments suggested that neither human placental collagen coating of the insert nor high cell seeding density result in markedly higher TEER values.

Conclusion:
ThinCert™(Greiner bio-one) 24 well inserts (cat. N° 662641) were selected for future permeability studies with BeWo cells and different test compounds. The screening has shown that Transwell inserts from different manufacturers can lead to results with high variations in TEER values. This makes a comparison of absolute TEER values difficult among different research groups. The optimization of the *in vitro* BeWo model is a critical step before predicting placental apparent permeability coefficients of compounds.

5367

V. Ginde[1], A. Ulusoy[2], C. Moreira[1], L. Jakobi[2], D. Di Monte[2], C. Baumann[1], D. Noain[1]

Effect of slow-wave sleep modulation over α-synuclein spreading in a AAV rat model of spreading of synuclein pathology

Department of Neurology, University Hospital of Zurich, University of Zurich.[1], German Center for Neurodegenerative Diseases (DZNE), Bonn, Germany[2]

Introduction:
Parkinson Disease (PD), the second most common human neurodegenerative disease, is characterized by the presence of intraneuronal proteinaceous inclusions containing α-synuclein. α-Synuclein possesses two pathological properties, i.e. the ability to aggregate and the property to spread from neuron to neuron and, thus, advance from one brain region to others. PD patients suffer from sleep-wake disturbances that may be related, at least partially, to pathological accumulation of α-synuclein in discrete brain regions. Recent research has suggested a role of sleep on amyloid-β plaque burden in Alzheimer Disease. Moreover, clearance of extracellular waste products through the glymphatic pathway has been proposed to occur during deep sleep, perhaps preventing brain accumulation of amyloid proteins. Furthermore, we have shown a positive effect of slow-wave sleep (SWS) enhancement in a transgenic mouse model of PD (VMAT2 LO), evidencing reduced accumulation of phosphorylated α-synuclein in prefrontal cortex of Xyrem®-treated mice compared to non-SWS enhanced ones. Here, our goal is to investigate mechanisms behind the reduction of α-synuclein accumulation after SWS enhancement. We hypothesize that increased SWS delta power (i.e. depth of sleep) enhances clearance of extracellular pathological α-synuclein through the glymphatic pathway by activating aquaporin-4 (AQP4) water channels. If so, increased SWS delta power would be expected to prevent neuron-to-neuron transfer and spreading of α-synuclein. To test this hypothesis, we will explore in our experiments the effect of sleep on the level/extent of human-α-synuclein spreading in a model of protein transmission triggered by targeted overexpression of human α-synuclein in the lower brainstem of rats.

Methods:
We implanted electroencephalogram/electromyogram (EEG/EMG) electrodes in a rats injected in their vagal nerves with AAV-human-α-synuclein, an experimental model of α-synuclein spreading (Ulusoy et al., 2013). Two weeks post-surgery (wps) we performed 24-hours baseline EEG/EMG recordings followed by two other EEG/EMG recordings at 7 and 11 wps. Currently, we are performing sleep modulation treatments with Xyrem® (400mg/kg, per os) and placebo after baseline recording and during 10 weeks. After perfusions, we will assess viral transduction in the pons and caudorostral spreading of a-synuclein pathology. The EEG/EMG data will provide insights on the changes in slow wave activity (SWA), and help to draw a correlation to the a-synuclein transduction and spreading. Other key outcomes, such as changes in slow wave energy and fragmentation, are being analyzed.

Results:
We expect to observe reduced human-α-synuclein spreading in Xyrem®-treated SWS-enhanced rats when compared to placebo-treated ones. Preliminary results show that SWA is slightly increased during most of the light period in Xyrem-treated animals and fairly unaffected during the dark period, whilst keeping the same amount of total sleep per 24 hours. Promisingly, these few animals presented reduced α-synuclein spreading in the pons, corroborating a correlation between steady and extended increase in deep sleep and improvements on a-synuclein pathology.

Conclusion:
We are currently executing these experiments. We will present preliminary results and conclusions in the 18th clinical research day at University hospital of Zürich, in April 2019.

5368

T. Skaria[1], E. Bachli[2], G. Schoedon[1]

RSPO3 impairs barrier function of human vascular endothelial monolayers and synergizes with pro-inflammatory IL-1

Medicine, University Hospital Zurich, Zurich[1], Medical Clinic, Uster Hospital, Uster[2]

Introduction:
Endothelial barrier dysfunction characterized by hyperpermeability of the vascular endothelium is a key factor in the pathogenesis of chronic inflammatory diseases and affects clinical outcomes. In states of chronic inflammation, mediators secreted by activated immune cells or vascular endothelium may affect the barrier function and permeability of the vascular endothelium. The matricellular R-spondin family member RSPO3 is produced by inflammatory-activated human monocytes and vascular endothelial cells, but its effects in the regulation of vascular endothelial barrier function remains elusive.

Methods:
The present study investigates the effects of RSPO3 on the barrier function of adult human primary macro- and micro- vascular endothelial monolayers. Tight monolayers of primary endothelial cells from human coronary and pulmonary arteries, and cardiac, brain, and dermal microvascular beds were treated with RSPO3 either alone or in combination with pro-inflammatory mediator IL-1β. Endothelial barrier function was assessed non-invasively in real-time using Electric Cell-substrate Impedance Sensing.

Results:
RSPO3 treatment critically affected barrier function by enhancing the permeability of all vascular endothelial monolayers investigated. To confer hyperpermeable phenotype in vascular endothelial monolayers, RSPO3 induced inter-endothelial gap formation by disrupting the β-catenin and VE-cadherin alignment at adherens junctions. RSPO3 synergistically enhanced the barrier impairing properties of the pro-inflammatory mediator IL-1β.

Conclusion:
Here, we show that the matricellular protein RSPO3 is a mediator of endothelial hyperpermeability that can act in synergy with the inflammatory mediator IL-1β. This finding stimulates further studies to delineate the endothelial barrier impairing properties of RSPO3 and its synergistic interaction with IL-1β in chronic inflammatory diseases.

5369

M. Wildschut[1], M. Van Oostrum[2], P. Schürch[1], T. Wilhelm[3], M. Huber[3], B. Wollscheid[2], A. Theocharides[1]

The Consequence of CALR Mutations on Proteostasis in Myeloproliferative Neoplasms

Experimental Hematology, University Hospital Zürich[1], Institute of Molecular Systems Biology, ETH Zürich[2], Institute of Biochemistry and Molecular Immunology, University Clinic RWTH Aachen University, Germany[3]

Introduction:
Myeloproliferative neoplasms (MPN) are a family of hematopoietic stem cell disorders characterized by disease-driving mutations in *JAK2*, *MPL*, and Calreticulin (*CALR*). Whereas JAK2 and MPL represent the families of tyrosine kinases and cytokine receptors, to which various oncogenes belong, CALR is best known as an endoplasmic reticulum (ER)-resident chaperone involved in glycoprotein folding. Mutant CALR gains ability to activate JAK/STAT signaling, while loss of CALR chaperone client MPO in *CALR*-mutated MPN patients could indicate a loss of chaperone function.

Methods:
To elucidate loss and gain of function effects of CALR chaperone mutations and their relevance for driving disease, an integrative proteomics-based approach was utilized. The approach integrated a cohort of *CALR*-mutated and *CALR*-wild type MPN patient samples and healthy donor samples, and a panel of parental and CRISPRed *CALR* mutant or knockout (KO) cell lines.

Results:
In this study, proteomics analyses on CRISPRed cells showed significantly affected proteostasis upon either mutation or KO of the CALR chaperone. A highly interacting network of ER stress chaperone proteins was consistently upregulated across *CALR* mutants and knockouts, indicating a loss of function effect of *CALR* mutation. Additional experiments validated deregulation of these ER chaperones, showed compensatory effects upon their inhibition, and indicated involvement of the ATF6 unfolded protein response (UPR) transcription factor. Finally, first proteomic analyses on MPN patient granulocytes validated ER chaperone upregulation, providing proof for validity and relevance of the CRISPRed cell line models for discovering translationally relevant effects.

Conclusion:
Our current data thus indicates a loss of CALR chaperone function and compensating upregulation of alternative ER chaperones. Analyzing an increasing number of MPN patient proteomes will enable further comparisons and discovery of deregulation of pathways and CALR chaperone client proteins and their relevance for MPN disease pathogenesis and development.

5370

R. Myburgh[1], J. Kiefer[2], N. Russkamp[1], A. Simonis[1], S. Pfister[1], C. Magnani[1], C. Wilk[1], A. Müller[1], M. Van den Broek[3], B. Becher[3], D. Neri[2], M. Manz[1]

Anti-Human CD117 CAR T-Cells Efficiently Eliminate Hematopoietic Stem and CD117-Positive AML Cells

Department of Medical Oncology and Hematology, University of Zurich and University Hospital Zürich[1], ETH Zurich, Department of Chemistry and Applied Biosciences[2], University of Zuerich, Institute of experimental immunology, Zuerich[3]

Introduction:
Acute Myeloid Leukemia (AML) originates from immature hematopoietic stem and progenitor cells (HSPC). While some AML are curable, disease relapse occurs in most of patients upon application of current standard chemotherapy approaches. Recently, eradication of leukemia or lymphoma cells by immunologically targeting lineage specific surface antigens (e.g. CD20, CD19, BCMA) has been achieved. To date, however, the search for AML-specific surface antigens has remained largely elusive. We thus propose in a proof of concept to target the HSPC antigen c-Kit (CD117) expressed by healthy HSPC as wells as by leukemic blasts in >90% of AML patients with CD117 specific CAR T cells, terminate the response, and subsequently conduct healthy/allogeneic HSC transplantation.

Methods:
We generated a lentiviral vector which incorporates the anti-CD117 CAR followed by a T2A ribosomal skip sequence and RQR8 as selection marker and depletion gene. Human CD117 was cloned in human CD117 negative HL-60 AML cells and cell lines with stable expression of CD117 at various levels were derived from these.

Results:
T-cells were isolated from healthy donors or AML patients in complete remission, respectively, and exhibited sustained growth after activation with recombinant human IL-2 and CD3/CD28 beads. In vitro, CAR T-cells eliminated more than 90% of $CD117^{high}$ leukemia cell lines within 24 hours at effector-to target ratios (E:T) of 4:1 and 1:1 and more than 50% at E:T of 1:4. CAR-mediated cytotoxicity correlated with levels of CD117 surface expression as the elimination of $CD117^{low}$ target cells was less efficient compared to $CD117^{high}$ and $CD117^{intermediate}$ cells. With primary cells, anti-CD117 CAR T-cells effectively depleted >90% of $lin^{-}CD117^{+}CD34^{+}CD38^{+}$ and >70% of $lin^{-}CD117^{+}CD34^{+}CD38^{-}$ cells from healthy bone marrow in vitro. Similarly, >70% of patient derived leukemic blasts were eliminated by autologous anti-CD117 CAR T-cells. To determine effectivity of anti-human CD117 CAR T-cells in vivo, humanized mice were engrafted with umbilical cord blood $CD34^{+}$ cells. A single injection of $2x10^{6}$ anti-CD117 CAR T-cells resulted in >90% depletion of $CD117^{+}$ cells in the bone marrow within 6 days. Finally, humanized mice transplanted with primary $CD117^{+}$ AML were treated with patient-derived autologous CAR T-cells. At 6 weeks after injection of CAR T-cells, >98% of hu-CD45 $CD117^{+}$ cells were depleted in the bone.

Conclusion:
We provide proof of concept for the generation of highly-potent CAR T-cells re-directed against CD117 from healthy human donors and AML patients. Strategies for the complete elimination of CAR T-cells are required before translation of this approach to the clinical setting.

5371

A. Jomard[5], O. Chavez-Talavera[6], A. Tailleux[6], P. Doytcheva[4], M. Bueter[3], A. Taheri[4], C. Wolfrum[5], T. Lutz[4], A. Von Eckardstein[1], F. Ruschitzka[2], B. Staels[6], E. Osto[1]

The Functional Relevance of Bile Acids in the Improvement of HDL-mediated Endothelial Protection After Bariatric Surgery

Institute of Clinical Chemistry, University Hospital of Zurich[1], Heart Center Zurich, University Hospital of Zurich[2], Department of Surgery & Transplantation, University Hospital of Zurich[3], Institute of Veterinary Physiology, University of Zurich and Zurich Center for Integrative Human Physiology (ZIHP)[4], Laboratory of Translational Nutrition Biology, IFNH, ETH Zurich[5], Universite Lille, Inserm, CHU and Institut Pasteur de Lille, Lille, France[6]

Introduction:
Roux-en-Y gastric bypass (RYGB) reduces cardiovascular mortality. We have previously shown that high density lipoproteins (HDL)-mediated vasoprotection is improved early after RYGB. Bile acids (BA) are signaling molecules increasingly recognized as regulators of cardio-metabolic homeostasis. BAs circulate in blood bound mainly to albumin, and in a lesser extent to HDL. The signaling role of HDL-bound BAs (HDL-BAs) is unknown, but we hypothesize that HDL could act as a vehicles, facilitating BAs delivery directly to endothelial cells where they could regulate vaso-protection properties. Circulating BAs systematically increase upon RYGB, and are candidates to contribute to the early and weight-loss independent metabolic improvements after surgery. Whether RYGB alters HDL-BAs and their role on the improved HDL vasoprotection is unknown. **Purpose:** We studied whether RYGB changes the composition of HDL-BA and their contribution to the RYGB-improvement of HDL vaso-protective properties.

Methods:
HDL were isolated by ultracentrifugation from 29 morbidly obese patients before and 1 year after RYGB. The HDL-BA composition was determined by liquid chromatography-mass spectrometry (LC/MS-MS) and the HDL vaso-protective properties were evaluated *ex-vivo* in human aortic endothelial cells (HAEC). Moreover, the size and abundance of HDL particles were determined by NMR spectroscopy in plasma.

Results:
Interestingly, the expected increase in total BA concentrations in plasma observed 1 year after RYGB also translated in higher concentration (up to 25%) of BA bound to HDL. Moreover, obesity-induced HDL dysfunction was reversed postoperatively, restoring HDL-mediated endothelial NO production, anti-apoptotic effects and cholesterol efflux capacity. The size-function analyses showed post-operatively a shift towards larger HDL. After RYGB there was a remodeling of BA bound to HDL, which are either agonists of the endothelial nuclear farnesoid X receptor (FXR), e.g. chenodeoxy-CA (CDCA), cholic acid (CA) and or for the membrane TGR5 receptor, e.g. deoxy-CA (DCA). The composition-function analysis revealed that among all BA subclasses present on HDL, the specific enrichment of CA and CDCA bound to HDL correlated with improved HDL's endothelial anti-apoptotic capacity (R -0.52, p=0.006 for CA-HDL and R -0.35, p=0.07 for CDCA-HDL). Further, exogenous loading of CA onto native HDL isolated from human serum significantly enhanced their endothelial anti-apoptotic function. This suggests that a crucial interaction between endothelial cells and BA may underlie the improved HDL functionality after RYGB.

Conclusion:
RYGB achieves a dual benefit by first increasing the concentration and second improving the function of HDL. One year after RYGB, higher amounts of BA bound to HDL may mediate HDL’s improved endothelial-protective effects via enhanced endothelial activation of FXR and TGR5.

5372

I. Iskender[1], S. Arni[1], T. Maeyashiki[1], N. Citak[1], M. Canic[2], S. Paal[3], T. Frauenfelder[4], I. Opitz[1], W. Weder[1], I. Inci[1]

Warm versus cold ischemic donor lung injuries activate distinct pathophysiological responses during ex vivo lung perfusion

Thoracic Surgery, University Hospital Zurich, Zurich[1], Surgical Research, University Hospital Zurich, Zurich[2], Cardiovascular Surgery, University Hospital Zurich, Zurich[3], Radiology, University Hospital Zurich, Zurich[4]

Introduction:
Outcomes of lung donation after circulatory death are comparable with standard brain-dead donors in lung transplantation. However, post-transplant inflammatory profiling between warm (WI) and cold ischemic (CI) donor lung injuries have been shown to be different in rats. In this study, we have looked at the post-reperfusion pathophysiology between WI and CI donor lung injuries in a large animal ex vivo lung perfusion (EVLP) model.

Methods:
Domestic female pigs were subjected to a cardiac death with administration of potassium chloride and left at room temperature for 2 hours followed by lung retrieval in the WI group. Donor lungs were preserved for 24 hours at 4 ° C after flushing with Perfadex in the CI group (n=6,each). EVLP was then performed for 6 hours according to the Toronto protocol. EVLP physiology, perfusate biochemistry and inflammatory responses were assessed.

Results:
Pulmonary vascular resistance was significantly higher in CI lungs throughout EVLP. Elevated potassium ion concentration and lactate production in perfusate were the distinct biochemical features observed in WI lungs. Interestingly, perfusate inflammatory response determined by IL-6, IL-8, IL-1β, and IL-18 were markedly higher in the CI group when compared to the WI.

Conclusion:
EVLP simulates ischemia-reperfusion injury. In this large animal model, warm versus cold ischemic donor lung injuries differ not only for inflammation but also for pulmonary vascular pressure and perfusate biochemistry. Alternative treatment strategies should be developed based on the underlying mechanisms of donor injuries to salvage more donor lungs for transplantation.

5373

K. Frauenknecht[1], M. Emmenegger[1], A. Chincisan[1], A. Aguzzi[1]

Incidence of naturally occurring anti-TREM2-antibodies in a large hospital cohort

Institute of Neuropathology, University Hospital of Zurich[1]

Introduction:
Microglia are essential for optimal function of the central nervous system (CNS) during health and disease. Many neurological diseases are accompanied by neuroinflammatory changes with the activation or dysfunction of microglia. A key feature of microglial function is the triggering receptor expressed on myeloid cells (TREM) 2. TREM2 could serve as a suitable therapeutic target for monoclonal antibodies by either blocking or accelerating TREM2 activation. Monoclonal antibody-based drugs have revolutionized the treatment of many disease. However, when translating into human therapy, mouse or phage-derived or even humanized antibodies often provide an unfavorably safety profile.

Methods:
To overcome this problem, we proposed to screen 20'000 patients for naturally occurring autoantibodies against TREM2 using a fully automated high-throughput microELISA platform.

Results:
Here we present the results from screening 17'145 patients for anti-TREM2 antibodies. Highly reactive samples were observed in 0.05 % of the patients tested (n = 8; 4 male and 4 female), these patients were older than patients with lower reactivity (high anti-TREM2: mean age: 64.57 ± 13.31; median age: 67 vs low anti-TREM2: mean age: 54.89 ± 17.78, median age: 55). Gender had no significant effect on anti-TREM2 reactivity. There was no specific disease associated with higher anti-TREM2 reactivity.

Conclusion:
Our preliminary results do not explicitly point to disease-causing effects by naturally occurring anti-TREM2 antibodies suggesting a favorable safety profile of naturally occurring anti-TREM2 antibodies. In summary, we were able to identify a small subset of carriers of anti-TREM2 antibodies in a large hospital cohort. The extraction and biobanking of PBMCs from high reactive patients will allow us subsequent cloning of anti-TREM2 antibodies. Further studies will be conducted to evaluate the function of these antibodies in vitro and in vivo.

5374

V. Lysenko[1], N. Wildner[1], K. Zimmermann[1], P. Schürch[1], C. Fritz[2], R. Flavell[4], P. Wild[3], S. Dirnhofer[5], M. Manz[1], A. Theocharides[1]

Enhanced support of myelofibrosis stem cells in next generation humanized mice

Division of Hematology, University and University Hospital Zurich[1], Institute of Pathology and Molecular Pathology, University Hospital Zurich[2], Dr. Senckenberg Institute of Pathology, University Hospital Frankfurt, Frankfurt am Main, Germany[3], Department of Immunobiology, Yale University, New Haven, Connecticut, USA[4], Institute of Pathology, University Hospital, University of Basel[5]

Introduction:
Pre-clinical patient-derived xenograft (PDX) mouse models have emerged as powerful tools for investigating normal and leukemic stem cells (HSCs and LSCs). Successful development of PDX models for aggressive neoplasms, such as acute leukemias, has been achieved. However, engraftment of less-aggressive neoplasms in PDX models is poor. Myelofibrosis (MF) is a chronic HSC disorder predominantly characterized by an expansion of myeloid cells followed by constant deposition of fibers in the bone marrow (BM) and transformation into AML depending on the clonal evolution of MF stem cells (MF SCs). We hypothesized that the constitutive expression of human cytokines and growth factors in humanized mice may provide a supportive microenvironment for MF SC development and could faithfully recapitulate disease phenotype and genetic heterogeneity allowing the development of a pre-clinical MF PDX model.

Methods:
Purified peripheral blood (PB) stem and progenitor (CD34+) cells from 13 MF patients were transplanted intra-hepatically into sub-lethally irradiated newborn MISTRG mice and NSG mice (controls). For secondary transplantations, human CD45+ cells purified from primary animals were transplanted intra-hepatically. Mice were sacrificed after 5-26 weeks and characterized by flow cytometry, immunohistochemistry and mutational profiling.

Results:
The total median human engraftment was significantly higher in the BM (29.20% vs 4.175%, $p<0.0001$), the PB (48.70% vs. 0.73%, $p<0.0001$) and the spleen (8.19% vs. 0.33%, $p<0.0001$) of MISTRG compared to NSG mice. Overall, the human BM engraftment (more than 2% human CD45 (hCD45)) was observed in all MISTRG mice (49/49, 100%) and 57.5% of NSG mice (23/40). MISTRG mice exhibited superior engraftment independent of risk categories (DIPSS, MIPSS70 and MYSEC), disease stage (chronic, accelerated) and diagnoses (primary, secondary MF). Both NSG and MISTRG mice supported substantial human myeloid (CD33+) engraftment in the BM, PB and spleen. In the BM of both mouse strains, there was an expansion of monocytes and granulocytes in the myeloid compartment. A higher percentage of monocytes to granulocytes was observed in the PB of NSG ($p=0.0044$) and MISTRG ($p<0.0001$) mice, while in the spleen, the ratio was higher for only MISTRG ($p=0.0254$) mice. Next, we characterized the CD34+ hematopoietic stem and progenitor cell compartment. Although, both NSG and MISTRG mice supported an expansion of human CD34 (hCD34) cells out of the hCD45 cell fraction (10.76% vs. 11.07%, $p=0.5640$), MISTRG mice supported higher engraftment of hCD34 cells out of all the cells (1.044% vs. 2.375, $p=0.0168$). Furthermore, immunohistochemistry revealed human megakaryocytic differentiation in both strains and reticulin fibers (Gömöri) only in 16.7% (3/18) of MISTRG mice. Since fibrosis is a timely process, we focused on mice that were analyzed after an extended period. Reticulin fibers were detected in 50% (3/6) of MISTRG mice observed over 16 weeks. To determine whether the engrafted human cells were derived from the MF clone, next generation sequencing comparing the mutational profile of primary samples to their corresponding engrafted xenografts was performed. This data showed maintenance of the original clonal composition in the xenografts. Finally, purified human MF cells isolated from primary mice showed significant myeloid reconstitution in secondary recipients.

Conclusion:
Overall, these results show that MISTRG mice support robust engraftment of MF SCs and are able to maintain repopulation capacity and the genetic heterogeneity found in patients. The MF PDX model will further be used to understand the disease pathogenesis and assess established and novel therapeutic agents in order to expedite their transition into clinical trials.

5375

D. Kreul[1], R. Kubik-Huch[1], J. Froehlich[2], M. Thali[3], T. Niemann[1]

Dual energy computed tomography with multiparametric mapping of parenchymatous organs: Normal distribution in a 12-month cohort.

Institute of Radiology, Kantonsspital Baden[1], Guerbet AG, Zürich[2], Institute of Forensic Medicine, Zurich[3]

Introduction:
The use of dual-energy computed tomography (DECT) has increased over the past years, allowing for several new applications for material and tissue characterization as well as organ assessment based on two different X-ray spectra.
The aim of this study was to retrospectively evaluate a 12-month cohort of DECT acquisitions of the abdomen of patients referred in a standardized clinical routine setting to establish a multiparametric normal distribution of different the parameters.

Methods:
500 DECT were included in the study. Each patient was examined using a standardized DECT-protocol to create unenhanced and enhanced acquisitions. For DE analysis syngo.via (Siemens Healthineers) was used.
Organ density in Hounsfield Units (HU), fat fraction, and ϱ/Z were measured standardized by placing ROIs (region of interest) of at least 0.5 cm2 (Fig. 1-3). Only mixed dual-energy reconstructions (based on the two different tube voltages) were used for measurements. Between two and six ROIs were placed in each organ. Included in the examination were liver, spleen, kidneys, muscle and fat tissue. A mean value for each tissue in each patient was estimated and transferred to the software IBM SPSS Statistics. All values were tested for normality, variance homogeneity and significance.

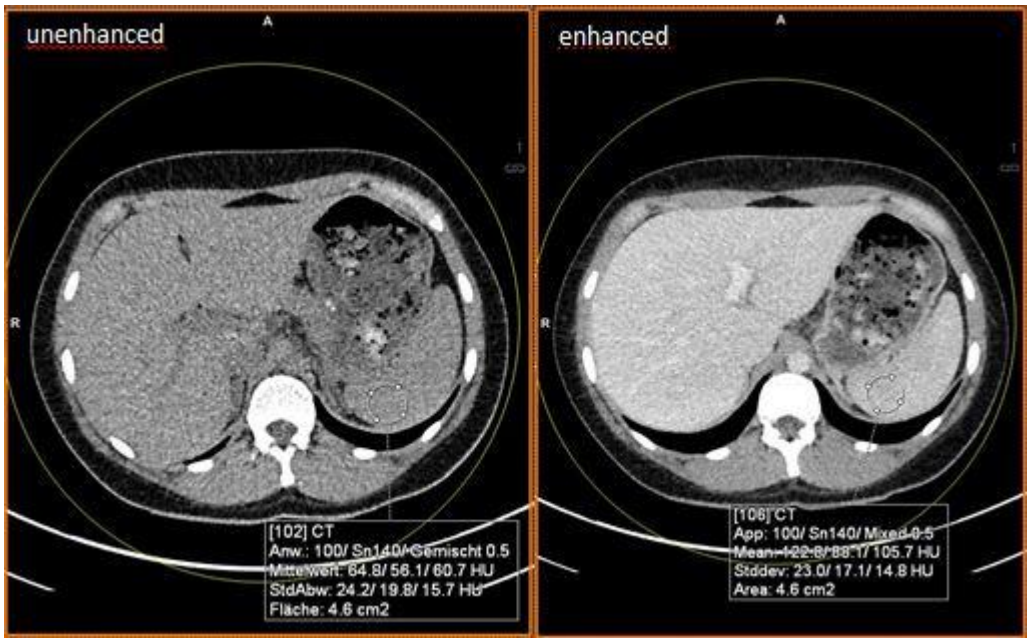

Fig. 1: Measurements of HU in the spleen

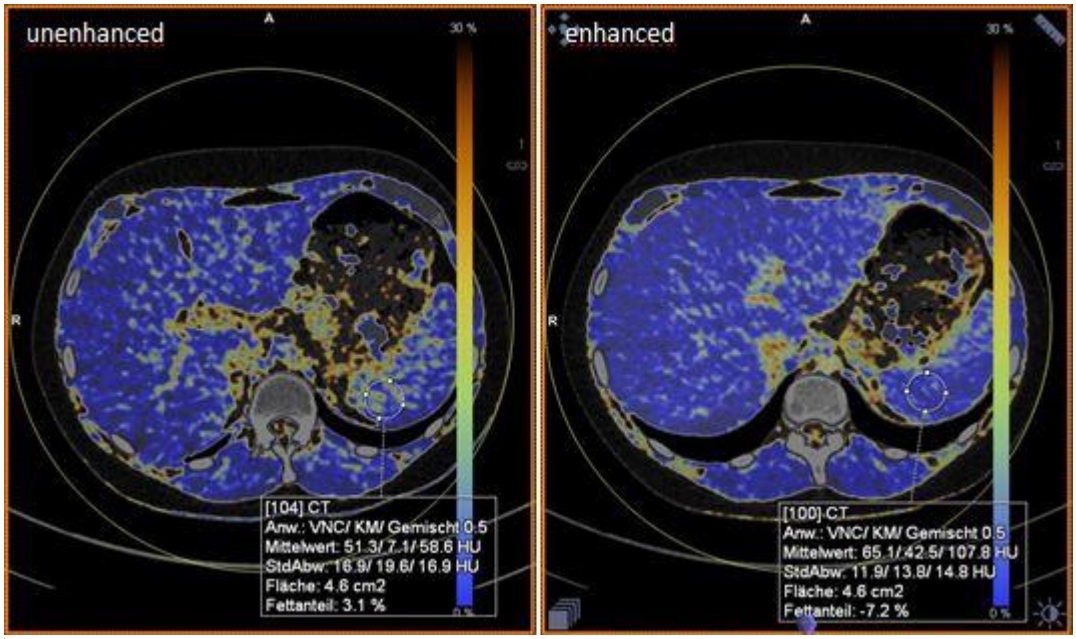

Fig. 2: Measurements of fat content in the spleen

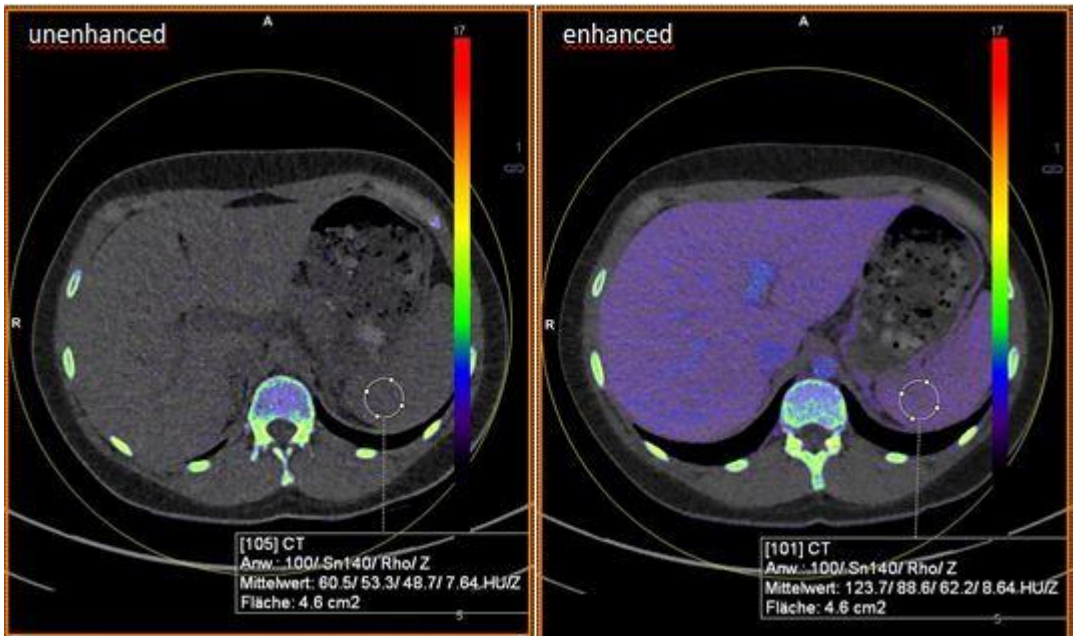

Fig. 1: Measurements of ϱ and Z in the spleen

Results:
In the following the mean values and standard deviations of the respective tissues in unenhanced DECT are given (Table1).
HU: liver 59.74 (±7.74); spleen 55.34 (±3.29); kidneys 37.38 (±4.36); muscle 55.57 (±5.72);fat tissue -103.14 (±5.58). Kidneys, fat tissue and liver differentiate significantly from every other organ (p<.001). No significant difference between spleen – muscle (p=1.0).
ϱ : liver 59.78 (±7.20); spleen 54.35 (±4.21); kidneys 32.57 (±3.87); muscle 56.33 (±6.23);fat tissue -71.01 (±4.64). Kidneys and fat tissue differentiate significantly from every other organ (p<.001). No significant difference between spleen – muscle (p=.160) and muscle – liver (p=.093).
Z: liver 7.35 (±0.11); spleen 7.39 (±0.10); kidneys 7.49 (±0.18); muscle 7.32 (±0.19); fat tissue 5.56 (±0.30). Kidneys and fat tissue differentiate significantly from every other organ (p < .001). No

significant difference between muscle – liver (p=1.0), muscle – spleen (p=.056) and liver – spleen (p=.275).
Percentage of fat: liver -5.14 (±5.60); spleen -1.51 (±3.37); kidneys 11.77 (±5.28); muscle -5.75 (±5.49); fat tissue 95.93 (±4.15). Kidneys, spleen and fat tissue differentiate significantly from every other organ (p < .001). No significant difference between muscle – liver (p=1.0).
In the following the mean values and standard deviations of the respective tissues in enhanced DECT are given.
HU: liver 96.14 (±15.77); spleen 98.08 (±10.56); kidneys 146.52 (±23.70); muscle 61.21 (±8.90); fat tissue -98.57 (±8.54). Kidneys, fat tissue and muscle differentiate significantly from every other organ (p < .001). No significant difference between liver – spleen (p=1.0).
ϱ: liver 63.58 (±7.93); spleen 60.90 (±4.81); kidneys 39.10 (±4.69); muscle 55.12 (±5.63); fat tissue -71.76 (±5.27). Kidneys, muscle and fat tissue differentiate significantly from every other organ (p < .001). No significant difference between liver – spleen (p=.440).
Z: liver 8.39 (±0.24); spleen 8.44 (±0.26); kidneys 9.97 (±0.32); muscle 7.51 (±0.27); fat tissue 6.00 (±0.42). Kidneys, muscle and fat tissue differentiate significantly from every other organ (p < .001). No significant difference between liver – spleen (p=1.0).
Percentage of fat: liver -7.07 (±5.92); spleen -16.60 (±4.58); kidneys 10.82 (±4.50); muscle -4.05 (±4.57); fat tissue 97.06 (±4.12). Kidneys and fat tissue differentiate significantly from every other organ (p < .001). No significant difference between liver – spleen (p=.923) and spleen – muscle (p=1.0).

Table 1: Overview of multiparametric mapping results.

acquisition	organ	organ	mean	(SD)	min	max
unenhanced	HU	liver	59.74	(7.74)	37.85	71.80
		spleen	55.34	(3.29)	44.90	62.55
		kidneys	37.38	(4.36)	26.80	49.45
		fat tissue	-103.14	(5.58)	-112.20	-79.85
		muscle	55.57	(5.72)	39.80	69.75
	ϱ	liver	59.78	(7.20)	40.20	70.63
		spleen	54.35	(4.21)	44.25	63.95
		kidneys	32.57	(3.87)	23.37	42.17
		fat tissue	-71.01	(4.64)	-79.55	-56.80
		muscle	56.33	(6.23)	40.40	67.15
	Z	liver	7.35	(0.11)	7.03	7.66
		spleen	7.39	(0.10)	7.09	7.63
		kidneys	7.49	(0.18)	6.99	7.89
		fat tissue	5.56	(0.30)	4.82	6.29
		muscle	7.32	(0.19)	6.74	7.94
	fat content	liver	-5.14	(5.60)	-15.15	9.75
		spleen	-1.51	(3.37)	-9.75	7.75
		kidneys	11.77	(5.28)	-1.98	26.02
		fat tissue	95.93	(4.15)	82.30	103.55
		muscle	-5.75	(5.49)	-20.50	8.65
enhanced	HU	liver	96.14	(15.77)	53.10	134.43
		spleen	98.08	(10.56)	75.65	130.10
		kidneys	146.52	(23.70)	67.80	202.80
		fat tissue	-98.57	(8.54)	-110.75	-72.60
		muscle	61.21	(8.90	37.90	74.20
	ϱ	liver	63.58	(7.93)	40.88	75.40
		spleen	60.90	(4.81)	48.80	73.35
		kidneys	39.10	(4.69)	28.20	51.05
		fat tissue	-71.76	(5.27)	-79.95	-54.25
		muscle	56.12	(5.63)	41.65	69.90
	Z	liver	8.39	(0.24)	7.82	8.99
		spleen	8.44	(0.26)	7.75	9.14
		kidneys	9.97	(0.32)	8.98	10.71
		fat tissue	6.00	(0.42)	4.85	7.23
		muscle	7.51	(0.27)	6.70	8.05
	fat content	liver	-7.07	(5.92)	-17.50	8.98
		spleen	-16.60	(4.58)	-6.03	2.35
		kidneys	10.82	(4.50)	-1.33	22.55
		fat tissue	97.06	(4.12)	82.85	103.20
		muscle	-4.05	(4.57)	-12.80	7.85

Conclusion:
Multiparametric DECT allows for improved organ characterization based on the atomic number and electron density. A normal distribution of upper abdomen organs and soft tissue could be established for various organs. The evaluation of the measured values shows that kidneys and fat tissue differ significantly from other organs in terms of all parameters. Based on our results further research should provide the possibility for reliable tissue identification of healthy organs and promote early and simple recognition of pathologically altered organs/areas.

5376

D. Kreul[1], R. Kubik-Huch[1], T. Niemann[1]

Influence of CT reconstruction parameters and on image quality and reconstruction efficiency in cinematic reconstructions

Institute of Radiology, Kantonsspital Baden[1]

Introduction:
Cinematic-rendering technique (CRT) depicts volumetric datasets in more photorealistic detail than does conventional volume-rendering technique (VRT). In VRT, simple ray casting is performed to compute images. CRT simulates a complex interaction between light and the density and associated transfer functions of the scanned object. The complex reconstruction algorithm currently needs enormous computer performance to be performed. Therefore, depending on the size of the dataset used for reconstructions the time needed for reconstructions can vary substantially and consume up to more than 10 hours.
The aim of this study was to evaluate the influence of reconstruction parameters from CT raw data on the quality and time consume of CRT-reconstructions.

Methods:
CT raw data set of a wrist was used to reconstruct CT-series with different slice thicknesses (0.6mm–6mm), increments (0,5–1) and kernels (n=2). Based on these, cinematic reconstructions using syngo.frontier software (Siemens Healthineers) were performed using five different quality presets (from very low to cinematic). The time to the finished reconstruction was measured and recorded. First two then four images with a 10° distance were reconstructed for each slice thickness for all image quality levels.

Results:
Substantial differences in time efficacy for the time consuming cinematic reconstructions for the different quality presets could be measured as shown in Table 1. The reconstruction of 4 images in the same application took about twice the time.
As shown in Fig.1 there exist huge differences in reconstruction quality based on slice thickness. Only minor differences could be depicted between the thinnest reconstructions (0.6mm and 1mm). Subjective, there is no major difference between the different quality presets.

Fig.2 compares the different quality levels. ‘Cinematic’ seems to be more soften.

Table 1: Reconstruction time for 2 images with 10° degree distance for different image quality levels; [time in minutes and seconds]

	Slice thickness [mm]	Image quality				
		Very low	Low	Medium	High	cinematic
bone window	6	0’22’’	0’45’’	1’29’’	2’14’’	3’46’’
	4	0’23’’	0’44’’	1’27’’	2’10’’	3’36’’
	3	0’23’’	0’45’’	1’26’’	2’09’’	3’34’’
	2	0’24’’	0’46’’	1’29’’	2’14’’	3’40’’
	1	0’23’’	0’45’’	1’28’’	2’11’’	3’36’’
	0.6	0’24’’	0’45’’	1’28’’	2’12’’	3’38’’

Fig.1: Reconstruction with different slice thickness (top left 0.6mm, top right 1mm, middle left 2mm, middle right 3 mm, bottom left 4mm, bottom right 6mm) ; image quality 'medium'.

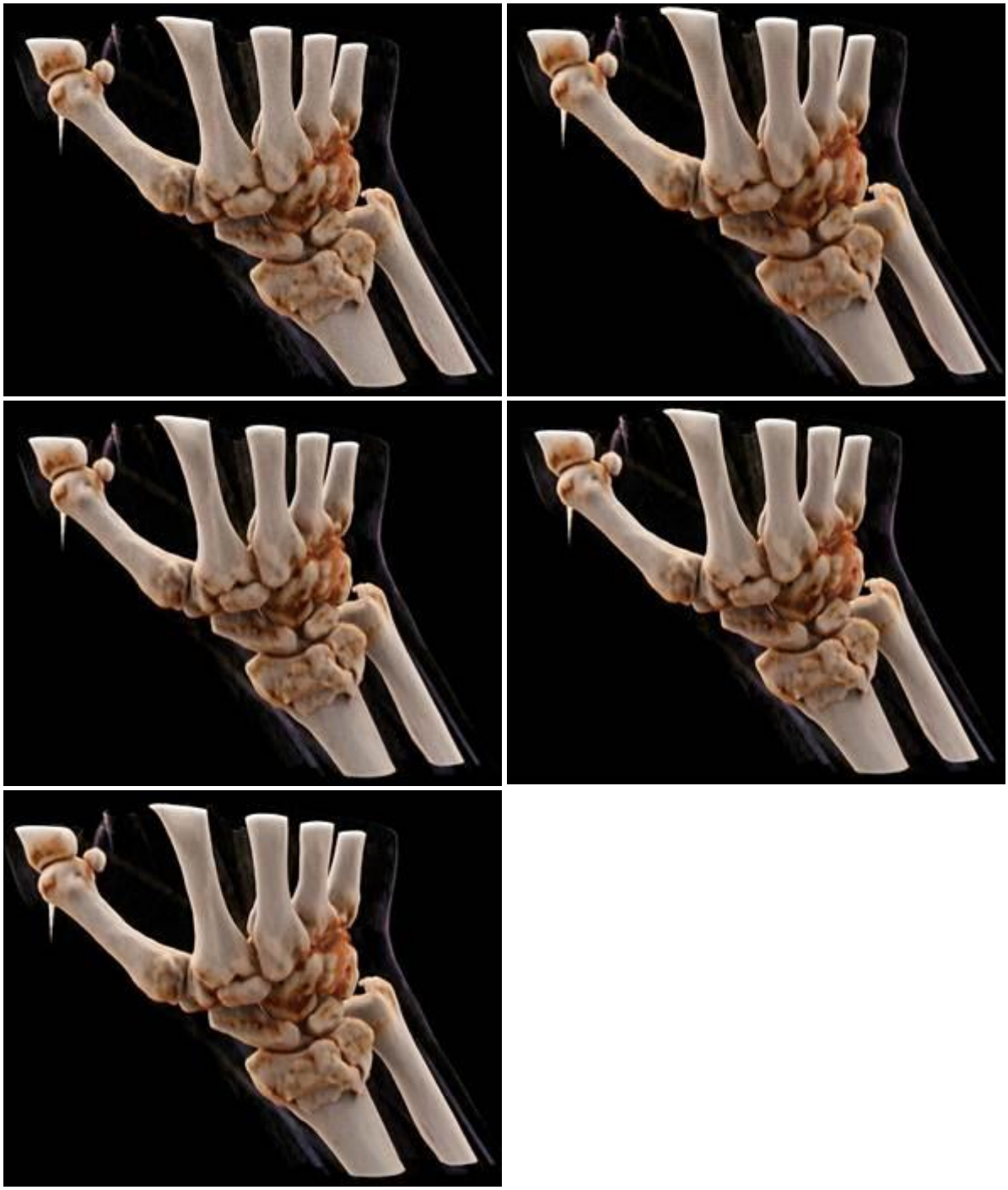

Fig.2: Reconstruction for same slice thickness (1mm) with different image quality presets (top left 'very low', top right 'low', middle left 'medium', middle right 'high', bottom left 'cinematic'.

Conclusion:

For cinematic CT-reconstructions image quality and reconstruction time vary substantially. These depend strongly on parameters used both for the CT image reconstruction series and the quality preset applied for image generation. Optimum choice of reconstruction parameters and image quality preset may substantially enhance efficacy in the use of cinematic reconstruction CT images. The slice thicknesses of 2–6mm do not represent suitable methods for an adequate representation, as shown in this case. For slice thicknesses of 4–6mm, it is not even possible for an unexperienced radiographer to detect the fracture in the distal radius. Best reconstruction quality is given for slice thicknesses of 0.6mm and 1mm. As shown in Fig.2, an adequate representation of the distal radius fracture is possible for all quality levels. Consequently, a lower quality level could be used to save time during reconstruction period.

5377

J. Prange[2], D. Mohr-Haralampieva[2], R. Alves de Sousa[2], F. Schmid[1], D. Eberli[1]

GMP-Verification processes of the final product in a clinical stem cell trial to treat Stress Urinary Incontinence

Urologie, Universitätsspital Zurich, Zurich[1], University of Zurich, Zurich[2]

Introduction:
Recent advances in cell-based therapies have provided a variety of opportunities to seek alternative solutions to restore damaged sphincter function in patients with urinary incontinence. Various pre-clinical studies have shown promising results towards successful skeletal muscle regeneration using autologous injection of patients muscle progenitor cells (MPCs). We aim to produce autologous MPCs for the injection into the sphincter muscle of female patients and to combine it with electro-magnetic stimulation. To successfully validate the manufacturing process of a clinical trial according to authority guidelines, the final product has to pass several verification processes: Excipient studies to define temperature range for the final product, Stability studies for the verification of the shelf life of the final product and Transport simulations to verify the transport process does not influence the quality of the final product. With the obtained results, the shelf life of the final product can be determined for the clinical trial.

Methods:
A defined amount of MPCs were prepared in collagen, as it is well established through pre-clinical trials, and stored in a syringe up to 24h at 2–8°C. Cell viability will be analyzed at several time points (4, 8, 12 and 24h) using a Nucleocounter NC-200 from Chemometec to determine the shelf life of the final product to provide sufficient time for release, transport and the application of the final product. The transport process is simulated in a pre-conditioned transport box equipped with temperature loggers and a specially designed cooling tool for the prepared syringe. Additionally, the impact of the application through a 20cm 18G needle on the MPCs is tested.

Results:
The Nucleocounter NC-200 allows analysis with calibrated cassettes containing a defined amount of Acridin Orange and DAPI to distinguish between dead and live cells. However, the viscous mix of MPCs in collagen needs to be highly diluted with growth medium to be measurable and to avoid false negative readouts from collagen interference.
Our results showed that the final product can be transported and stored for at least 4h at 2–8°C. After 24h however, the cell viability was already below 80% which is one of the release criteria of the final product. Independently from the application speed of normal injection, the viability of the cells was not affected by the sheer stress of the needle. These results are confirmed in a GMP-conform set up.

Conclusion:
4h shelf life is very short for the release of advanced therapeutic medicinal products in a first phase clinical trial as the complete batch record of the production process has to be approved and the final product needs to be transported and applied during these 4h. Therefore, a longer shelf life is advantageous for the continuation of the trial into phase 2 which could be set up as a multi-centric trial to acquire larger patient numbers.

5378

S. Hörmann[1], Z. Gai[1], G-A. Kullak-Ublick[1], M. Visentin[1]

Effect of the cellular lipid composition on the transport properties of the organic cation transporter 2 (OCT2)

Department of Clinical Pharmacology and Toxicology, University Hospital of Zurich, Zurich[1]

Introduction:
The human organic cation transporter 2 (OCT2) is a polyspecific cation transporter primarily located at the basolateral plasma membrane of renal proximal tubule cells. It mediates the first step of tubular secretion by translocating various substrates from the interstitium (blood side) into the proximal tubule cells. Compounds being transported are several endogenous substances like an array of neurotransmitters and choline, and clinically relevant drugs like cimetidine, oxaliplatin, cisplatin, gentamicin, metformin and others. As an integral membrane protein with 12 predicted transmembrane domains, OCT2 is embedded in and influenced by, the surrounding microenvironment. Cholesterol for example, is not only known to regulate the fluidity and permeability of biological membranes, it is also thought to influence the function of membrane proteins via its accumulation in lipid rafts or even directly by lipid-protein interactions. The plasma membrane lipid content of proximal tubule cells is highly dynamic and subjected to substantial changes - physiologically during aging or in several pathological conditions such as acute kidney injury - and may influence the process of tubular secretion, a major route of elimination of drugs and potential uremic toxins (e.g. Trimethylamine N-oxide, TMAO). Here we chemically manipulated the cellular lipid content and characterized the transport properties of OCT2.

Methods:
To study the transport properties of OCT2, we used human embryonic kidney 293 cells stably transfected with the open reading frame of OCT2 (OCT2-HEK293) and wild-type HEK293 cells as control (WT-HEK293). For cellular cholesterol depletion, methyl-β-cyclodextrin (mβcd), a torus-shaped cyclic oligosaccharide able to encapsulate cholesterol in its hydrophobic cavity, was used empty (mβcd) or loaded with cholesterol (RAMEB). Lipid content was quantify by thin layer chromatography (TLC). The effect of mβcd incubation on cell viability was assessed by Trypan blue exclusion assay. The effect of mβcd incubation on OCT2 protein stability was evaluated by immunofluorescence microscopy. Transport activity of OCT2 was measured by measuring the intracellular accumulation of radioactively labelled 1-methyl-4-phenylpyridinium (MPP^+), a commonly used model substrate of OCT2. Transport kinetics data were analyzed using nonlinear and linear regression analyses.

Results:
Incubation of WT-HEK293 cells with 10 mM mβcd for 20 minutes at 37°C and 5% CO_2 slightly affected cell viability/membrane permeability and markedly reduced the cholesterol amount as compared with that in untreated cells (8.6±6.1 vs 25.5±5.5 µg/mg of protein). The cholesterol content was replenished or even enriched by co-incubation with increasing concentrations of RAMEB. The phospholipid content was not affected by mβcd exposure. OCT2-mediated uptake of MPP^+ was reduced by more than 50% (1.0±0.1 vs 2.6±0.2 pmol/mg of protein/sec) after 20 minutes of preincubation with 10 mM mβcd at 37°C. Such an effect was not observed after incubation with mβcd and RAMEB in equimolar concentrations. Coincubation of mβcd did not show any reduction in MPP^+ influx. The MPP^+ influx kinetics was sigmoidal in presence of cholesterol, indicating two allosteric binding sites. The curve was best fitted to the Michaelis-Menten equation when the cholesterol was removed, suggesting a one binding site influx kinetics.

Conclusion:
Removal of cellular cholesterol changed the transport properties of OCT2 *in vitro*. The MPP^+ influx kinetics after preincubation with mβcd indicates that in absence of cholesterol only the OCT2 high-affinity binding site is accessible to the substrate, perhaps because of an augmented rigidity of the membrane, which constrains the mobility of the transporter. Our findings suggest that changes in cellular cholesterol content may affect the renal clearance of potential uremic toxins and drug, substrates of OCT2, and may lead to unexpected drug-drug interactions, especially in polypharmacy.

5379

D. Kreul[1], D. Gascho[2], S. Franckenberg[3], S. Eggert[2], B. Fliss[2], R. Kubik-Huch[1], M. Thali[2], T. Niemann[1]

Determining postmortal liver steatosis. A retrospective study comparing dual-energy computed tomography to histological graduation

Institute of Radiology, Kantonsspital Baden[1], Institute of Forensic Medicine, Zürich[2], Institute for Diagnostic and Interventional Radiology, University Hospital Zurich[3]

Introduction:
The use of dual-energy computed tomography (DECT) has increased over the past years, allowing several new applications for material characterization and organ assessment based on two different X-ray spectra.
The aim of this study was to retrospectively evaluate post mortal DECT acquisitions of the liver to analyze the fat percentage and organ characterization based on atomic structure (ϱ/Z) and to correlate it to histological graduation of steatosis hepatis of the same specimen.

Methods:
121 postmortal DECT were included in the study. Multiparametric analysis was performed using syngo.via (Siemens Healthineers) for unenhanced DECT acquisitions in a standardized acquisition protocol. Organ density (Hounsfield Unit; HU), fat fraction and ϱ/Z were measured standardized by placing four ROIs (region of interest) of at least 2 cm^2 in the liver (Fig. 1-3). Locations of measurements were chosen avoiding visible organ lesions or potential vascular structures. Samples for histological examination were taken during autopsy and classified according to the percentage of fat vacuoles in microscopy. A mean value for each patient was estimated and transferred to the software IBM SPSS Statistics. Data were categorized depending on the known histological graduation (grade I N = 86; grade II N = 21; grade III N = 14). Data was tested for normality, variance homogeneity and significance.

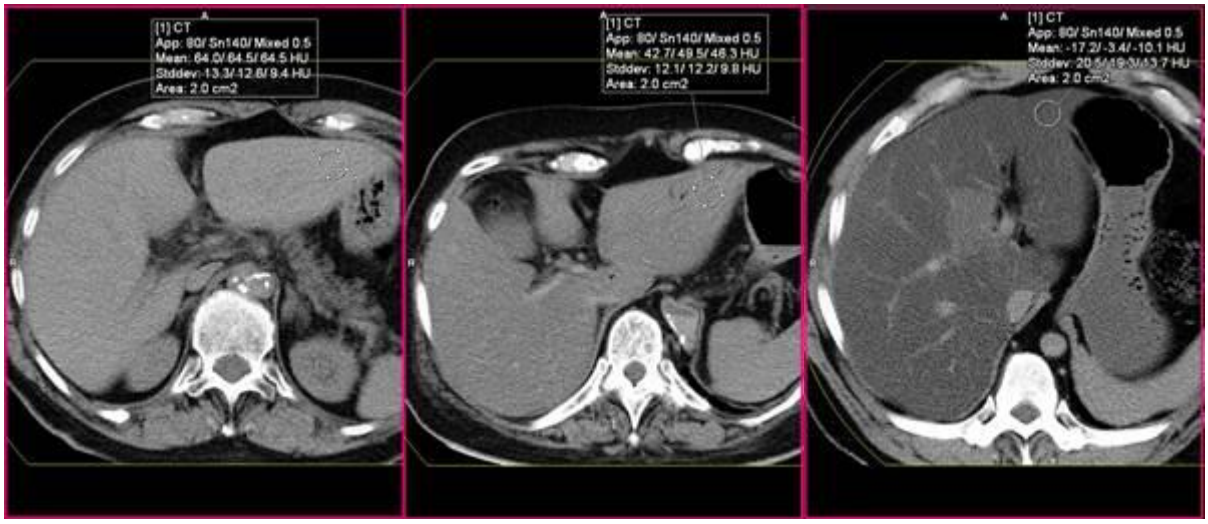

Fig. 1: Measurements of HU for three different grades of steatosis (left grade I, middle grade II, right grade III).

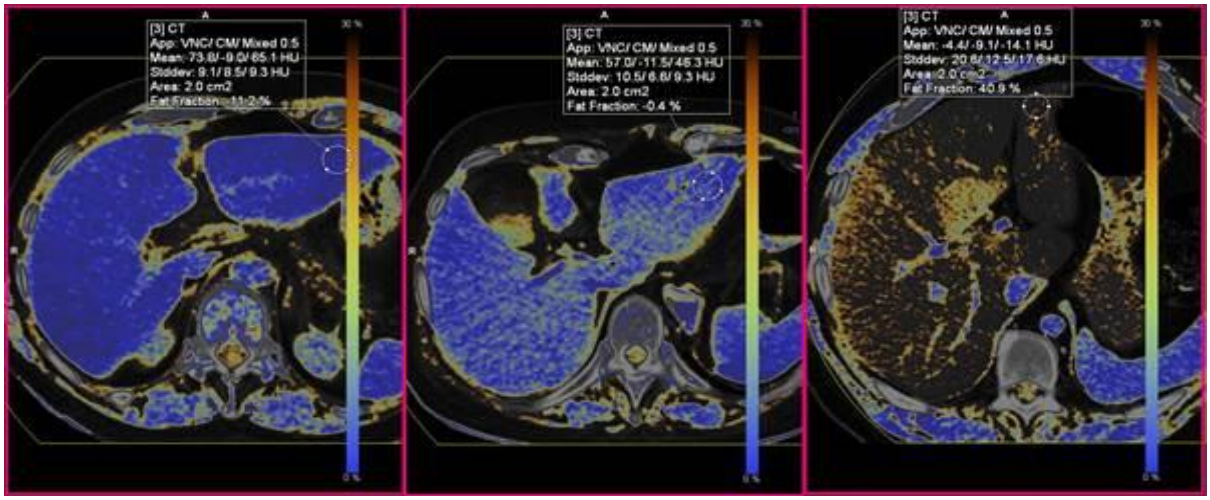

Fig. 2: Measurements of fat content for three different grades of steatosis (left grade I, middle grade II, right grade III).

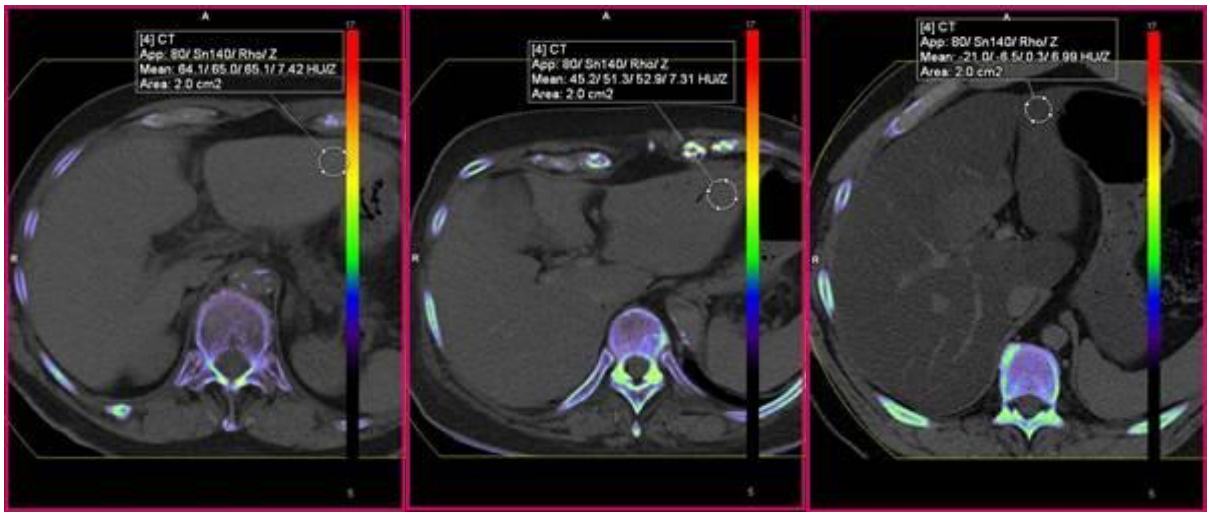

Fig. 3: Measurement of ϱ and Z for three different grades of steatosis (left grade I, middle grade II, right grade III).

Results:
In the following the mean values and standard deviations of the three histological grades of steatosis are given.

HU: grade I 57.5 (±10.16), grade II 44.6 (±12.13), grade III 25.7 (±18.72).

ϱ: grade I 61.59 (±9.10), grade II 52.69 (±11.08), grade III 36.38 (±16.07).

Z: grade I 7.28 (±0.17), grade II 7.18 (±0.11), grade III 7.06 (±0.19).

Percentage of fat: grade I -7.79 (±7.17); grade II -0.24 (±8.27), grade III 12.13 (±12.90).

Since the determination of fat content in fat mapping follows a linear equation, values above 100% and under 0% are possible. Nevertheless, values >100% mean 'is fat tissue' and values under <0% mean 'has no fat'.

Normality for all three graduation levels but no variance homogeneity was given. Significance test showed:

- Hounsfield Unit: significant difference between I – II (p<.001), I – III (p<0001); no significant difference between II – III (p=.061)
- Fat fraction: significant difference between I – II (p=.001), I – III (p<0001); no significant difference between II – III (p=.075)
- < >: significant difference between I – II (p=.007), I – III (p<.001) and II – III (p=.042)

  Z: significant difference between I – II (p=.017), I – III (p<.001); no significant difference between II – III (p=.195)

The resulting multiparametric 3D maps are shown in Fig. 4.

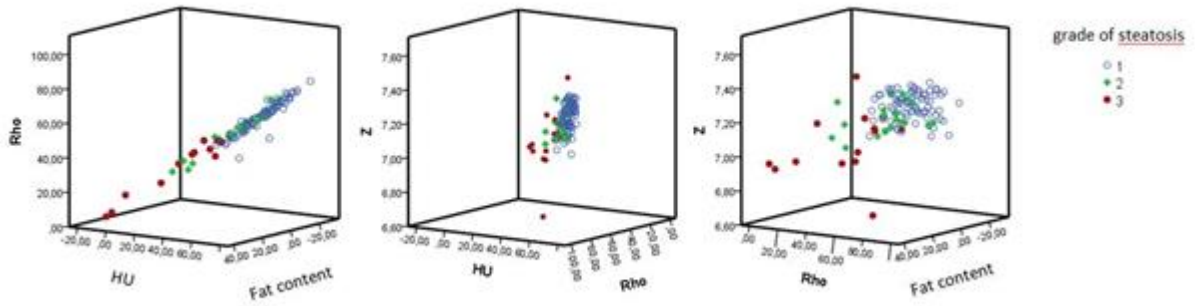

Fig. 4 Mapping results for three different grades of steatosis; Creation of 3D graphs using IBM SPSS Statistics.

Conclusion:
Multiparametric non-contrast dual energy analysis of the liver for steatosis estimation is a feasible and suitable method to gain initial knowledge about liver characterization before an autopsy. It allows to separate a grade of steatosis I from a grade of steatosis III. Accurate demarcation of grade II was difficult and did not provide significant results. The methodology can be regarded as an additional gain and under no circumstances as a substitute for the gold standard (histological examination). Further studies should work with a larger collective of grade II and III. Further studies including contrast examinations may enhance feasibility of grade II staging and increase significance levels.

5380

M. Kirschner[1], M. Friess[1], V. Orlowski[1], B. Gray-Stocker[1], W. Weder[1], I. Inci[1], R. Schüpbach[3], D. Bettex[4], S. Ulrich[2], I. Opitz[1]

Expression of microRNAs in surgical specimens of patients with Chronic Thromboembolic Pulmonary Hypertension

Department of Thoracic Surgery, University Hospital Zurich[1], Department of Pulmonology, University Hospital Zurich[2], Department of Intensive Medicine, University Hospital Zurich[3], Department of Anesthesiology, University Hospital Zurich[4]

Introduction:
Chronic thromboembolic pulmonary hypertension (CTEPH) – as a special form of pulmonary hypertension (PH) - is a rare and debilitating disease that can develop as a result of recurring pulmonary embolism. Thus far, it is unclear, what predisposes this subset of patients to develop this rare complication of PH. Furthermore, the exact pathophysiology, including the detailed mechanisms leading to fibrosis and remodelling of the pulmonary arteries, which ultimately lead to CTEPH remain largely unknown.
In recent years, microRNAs have emerged as important players in regulation of physiological processes, and dysregulation of microRNA expression has been linked to various diseases. So far, only a limited number of studies has investigated microRNAs in CTEPH. Therefore, the aim of this study was to investigate whether microRNAs are also detectable in tissue specimens obtained from patients undergoing pulmonary endarterectomy (PEA), since differential expression in the tissues could suggest a role of these microRNAs in disease development.

Methods:
Tissue specimens were obtained from 16 patients undergoing PEA at the University Hospital Zurich, between 2016 and September 2018. RNA was extracted from FFPE blocks, and expression levels of three microRNAs identified as potential players in CTEPH development through a study of circular RNAs (Miao et al, Medicine 2017), miR-939, miR-942 and miR-92a-2*, were measured by microRNA-specific RT-qPCR. In addition, miR-210, the most important microRNA in regulation of hypoxia was measured. Expression of microRNAs was correlated to various clinical factors**.**

Results:
Of the three miR-candidates measured in plasma before, miR-939 and miR-942 were detectable in PEA tissue specimens. In addition, the hypoxamiR miR-210 was also detectable and represented the microRNA with the highest expression levels. Expression of miR-939 showed a significant negative correlation with peripheral oxygen saturation ($p=0.03$; Spearman's $R=-0.548$) and pulmonary vascular resistance ($p=0.05$, $R=-0.502$), while miR-942 expression negatively correlated with Jamieson Classification ($p=0.04$, $R=-0.623$).

Conclusion:
This pilot study has shown for the first time that microRNAs are readily detectable in material extracted during PEA. Our data shows that microRNAs are differentially expressed between different patients, and that microRNA expression is correlated with various factors of clinical presentation. Thus, our data highlight that microRNA expression warrants further investigation as their dysregulation might be involved in the development of CTEPH. Hence, we are currently evaluating additional microRNAs in a larger sample set.

5381

R. Chen[1], T. Hornemann[2], W. Yu[2], S. Camargo[3], R. Graf[1], S. Sonda[1]

1-DEOXY-SPHINGOLIPIDS, novel biomarkers of diabetes, are cytotoxic for exocrine pancreatic cells

Swiss Hepato-Pancreatico-Biliary(HPB) Centre, Division of Surgical Research, Department of Visceral & Transplantation Surgery, University Hospital Zurich[1], Institute for Clinical Chemistry, University Hospital Zurich[2], Institute of Physiology, University of Zurich[3]

Introduction:
Exocrine pancreatic insufficiency and exocrine function alterations are characteristics of pancreatitis. They are frequent in diabetes mellitus (DM) patients with a prevalence up to 50%. Although reduced levels of insulin may explain many of the proposed mechanisms of pancreatic dysfunction following DM, the same phenotype is also detected in insulin-independent DM. This highlights the concept that additional factors are likely to contribute to the pathophysiology of acinar cells.
We recently discovered that 1-deoxy-sphingolipids (1-deoxySLs), the levels of which increase in DM and metabolic syndrome are cytotoxic for beta cells. Our preliminary results showed that 1-deoxySLs are also cytotoxic for acinar cells *in vitro*. Furthermore, the high level of 1-deoxySLs in diabetic animal model aggravated acinar cell damage whereas lowering levels of 1-deoxySLs improved cell deterioration. In this research, we investigate molecular and cellular factors that contribute to compromise acinar cell functionality in the context of DM. Based on the endocrine and exocrine pancreas crosstalk, we hypothesize that elevated 1-dSeoxyLs levels affect directly the pancreatic exocrine compartment by compromising pancreatic acinar cells in DM, thus increasing its predisposition to develop exocrine pancreatic diseases.

Methods:
In this study, we used *in vivo* mouse models with STZ-induced diabetes and cerulein-induced pancreatitis. Reduction of 1-deoxySLs synthesis was achieved by oral L-serine supplementation. Disease severity was assessed with biochemical and immunohistochemical methods. Cellular mechanisms of 1-deoxySL-dependent toxicity were evaluated *in vitro* on AR42J pancreatic acinar cells, with focus on mitochondrial analysis by Seahorse XFp technology and high-resolution microscopies.

Results:
In vitro studies showed that treatment with 1-deoxysphinganine, one of the early products of 1-deoxySLs synthesis at low concentration reduced replication and promoted programmed cell death in pancreatic acinar cells. Particularly, 1-deoxySL-mediated cytotoxicity affected mitochondrial functions by deteriorating mitochondrial respiration and ATP synthesis. Consequently, it triggered overproduction of reactive oxygen species (ROS) followed by endoplasmic reticulum stress and DNA damage.
In our animal model, DM induction resulted in increased 1-deoxySL levels but also atrophy and fibrosis of pancreatic parenchyma. The increase of ROS and Apoptosis observed *in vitro* were confirmed here *in vivo*. In addition, reduction of 1-deoxySL synthesis by oral L-serine supplementation ameliorated the damage of the exocrine pancreatic tissue with decrease of ROS and apoptotic cells, however, without restoring insulin production in beta cells. This suggests that elevated 1-deoxySLs rather than insulin deficiency contribute to the exocrine damage in DM.

Conclusion:
Our work revealed that 1-deoxySLs are cytotoxic for exocrine pancreatic cells, suggesting a role for these lipids in the exocrine dysfunctions following DM. Oral L-serine supplementation could be a therapeutic treatment for ameliorating exocrine pancreatic diseases in diabetic patients.

5382

J. Schniering[1], M. Brunner[1], O. Distler[1], M. Guckenberger[2], M. Bogowicz[2], D. Vuong[2], C. Müller[3], T. Frauenfelder[4], S. Tanadini-Lang[2], B. Maurer[1]

Texture-based radiomics features discriminate different stages of experimental interstitial lung disease

Center of Experimental Rheumatology, University Hospital Zurich[1], Department of Radiation Oncology, University Hospital Zurich[2], Center for Radiopharmaceutical Sciences, Paul Scherrer Institute (PSI), Villigen[3], Institute of Diagnostic and Interventional Radiology, University Hospital Zurich[4]

Introduction:
Interstitial lung disease (ILD) is a life-threating complication in systemic sclerosis (SSc). There is an unmet need for validated, routinely available biomarkers for disease staging and individualized patient stratification. In that respect, high-resolution computed tomography (HRCT), routinely performed in the work-up of SSc-ILD patients, has great potential as a source for non-invasive imaging biomarkers. Recently, radiomics, the quantitative extraction of hundreds of radiologic image features, has emerged as a powerful tool for biomarker research and precision medicine approaches; however, so far, has only been applied in oncology.
In this study, we aim to evaluate the performance of CT-based radiomics for disease detection, staging and as surrogate marker of the tissue pathophysiology in the model of bleomycin (BLM)-induced lung fibrosis.

Methods:
To mimic different stages of SSc-ILD, CT imaging was performed at days 3, 7, and 14 after the instillation of BLM or saline solution, respectively (n=5-6 mice/group). Trained observers manually segmented the left and right mouse lungs, and 154 radiomics features were extracted including 17 histogram- and 137 texture-based features using the in-house developed software Z-Rad (Python 2.7). To link the radiomics features with the underlying pathophysiology, Pearson correlation analysis between radiomics and histological features (Ashcroft score, Sirius red and CD45 staining positivity) was performed.

Results:
As anticipated, CT imaging visualized morphological changes of the lung architecture in BLM-treated mice, as evidenced by a time-dependent increase of grey consolidations on chest CT images and a gradual increase in tissue density on density-masked lungs. Accordingly, 6 out of 17 classical histogram features (e.g. mean CT density, skewness and kurtosis) precisely distinguished diseased from healthy mice with area under the curve values (AUCs) of >0.87 ($p<0.05$) and thus detected lung remodelling. However, histogram-based features failed to differentiate between the different time points and thus stages of experimental lung fibrosis as investigated by receiver operating characteristic curve analysis and by hierarchical clustering. In contrast, 59 out of 137 texture-based radiomics features, including features describing image homogeneity or contrast detected ILD and distinguished the different stages with excellent accuracy (AUCs>0.84; $p<0.05$) and thus outperformed the classical histogram features. In addition, texture-based, but not histogram-based features were significantly associated ($R^2>0.5$, $p<0.05$) with histological parameters, thereby possibly reflecting changes in lung (micro-)architecture, which may result from both inflammatory and/or fibrotic changes.

Conclusion:
If developed further and confirmed in SSc-ILD, texture-based radiomics features have great potential to provide biological and stage-specific quantitative information on lung (micro-)architecture and thus could serve as quantitative imaging biomarkers for guided decision making in SSc-ILD.

5383

L. Liberale[1], A. Akhmedov[1], V. Nageswaran[1], S. Costantino[1], N. Bonetti[1], J. Pahla[1], C. Matter[1], J. Beer[1], F. Paneni[1], T. Luscher[1], G. Camici[1]

Endothelial SIRT6 exerts a beneficial role in cerebral ischemia/reperfusion injury by preserving blood-brain barrier integrity

Center for Molecular Cardiology, Division of Cardiology, University Hospital of Zurich, University of Zurich[1]

Introduction:
Stroke is a major cause of mortality and morbidity worldwide. Yet, therapeutic strategies are limited to the early restoration of blood flow which can, on the other hand, worsen the brain damage trough ischemia/reperfusion (I/R) injury. During stroke, blood-brain barrier (BBB) is damaged and its impairment is associated with worsened outcome. Aging is a major risk factor for stroke and several genes regulating lifespan also contribute to the determination of cerebral damage during I/R injury. Given the pivotal role of endothelial cells in BBB, we hypothesized that the endothelial-specific expression of the longevity gene SIRT6 may protect the BBB from ischemia/reperfusion damage thus having a beneficial role on stroke outcome.

Methods:
Endothelial-specific SIRT6 knockout (eSIRT6-/-) and wild type (WT) mice underwent transient middle cerebral artery occlusion (tMCAO) for 45 min followed by 48 h of reperfusion. Survival rate, infarct size by triphenyltetrazolium chloride staining as well as neurological impairment by RotaRod test and Bederson scale were assessed after tMCAO. In order to test the relevance in human cells, primary human brain microvascular endothelial cells (HBMVECs) were transfected with either SIRT6 (siSIRT6) or scrambled (siSCR) small interfering RNA and subjected to hypoxia/reoxygenation (H/R). An in vitro BBB model consisting of a monolayer of siRNA-treated HBMVECs seeded at confluence in electric cell-substrate impedance sensor electrode chambers was established and barrier function was assessed by 48 h-lasting transendothelial electrical resistance measurement. Molecular pathways underlying the observed effects were investigated. In addition, SIRT6 expression was determined in peripheral blood monocytes (PBMCs) of ischemic stroke patients and correlated with the stroke outcome.

Results:
eSIRT6-/- displayed higher infarct volumes and lower survival rate compared to WT mice 48 h after tMCAO. The increased infarct volume was functionally relevant as eSIRT6-/- also showed worse post-stroke neurological impairment.
In vitro, H/R reduced SIRT6 expression in HBMVECs. Of interest, SIRT6 silencing impaired the barrier function of HBMVECs as siSIRT6-treated cells showed lower resistance values as compared to siSCR-treated ones 48 h after exposure to H/R. In line with this, SIRT6-silenced HBMVECs showed reduced viability, increased cleaved-caspase 3 expression and reduced activation of the anti-apoptotic survival pathway Akt as compared to control cells after H/R; no difference were shown under normoxic conditions. Furthermore, the direct interaction between SIRT6 and Akt was confirmed by co-immunoprecipitation.
Lastly, PBMCs from ischemic stroke patients showed similar SIRT6 levels as compared to cells from healthy controls. Of interest, monocyte SIRT6 expression was higher in patients with a positive in-hospital clinical course than in those with a negative one as assed by NIHSS difference at the time of admission and discharge (delta_NIHSS). Also, a significant negative correlation was showed between SIRT6 levels and delta_NIHSS.

Conclusion:
Endothelial SIRT6 exerts a beneficial role in ischemic stroke by blunting I/R-mediated BBB damage. Specifically, SIRT6 reduces I/R-induced apoptotic death through activation of the protective Akt pathway. The longevity gene SIRT6 may represent a novel therapeutic target for the treatment of ischemic stroke.

5384

I. Jelcic[1], F. Al Nimer[2], J. Wang[1], V. Lentsch[1], R. Planas[1], Il. Jelcic[1], A. Madjovski[1], S. Ruhrmann[2], W. Faigle[1], K. Frauenknecht[3], C. Pinilla[4], R. Santos[5], C. Hammer[6], Y. Ortiz[1], L. Opitz[7], H. Grönlund[8], G. Rogler[9], O. Boyman[10], R. Reynolds[11], A. Lutterotti[1], M. Khademi[2], T. Olsson[2], F. Piehl[2], M. Sospedra[1], R. Martin[1]

Memory B Cells Activate Brain-Homing, Autoreactive CD4+ T Cells in Multiple

Neuroimmunology and MS Research Section (NIMS), Neurology Clinic, University of Zurich, University Hospital Zurich[1], Neuroimmunology Unit, Department of Clinical Neuroscience, Karolinska Institutet, Stockholm, Sweden[2], Institute of Neuropathology, University of Zurich, University Hospital Zurich[3], Torrey Pines Institute for Molecular Studies (TPIMS), San Diego, CA, USA[4], Torrey Pines Institute for Molecular Studies (TPIMS), Port St. Lucie, FL, USA[5], School of Life Sciences, École Polytechnique Fédérale de Lausanne,Lausanne[6], Functional Genomics Center Zurich, Swiss Federal Institute of Technology and University of Zurich[7], Therapeutic Immune Design Unit, Department of Clinical Neuroscience, Karolinska Institutet, Stockholm, Sweden[8], Department of Gastroenterology and Hepatology, University of Zurich, University Hospital Zurich[9], Department of Immunology, University of Zurich, University Hospital Zurich[10], Division of Brain Sciences, Department of Medicine, Imperial College London, London, United Kingdom[11]

Introduction:
Multiple sclerosis (MS) is an autoimmune disease of the central nervous system, caused by an interplay of genetic - most importantly HLA-DR15 - and environmental risk factors. How these etiologic factors generate and maintain an autoreactive CD4+ T cell repertoire has remained elusive.

Methods:
Previously, we have shown increased autoproliferation *in vitro* in MS patients using PBMCs in the absence of any exogenous stimulus and serum-free conditions. We developed this assay further by using a CFSE-labeling protocol, which allows characterization of autoproliferating cell populations in flow cytometry. PBMCs of healthy donors and MS patients were then tested for their degree of autoproliferation, the cellular composition, the TCR repertoire, mechanistic insights in the inducing cell populations and their antigen specificity.

Results:
Autoproliferation involves mainly effector memory cells with a Th1/Th1* phenotype, is increased in MS patients during inactive state of the disease whereas MS patients in relapse showed a significant decrease of response. This proliferative response was in particular associated with the major risk factor HLA-DR15 rather than with MS-associated non-HLA risk SNPs. Moreover, we provided mechanistic insights in this phenomenon by demonstrating that autoproliferation of T helper cells is directly mediated by the interaction of memory B cells via HLA-DR - T cell receptor (TCR) contact. We further dissected the B-T cell interactome revealing multiple co-receptor-ligand pairs that might also contribute in this interaction. TCR deep sequencing of brain-infiltrating and *in vitro* autoproliferating T cells shows that the latter are enriched for brain-homing T cells. Using this methodology we have been able to isolate multiple HLA-DR15-restricted T cell clones from the autoproliferating compartment of the peripheral blood from MS patients. We then addressed the specificity of these T cell clones towards myelin antigens and further employed an unbiased epitope discovery approach in order to identify new cognate self-antigens that might be also expressed in the inducing B cell population.

Conclusion:
Collectively, our data indicate that B-T cell interactions are at the core of MS pathogenesis. These findings are instrumental to approach numerous questions on the dynamics of pathogenic T-B cell interactions in MS that we will be now able to investigate *in vitro*. Furthermore, we now have a promising *in vitro* approach that can be used to dissect the antigen-specificity in MS relevant T cell clonotypes in peripheral blood and as a drug screening platform for the identification of future therapeutic targeting.

5385

D. Mohr-Haralampieva[1], J. Prange[1], R. Alves de Sousa[1], F. Schmid[1], D. Eberli[1]

Towards Implementing a Multisystem Cell Therapy for Improvement of Urinary Continence: MUS.I.C. project

Urology, University Hospital Zurich[1]

Introduction:
Stress Urinary Incontinence (SUI) is a disease affecting over 200 million people worldwide and is twice as common in women as in men. Childbirth and menopause are major reasons of the increased prevalence in women, whereas prostatectomy is one of the main causes in men. The significantly reduced quality of life; high healthcare costs and complication rates, with rather limited success of the available therapies; and the constantly aging population are just some of the main factors, showing the urgent clinical need for novel treatment modalities.

Methods:
Early clinical trials using stem, or progenitor cells in both male and female patients have promising functional results with minimal adverse effects. However, as simple as it seems to be, the precise identification, isolation and transplantation of these cells seems to be more complex than originally expected.

Results:
Within our international, H2020-funded, project consortium MUS.I.C., we identified some points, which seem to be fundamental for the long-term success of this TE therapy: (1) the production of autologous cells needs to skip the costly GMP-site to become more affordable and efficient;(2) the final product needs to be completely xeno-free;(3) the cell-transplantation needs particular precision and (4) it needs to be supported by pelvic floor stimulation with neuromuscular-electromagnets for effective functional regeneration of the urinary sphincter.

Conclusion:
Together, with combined expertise and efforts, we are working towards providing such a novel autologous progenitor-cell-based multisystem-therapy, which already shows great potential as a feasible solution for the current bottlenecks of applying a cellular therapy to SUI patients, that we currently face in a PhI clinical trial.

5386

T. Maeyashiki[1], S. Arni[1], I. Iskender[1], W. Weder[1], I. Inci[1]

Sub-normothermic ex-vivo lung perfusion attenuates ischemia reperfusion injury from donation after circulatory death donors

Universitätsspital Zürich, Department of Thoracic Surgery[1]

Introduction:
Evaluation of a potential lung graft in an ex-vivo lung perfusion (EVLP) system has gained an increased use among transplantation centers. Current standard of organ assessment before transplantation with machine perfusion are performed with normothermic temperature but sub-normothermic setting is under clinical use among several solid organs. Our aim was to investigate the impact of sub-normothermic EVLP from donation after circulatory death donor lungs in a rat model.

Methods:
Male outbred Sprague Dawley rats were euthanized and left at room temperature for 2 hours. Donor lungs were retrieved and perfused in a rat EVLP system for 4 hours at sub-normothermic setting including 21C° (n = 4) and 28C° (n = 6), and compared with the normothermic temperature (37C°) (n = 6). We examined the EVLP physiology, perfusate biochemistry, lung tissue ATP and cytokines content in the perfusate after 4 hour EVLP.

Results:
Both pulmonary vascular resistance and dynamic lung compliance at 21C° were significantly lower than those at 37C° ($p < 0.05$), but, those of 28C° were statistically comparable to the 37C° values. Potassium ion and lactate concentrations under 28C° perfusion were significantly lower than those at 37C°. The tissue ATP at 28C° and 21C° showed trends toward better ATP preservation. In the perfusate under 28C°, IL-6, GRO/KC/CINC-1 and MIP-2 were statistically lower than the value observed at 37C°.

Conclusion:
EVLP with perfusate temperature of 21C° showed significantly worst lung physiology whereas EVLP at 28C° were functionally comparable to 37C°. Nevertheless, at EVLP temperature lower than 28C°, low energy consumption and low inflammatory response were significantly recorded. This study suggests that sub-normothermic EVLP temperature of 28C° would be an appropriate setting to reduce ischemia-reperfusion injury.

5387

S. Salemi[1], B. Kranzbühler[1], T. Sulser[1], D. Eberli[1]

ARN-509 (Apalutamide) combined with autophagy inhibitors: Promising double therapy for advanced prostate cancer

Laboratory for Urologic Tissue Engineering and Stem Cell Therapy, Zurich[1]

Introduction:
ARN-509 is a unique androgen receptor (AR) antagonist for the treatment of castration-resistant prostate cancer. It inhibits AR nuclear translocation, DNA binding and transcription of AR gene targets. ARN-509 has the same binding site as bicalutamide, but shows a 7-10 fold greater affinity to the AR. Dysregulation of autophagy, a conserved lysosomal degradation pathway, has been shown in prostate cancer. Targeting autophagy is thought to be a potential approach to overcome early therapeutic resistance. Therefore, we investigated the characteristics of autophagic response to ARN-509 treatment in androgen sensitive prostate cancer cells. Furthermore, we investigated, if a combination of ARN-509 with autophagy inhibitiors could further increase the antitumor activity.

Methods:
Human prostate cancer cells (LNCaP) were cultured in steroid-free medium. Cells were treated with ARN-509 (50 and 100 µM) alone or in combination with the autophagy inhibitors 3-methyladenine (3MA, 5 mM) or chloroquine (CHQ, 20 µM). Cell Viability was detected by WST-1-assays after 1, 3 and 7 days. Autophagic activity was screened by western blot (WB) and immunocytochemistry for the expression of LC3-I/II, Atg5, Beclin1 and P62. Autophagosome increase was detected by Autodot staining.

Results:
Treatment with ARN-509 led to dose dependent cell death up to 30% with 50 uM and 50% with 100 uM in a time dependent manner after 1, 3 and 7 days. Combination of ARN-509 with autophagy inhibitors showed further increase in cell death 50 uM (70% for CHQ and 60% for 3MA) and 100 uM.(70% for CHQ and 70% for 3MA) after 7 days. Immunostaining results showed that ARN-509 induced autophagy in LNCaP cells as evidenced by elevated levels of Atg5, Beclin1 and LC3 punctuation and increase in LC3-II band detected by WB. Autophagic flux was restored by the treatment of cells with with CHQ, increasing the LC3-II band. These findings were further supported by an increase in autophagosome punctuation observed by Autodot staining.

Conclusion:
Taken together, this data demonstrates that treatment with ARN-509 leads to increased autophagy levels in LNCaP cells. Given its potential for a high therapeutic index, ARN-509 in combination with autophagy inhibitors significantly increases its antitumor effect providing a new therapeutic approach potentially translatable to patients.

5388

A. Irmisch[1], The. Melanoma molecular analysis R&D team[2], R. Dummer[1], M. Levesque[1]

In depth molecular profiling of metastatic tissue from melanoma patients- a multi-institutional feasibility study

Dermatologische Klinik, Universitätsspital Zürich, Zürich[1], ETH Zürich, Institute of Molecular Systems Biology, Department of Biosystems Science and Engineering, Department of Informatics; Universität Zürich, Insitute of Molecular Life Sciences; Universitätsspital Zürich, Institut für Pathologie und Molekularpathologie[2]

Introduction:
Molecular profiling for therapeutic decision support in oncology typically includes NGS-based gene panel or whole exome sequencing techniques. Although these approaches yield genetic variants that are targetable by approved drugs, it is in many cases unclear whether these variants are actually expressed or functional in tumor proliferation. We here present a pilot feasibility study in which metastases from 11 patients with stage III or IV melanoma, in addition to gene panel sequencing on formalin-fixed paraffin embedded (FFPE) material, were analysed by multiple innovative molecular techniques utilising live tumor cells. The aim was to show technical feasibility, gain initial experience in providing therapeutic decision support and feasibility of biomarker discovery.

Methods:
Metastasis tissue from routine surgical resection of 11 melanoma patients was analysed by Foundation One cancer gene panel sequencing as well as single cell RNA sequencing, imaging and solution CyTOF (mass cytometry), pharmacoscopy (drug sensitivity testing), deep drug screening, proteomics and immune-pathology analysis. The resulting data was integrated into a research report containing a clinically relevant summary page, which was discussed in a molecular tumor board.

Results:
We could show that in-depth molecular analysis of live tumor material is feasible provided tumor material quantity and quality is sufficient. Furthermore, we were able to integrate the wealth of molecular data into a clinically relevant report. For all patients analysed the molecular data refined the therapeutic decision support of gene panel sequencing and provided potential additional therapy options for most patients.

Conclusion:
Based on the feasibility study presented here we have started an observational clinical trial to discover novel biomarkers of treatment response, resistance and toxicity in metastatic melanoma and further develop our molecular platform for therapeutic decision support.

5389

P. Manogaran[1], M. Samardzija[3], A. Schad[4], C. Wicki[6], C. Walker-Egger[2], M. Rudin[5], C. Grimm[3], S. Schippling[2]

Longitudinal characterization of optic nerve and retinal pathology in experimental optic neuritis

Department of Information Technology and Electrical Engineering, Swiss Federal Institute of Technology, Zurich[1], Neuroimmunology and MS Research, Department of Neurology, University Hospital Zurich and University of Zurich[2], Lab for Retinal Cell Biology, Department of Ophthalmology, University of Zurich, Zurich[3], Department of Biology, University of Zurich, Zurich[4], Institute for Biomedical Engineering, Swiss Federal Institute of Technology and University of Zurich, Zurich[5], Department of Health Sciences and Technology, Swiss Federal Institute of Technology, Zurich[6]

Introduction:
Optic neuritis (ON) is a common manifestation in multiple sclerosis (MS) and its animal model, experimental autoimmune encephalomyelitis (EAE). The visual pathway including its unmyelinated retinal axons, can serve as a prototypic model to characterize the pathological mechanisms and define the chronological sequence of events leading to neurodegeneration. Therefore, a longitudinal experiment involving optical coherence tomography (OCT) along with immunohistochemical analysis was conducted at various time points in experimental ON.

Methods:
30 EAE-MOG_{35-55} and 14 healthy female C57BL/6J mice were used in this study. Distribution of marker proteins for microglia (IBA1), gliosis (GFAP), myelin (MBP), axons (NEFM/APP), T-cells (CD3), retinal ganglion cells (RGC; NEUN), and apoptosis (TUNEL) was assessed by immunofluorescence staining of retinal and optic nerve tissue. Retinal mRNA levels of *Brn3a* (transcription factor expressed in RGCs), *Gfap*, brain-derived neurotrophic factor (*Bdnf*), tumor necrosis factor (*Tnf*), caspase-1 (*Casp1*), and chemokine ligand 2 (*Ccl2*) were assayed using real-time PCR. Retinal protein levels were determined by western blotting using specific antibodies. While, histological morphology was assessed in the optic nerves and retinas. Inner retinal layer (IRL) thickness was obtained from a volume scan centered over the optic nerve head using the Spectralis OCT-2 Plus device. Data was acquired at baseline, 7, 9, 11, 15, 20, 28 and 33 days post immunization (dpi).

Results:
A sharp increase in IRL thickness was observed by OCT at 11 dpi followed by a steady decline in thickness until the final observational time point in EAE mice compared to healthy controls. Activated microglia and gliosis signal presented as early as 7 dpi and 9 dpi respectively in the optic nerve and retina. At 11 dpi, massive cellular infiltration was observed including T-cells, microglia and gliosis in the optic nerve. Upregulation of inflammatory markers in the retina such as *Tnf, Ccl2, Gfap,* and *Casp1* persisted until 33 dpi. First signs of demyelination and axonal damage were observed at 11 dpi in the optic nerve, which continued until 33 dpi where profound signs of myelin disorganization and axonal degeneration were observed. In the retina, axonal degeneration was present from 20 to 33 dpi while APP immunoreactivity increased as early as 11 dpi in EAE mice. A decrease in RGC bodies along with apoptosis was detected at 28 and 33 dpi. Retinal expression of *Bdnf*, a marker for neuronal survival, decreased at 20 and 28 dpi in EAE mice compared to healthy controls. No notable gross changes were observed in retinal histology of EAE mice.

Conclusion:
Massive cellular infiltration (including peripheral T-cells) concurring with onset of clinical symptoms was observed in the optic nerve of EAE mice similar to previously described findings in the brain and spinal cord. The immune response within the retina appears to be secondary to ON. Thus, the increased IRL thickness observed at disease onset coincides with the immune response. Demyelination and axonal degeneration occur concurrently with cellular infiltration in the optic nerve

while axonal damage within the retina appears later. Structural damage persisted in both compartments. Furthermore, RGC cell death and elevated apoptotic response in the retina coincides with decreased IRL thickness at later time points in EAE. These results add morphological substrate to our previously uncharacterized retinal thickness changes observed by OCT. The extent and rapid onset of axonal and neuronal damage in this model appears relevant for testing interventions scaled to human ON.

5390

S. Chaudron[1], K. Metzner[1], C. Leemann[1], K. Kusejko[1], H. Nguyen[1], A. Marzel[1], J. Böni[3], S. Yerly[2], T. Klimkait[4], M. Perreau[5], R. Kouyos[1], H. Günthard[1]

A molecular epidemiology method to screen for HIV-1 superinfection in the swiss HIV cohort study

Department of Infectious Diseases and Hospital Epidemiology, University Hospital Zurich[1], Laboratory of Virology, Geneva University Hospitals[2], Institute of Medical Virology, University of Zurich[3], Department of Biomedicine, University of Basel[4], Faculty of Biology and Medicine, University of Lausanne[5]

Introduction:
HIV-1 superinfection (SI) is the infection of an already HIV-infected individuals by another HIV-1 virus. SI has been associated with viral recombination, immune escape and disease progression. SI identification remains challenging for various reasons: 1. SI is difficult to discern from co-infection. 2. Within subtypes SI is difficult to prove due to viral similarity. 3. SI strain may outcompete or be outcompeted by the first strain. 4. Sampling frequencies are too low and systematic screens of large populations to date are missing due to lack of needed longitudinal samples in untreated patients. We thus aimed to develop a molecular epidemiology method to screen for SI in longitudinal cohorts. We profited from 2 well characterized longitudinal studies: the Zurich Primary HIV Infection Cohort Study (ZPHI, >360 patients) and the Swiss HIV Cohort Study (SHCS, >19,000 HIV infected individuals) to establish our workflow.

Methods:
22,243 HIV-1 pol Sanger sequences of longitudinal time points from 12,080 patients were used for phylogenetic reconstruction. Intra-patient HIV-1 sequence diversity from a single infection can reach 5%. Considering this, two criteria were applied to patients with ≥2 longitudinal sequences available to select for SI: 1. a phylogenetic cluster diversity of at least 20 patients for each individual patient's cluster and 2. a genetic distance ≥5% between each focal patient's sequences. The time of SI for each patient was estimated around the time point with the highest genetic distance to the other time points. The number of longitudinal sequences and their topology in the phylogeny was used to rank the potential cases. Category 1 patients only have 2 sequences available. Category 2 patients have >2 sequences with one sequence away for the others in the phylogeny. Category 3 also have >2 sequences with ≥1 sequences clustering away from the others. ≥3 longitudinal plasma samples from 15 category 3 patients, around the supposed SI window, were chosen. HIV-1 full-length genome was amplified, and next generation sequenced (NGS).

Results:
Of 4,775 HIV-infected individuals with ≥2 sequences, 325 potential HIV-1 SI were identified. For 15 category 3 patients, the longitudinal NGS and the Sanger sequences were used to build a phylogeny for the pol gene. We see in the phylogeny that the NGS sequences co-localize with the Sanger sequences of the same focal patient. In addition, the genetic distance between patient' NGS sequences was >5% for 13 patients, confirming our first Sanger sequences analysis. Thus 13 SI cases out of 15 first sequenced were confirmed by our method.

Conclusion:
This molecular epidemiology approach is the largest screen to study SI. 173 plasma samples from 46 categories 2 and 3 potential SI were additionally ordered for HIV-1 full-length NGS. It sets the ground to further characterize HIV-1 SI in our cohort. The use of NGS will allow to study in depth recombination as well as the within patient viral diversity during SI. Finally, with our well documented cohort registries, the epidemiological profiles, risk behaviours and incidence for SI can be determined.

5391

N. Citak[1], L. Guglielmetti[1], Y. Aksoy[2], O. Isgörücü[3], M. Metin[2], A. Sayar[3], I. Opitz[1], D. Schneiter[1], W. Weder[1], I. Inci[1]

Stage IIIA should be divided in two different subgroups according to T and N status in patients with resected lung cancer: validation with another center database

Universitätsspital Zürich, Department of Thoracic Surgery[1], Yedikule Thoracic Surgery and Chest Disaese Research and Education Hospital, Department of Thoracic Surgery, Istanbul[2], Bakirkoy DSK Research and Education Hospital, Department of Thoracic Surgery, Istanbul[3]

Introduction:
Stage IIIA-NSCLC includes a very heterogeneous group of patients depending on tumor localization, and extension of nodal disease. Therefore therapy still remains very controversial. The purpose of our study was to compare the survival between Stage IIIA-subsets (T3N1-T4N0/1 versus T1/2N2), and to validate our results with another center database.

Methods:
Between 2007 and 2017, completely resected patients with Stage IIIA/B-NSCLC were retrospectively analyzed. There were 424 patients had Stage IIIA and 82 patients had Stage IIIB (T3/4N2). Stage IIIA were divided into two subsets according to tumor localization (T3N1-T4N0/1, IIIA-T group; n=308) and extension of nodal disease (T1/2N2, IIIA-N2 group; n=116). Survival rate was compared with another Thoracic Surgery Center database for validation.

Results:
IIIA-N2 group had more adenocarcinoma than IIIA-T group (52.6% vs 29.5%, p<0.001), and pneumonectomy was more performed in IIIA-T group (51.0% vs 32.8%, p=0.001)**.** In multivariate analysis, N2 and age > 65 were significant independent negative prognostic factors (p<0.0001). Five-year survival for patients in IIIA-T group was 51.3% (median 64 months), whereas it was 25.7% (median 31 months) for IIIA-N2 patients (HR: 1.834, 95%CI [1.345-2.501], p<0.0001). There was no statistically difference regarding the survival between IIIA-N2 and Stage IIIB (25.7% vs 25.3%, p=0.4). According to the results, we performed a re-staging for Validation Cohort patients as; Stage IIIA-T (including T3N1 and T4N0/1) (n=139), Stage IIIA-N (including T1/2N2) (n=104), and Stage IIIB (n=50). Stage IIIA-T had a statistically better survival than Stage IIIA-N (50.5% vs 27.1%, HR: 1.707, 95%CI [1.231-2.366], p=0.0007), whereas five-year survival rates were similar for Stage IIIA-N and Stage IIIB (27.1% vs 27.1%, p=0.9).

Conclusion:
We propose to divide stage IIIA into two different subgroups according to the primary tumor extension (T) and mediastinal lymph node involvement (N) in the next TNM classification. This allows better patient selection for resection.

5392

F. Schmid[1], A. Mortezavi[1], J. Sonderer[1], J. Bruhin[1], T. Sulser[1], D. Schindele[2], D. Eberli[1], M. Schostak[2]

Prospective Multicentre Study using High Intensity Focused Ultrasound (HIFU) for the Focal Treatment of Prostate Cancer: Safety Outcomes and Complications

Department of Urology, University Hospital Zurich[1], Department of Urology, University Hospital Magdeburg, Otto von Guericke University Magdeburg, Magdeburg[2]

Introduction:
Radical prostatectomy and irradiation in men with prostate cancer (PCa) are associated with significant genitourinary and rectal side-effects. High intensity focused ultrasound (HIFU) is emerging as an alternative to radical whole-gland therapy. In this prospective multicentre trial, we analyzed safety and complications in patients (pts) treated by focal HIFU for localized PCa.

Methods:
Men aged >45 years were eligible for this multicentre prospective cohort study if they had low to intermediate risk and localized PCa (Gleason score ≤4 + 3, PSA ≤15 ng/ml, stage ≤T2) with no prior treatment. After identifying tumors on multiparametric MRI and prostate biopsy, pts received focal therapy using HIFU (Focal One, EDAP) of the PCa lesions with a safety margin of 8 mm. The 30-day and 90-day adverse events (AE) and interventions were assessed and stratified on treatment localisations.

Results:
Between May 2014 and January 2018 we included 89 men with a median age of 66 years (50 – 78y) in two European centers. Overall, 37 pts (41.6%) experienced AEs in the first 30 days after HIFU intervention (all Clavien-Dindo grade ≤ II): 15 pts (16.9%) had a postoperative urinary tract infection and 22 pts (24.7%) urinary retention. Only three pts (3.4%) underwent subsequent TURP. The complication rate between 30 and 90 days postoperatively was low (2.2%). Zonal analysis of quarters of the prostate revealed that tumors located at the anterior base had the highest complication rate with 55.6%, followed by the dorsal base with 43.5%. Complications were less common after ablation in the dorsal apex or anterior apex (39.5% and 20%, respectively). The inclusion of the urethra in the ablation zone led to AEs in 37 out of 43 pts (86%). However, it was no significant criterion for complications within 30 days (OR = 1.79, 95% CI: 0.76 to 4.20, p = 0.180). In a linear regression analysis, the size of the treated tumor volume was no significant predictor of complications (OR = 1.1, 95% CI: 1.00 to 1.21), p = 0.057).

Conclusion:
Focal therapy of prostate cancer lesions with a robotic HIFU-probe is safe and leads to an acceptable rate of early genitourinary side-effects. Tumors treated in the anterior base of the prostate, as well as the inclusion of the urethra, tend to develop more complications than other regions.

5393

F. Schmid[1], M. Wettstein[1], T. Thomas[2], A. Boss[3], T. Hermanns[1], D. Eberli[1]

Contrast Media Kinetics in Multiparametric MRI before Radical Prostatectomy Predicts Probability of Postoperative Incontinence

Department of Urology, University Hospital Zurich[1], Balgrist University Hospital, Department of Neuro-Urology, Zurich[2], University Hospital Zurich, Department of Radiology, Zurich[3]

Introduction:
While radical prostatectomy (RP) renders good cancer control, urinary incontinence (UI) remains a major morbidity issue and significantly influences the postoperative quality of life. With the possibility of predicting the chances of UI, urologists receive an important tool in their prognostic armamentarium, which will influence consulting and treatment strategies. The aim of the study was to use data from routine preoperative MRI to estimate the risk of UI after RP.

Methods:
We analyzed patients who underwent robot-assisted RP for localized prostate cancer at our institution between July 2015 and April 2017. Preoperatively, all patients received a multiparametric MRI of the prostate (3 Tesla Siemens Magnetom). Prospectively collected questionnaires regarding UI were evaluated one year postoperatively (ICIQ-Score). “Tissue 4D” software from Siemens on “Syngo Multimodality Workplace” was used to measure the contrast media (CM) kinetics (median initial area under the curve for the first 60 seconds after injection of CM [median iAUC]). With this technique, we were able to visualize the preoperative perfusion quality of the pelvic floor (levator ani muscle) in comparison to the surrounding pelvic muscle structures (reference). Outcomes were dichotomized into groups “continent” (ICIQ-score = 0-5) and “incontinent” (ICIQ-score≥ 6). In each patient, we determined the ratio between the median iAUC of the levator ani muscle to the median iAUC of the surrounding pelvic muscle structures. The resulting perfusion ratios among the group of continent patients were then compared to the ratios of the incontinent patients.

Results:
In total 42 patients were included in this study (n=22 in “continent”, n=20 in “incontinent” group). The groups did not differ with regard to clinically relevant characteristics (age, PSA, Gleason-Score and nerve sparing). The perfusion ratio from the continent group was significantly higher than the one from the incontinent group (1.61 vs. 1.15, respectively; difference in perfusion ratios = 0.45; 95% confidence interval (CI): 0.09 to 0.81, p = 0.015). In a further analysis of excellent outcomes (ICIQ = 0) vs. poor outcomes (ICIQ ≥ 10) of 10 patients in each group, the perfusion ratio of excellent outcomes was also significantly higher (1.48 vs. 0.94, respectively; difference in perfusion ratios = 0.53; 95% CI: 0.04 to 1.03, p = 0.036).

Conclusion:
Our data demonstrate a promising new strategy to assess the perfusion of pelvic muscle structures with CM kinetics to predict continence after RP. This may facilitate preoperative patient consulting and decision making.

5394

M. Huemer[1], S. Mairpady Shambat[1], S. Söderhom[2], S. Götschi[1], M. Boumasmoud[1], C. Vulin[4], D. Bumann[2], R.A. Schüpbach[3], A.S. Zinkernagel[1]

Combination of high virulence and antibiotic persistence in a Staphylococcus aureus strain resulting in treatment failure

Division of Infectious Diseases and Hospital Epidemiology, University Hospital Zurich, University of Zurich[1], Focal Area Infection Biology, Biozentrum, University of Basel[2], Institute of Intensive Care Medicine, University Hospital Zurich[3], Department of Environmental Microbiology, Eawag, ETH Zurich, Dubendorf[4]

Introduction:
Staphylococcus aureus is well known for causing a variety of community and hospital acquired infections, e.g. superficial skin infections and severe invasive infections like endocarditis. Approximately 50% of the human population are colonized intermittently or permanently with *S. aureus*, which is associated with a higher infection risk. *S. aureus* easily acquires antibiotic resistances, but even susceptible bacteria can survive antibiotics by forming persisters. Persisters are a phenotypic subpopulation that tolerate and survive high antibiotic concentrations. Here, we present a clinical case of a methicillin susceptible USA300 *S. aureus* endocarditis. Despite state-of-the-art therapy including multiple antibiotics and surgical interventions, the infection was not controlled and the patient died. We investigated in detail the strain's ability to survive antibiotics and characterized a cytotoxic strain that displayed an antibiotic persisting phenotype at the same time.

Methods:
We analyzed bacterial growth directly from patient's abscess material by automated agar plate imaging and mimicked the patient's treatment regimen *in vitro* as well as in an *in vivo* murine abscess model. Additionally we performed whole genome sequencing (WGS), measured intracellular ATP levels, analyzed the interaction of the strain with human neutrophils and performed quantitative proteomics of pH-stressed bacteria. Finally, we tested the synthetic retinoid CD1530 for its ability to reduce persisters and increase bacterial clearance.

Results:
We found that the clinical isolate CI1149 grew very heterogeneously resulting in various colony sizes when directly grown from the patient's abscess as compared to growth under standard conditions. This was reflected in an increased bacterial lag time, which we previously linked to protection from antibiotic killing. Even though the strain was susceptible to all the antibiotics used for treatment, *in vitro* and *in vivo* modelling of the infection showed that the clinical isolate survived high concentrations of better than the laboratory strain Cowan I as well as other USA300 strains, indicating a tolerant phenotype. The clinical isolate had the lowest intracellular ATP levels in stationary phase, corresponding to a reduced metabolic state. Exposure of CI1149 to an acidic environment enhanced its resistance to killing by neutrophils and intracellular survival. Proteomic analysis of the clinical isolates after pH 5.5 stress showed decreased abundances of proteins important for electron transport, transcription, and biosynthesis compared to pH 7.4. On the other hand, proteins related to nitrogen utilization, which have been shown to be important in acidic stress response, for oxidative stress response, for protein degradation and for pathogenicity were upregulated. Finally, we showed that combination of conventional antibiotics and CD1530 reduced the bacterial load below the detection limit *in vitro* as well as *ex vivo* when bacteria where taken from murine abscesses.

Conclusion:
Despite state-of-the-art treatment and susceptibility of the clinical *S. aureus* isolate, the infection could not be controlled leading to the death of the patient. We showed that this clinical isolate adapted dynamically to stress conditions encountered within the host resulting in a highly virulent state. At the same time, a large subpopulation of persister cells was formed enabling the strain to survive antibiotic treatment. Combination of conventional antibiotics with the "persister-killing molecule" CD1530 eradicated the bacteria including the persister population.

5395

R. Pfeifer[1], S. Schick[2], W. Hell[2], S. Halvachizadeh[1], K. Sprengel[1], K. Jensen[1], H-C. Pape[1]

Analysis of Injury and Mortality Patterns in Deceased Patients with Blunt Trauma: An Autopsy Study

Department of Trauma Surgery, Zurich University Hospital, Zurich[1], Institute of Legal Medicine, University of Munich, Munich, Germany.[2]

Introduction:
Despite improvements in prevention and rescue, mortality rates after severe blunt trauma continue to be a problem. Moreover, the previous studies are not standardized and show high variability in inclusion and exclusion criteria. The present study analyzes mortality pattern in representative blunt trauma population and the impact of demographic, injury patterns, locations, and timing of death.

Methods:
Patients deceased between 01.01.2004 and 31.12.2005 due to a traffic injury were subjected to a standardized autopsy. Inclusion criteria: death from blunt trauma due to road traffic injuries (injury severity score ≥ 16), patients from a defined geographical area, death on scene or in the hospital. Exclusion criteria were: suicide, homicide, penetrating trauma, monotrauma including isolated head injury. Parameters studied: Patient demographics, injury severity, (based on Injury severity score (AIS/ISS), exact time and cause of death assessed by rescue documents and autopsy. Statistics: Student's *t*-Test/Wilcoxon (nonparametric test), Mann-Whitney-U-test (parametric test) or Chi-square. For representativity calculations *Kirkman-Test*. P-value of 0.05 was deemed significant.

Results:
277 consecutive injured patients were included. Mean age: 46.1 ± 23 years, 67.5% males, 40.5% of the victims showed an ISS of 75. We have identified a "unimodal" distribution of mortality in blunt trauma patients. The most frequently injured body regions were head (38.6 %), chest (26.7%) or head/chest injuries (11.0%). The cumulative demonstration of mortality has shown that several factors, such as injury pattern and regional location of accident also affects the pattern of mortality.

Conclusion:
The majority of patients died on scene from severe head and thoracic injuries. A homogenous distribution of death after initial peak on scene was found. Moreover, it could be shown that several factors, such as injury pattern and regional location of accident may affect the pattern of mortality as well.

5396

L. Pasterk[1], N. Bonetti[1], S. Gobbato[1], M. Frick[2], S. Meier[2], G. Camici[1], T. Lüscher[1], M. Egloff[2], P. Köpfli[2], H. Schmid[2], J. Beer[2]

The effects of PCSK9 inhibitor therapy on platelet structure and function

Center for Molecular Cardiology, Division of Cardiology, University Hospital of Zurich, University of Zurich[1], Department of Internal Medicine, Cantonal Hospital Baden, Baden[2]

Introduction:
PCSK9 inhibitors, a novel class of lipid lowering agents, may reduce plasma LDL-C levels to ultralow levels of less than 0.4mmol/l in 9% of the treated study population. Although “the lower, the better” is a guideline approved and welcome concept in preventing cardiovascular complications, pleiotropic effects of PCSK9-inhibitors remain to be investigated. Given that emerging evidence suggests a direct activatory role of LDL-C on platelets and novel findings indicate that PCSK9 levels are associated with platelet reactivity, the aim of this study is to investigate potential effects of PCSK9-inhibitors on platelets

Methods:
In this pilot study, citrated blood from patients on PCSK9-inhibitor therapy (n=16) and matched controls (n=16) was collected in order to investigate platelet numbers, structure and functional aspects. Platelet rich plasma (PRP) was analyzed for aggregation using ADP, collagen and TRAP as stimuli. In addition, the platelet receptor GPIb and the activation-dependent glycoproteins P-selectin and GPIIb/IIIa were quantified by flow cytometry.

Results:
Platelet aggregation to a low concentration of TRAP (5µM) was decreased by almost 50% in patients on PCSK9-inhibitor therapy compared to controls (P=0,0381), while no significant differences could be observed in ADP and collagen-induced platelet aggregation. In line with these results, the early platelet activation marker P-selectin was downregulated ~30 % (P=0,0188) in TRAP stimulated platelets of patients on PCSK9-inhibitor therapy. Activation of the major platelet integrin GPIIb/IIIa was not significantly affected by stimulation with ADP, collagen or TRAP. Of note, the PCSK9 inhibitor therapy did not affect the expression profile of the fibrinogen receptor GPIb as well as the total number of platelets.

Conclusion:
Our data support the hypothesis that platelets from patients treated with PCSK9-inhibitors show a reduced reactivity. This is particularly evident in platelet aggregation and P-selectin expression upon TRAP stimulation, indicating an important mechanistic role for the platelet PAR receptors. Whether these pleiotropic effects result from LDL-C reduction and/or different plasma levels of PCSK9 need to be further investigated in the ongoing study.

5397

L. Gstrein-Prause[1], A. Mortezavi[1], C. Millan[1], S. Wyler[2], T. Sulser[1], F. Recker[2], M. Kwiatkowski[2], D. Eberli[1]

Influence of regular aspirin intake on PSA values, prostate cancer incidence and overall survival in a prospective screening trial cohort (ERSPC Aarau)

UniversitätsSpital Zürich, Department of Urology[1], Kantonsspital Aarau, Department of Urology[2]

Introduction:
Chemoprevention of prostate cancer (PCa) has been extensively investigated in the last decades. So far only 5-alpha-reductase-inhibitors (5-ARI) are supported by clinical evidence to have chemopreventive effect on PCa incidence, hence unclear in terms of prevention of aggressive PCa. Evidence for an effect of ASA on PCa is conflicting. The exact interaction pathways between ASA and carcinogenesis are still to be established. The aim of the study was to analyze the influence of ASA intake on PSA values and PCa development.

Methods:
A population-based analysis including 4314 men from the European Randomized Study of Screening for Prostate Cancer (ERSPC) database was conducted. Data about drug intake, age, family history and symptoms was obtained by a self-administered questionnaire. A transrectal ultrasound guided prostate biopsy was performed in men with a PSA-level > 3 ng/ml. Tumor stage and grade were registered; incidence and mortality data were obtained through registry linkages. PCa incidence and grade, total PSA value, free-to-total PSA and overall survival were compared between ASA users and non-users, respectively.

Results:
Median follow-up time was 9.6 years. In all, n = 789 (18.3%) men used aspirin [ASA+]. Although overall PCa incidence was significantly lower among aspirin users ([ASA+] 54 (6.8%) vs. [ASA-] 338 (9.6%), p 0.015), the multivariate cox-regression analysis did not show the decreased risk to be diagnosed with PCa ([ASA+] hazard ratio (HR) 0.78, 95% confidence interval (CI) 0.57 to 1.08) to be statistically significant. Total PSA values were significantly lower in aspirin users for both baseline (1.6 vs. 1.8 ng/ml, p 0.0072) and follow-up-visits after four years (1.75 vs. 2.1 ng/ml, $p < 0.001$). Multivariate cox-regression analysis predicted significantly higher overall mortality among ASA users compared to non-users ([ASA+] HR 1.58, 95% CI 1.17 to 2.13).

Conclusion:
In our study population we could demonstrate that ASA intake did not alter overall PCa risk in a statistically significant manner. However, the finding of persistently lower PSA values in ASA users is of potential clinical importance. It suggests that PSA cutoff values should be lowered in ASA users otherwise it may introduce potential bias towards delayed PCa detection in this group, especially outside a screening setting. On the other hand, lower PSA values may suggest a protective effect of ASA on PCa development

5398

L. Roth[1], E. Breuer[1], R. Graf[1], P-A. Clavien[1], A. Gupta[1], K. Lehmann[1]

The impact of hyperthermic intraperitoneal chemotherapy (HIPEC) on the anticancer immune response

Surgical Oncology Research Laboratory, Department of Surgery and Transplantation, University Hospital Zurich[1]

Introduction:
The combination of cytoreductive surgery (CRS) and hyperthermic intraperitoneal chemotherapy (HIPEC) has improved survival of selected patients with peritoneal metastasis from colorectal cancer. Nevertheless, peritoneal recurrence, presumably due to remnant cancer cells, is common and requires further optimization of this locoregional treatment. Therefore, it is important to understand mechanisms operating behind HIPEC. We hypothesize that the combination of chemotherapy and heat might not only be cytotoxic, but may also induce strong immunogenic changes within the tumor microenvironment. We therefore assessed effects of Mitomycin C/Doxorubicin (M/D) and Oxaliplatin (Oxa), widely used in clinical settings, on the immunogenicity of colorectal cancer cells in-vitro. We examined the expression of immunogenic cancer-testis antigens (CTAs) on cancer cells after HIPEC-like conditions in-vitro and subsequent monocyte-derived dendritic cell (Mo-DC) maturation and cytotoxic T-cell activation (CD8+ T-cells).

Methods:
Multiple colorectal cell-lines were treated with M/D or Oxa for 30 minutes with and without hyperthermia (43^0C). 72 hours after treatment, CTA expression was analyzed using qPCR and western blot. To assess Mo-DC maturation, we set up a co-culture between differentially treated colorectal cells and Mo-DC`s. We analyzed surface markers such as HLA-DR and CD 83 to assess Mo-DC maturation using flow cytometry. Further, Mo-DC`s that were pre-incubated with treated and untreated colorectal cancer cells were added to purified CD8+ T-cells to measure their activation via intracellular IFN-y staining.

Results:
Multiple colorectal cell-lines were treated with M/D or Oxa for 30 minutes with and without hyperthermia (43^0C). 72 hours after treatment, CTA expression was analyzed using qPCR and western blot. To assess Mo-DC maturation, we set up a co-culture between differentially treated colorectal cells and Mo-DC`s. We analyzed surface markers such as HLA-DR and CD 83 to assess Mo-DC maturation using flow cytometry. Further, Mo-DC`s that were pre-incubated with treated and untreated colorectal cancer cells were added to purified CD8+ T-cells to measure their activation via intracellular IFN-y staining.

Conclusion:
HIPEC treatment induces immunogenic changes in colorectal cancer cells via upregulation of two CTAs, Cyclin A1 and SSX-4, on mRNA and protein level. Furthermore, HIPEC leads to Mo-DC maturation and subsequent cytotoxic T-cell activation. These novel insights may explain observed long-term effects in selected patients, and represent a novel aspect of HIPEC, beyond cytotoxicity allowing fine tuning of this treatment approach.

5399

D. Lenggenhager[1], M. Amrutkar[2], P. Sántha[5], M. Aasrum[2], J. Löhr[6], I. Gladhaug[4], C. Verbeke[3]

Comparison of different pancreatic stellate cell cultures currently used for the in vitro study of human pancreatic cancer

Department of Pathology and Molecular Pathology, University Hospital Zurich[1], Department of Pharmacology, Institute of Clinical Medicine, University of Oslo, Norway[2], Department of Pathology, Institute of Clinical Medicine, University of Oslo, Norway[3], Department of Hepato-Pancreato-Biliary Surgery, Institute of Clinical Medicine, University of Oslo, Norway[4], Department of Pathology, Oslo University Hospital Rikshospitalet, Norway[5], Department of Clinical Science, Intervention and Technology, Karolinska Institutet, Stockholm, Sweden[6]

Introduction:
The tumor microenvironment of pancreatic ductal adenocarcinoma (PDAC) is characterized by an exceedingly prominent stroma, in which pancreatic stellate cells (PSCs) play a central role. Not only are they the main producers of collagens and other extracellular matrix proteins, they also play an important role in tumor progression and in the pronounced chemoresistance of PDAC. Currently, much of the research in this field is still based on *in vitro* studies. Given the limited availability of patient-derived PSCs from PDAC, laboratories around the world use many different pancreatic stellate cell models for their experimental studies of human PDAC, which are mostly of human or murine origin, may be primary or immortalized, and derived from normal pancreas, chronic pancreatitis or pancreatic cancer. Despite these considerable differences, possible divergence in phenotype and functions have not been investigated, leaving unanswered questions about the comparability of data from studies using different PSC cultures.

Methods:
Therefore, in this study, a panel of seven commonly used PSC cultures was characterized regarding key phenotypical and functional features: three primary PSC cultures from human PDAC (hPSC-1, hPSC-2, hPSC3), one primary PSC culture from normal human fetal pancreas (HPaSteC), one immortalized human PSC culture (i-hPSC) and two immortalized mice PSC cultures (i-mPSC C2 and C3). The interaction with pancreatic cancer cells was analyzed by exposure of two commercially available cancer cell lines (BxPC-3 and MIA PaCa-2) to the soluble factors produced by the different PSC cultures.

Results:
As expected, the three primary PDAC-derived PSC cultures consisted of an activated PSC phenotype with expression of the PSC activation marker a-SMA. They showed a significant induction of collagen synthesis by TGF-b-stimulation, and had a significant effect on the cancer cells with induction of proliferation, migration and chemoresistance to gemcitabine. None of these features were observed with the immortalized human PSC culture, whereas the two immortalized mice PSC cultures showed only some of them. However, the high proliferation rate and unlimited passaging of the immortalized PSC cultures makes them easier to handle than the primary PSC cultures from human PDAC. Unexpectedly, the commercially available HPaSteC culture (derived from normal human pancreas in which PSCs are expected to be quiescent) proliferated at a rate similar to that of the immortalized human PSC culture, while interestingly, it reproduced other functional features and in particular the interaction with cancer cells even better than the primary PDAC-derived cultures. Differences in the interaction with pancreatic cancer cells were reflected by differences in the secretome composition of the various PSC conditioned media.

Conclusion:
The study reveals considerable differences in features and functions that are key to PSCs and in their interactions with pancreatic cancer cells. Awareness of these differences is important when selecting the most appropriate PSC culture for a given experiment, as well as when comparing results from studies that used different PSC cultures.

5400

C. Millan[1], L. Gstrein[1], F. Clement[1], D. Eberli[1]

Developing a liquid biopsy diagnostic for prostate cancer based on extracellular vesicles

Klinik für Urolgie, Universitätsspital Zürich[1]

Introduction:
Extracellular vesicles (EVs; e.g. exosomes) – which are shed by cancer cells during all stages of tumor development into the blood and carry a milieu of proteins, DNA, and RNA specific to their cell of origin – are an especially promising liquid biopsy target. Here, we have developed a 3-dimensional tumor model that leads to recapitulation of the EV secretion behaviors observed in vivo including enrichment of tumor-specific proteins and RNAs. The molecular cargo of EVs produced by cancer cells cultured this way was analyzed during discovery to identify novel protein and lncRNA "hits" that have potential to be used as biomarkers for prostate cancer diagnostics. The first of these hits have been validated on a small cohort of retrospective clinical samples.

Methods:
For a range in comparisons we focused on 4 cell types: PC3 (aggressive prostate cancer cells), LNCaP (less aggressive prostate cancer cells), PNT1 (benign prostate epithelial cells), and adipose-derived stem cells (ASCs; non-prostate cells included as controls). EVs secreted by cells in 3D were compared to those secreted by the same cells cultured in 2D (tissue culture plastic). Overall EV production was quantified by Bradford assay, EV size distributions assessed by nanoparticle tracking analysis and TEM, and molecular cargo was compared by LC-MS/MS and RNAseq. Protein and lncRNA hits were then validated via western blot and qPCR in a small cohort of patient samples over wide ranging Gleason scores and PSA levels.

Results:
All cell types showed heightened EV production when cultured in 3D, ranging from 2-5x increased EV-protein per cell. EV-diameters did not vary across cell types or culture conditions. Next generation sequencing (NGS) and proteomics analyses revealed dramatic alterations in EV content as a result of 3D culture. Principle component analysis performed on NGS data of the 500 genes of highest variance exhibited the highest magnitude of expression changes for the PC-3 cells and the ASCs. Gene ontology enrichment indicated ubiquitous down-regulation of genes involved in directing intracellular protein traffic for all cell types. Differences seen in proteomics were equally stark – an average of 400 extra proteins were detected in proteomics of 3D-EVs that were not found in 2D-EVs of the same cell type. Comparing these lists with public databases, including ExoCarta and Vesiclepedia, revealed numerous proteins found in 3D-EVs that have not previously been reported as cargo in EVs. In patient plasma, EV concentrations correlated with Gleason Scores, while PSA levels did not.

Conclusion:
Utilization of our 3D cell culture model has led to the potential uncovering of novel biomarkers that could be used as targets for liquid biopsy tests to detect and monitor prostate cancer. Above all, the data presented here speaks to the importance of the in vitro model used for characterization of EVs, especially for clinical applications. Further clinical validation on a larger patient cohort is underway.

5401

S. Deycmar[1], S. Gruber[2], W. Dörr[2], A. Lomax[3], M. Pruschy[1]

The HSP90 inhibitor ganetespib specifically sensitizes cancer cells for clinical SOBP proton beam irradiation in comparison to photon irradiation.

Laboratory of Applied Radiobiology, Dept. of Radiation Oncology, University Hospital Zurich[1], Applied and Translational Radiobiology, Dept. of Radiation Oncology, Medical University Vienna, Austria[2], Center for Proton Therapy, Paul Scherrer Institute, Villigen[3]

Introduction:
Recent data suggest an elevated dependence on homologous recombination (HRR) to repair DNA double strand breaks (DSB) subsequent to proton irradiation. We investigate the effect of HSP90 inhibition by ganetespib and the role of DNA DSB repair deficiencies for specifically sensitizing cancer cells towards proton irradiation.

Methods:
NSCLC (A549) cells were irradiated with 200kV photon irradiation and a proton pencil beam at a proximal (LET 1,97 keV/µm) and a distal position (LET 4,43 keV/µm) of a 8 cm SOBP in a PMMA/water phantom and clonogenic survival fractions were determined. Physical doses are stated and nuclear repair foci assays were used to monitor the DSB repair response.

Results:
Inhibition of HSP90 strongly sensitizes A549 cells for proton irradiation within the proximal SOBP. The dose-modifying factor (DMF) at 50%, 10%, and 1% cell survival was 1.18, 1.10, and 1.06 for photons, and 1.17, 1.09, and 1.05 for cells irradiated at the distal position of the SOBP. Interestingly, the DMF was increased to 1.35, 1.22, and 1.16 for cell irradiated at the proximal position of the SOBP.

Conclusion:
Administration of ganetespib provides a novel approach to specifically sensitize cancer cells to proton irradiation. Our data suggest that combinatorial approaches induce a differential cellular response when administered with photon respectively proton irradiation. Thus, extensive testing will be required to convert from routine photon protocols to a proton radiotherapy setting.

5402

L. Roth[1], X. Muller[1], R. Graf[1], Y. Tian[1], B. Imthurn[2], P. Imesch[4], N. Ochsenbein-Kölble[3], P-A. Clavien[1], P. Dutkowski[1], O. De Rougemont[1]

Prolonged Cold Preservation Exposes Uterus Grafts to Major Ischemia-Reperfusion Injury

Department of Surgery and Transplantation, University Hospital Zurich[1], Department of Reproductive Endocrinology, University Hospital Zurich[2], Department of Obstetrics, University Hospital Zurich[3], Department of Gynecology, University Hospital Zurich[4]

Introduction:
In Switzerland, over 1500 women have an absolute uterine factor infertility (AUFI) with the main underlying causes being the Mayer-Rokintansky-Küster-Hauser-Syndrome and previous hysterectomy. Uterus transplantation offers the possibility of a pregnancy for those patients. The feasibility, safety and success of the procedure have been shown with the first birth in Sweden in 2015. Since then over 50 uterus transplantations have been performed worldwide. Although most programs worldwide actually use live donor grafts, some, e.g. Belgium, Czech Republic and Brazil opted for a deceased donation program. In 2017, the first baby was born from a deceased graft in Brazil. In uterus transplantation, as for transplantation of solid organs in general, the succession of cold preservation of the graft and subsequent transplantation may lead to considerable damage to the organ. However, no systematic quantification of ischemia-reperfusion injury (IRI) in the setting of uterus transplantation from deceased donors has been performed so far. As a prerequisite for a successful uterus transplantation, this study investigates the IRI of uterus grafts, and its impact on graft viability. IRI occurs during the first 30 minutes of transplantation of a cold stored solid organ. To study these early events of transplantation, we used an isolated ex-vivo uterus perfusion model.

Methods:
We included a control group consisting of uterus grafts, which were directly perfused after harvesting from healthy female pigs, and a study group of uterus grafts, which underwent extensive cold storage (24hours) prior to perfusion. For all experiments, transplantation was simulated by ex-vivo perfusion with autologous pig blood for 3 hours. Quantification of IRI was performed by analysis of tissue and perfusate samples in situ, before and after cold preservation as well as during the entire perfusion.

Results:
After uterus harvesting (median duration 40 minutes), four uteri were included in the control group with a median cold preservation time of 2 hours and 2 were included in the study group with a cold preservation time of 24 hours. After cold storage, histological analysis of the uteri of both groups showed no difference compared to the in situ samples. Upon ex-vivo perfusion, the uteri in the control group showed sustained and homogenous tissue perfusion resulting in rhythmic muscle contractions. On histological analysis, the endometric glands and adjacent submucosal structure were well preserved during the entire perfusion. In contrast, the uteri undergoing 24 hours of cold preservation showed inhomogeneous perfusion with rapid tissue swelling resulting in necrotic tissue areas. No muscle contractions were observed. Histological analysis showed a disrupted endometrium with extensive intramural bleeding.

Conclusion:
Our study shows that prolonged cold preservation of uterus grafts leads to major IRI, resulting in extensive tissue swelling and necrosis. In the setting of clinical transplantation, this may have significant impact on organ viability, recipient safety and potentially pregnancy rate. Reducing cold preservation duration and using strategies to dampen IRI are a prerequisite for a successful uterus transplantation.

5403

L. Michels[1], R. Büchler[1], K. Kucian[2]

Structural hyperconnectivity in brain regions for number line processing and memory in children with developmental dyscalculia

Department of Neuroradiology, University Hospital Zurich, University of Zurich[1], Center for MR-Research, University Children's Hospital, Zurich[2]

Introduction:
Developmental dyscalculia (DD) is a developmental learning disability associated with deficits in processing numerical and mathematical information. Several studies demonstrated functional network alterations in DD. Yet, there are not studies which examined the structural network integrity in DD.

Methods:
We used structural covariance network analysis in order to compare brain volume based structural connectivity between 19 children with DD and 18 typically developing children (TD).

Results:
We found hyperconnectivity of the left intraparietal sulcus to the left cingulate cortex and angular gyrus but also to the right middle frontal and superior temporal gyrus as well as superior parietal lobe ($p < 0.05$, corrected). In addition, the right hippocampus showed hyperconnectedness to right middle frontal- and lateral occipital cortex. In contrast, the bilateral Heschl's gyrus were hypoconnected in DD.

Conclusion:
Our results extend functional resting-state connectivity studies by revealing abnormal connectivity in DD on the structural level in areas involved in number processing and memory function.

5404

C. Wicki[1], C. Walker-Egger[2], T. Simic[2], J. Hanson[3], S. Schippling[2]

Repetitive transorbital alternating current stimulation in acute autoimmune optic neuritis: Pathobiological basis and design of a phase I/ IIa pilot study

Department of Health Sciences and Technology, ETH Zurich[1], Neuroimmunology and Multiple Sclerosis Research Section, Department of Neurology, University Hospital Zurich[2], Department of Ophthalmology, University Hospital Zurich[3]

Introduction:
Optic neuritis (ON) is an acute inflammatory, demyelinating attack of the optic nerve, frequently of autoimmune origin, and a common clinical manifestation of multiple sclerosis. ON triggers neurodegeneration in the entire visual pathway; translating into visual dysfunction. Currently, no neuroprotective therapy or visual rehabilitation with satisfying evidence can be offered to patients. Repetitive transorbital alternating current stimulation (rtACS) is a methodology applied to electrically stimulate the retina and the optic nerve, and is considered having neuroprotective- and restorative potential through remyelination-dependent but also independent mechanisms. While rtACS based on (pre-) clinical evidence holds promise as an interventional approach, clinical evidence of safety and efficacy supporting this approach in patients with autoimmune ON is not yet available.

Methods:
We are planning to run a prospective, randomized, patient-blinded, sham-controlled pilot study to generate safety and preliminary efficacy data on the effects of rtACS on functional visual as well as structural outcomes in a first-ever acute ON, using low-contrast visual acuity testing and optical coherence tomography-derived measures such as the thickness of the macular ganglion cell and inner plexiform layer (marker of neurodegeneration).

Results:
For optimizing timing and patient selection in this interventional study, we recently completed a longitudinal study exploring the temporal dynamics of structural and functional visual changes following a first-ever episode of acute ON. Retinal atrophy was most pronounced at early stages of the disease course, therefore early or even hyperacute intervention may be the most promising strategy to prevent irreversible neuroaxonal degeneration. Furthermore patients who are diagnosed with a first-ever episode of acute ON are therefore the most suitable patients for this specific study design.

Conclusion:
ON is an important manifestation and major source of persistent disability in MS. Developing neuroprotective or -regenerative therapies, that specifically target neurodegeneration, is a clear unmet medical need. Demonstrating safety and satisfying tolerability together with neuroprotective and -regenerative efficacy of a novel, non-pharmacological treatment approach in ON would be a major breakthrough.

5405

F. Tschanz[1], M. Pruschy[2]

ADAM17-Dependent paracrine and intercellular communication in response to irradiation

University of Zurich[1], University Hospital Zurich and University of Zurich[2]

Introduction:
Cancer is a leading cause of death worldwide. For most solid tumors, the first line strategy consists of radiotherapy alone or in combination with other anti-cancer agents. Irradiation (IR) induces the formation of reactive oxygen species that induce DNA damage and chromosomal aberrations which eventually result in mitotic catastrophe and cell death. The response to IR depends on several factors and there is a difference in radiosensitivity for different cell types. The Laboratory of Radiation Oncology recently demonstrated in an IR-dependent large scale secretome analysis that, among other factors, the metalloproteinase ADAM17 (a disintegrin and metalloproteinase 17) is upregulated following irradiation in a time and dose dependent manner. Increased ADAM17 activity correlates with increased radiation resistance and is therefore an interesting candidate target for optimizing the impact of IR. ADAM17 is a single-pass transmembrane protein and is involved in the cleavage and release of soluble membrane-bound pro-proteins from the extracellular surface. Substrates undergoing ADAM17 shedding include tumor necrosis factor alpha, transforming growth factor alpha and epidermal growth factor among others. Furthermore, ADAM17 is also associated with the release of various membrane-anchored cytokines, cell adhesion molecules, receptors, ligands and enzymes. This presents ADAM17 as a crucial mediator of treatment resistance and a promising target to develop novel treatment strategies. Our aim is to elucidate the effects of IR-induced ADAM17-dependent paracrine and intercellular communication, the respective signaling pathways and the resulting implications for cancer therapy.

Methods:
The effect of ADAM17 pro- or deficiency is assessed on the level of intercellular communication by the co-culturing of cells with different ADAM17-status (wild-type or knockdown) in combination with irradiation. Paracrine communication is investigated with endothelial cells (ECs) migrating towards ADAM17 wild-type or knockdown cells. Furthermore, signaling entities involved in ADAM17-regulated pathways are mechanistically studied. *In vivo* experiments combining IR and a monoclonal antibody against ADAM17 can give insight into the ADAM17-dependent communication of tumor cells, the (tumor-)microenvironment and presumably cell collectives at more distant sites within an organism.

Results:
As demonstrated in the Laboratory of Radiation Oncology, ADAM17 inhibition in combination with IR results in decreased clonogenicity across several cancer cell lines *in vitro*. *In vivo*, the pharmacological inhibition of ADAM17 in combination with radiotherapy resulted in a significant tumor growth delay. As a paracrine readout, we observed increased migration of irradiated ECs toward the non-small cell cancer cell lines A549 and H358. This increase in migration could be abrogated by inhibiting ADAM17 either via inducible short hairpin constructs targeting ADAM17 or via a monoclonal antibody. Additionally, our results demonstrated decreased survival of irradiated wild-type cells when co-cultured with ADAM17-deficient cells.

Conclusion:
Radiosensitization of several cancer cell lines and the decrease in migration of ECs upon ADAM17 inhibition suggests this metalloproteinase as a promising target in cancer treatment. Additional experiments need to be performed to understand the mechanistic role of ADAM17 shedding and to identify the key players within promoted signaling pathways.

5406

Y. Nonomura[1], O. Eichhoff[1], M. Levesque[1], R. Dummer[1]

New treatment strategy in melanoma patients with c-kit mutations targeting the tyrosine phosphatase SHP2

University Hospital Zurich, Dermatology, Zurich[1]

Introduction:
In recent years, targeted therapies have drastically improved the prognosis of malignant melanoma patients with BRAF mutations. However, melanoma patients without BRAF mutations are left with few treatment options in their advanced stages. Mutations in the cKit kinase have been reported also in melanoma patients, especially in those with acral lentiginous (ALM), and mucosal melanoma which are highly malignant clinical subtypes. C-kit mutations are rare, occurring in about 2-8% of all melanomas and in about 15-20% of ALMs or mucosal subtypes. C-kit is a receptor tyrosine kinase type III, which binds to stem cell factor (SCF). Upon ligand binding, cKit receptor forms a protein dimer that activates its intrinsic tyrosine kinase activity, which in turn phosphorylates and activates signal transduction molecules that propagate the activation of receptor tyrosine kinase (RTK) signalling. Tyrosine-phosphatase SHP2 (src homology region 2) is known to be a positive effector molecule for RTK signalling.
A large-scale shRNA screen of over 250 cancer cell lines (CCLE data base) revealed that the depletion of the tyrosine phosphatase SHP2 RNA caused a reduction in the viability of only a subset of cell lines which are dependent on RTK signalling (e.g. EGFR amplification in breast cancer cells). This finding led to the development of the small molecule SHP099, which is an orally bioavailable inhibitor of SHP2. It stabilizes SHP2 in an auto-inhibited conformation and supresses MAPK signalling and blocks the proliferation of receptor tyrosine kinase-driven human cancer cells in vitro and in vivo.
Here we investigate the effects of tyrosine-phosphatase SHP2 inhibition by SHP099 in patient-derived ALM cultures with confirmed cKit mutations.

Methods:
We established primary melanoma cell cultures derived from ALM patients harbouring c-kit mutations (n=4) and melanoma patients not harbouring c-kit mutations (n=3). The mutation in each cell culture was confirmed by PCR. Melanoma cell cultures were treated with SHP099 or in combination with other compounds including Imatinib. Western blot (WB) analysis of different effector molecules (ERK1/2, p38, or PI3K) was performed to assess the activity of different signalling pathways.

Results:
The SHP inhibitor SHP099 significantly reduced the viability of c-Kit mutated primary melanoma cell cultures (paired t test, p=0.023, IC50 of 1.16–2.18, 1.75 μM on average) as well as of 3D melanoma. In contrast, cutaneous melanoma cultures and 3D spheroids harbouring BRAF or NRAS mutations were not affected by SHP099 treatment (IC50 of 56-630, 291 μM on average). The combination of Imatinib and SHP099 did not show synergistic effects. WB analysis revealed that pERK expression was significantly downregulated in c-kit mutated melanoma cell lines after treatment with SHP099 (paired t test, p=0.049) while pAKT expression did not change.

Conclusion:
The SHP2 inhibitor SHP099 reduced the proliferation of c-kit mutated melanoma cells through the down-regulation of the MAPK pathway. Our results suggest that SHP2 may have potential for clinical application of cKit-mutated melanomas.

5407

N. Schneider[1], M. Ferster[2], C. Lustenberger[2], W. Karlen[2], H. Fehr-Duda[3], E. Fehr[4], R. O'Gorman[5], R. Huber[6], C. Baumann[1], A. Maric[1]

Linking the change in decision-making after sleep restriction to the restorative function of sleep

Department of Neurology, University Hopsital Zurich[1], Department of Health Sciences and Technology, ETHZ Zurich[2], Department of Banking and Finance, University of Zurich[3], Department of Economics, University of Zurich[4], Center for MR-Research, University Children's Hospital Zurich[5], Child Development Center, University Children's Hospital Zurich[6]

Introduction:
Increasing sleep loss in modern society presents a major socio-medical problem. Despite that, chronic sleep restriction (cSR) has not been thoroughly studied in the past. In 2017, we were able to show for the first time that cSR leads to a subjectively unnoticed increase in financial risk seeking. We further found that low levels of slow wave (SW) energy, a marker for the restorative function of sleep, during shortened sleep were associated with this change in behaviour. Time-locked acoustic stimulation during sleep enables modulating SWs and therefore allows to eventually proving the causality of insufficient sleep-dependent restoration of particular brain areas during cSR causing altered behaviour.

Methods:
Healthy, young male subjects (21-30 years; targeted n = 20) undergo 7 consecutive nights of cSR, that is 5 hours sleep per night, twice - once with acoustic stimulation and once without - in a double-blinded, counterbalanced crossover design. The subjects spend all of these nights in the sleep laboratory at the Institute of Pharmacology of the University of Zurich. During sleep, SWs will be targeted using a real time phase locked loop (PLL) algorithm. The auditory stimulus is presented in the up-phase of ongoing SWs in a 6 second ON window followed by a 6 second OFF window in which no stimulus will be presented regardless of SW occurrence or absence. Sleep is recorded via 128 channel high density (hd) electroencephalography (EEG). Financial risk seeking behavior and other behaviour parameters and physiological markers are assessed before the first SR night (baseline) and on the last day of SR in each of the two cSR weeks. Magnetic Resonance (MR) spectroscopy of the right and left prefrontal cortex and pupillometry are also be assessed during those time points. Vigilance is measured every 2-5 hours every day.

Results:
We recently started data collection, which is currently ongoing. Analysis of the first subject completing the study showed that SW activity , that is averaged spectral power in the SW range of 1 – 4.5 Hz, was consistently higher within the ON windows compared to the OFF windows in all 7 consecutive cSR nights ($p < 0.05$ in all nights) in the cSR week with acoustic stimulation. Importantly this was 1) not observed in the condition without acoustic stimulation and 2) did not reflect a decrease of SW activity during the OFF windows, indicating that modulation of SWs during the ON window was successful.

Conclusion:
The current study will create an extensive data set, which, to our knowledge, is so far unique. Our first data analysis shows that acoustic stimulation can significantly modulate SW activity also in healthy young subjects under increased sleep pressure during cSR - something that has not been shown so far. By combining hd EEG with precise acoustic stimulation and the readout of different behavioral parameters, we have the chance to prove that SWs are causally influencing risk seeking behavior and other important higher-order cognitive processes.

As decision making is important in everyday life, this study not only gathers basic research knowledge but also bridges into applied clinical research. Future results will bring new insight in how cSR affects behavior and therefore might influence future treatment of insufficient sleep in society. As acoustic stimulation is completely non-invasive, it might be easily applied to a broad range of patients suffering from insufficient sleep.

5408

M. Luciani[1], N. Bonetti[1], A. Akhmedov[1], L. Liberale[1], F. Maisano[2], T. Lüscher[1], G. Camici[1]

N-Terminal Pro-B-Type Natriuretic Peptide: From Sensor To Effector of Damage?

Center for Molecular Cardiology, Division of Cardiology, University Hospital of Zurich, University of Zurich[1], Department of Cardiovascular Surgery, University Hospital Zürich[2]

Introduction:
B-type natriuretic peptide (BNP) is synthetized by neurons and cardiomyocytes and elicits beneficial pleiothropic effects on different organ targets, such as natriuresis, vasodilation and lypolisis. BNP is synthetized as a pre-pro-hormone and subsequently released in the extracellular space upon cleavage together with its biologically inactive counterpart called N-terminal proBNP (NT-proBNP). The latter fragment is widely employed as a biomarker for heart failure and more recently in demented patients in light of its longer half-life, a preferred urinary excretion route, and higher resistance against degrading enzymes (e.g. neprilysin). Interestingly, a number of studies have detected in patients with heart failure a divergence between plasma and urinary levels of NT-proBNP in favour of blood accumulation suggesting a putative prognostic role of urinary sampling.
In line with the above, we aim at investigating the role of NT-proBNP per se by assessing its effect on cell viability, cell and organ damage or protection in two distinct yet common sources: heart and brain.

Methods:
Human Cardiac and Brain Micro-Vascular Endothelial Cells (HCMVECs and HBMVECs) were chosen as *in vitro* platforms to test NT-proBNP effect exposure at a single cell level. Together with NT-proBNP, TNF**-**α was added in order to mimick an aging condition.
Young (4 months old) and old (21 months old) WT C57BL/6 mice were employed as an *in vivo* model to observe NT-proBNP levels in plasma and urine. Heart and brain morphology and function in respect to age and to peptide levels will be evaluated.

Results:
At 24 hours exposure, both HBMVECs and HCMVECs cultured with NT-proBNP + TNF**-**α enriched exhausted medium showed significantly higher levels of LDH compared to control medium (33.3% vs 20.4% $p=0.02$) (45.1% vs 26.2% $p<0.001$). Of note, are the higher levels of LDH observed with NT-proBNP + TNF**-**α medium compared to TNF**-**α alone (33.3% vs 26.6% for HBMVECs) (45.1% vs 38.7% for HCMVECs). This trend was not observed with NT-proBNP when compared to baseline conditions.

Conclusion:
These preliminary data are suggestive of possible noxic effects elicited by NT-proBNP in stressed cells as observed in pathological and chronic condition such as heart failure and dementias. Further experiment are ought to be conducted at *in vitro* and *in vivo* level in order to evaluate the effect on cell and organ function.

5409

N. Bonetti[1], C. Diaz-Canestro[1], L. Liberale[2], A. Akhmedov[1], M. Reiner[3], M. Merlini[4], F. Ruschitzka[5], T. Lüscher[6], J. Beer[7], G. Camici[1]

Tumor necrosis factor-Alpha inhibition improves stroke outcome in a mouse model of rheumatoid arthritis

Center for Molecular Cardiology, Division of Cardiology, University Hospital of Zurich, University of Zurich[1], First Clinic of Internal Medicine, Department of Internal Medicine, University of Genoa, Italy[2], Clinic for Internal Medicine, University Hospital Zurich[3], Gladstone Institute of Brain Research, UCSF, San Francisco, USA[4], University Heart Center, Cardiology, University Hospital Zurich[5], Royal Brompton and Harefield Hospital Trust, London, UK[6], Clinic for Internal Medicine, Cantonal Hospital Baden[7]

Introduction:
Rheumatoid Arthritis (RA) is a chronic inflammatory disorder, where incidence and severity of myocardial infarction are increased. Data on the incidence and outcome of stroke are conflicting. Thus, we investigated outcome after Ischemia/Reperfusion (I/R) brain injury in a mouse model of RA and assessed for the role of the tumour necrosis factor-alpha (TNF-alpha) inhibitor Infliximab herein.

Methods:
We used a TNF-alpha reliant mouse model of RA. RA and wildtype (WT) animals were treated with vehicle (RA/WT) or Infliximab (RA Infliximab) for 4 weeks, before undergoing I/R brain injury. Stroke size was analysed by TTC staining. Blood brain barrier (BBB) permeability; tight junction protein (TJP) expression; matrix-metalloproteinase (MMP) expression; lipid peroxidation and counts of microglia and invading macrophages were assessed by immunohistochemistry.

Results:
RA-animals displayed larger strokes and poorer neurological performance. Immunohistochemistry on brain sections revealed increased numbers of resident and peripheral innate immune cells (microglia and macrophages); increased BBB-disruption; decreased levels of TJPs claudin-5 and occludin; increased expression of MMP-3 and -9 and enhanced lipid peroxidation. Treatment with Infliximab corrected these alterations.

Conclusion:
We show that RA associates to worse stroke-outcome via exacerbated BBB degradation by decrease of the TJPs claudin-5 and occludin. We identified MMPs-3 and -9 and increased oxidative stress as potential mediators thereof. Increased numbers of resident and peripheral innate immune cells (microglia and macrophages) may in turn contribute to all these effects. Infliximab-treatment restored the phenotype of RA-mice to baseline. Our data provide evidence clearly linking RA to adverse stroke-outcome in mice and indicate an approved TNF-alpha inhibitor as a potential strategy to reduce stroke-burden in this setting.

5410

S. Steiner[1], T. Reding[1], D. Lenggenhager[2], M. Healy[2], A. Gupta[1], G. Wanner-Seleznik[1], R. Graf[1]

Tumor suppressive mechanisms of Gastrokine 1 in pancreatic carcinogenesis

Department of Visceral & Transplantation Surgery, University Hospital Zurich[1], Department of Pathology and Molecular Pathology, University Hospital Zurich[2]

Introduction:
Late detection of pancreatic ductal adenocarcinoma (PDAC) and limited treatment options lead to poor survival of PDAC patients. A better understanding of the pathomechanism leading to PDAC may help to identify biomarkers for early detection. Pre-malignant lesions such as pancreatic intraepithelial neoplasia (PanIN) follow a multistage development process to form PDAC. While studying a K-Ras driven mouse model (KC mice) of PDAC, which recapitulates the stepwise progression of pancreatic cancer, we serendipitously identified Gastrokine 1 (GKN1) in early PanIN lesions. GKN1 is a stomach-derived secreted protein that maintains gastric homeostasis. Loss of GKN1 in gastric cancer suggested that it might act as tumor suppressor. We further confirmed presence of GKN1 in human PDAC samples, and its secretion in cystic lesions. The discovery of GKN1 in pancreatic carcinogenesis is of great importance, as normal pancreas do not express GKN1.Therefore, we aim to investigate the function of GKN1 in the pancreas, to understand the early events that underlie the development of premalignant lesions leading to pancreatic carcinogenesis.

Methods:
We intercrossed KC mice with GKN1-/- mice. GKN1-/- KC & GKN1+/+ KC pups were analyzed at the age of 3- and 9 months for the quantification of PanIN lesions and appearance of tumors via histology. Furthermore, mRNA transcripts were also analyzed to assess genes (relevant for apoptosis, EMT or tissue remodeling and stroma) involved in tumorigenic processes. Using IHC, pancreatic tissues were analyzed to quantify tumor stroma, markers of cell proliferation and apoptosis.

Results:
As noticed previously, GKN1 expression is restricted to low grade premalignant lesions. Analysis of pancreatic tissue from 3 months old GKN1-/- KC mice, showed more PanINs compared to GKN1+/+ KC mice. A significant difference in the mRNA screen revealed a different apoptosis regulation in GKN1-/- KC mice. IHC analysis of Cleaved caspase-3 also suggested decreased apoptosis in the absence of GKN1. We also noticed a significant decrease in Fas protein, a marker for extrinsic apoptosis pathway, in these animals. Nine months old GKN1-/- KC mice, showed increased tumor incidence (40.7% vs 13%). The histological comparison at 9-months showed that GKN1-/- KC mice developed a collagen-rich dense stroma around the pancreatic lesions compared to sparse stroma in KC animals.

Conclusion:
We conclude that the absence of GKN1 leads to accelerated PanIN development. We suggest that GKN1 influences apoptosis avoidance at an early age and development of dense stromal reaction in later stages leading to an increased tumor incidence. In summary, we confirm that GKN1 acts as tumor suppressor in pancreatic cancer.

5411

K. Frontzek[1], M. Carta[1], M. Losa[1], M. Epskamp[1], G. Meisl[3], U. Camenisch[2], S. Hornemann[1], A. Aguzzi[1]

The presence of autoantibodies against the prion protein is independent of PRNP mutations

Institute of Neuropathology, University Hospital of Zurich[1], Department of Pathology, University Hospital Zurich[2], Department of Chemistry, Cambridge University, Cambridge, UK[3]

Introduction:
Genetic prion diseases are rare, inherited and as yet incurable diseases of the central nervous system caused by highly penetrant mutations of the prion protein gene *PRNP*. Carriers of pathogenic *PRNP* variants often develop clinically manifest disease only at high age. This is indicative of protective factors. Structural analysis of disease-causing mutations of the prion protein PrP^C revealed subtle conformational alterations that could act as immunogenic “neo-“epitopes, raising the question whether such protective factors may consist, at least in part, of anti-PrP^C autoantibodies.

Methods:
In this case-control study, we have collected blood samples from n = 134 individuals encompassing a wide spectrum of *PRNP* variants. Individuals with a positive family history of genetic prion disease (n = 79) but lacking any pathogenic *PRNP* mutations served as controls. Antibody reactivity was measured using an indirect enzyme-linked immunosorbent assay for the detection of human IgG_{1-4} antibodies against full-length, recombinant human prion protein. We evaluated the effects of age, gender, *PRNP* mutations, *PRNP* p.129 polymorphism, clinical signs of prion disease and total IgG levels on autoantibody reactivity. In a subset of patients, autoantibody reactivity was assessed longitudinally up to two years after baseline measurements.

Results:
We found that antibody reactivity was present in both *PRNP* mutation carriers and controls. Elder individuals were at lower odds for the presence of anti-PrP^C autoantibodies, independently of total IgG levels or *PRNP* genotype. Gender, clinical signs of prion disease, pathogenic *PRNP* variants or p.129 polymorphism did not influence autoantibody reactivity. Moreover, levels of anti-PrP^C IgG were stable over up to two years.

Conclusion:
Pathogenic *PRNP* variants do not notably stimulate antibody-mediated anti-PrP^C immunity. Moreover, anti-PrP^C IgG autoantibodies are independent of overt signs of prion disease. The presence of anti-PrP^C autoantibodies in the general population without any disease-specific association suggests that such naturally occurring antibodies might be well-tolerated and could serve as anti-prion therapeutics.

5412

I. Olivares-Rivas[1], E. Katkeviciute[1], P. Busenhart[1], K. Bäbler[1], A. Niechcial[1], L. Hering[1], K. Atrott[1], C. Gottier[1], S. Lang[1], G. Leventhal[3], T. De Wouters[2], M. Spalinger[1], M. Scharl[1], A. Montalban-Arques[1]

Supplementation with butyrate producing bacteria reduces tumor load in a mouse model of CRC

Department of Gastroenterology and Hepatology, University Hospital Zurich, University of Zurich[1], Laboratory of Food Biotechnology, Institute of Food, Nutrition and Health, ETH Zürich[2], Department of Civil and Environmental Engineering, Massachusetts Institute of Technology , Cambridge, MA, USA[3]

Introduction:
Colorectal carcinoma is still a severe complication in patients with longstanding and severe ulcerative colitis. Current guidelines suggest that surgical total proctocolectomy must be considered in patients with high-grade dysplasia. Pharmacologic treatments that could prevent the onset of carcinoma in UC patients would be a milestone in the therapy of these patients. Here, we studied how the intestinal microbiota contributes to the onset/prevention of inflammation-induced colorectal carcinoma.

Methods:
Colitis associated tumors were induced in wild-type (WT) and RAG2$^{-/-}$ C57BL/6 mice via administration of three cycles of DSS in the drinking water (7 days DSS, 10 days recovery, each) + AOM injections at day 1 and 8 of each DSS cycle. *Peptostreptococcus stomatis* or a mix of 4 butyrate-producing strains (*A.caccae, E.hallii, F.prausnitzii*, and *R.intestinalis*) was supplemented via daily oral gavage on days 8-10 of each AOM/DSS cycle.

Results:
We found that tumor burden in the DSS/AOM model was associated with increased levels of fecal *P. stomatis*, but overall reduced levels of butyrate producers. In DSS/AOM-treated WT mice, supplementation with *P. stomatis* significantly enhanced tumor load when compared to PBS-treated controls ($p<0.01$, n=10, each). In contrast, only a small fraction of WT mice supplemented with butyrate producers developed tumors (n=10; $p<0.05$ vs. PBS group). Supplementation with *P. stomatis* was associated with increased intestinal inflammation as assessed in endoscopy and histology ($p<0.05$, each) after each AOM/DSS cycle. As causative mechanisms, we found elevated numbers of PD-L1+/PD-L2+ tumor-associated macrophages ($p<0.05$) in *P. stomatis* supplemented mice, while numbers of regulatory T cells were not affected. In mice receiving butyrate producers, DSS-induced intestinal inflammation was similar to DSS/AOM-treated control mice; however, we observed increased numbers of IFNg+ CD8+ cytotoxic T- cells and IFNg+ NK cells specifically within the tumor tissue, indicating that supplementation with butyrate producers promoted increased anti-tumor immune responses. Further, the increase in PD-L1+/PD-L2+ tumor-associated macrophages was absent in those mice. Of interest, the protective effect of supplementation with butyrate producers was completely abrogated in RAG-/- mice, indicating that T cells are crucially involved in mediating the anti-tumor effect.

Conclusion:
Our results indicate that oral supplementation with selected butyrate producers protects from colitis-associated tumor development via promoting anti-tumor T cell responses in vivo. Our findings suggest that manipulation of the intestinal microbiota might be a promising novel approach to promote anti-cancer immune responses.

5413

Ö. Altintas[1], A. Franchini[1], D. Heuberger[1], R. Schuepbach[1]

Novel tool for PAR1 activation

Institute of Intensive Care Medicine, University Hospital Zurich, University of Zurich[1]

Introduction:
Protease-activated receptor 1 (PAR1) is a key receptor orchestrating vascular barrier function regulation. PAR1 belongs to a small family of G protein-coupled receptors, which are named protease-activated receptors (PARs). PARs, uniquely in terms of activation, are lacking physiological soluble ligands but are activated by a tethered ligand generated by proteolytic cleavage of the N-terminus. Enzyme-dependent activation of PARs leads to various downstream effects via G protein activation. For instance, endothelial-expressed PAR1 activation by thrombin results in barrier disruption while activation of PAR1 by aPC protects the endothelial barrier function. The regulation of the barrier function by PAR1 is crucial in pathological conditions such as chronic or acute inflammation like sepsis and thus, a few PAR1 modulators as vorapaxar or the pepducin PZ-128 have been tested in clinical studies. Despite abundant research has been conducted to understand the complex mechanisms of PAR1 activation in terms of barrier function and inflammation, so far, no specific cleavage-independent PAR1 activating peptide has been tested in pre-clinical studies.
We hypothesize that peptides corresponding to the cleaved N-terminus of PAR1 tethered to scFv specifically induce barrier disruptive or protective effects when co-localized to a PAR1 co-receptor.

Methods:
We engineered a scFv construct carrying the PAR1 N-terminal sequence corresponding to the thrombin-cleaved PAR1 tethered-ligand. In HEK 293T cells overexpressing PAR1 and the NF-κB reporter plasmid pGL4.32[luc2P/NF-κB-RE/Hygro], we tested whether scFv-PAR1-TFLLR, similar to thrombin, induced NF-kB DNA binding activity via PAR1 activation. Next, we tested whether the recruitment of the scFv-PAR1-TFLLR to the cell surface further induced the efficiency of NF-kB DNA binding. The NF-κB DNA binding activity was measured by luciferase assay.

Results:
Thrombin and scFv-PAR1-TFLLR significantly induced NF-κB DNA binding activity. The PAR1-dependent NF-κB DNA binding activity was only induced by a functional recruitment of the scFv-PAR1-TFLLR to the cell surface.

Conclusion:
In a human overexpressing system, we were able to show that our scFv-PAR1-TFLLR construct, comparable to thrombin, efficiently induces NF-κB DNA binding activity via specific PAR1. Our data provide proof of concept, that scFv-tethered ligands might serve as specific PAR1 agonists and thus can regulate endothelial barrier function.

5414

M. Reinehr[1], C. Micheloud[2], F. Grimm[3], P. Kronenberg[3], J. Grimm[4], A. Beck[4], J. Nell[4], E. Furrer[2], B. Müllhaupt[5], T. Barth[4], P. Deplazes[3], A. Weber[1]

Pathology of echinococcosis - A morphological and immunohistochemical study on 138 cases with focus on the differential diagnosis between cystic versus alveolar echinococcosis

Pathology, University Hospital, Zurich[1], Epidemiology, Biostatistics and Prevention Institute, Department of Biostatistics, University of Zurich[2], Institute of Parasitology, University of Zurich[3], Institute of Pathology, University Ulm, Ulm, Germany[4], Clinics of Hepatology and Gastroenterology, University and University Hospital Zurich[5]

Introduction:
Accidental infection of humans by the larval stage of mainly *Echinococcus granulosus (EG)* or *Echinococcus multilocularis (EM)* in humans (dog or fox tape worm) causes cystic (CE) and alveolar echinococcosis (AE), respectively. The infection is a life threatening helmintic zoonosis with significant health burden in many areas of the world. Cystic lesions, mostly in the liver, are the clinicopathologic hallmark of both, AE as well as CE. However, the biologic course of the disease, its prognosis and patients management decisively differ between the two diseases. While there is a clear requirement to reliably diagnose and subtype echinococcosis in liver and other organ specimens, the wide and overlapping spectrum of morphological appearances described, and limited availability of ancillary tools are challenges for pathologists.

Methods:
To address this issue and aiming to develop a diagnostic algorithm, we comprehensively and systematically analyzed the pathological spectrum in a clinically and molecularly defined echinococcosis cohort (138 specimens from 112 patients). A newly developed monoclonal antibody (EmG3) was evaluated for immunohistochemistry, in particular for its combined application together with the Em2G11 antibody.

Results:
We identified the following morphologic criteria to sufficiently discriminate between CE and AE infection: Smallest size of cysts (AUC of 0.97 with 95%-CI from 0.92 to 1.00), number of cysts (sensitivity of 0.95 with 95%-CI from 0.85 to 0.99 and specificity of 0.90 with 95%-CI from 0.76 to 0.97), largest size of cysts (AUC of 0.92 with 95%-CI from 0.85 to 0.98), thickness of laminated layer (AUC of 0.99 with 95%-CI from 0.97 to 1.00), striation of the laminated layer (sensitivity of 0.89 with 95%-CI from 0.78 to 0.96 and specificity of 0.97 with 95%-CI from 0.87 to 1.00), and thickness of the fibrotic rim of single peripheral cysts (AUC of 0.89 with 95%-CI from 0.80 to 0.96). Albendazole therapy did not impact on any of the morphologic criteria that were tested. A decision tree based on two criteria, i.e. the thickness of the laminated layer and the thickness of the fibrotic rim of a single cyst, already allowed to sufficiently discriminate between CE and AE in 93% of the cases. Combined immunohistochemistry with Em2G11 and EmG3 antibodies was equally sensitive and specific as the gold standard of PCR-based molecular testing.

Conclusion:
In summary, we have identified morphologic criteria, which robustly discriminate between CE and AE, and introduced a highly sensitive and specific immunohistochemical panel. We expect our findings to improve diagnosis of echinococcosis, having impact on the management of echinococcosis patients.

5415

A. Akhmedov[1], M. Crucet[1], N. Bonetti[1], C. Ospelt[2], S. Briand[1], M. Amrollahi-Sharifabadi[1], A. Ciurea[2], O. Distler[2], G. Kollias[3], B. Simic[1], F. Ruschitzka[4], R. Laaksonen[5], P. Vanhoutte[6], T. Lüscher[1]

Anti TNFα treatment restores endothelial function in rheumatoid arthritis by inhibiting LOX-1 and arginase

Center for Molecular Cardiology, University of Zurich, Schlieren[1], Department of Rheumatology, University Hospital Zurich[2], Institute for Immunology, Biomedical Sciences Research Center Alexander Fleming, Vari, Greece[3], University Heart Center, Department of Cardiology, University Hospital Zürich[4], Finnish Cardiovascular Research Center, University of Tampere and Finnish Clinical Biobank Tampere, Tampere University Hospital, Tampere, Finland[5], Department of Pharmacology, Hongkong University, P.R.C.[6]

Introduction:
Chronic inflammatory diseases such as rheumatoid arthritis (RA) are associated with increased cardiovascular (CV) risk. In patients with RA, endothelium-dependent responses are impaired. However, the molecular mechanisms causing endothelial dysfunction (ED) in rheumatoid arthritis are poorly understood.
Purpose: We studied endothelial dysfunction in TNFα transgenic mice that develop RA and characterized the molecular mechanisms involved.

Methods:
Two transgenic mouse lines developing mild or severe form of RA were used to study disease progression. Endothelial function was assessed in both lines and controls at different time points using organ chamber myograph. Transgenic mice were also randomly receiving anti-TNFα treatment starting before the onset of ED.

Results:
Endothelium-dependent vasorelaxation to acetylcholine was impaired in both lines. This was associated with increased aortic expression of LOX-1 in transgenic mice. Anti-TNFa treatment with infliximab improved ED in both lines, which was paralleled with decreased arginase activity as well as lower expression and serum levels of LOX-1 in both lines. The same profile for arginase and LOX-1 was also seeing in RA patients.

Conclusion:
We show here that RA induced by TNFα overexpression leads to a time- and dose-dependent ED due to increased expression of LOX-1 receptor and increased arginase activity, while anti-TNFα treatment reduced LOX-1 expression and arginase expression and activity in RA mice. Moreover, anti TNFα therapy also reduced LOX-1 levels and arginase activity in RA patients. These translational results highlight the fact that inflammation itself leads to endothelial dysfunction that may explain the increased CV risk of RA patients.

5416

J. Bremer[1], A. Aguzzi[1]

Three-dimensional analysis of skin and peripheral nerve biopsies

Neuropathology, University Hospital of Zurich, Zurich[1]

Introduction:
Skin and nerve biopsies are routinely performed to diagnose peripheral nerve disorders. Serial sections are required to determine the density of intraepidermal nerve fibers in skin biopsies and laborious techniques like fiber teasing are sometimes needed to diagnose demyelination in nerve biopsies. To facilitate diagnostics, we aim at establishing a protocol for the three-dimensional analysis of nerve fiber density and myelin sheet thickness in skin and peripheral nerve biopsies.

Methods:
We combine tissue clearing of the unsectioned biopsy material with antibody or dye labeling of axons and myelin. Using confocal microscopy, this would allow us to visualize axon density and myelin sheet thickness in three dimensions in a large volume or even in the whole biopsy.

Results:
Initital attempts using the clearing method iDISCO have allowed us to visualize neurofilament-labeled axons in stacks of more than 100 µm.

Conclusion:
The integration of clearing techniques into neuropathological routine diagnostics has the potential to significantly facilitate and improve neuropathological analysis of skin and nerve biopsies.

5417

A. Reuss[1], D. Kirschenbaum[1], P. Nilsson[2], A. Aguzzi[1]

Establishing a 3D histological grading system for early and late amyloid beta and tau pathology in Alzheimer's disease patients

Neuropathology, University Hospital of Zurich, Zurich[1], Division of Chemistry, Linköping University, Sweden[2]

Introduction:
The grading of disease stages of the *NIHAA* classification system in Alzheimer's disease is based on amyloid beta density (Mirra *et al.,* 2002) as well as on amyloid beta and tau spread in distinct brain regions according to the *Thal* phases (Thal *et al.,* 2002) and *Braak & Braak* stages (Braak & Braak, 1991), respectively. Neuropathological diagnoses are currently made via 2D histology, cutting tissue blocks into very thin sections and staining with distinct dyes and antibodies on different slices. However, topographical information may get lost and the evaluation of colocalization is often difficult. 3D histology preserves topographical information of the whole tissue block and allows distinguishing real colocalization from accidental overlap of morphological structures in distinct planes.

Methods:
Region-specific tissue samples from human autopsy patients with clinically described dementia and age-matched controls are collected. The whole 7 mm thick tissue blocks of the regions of interest are cleared via iDISCO/CRYSTAL and stained for amyloid beta and tau via luminescent conjugated polythiophenes (LCPs) that allow distinguishing between distinct maturation stages of these protein deposits. Furthermore, the samples are stained for surrounding morphological structures like neurons, astrocytes, microglia, white matter, and blood vessels. Image acquisition will be achieved via a custom-made selective plane illumination microscope termed mesoSPIM.

Results:
Formalin-fixed human brain tissue from autopsy cases has been successfully cleared via CRYSTAL/iDISCO, and stained for different dyes and antibodies to display neurons, astrocytes, microglia, white matter, and blood vessels.

Conclusion:
Within the first year of this project, the main stainings for depicting structures within the cleared human brain tissue have been established so that the sample collection of Alzheimer's disease patients and age-matched controls can be started for staining with LCPs in relation to surrounding structures. Following the current *NIHAA* classification system, a 3D histological grading for early and late amyloid beta and tau pathology will be established.

5418

M. Carta[1], C. Scheckel[1], C. Schiavi[1], E. Kara[1], M. Losa[1], A. Aguzzi[1]

Targeted production of murine antibodies using sorted specific B cells

Neuropathology, University Hospital of Zurich, Zurich[1]

Introduction:
Murine or chimeric mouse-human antibodies against proteins associated with neurodegeneration are often unavailable and the sequences of well-characterized antibodies are mostly proprietary. In this project, we aim to establish a reliable high-throughput production pipeline for high-affinity antibodies.

Methods:
Wildtype or antigen-knockout mice are immunised with a protein of interest. Next, we obtain lymphoid tissues from the immunised animals and label the antigen-specific B cell receptors, using antigen baits conjugated to fluorescent molecules. We sort the specific B cells and isolate and reverse transcribe their mRNA, allowing amplification of the recombined immunoglobulin light and heavy chain genes with a primer set that covers a large variety of possible transcripts. The PCR products are expressed *in vitro* using phage technology or ribosomal display, which enables us to identify sequences that code for high-affinity immunoglobulins.

Results:
We have successfully sorted antigen-specific B cells after labelling them with fluorescent antigen baits. To increase the specificity of the sort, we use two different baiting strategies in parallel. As we expect antigen-specific B cells to exhibit a spectrum of binding affinities, we sort B cell subpopulations that are likely to express high-affinity antibodies, such as germinal centre or memory B cells. Furthermore, the recombined immunoglobulin genes of bulk-sorted cells can be reliably amplified via PCR, using high coverage primer set.

Conclusion:
We demonstrate a versatile method for sorting antigen-specific B cells from mouse lymphoid tissues. The method can be easily modified to target a variety of antigens and B cell populations. In a next step, we aim to optimise high-throughput cloning and protein production steps and clone high-affinity antibodies.

5420

I. Isringhausen[1], U. Suessbier[1], L. Kovtonyuk[1], N. Kräutler[2], P. Helbling[1], A. Gomariz[1], H. Wong[1], A. Oxenius[2], M. Manz[1], C. Nombela-Arrieta[1]

Chronic viral infections induce persistent loss of hematopoietic stem cell function through disruption of bone marrow stromal cell networks

Department for Medical Oncology and Hematology, University Hospital Zurich[1], Institute of Microbiology, ETH Zurich[2]

Introduction:
Hematopoiesis is a highly demand-adapted and tightly regulated process that is sustained by a rare population of self-renewing, multipotent hematopoietic stem and progenitor cells (HSPCs) residing in specialized microenvironments within bone marrow (BM) cavities. These cavities are built by an intricate network of nonhematopoietic or stromal cells of mesenchymal, neural and vascular origin that jointly build a basic tissue infrastructure throughout the entire BM.
Beyond providing a structural scaffold for hematopoietic cells, stromal cells are critically involved in the fine regulation of different stages of hematopoiesis. Whereas there is a basic understanding on the functional interplay of stromal components with hematopoietic cells during homeostasis, little is known about how inflammatory conditions may alter this relation. Viral infections act as major stressors to the hematopoietic system, inducing a massive and adaptive response in cellular output. Whether viral infections alter BM stromal scaffolds and thus shape hematopoietic responses remains unknown. We herein investigated the structural and functional alterations imposed on the BM after chronic infection with Lymphocytic Choriomeningitis Virus (LCMV).

Methods:
Mice were infected with LCMV-cl13 strain by intravenous (i.v.) injection of $2x10^6$ pfu LCMV in 6-10 week old female mice. Viral titers were determined by plaque assay. For most readouts, we combined multi-parameter flow-cytometric analyses with parallel 3D confocal imaging of the contralateral femur bone.
For transplantation experiments, HSPCs were FACS-sorted and then injected i.v. into lethally irradiated recipient mice. Enzyme-linked immunosorbent assays (ELISA) was performed in order to measure total BM protein levels. Interferon receptor signaling blocking was performed using commercially available blocking antibodies for IFNαR and IFNγ (BioXCell).

Results:
Our data shows that chronic LCMV infections result in a substantial alteration of the BM endothelial and mesenchymal stromal progenitor cell populations and a decrease in their capacity to produce HSPC-sustaining factors. Moreover, using deep tissue imaging we observed a profound and durable decimation in the number and density of CXCL12-abundant reticular (CAR) cells. Importantly, in-depth analysis showed that after chronic LCMV infection CAR cells are functionally impaired in their support for HSC quiescence. Major damage to BM stromal integrity is accompanied by a profound and sustained reduction in the number of both HSPCs as well as hematopoietic stem cells by phenotype. Competitive repopulation assays revealed a striking and persistent loss of HSC function after chronic LCMV infection. Finally, our results indicate that the observed alterations in the BM are mediated by virus-specific $CD8^+$ T cells and partly dependent on the production of systemic IFNα expression. Our observations thus indicate that chronic infections result in persistent damage to HSPC function, which can be explained by an impaired regulatory function of the stromal compartment of the BM.

Conclusion:
Chronic infections in humans are estimated to affect up to a third of the world population and can cause BM suppression. With an estimated 180 million people infected by hepatitis C virus and 34 million people infected with HIV, chronic virus infections pose a substantial demographic burden. We herein report that chronic viral infections as exemplified by the model organism LCMV lead to massive

alterations in the hematopoietic and stromal compartments in the BM. Intriguingly, the functionality of HSCs as well as mesenchymal stromal cells stays impaired even at time points of immunological exhaustion long after the initial infection. Considering the long standing clinical observation of an increased transplant rejection within chronically CMV-infected patients, precisely delineating the mechanisms that govern loss of functionality and immune pathology might pave the way for clinical applications in the future.

5421

O. Rus-Oswald[1], J. Reinhardt[1], C. Burki[2], S. Bridenbaugh[2], C. Stippich[1], R. Reto[2], M. Blatow[1]

A clinical fMRI protocol for cognitive-motor dual task

Neuroradiology, University Hospital Zürich[1], Felix Platter-Hospital, University Center for Medicine of Aging, Basel[2]

Introduction:
Gait analysis involving cognitive-motor dual task (DT) is used as a diagnostic tool in geriatric populations (e.g. "walking while talking")[1]. Cognitive-motor interference effects, measured as decrease of walking speed and increase of step variability during DT as well as decreases in cognitive performance have a high predictive value for future fall risk and cognitive decline[5]. In our previous study, we demonstrated the feasibility of performing the cognitive-motor DT in the fMRI environment using an MRI-compatible stepping device and evaluated the neural correlates of the DT costs [2].
In the present study, we aimed to optimize the DT fMRI protocol with respect to task difficulty, duration and signal robustness in order to be able to apply this fMRI protocol in clinical context. Furthermore, we compared the stepping DT paradigm to a finger tapping DT paradigm, to evaluate if the latter brings similar results in terms of DT difficulty and signal robustness.

Methods:
30 elderly healthy subjects (mean age ± SD: 70.2 ± 4.97) participated in the fMRI study which included the performance of a cognitive task (verbal fluency and serial subtraction) and a motor single task (ST; stepping or finger tapping) and the combination of both, i.e. a cognitive-motor DT. Data analysis was performed using standardized routines in BrainVoyager. First, the group level analysis based on the contrast task vs. baseline, was performed using a separate subjects fixed effects analysis. Second, a region-of-interest analysis (ROI) at the individual level of each subject was performed, employing a dynamic threshold technique[3, 4]. Further, the ROI based DT costs were computed based on the individual difference of activation between ST and DT.

Results:
During cognitive-motor DT the primary and secondary motor as well as parietal and prefrontal areas were active at group level. Activation of motor areas was decreased in DT as compared to the motor ST, according to our previous findings[3]. Activation of parietal and prefrontal areas was on average equivalent or increased in DT as compared to ST. The stepping DT paradigm was more distinctive (higher ROI occurence and activation strength on individual level) between ST and DT than the finger tapping DT paradigm. At the individual level the following ROIs showed robust activations in terms of occurence probability and signal strength, measured in the left hemisphere: primary motor cortex (M1), supplementary motor area (SMA) and superior parietal lobule/intraparietal sulcus (SPL/IPS). The neural correlates of DT costs computed in the stepping condition in SPL/IPS enabled to descriptively separate the subjects into two groups, one with high and one with low DT costs based on their individual activation differences.

Conclusion:
With this study, we propose an optimized cognitive-motor DT fMRI protocol and a standardized individual analysis routine to measure the neural correlates of cognitive-motor interference effects during DT. In the future this fMRI protocol may be evaluated in the clinical setting, i.e. in patients with mild cognitive impairment and might enable the early detection of motor and cognitive decline based on the obtained neurofunctional markers and preferably before the structural degeneration process occurs.

5422

G. Grossi[1], H. Beer[1]

Exploring the molecular mechanisms of UVB-induced cell death in human keratinocytes

University Hospital Zürich[1]

Introduction:
Exposure to ultraviolet (UV) light is the most important risk factor for the development of non-melanoma skin cancer (NMSC), the most prevalent type of cancer in Caucasians, with increasing incidence worldwide. Basal cell carcinoma and squamous cell carcinoma account for the majority of NMSC cases and arise from epidermal keratinocytes. In particular, UVB radiation represents a carcinogen, as it is able to induce direct DNA damage, which, if not correctly repaired, can lead to mutations in keratinocytes and subsequently to skin cancer *in vivo*. On the other hand, UVB-induced apoptosis of the damaged keratinocytes antagonizes the malignant transformation and therefore represents a protective pathway. However, the molecular mechanisms underlying this process are not fully elucidated.
We have previously shown that caspase-1 is required for UVB-induced apoptosis of human primary keratinocytes (HPKs) and aimed to further characterize its role in this process.

Methods:
We established a system based on stable genetic modification of HPKs and inducible overexpression of caspase-1, and employed a proteomics approach termed TAILS for identification of endogenous caspase-1 substrates potentially involved in UVB-induced cell death.

Results:
We identified a specific cleavage of the major vault protein (MVP) by caspase-1 at the aspartate 441. MVP is part of huge cytoplasmic ribonucleoprotein particles termed vaults, whose functions are poorly understood. Cleavage of MVP was never described before and, interestingly, we found that this protein is also cleaved by the apoptotic caspase-9. Cleavage of endogenous MVP occurs in HPKs in response to UVB-induced apoptosis and is dependent on expression of caspase-1 and -9. Furthermore, MVP is involved in cell death resistance of HPKs and is degraded during cell death. Overexpression of a cleavage resistant variant of MVP protects the cells against UVB-induced cell death, suggesting an important role of this cleavage event in this pathway.

Conclusion:
Our results provide better insights about the role of caspase-1 and -9 in UVB-induced apoptosis and identify MVP cleavage as a novel molecular feature occurring as the result of caspase activation during this cell death process. Further studies will reveal whether MVP has a role in NMSC development.

5424

U. Süssbier[1], H. Wong[1], A. Gomariz[1], S. Isringhausen[1], P. Helbling[1], T. Nagazawa[2], A. Müller[1], M. Manz[1], C. Nombela-Arrieta[1]

Functional and structural dynamics of the bone marrow stromal microenvironment after cytoreductive treatments

Hematology and Oncology, University Hospital Zurich[1], Institute for Frontier Medical Sciences, Kyoto University, Kyoto, Japan[2]

Introduction:
Bone marrow (BM) cavities are the primary sites of the high throughput, continuous and tightly regulated production of mature blood cells throughout the whole lifespan, called hematopoiesis. To assure hematopoiesis, the BM contains hematopoietic cells including hematopoietic stem and progenitor cells (HSPCs). The proliferation and differentiation of HSPCs are tightly regulated by signals emanating from the BM microenvironment, which consists of non-hematopoietic stromal cells from different origin including mesenchymal, endothelial and neural cells.
For many different haematologic and non-haematologic malignancies chemotherapy is the primary therapeutic approach. In particular, 5-fluorouracil (5-FU), which targets cycling cells, is one of the most commonly used chemotherapeutic reagents to investigate the effect of myeloablative treatment. For that reason, effects on the hematopoietic compartment are extensively described. Nevertheless, the structural effects, especially the kinetics of the destruction and recovery of the BM microenvironment and its different components are less characterized.
Novel 3D-imaging techniques combined with flow cytometry enabled us to gain a better insight in structural changes of the BM microenvironment as well as quantitative changes of particular stromal cell populations.

Methods:
In our study we provide a comprehensive analysis of the changes in the BM upon5-FU treatment through two complementary approaches. By combining advanced flow cytometric protocols, 3D-imaging techniques and newly developed computational tools that enabled the quantitative analysis of images, we could study quantitative changes of the hematopoietic and especially of the stromal compartment but also investigate effects on the murine BM microarchitecture, in particular with regard on the vasculature.

Results:
-Ter119^{-}Sca1^{+}CD31^{+}endothelial cells within 7 days with a subsequent recovery of cell numbers between 14 to 28 days post 5-FU treatment was seen by flow cytometry. These results were reflected by 3D-imagingwhere we observed a massive sinusoidal vasodilation followed by a complete disruption of the vessel walls. Similar to the recovery of cell numbersthe vascular network started to reorganize, eventuallyregenerating a normal microvascular network 28 daysafter treatment. In contrast to the analysis by flow cytometry, CXCL12 abundant reticular stromal cells were only slightly affected when quantified by 3D-imaging. The striking regenerative potential of the BM aftersevere tissue damage is remarkably robust. Indeed similar kinetics of recoverypost 5FU-induced stress were alsoobserved inthe BM microenvironment ofaged mice (<2 years), as well as after repeated challenge of the system through 3 consecutive treatments with 5-FU.

Conclusion:
Our observations demonstrate that, in contrast to hematopoietic cells, mesenchymal stromal cell populations are highly resistant to cytoreductive damage with 5-FU and most likely drive the complex process of rapid and complete regeneration of BM tissues after injury.

5425

L. Barrios[1], A. Maeder[2], P. Oldrati[1], S. Demirci[1], S. Santini[3], A. Lutterotti[2]

Digital Biomarkers for autonomic dysfunction in Multiple Sclerosis

ETH Zürich[1], Neurology, University Hospital, Zurich[2], Faculty of Informatics, Universita della Svizzera italiana, Lugano[3]

Introduction:
The recent advances in mobile and wearable technologies opened up opportunities to improve healthcare monitoring systems. Using devices like smartphones and smartwatches it is possible to collect mobility or physiological data continuously using wearable sensors. This is particularly promising for the management of chronic conditions, where the monitoring of patients' physiological parameters over extended periods of time could lead to a better understanding of the disease and improvement of therapies. Using smartphone based applications and wearable sensors we aim to correlate measurements of daily activities, fatigability and autonomic nervous system function with the frequency and severity of fatigue in MS patients.
The aim of the study is to develop new objective measures to follow fatigue and fatigability in MS patients. The study engages patient with MS carrying a wearable sensor continuously over time in combination with App-based tests for cognitive and motor fatigue and patient reported outcomes.

Methods:
We have validated two off-the-shelf sensors capable of measuring heart rate through photoplethysmography (PPG) and electrodermal activity (EDA): the Empatica E4 (Empatica Inc) and the Everion (Biovotion AG) devices comparing the sensor data with standard Holter ECG in a defined protocol initiating with 5 minutes of resting period followed by five activities: biking (60W), biking (120W), walking (5km/h), jogging (8km/h) and running (10km/h). Each activity lasts for 5 minutes and between each activity there is a resting period of 5 minutes.

Results:
Overall there is a good agreement of the data from the wearable sensor with standard Holter-ECG with regard to HR and several time and frequency domain measures of heart rate variability. The app generated to assess motor and cognitive fatigability was validated in healthy controls and MS patients comparing standard measures for fatigability.

Conclusion:
We report results on the feasibility of off-the-shelf devices and newly developed App-based measures for motor and cognitive fatigue to be used to monitor the function of the autonomous nervous system and chronic fatigue in patients with MS.

5426

V. Waller[1], M. Pruschy[1], P. Knobel[1]

Exploring the interactome of ADAM17 in the tumor microenvironment and its role for radiation resistance

Department of Radiation Oncology, University Hospital Zurich[1]

Introduction:
In addition to DNA damage and genomic instability, ionizing irradiation (IR) also affects intra- and intercellular processes that induce a multilayered stress response and determines the tumor response to radiotherapy. Growth and survival of NSCLC cells are often dependent on ectodomain shedding, which includes proteolytic cleavage of the extracellular part of membrane proteins primarily mediated by membrane-anchored metalloproteases. Most of the members of the ADAM (A disintegrin and metalloproteinase) family have proteolytic activity and are actively associated with the process of proteolytic 'shedding' of membrane-bound proteins and hence the rapid modulation of key signals in the tumor microenvironment. ADAM17 represents one of the best studied members of the ADAM family. In patients suffering from NSCLC increased ADAM17 expression is associated with aggressive progression and poor prognosis. ADAM17 drives pleiotropic pathways that are involved in auto- and paracrine signaling by regulating the processing of multiple key oncogenic growth factors, cytokines and adhesion molecules.
As part of an IR-dependent secretome analysis, our laboratory demonstrated that adenocarcinoma cells respond to IR with elevated ADAM17 activity that negatively influences the outcome of non-small-cell-lung-cancer (NSCLC) to treatment. Direct targeting and inhibition of ADAM17 sensitizes multiple adenocarcinoma cell lines to radiotherapy *in vitro* and *in vivo,* which makes it a promising target for novel combined treatment modalities.
We are highly interested in gaining additional insights into the mechanisms of IR-induced and ADAM17-mediated modulation of key signals in the tumor microenvironment. We aim to identify substrates of ADAM17 in the primary tumor or metastatic tumor sites that could be targeted to increase the sensitivity of the tumor towards radiotherapy.

Methods:
The novel BioID method will be applied to identify ADAM17 proximity interactors and to determine how ADAM17 influences its microenvironment. The principle of the BioID method is based on proximity-dependent biotin labeling of primary amines of proteins by a promiscuous *Escherichia coli* biotin protein ligase (BirA), fused to either the C- or N-terminus of a protein of interest. Biotinylated proteins are purified via streptavidin and identified by mass spectrometry. For this project, BirA was fused to the extracellular N-terminus of murine ADAM17 and overexpressed in multiple murine and human lung cancer cell lines, such as SV2, H358 and A549. Promising candidates identified by mass spectrometry (MS) will be tested in *in vitro* approaches and *in vivo* in immune competent orthotopic lung tumor models.

Results:
Overexpression of Flag-tagged BirA biotin ligase fused to the N-terminus of murine ADAM17 in HEK AD293T cells resulted in the extracellular colocalization of biotinylated proteins with the transfected BirA-Flag-mADAM17 construct. To follow up, stable human and murine cell lines were generated, expressing the BirA-ADAM17 fusion protein, via lentiviral transduction.

Conclusion:
After confirming the functionality of the biotin ligase and ADAM17 in the BirA-Flag-mADAM17 construct, BioID-MS will be applied to identify the first promising interactors of ADAM17 *in vitro*. The significance, but also the challenge of this project lies in the implementation of the BioID technology in the extracellular space. Since its development in 2012, the BioID method was exclusively used to study intracellular protein interactions. However, applying it to explore extracellular sites, could be an elegant strategy for the identification and characterization of novel markers to deepen the understanding of the complex heterogeneity of a tumor microenvironment.

5427

M. Docampo[1], M. Hohmann[1], C. Sellés-Moreno[1], C. Cruciani[2], M. Mikolin[2], H. Hayward-Koennecke[2], T. Müller[1], A. Zaugg[2], M. Foege[1], T. Ludersdorfer[1], A. Lutterotti[2], R. Martin[2], M. Sospedra[2]

Immunosafety and Characterization of Tolerance Mechanisms Following Treatment with Myelin Peptide-Pulsed Red Blood Cells (ETIMSred Phase Ib trial)

Wyss Zurich, University of Zurich / ETH Zurich[1], Neuroimmunology and MS Research (NIMS), Neurology Clinic, University of Zurich, University Hospital Zurich[2]

Introduction:
Autoimmune diseases are characterized by unwanted immune reactions against self-antigens. Multiple sclerosis (MS) is a prototypic example, and autoreactive T cells with specificity for myelin- and a few non-myelin autoantigens as well as proinflammatory B cells play important roles in its pathogenesis. Despite the availability of several approved and in part very active treatments, there is still a strong need for antigen-specific therapies that block the autoimmune process very early and without major side effects. Antigen-specific tolerance induction would be the best approach if effective methods can be developed to achieve this in MS and other autoimmune diseases. We pursue tolerance induction with myelin peptide-pulsed red blood cells (RBCs; abbreviation ETIMS^{red}) and have successfully completed a phase I clinical trial in relapsing-remitting MS patients.

Methods:
10 MS patients were enrolled and treated with ETIMS^{red} cell product, i.e. 1x10^{10} - 3x10^{11} autologous RBCs pulsed with 7 myelin peptides derived from three myelin proteins (MBP, MOG, PLP). Besides standard hematological parameters, a multi-panel flow cytometry protocol characterized all major immune cell types and relevant subpopulations before and after tolerization. Two methods were applied to test antigen-specific proliferation against the 7 myelin peptides and controls and for both peripheral blood- and cerebrospinal fluid (CSF)-derived T cells. Serum- and CSF cytokine testing and several other assays are currently being performed to characterize potential mechanisms of this tolerization approach in depth.

Results:
Tolerization with ETIMS^{red} did not induce unwanted immune reactivity against the tolerizing peptides. Detailed immune cell phenotyping supports immunosafety of the treatment, and none of the large number of examined cell types showed significant changes at the level of bulk peripheral blood or CSF cells. Antigen specificity testing shows a decrease and/or lower activity of peripheral blood and CSF T cells after treatment when compared to before tolerization at the high dose of the cell product.

Conclusion:
The current mechanistic study, which is part of the phase Ib trial of ETIMS^{red}, provides a detailed analysis of potential tolerance mechanisms induced by the treatment with myelin peptide-coupled red blood cells. Although the data are still preliminary, results are very promising that antigen-specific tolerization can be achieved in MS.

Acknowledgment: Supported by a grant of the Wyss Zurich (Lutterotti) and ERC grant 340733 – HLA-DR15 in MS (Martin)

Disclosures:
A. Lutterotti: Received financial compensation and/or travel support for lectures and advice from Biogen, Merck, Novartis, Teva, Genzyme, Bayer, Celgene. A Lutterotti is a co-founder of Cellerys and co-inventor on a patent held by the University of Zurich on the use of peptide-coupled cells for treatment of MS. R. Martin: received unrestricted grants or financial compensation for lectures/advice from Biogen, Merck, Novartis, Roche, Teva, Genzyme, Celgene, Neuway and CellProtect. R. Martin is a co-founder/-owner of Cellerys and co-inventor of University Zurich-owned, Cellerys-related patents. M. Sospedra is a co-founder of Cellerys and co-inventor on related patents held by the University Zurich.

5428

C. Cruciani[1], W. Faigle[1], P. Tomas-Ojer[1], C. Selles Moreno[1], B. Roschitzki[2], W. Wolski[2], N. Schaeren-Wiemers[3], T. Zeis[3], R. Reynolds[4], M. Sospedra[1], R. Martin[1]

Reactivity of autoreactive T cells against post-translational modifications of brain proteins, specifically citrullinated peptides in MS

Department of Neuroimmunology and MS Research, Neurology Clinic,University Hospital Zürich[1], Functional Genomic Center, ETH and University of Zurich [2], Department of Biomedicine, University Hospital Basel [3], Division of Brain Sciences, Imperial College London, UK[4]

Introduction:
Extensive effort has been made to identify the target antigen/s in multiple sclerosis (MS), and the greatest attention has been directed to myelin proteins. The identification of $CD4^+$ T cells reactive to epitopes of several myelin proteins has been a consistent finding. Among the myelin proteins, myelin basic protein (MBP) is the best studied. Interestingly, reactivity of autoimmune T cells against post-translational modifications of autoantigens, specifically against citrullinated peptides, has been observed in MS. It has been shown that T cell reactivity against citrullinated MBP is elevated in peripheral blood of MS patients, supporting the hypothesis that T cells specific for citrullinated epitopes may escape central immune tolerance. Since citrullination/deimination of MBP induces the generation of new epitopes triggering as a consequence autoreactivity, we aimed to investigate the specificity of cerebrospinal fluid (CSF)-infiltrating $CD4^+$ T cells against immunodominant myelin- and citrullinated versus non-citrullinated peptides.

Methods:
Snap frozen brain tissue from MS and control brains was used in a bottom-up proteomics study using pressure cycling technology. The newly identified citrullinated peptides together with myelin peptides were used to address the recognition of brain- and CSF-infiltrating CD4+ T cells from MS patients, measuring proliferation (3H-thymidine incorporation), cytokine production.

Results:
The proteomics study identified 8 new sites of citrullination in the MBP molecule that were expressed at high levels in the white matter of MS cases compared to healthy controls. Also, citrullination of glial fibrillary acidic protein (GFAP) is found more abundantly in the white matter of MS brains. We did not observe specific recognition of citrullinated- and non-citrullinated peptides. When we analyzed the IFN-γ secretion in the culture supernatant, we did also not detect a strong IFN-γ release upon exposure to citrullinated MBP peptides, but weak responses in only a few patients.

Conclusion:
Given these results, we conclude that the non-modified peptides are more frequently recognized by CSF-infiltrating CD4+ T cells compared to the citrullinated version and that the reactivity to the latter is overall very low. Our findings show that recognition of citrullinated MBP epitopes is almost absent and thus unlikely to play a role in the MS autoimmune response.

5429

M. Puthenparampil[1], C. Cruciani[1], P. Tomas-Ojer[1], M. Hohmann[1], C. Sellés-Moreno[1], I. Jelcic[1], J. Wang[1], M. Mikolin[1], R. Martin[1], M. Sospedra[1]

CSF CD4+ T cells reactivity against auto-antigen in MS patient

Neuroimmunology and MS Research Section (NIMS), Neurology Clinic, University of Zurich, University Hospital Zurich[1]

Introduction:
Multiple sclerosis (MS) is an immune-mediated autoimmune disorder affecting the central nervous system and that develops in genetically susceptible individuals, likely requiring environmental co-factors. The auto-antigens triggering the autoimmune response in MS remain incompletely understood. Recently, data from our laboratory showed that not only myelin-derived peptides, but also RASGRP2 (which is expressed in grey matter and B cells) and TSTA-3 (which is ubiquitously expressed) recognition by cells of the immune system could be demonstrated in MS patients.

Methods:
The previously identified peptides derived from RASGRP2 and TSTA-3 and immuno-dominant myelin peptides (i.e., MBP, PLP and MOG) were used to address the recognition of CSF-infiltrating CD4+ T cells from MS patients, measuring proliferation (3H-thymidine incorporation), cytokine production and functional phenotype.

Results:
Until now, we analyzed 61 patients with a diagnosis of MS in agreement with 2017 McDonald criteria. Overall CSF $CD4^+$ T-cell reactivity could be demonstrated in twenty-seven patients. Specifically, 18.0% of patients responded exclusively to MOG_{35-55} peptide, while 16.4% responded to at least one TSTA-3 peptide; from these latter patients, 36.4% recognized also MBP-derived peptides. Finally, only 3 patients reacted exclusively against MBP-derived peptides and wide antigen recognition (i.e., MOG2 and TSTA3 and MBP) was documented in 3 patients.
To what extend RASGRP2 is recognized by CSF $CD4^+$ T-cells is still under investigation. So far only 3 patients were tested, finding a strong positive response in one.

Conclusion:
Our findings confirm that specific peptides recognition is detectable in MS patients and can be demonstrated in 44% of the investigated patients. Furthermore, the evaluation of additional 30 patients is currently ongoing as well as serum and CSF cytokine concentration and HLA-typing on our entire cohort. All these variables will be pooled together with clinical data to depict specific pattern of MS.

5430

H. Hayward-Koennecke[2], F. Fuchs[2], C. Kaiser[3], F. Von Kaenel[3], S. Iseli[3], O. Mujkic[3], S. Broicher[2], O. Geisseler[2], R. Martin[2], E. Hafen[1], S. Bignens[3], A. Lutterotti[2]

The MitrendS App – a new tool to follow MS patients using the citizen controlled MIDATA platform.

ETH Zürich[1], Neurology, University Hospital, Zurich[2], Bern University of Applied Sciences[3]

Introduction:
Individualization of outcome parameters according to specific impairments in single patients is an important step towards personal risk assessment and to showing efficacy of treatments in individuals. There is a clear medical need for establishing sensitive parameters as basis for treatment decision in patient care and as outcome parameter in clinical trials. New technologies using App-based tests and/or wearable sensors offer the opportunity for continuous assessment of neurological function and individualization of outcome parameters.

Methods:
We have started to approach this goal by developing a MS-specific App (MitrendS) for tablet computers to assess motor function, cognition, fatigue, quality of life and gait (smartphone-based) with a combination of objective neurological tests and patient-reported outcome measures. MitrendS was developed to monitor disease progression in individual MS patients.

Results:
A validation study demonstrated excellent usability of the MitrendS App. During the validation study motor function tests on the app were correlated with results of the Nine-Hole-Peg Test. Data safety and storage is provided through citizen controlled data management in the MIDATA cooperative. MIDATA.coop is organized as a citizen-owned not-for-profit cooperative that runs and operates a cloud-based IT platform, on which patients and citizens securely store and manage their personal data. Users of the platform own their personal data account, where they store data imported from Apps, medical records and other sources. The users decide, with whom they share their data sets. Users can become members of the cooperative. Members have the same rights as users on the platform, but in addition they take part in the governance of the cooperative (e.g. election of the members of the board, decisions on how revenues will be invested in projects that benefit society at large). In this way, members take control over the use of their own medical data and also participate in the governance of the MIDATA ecosystem.

Conclusion:
We report results from a validation study of the MitrendS App in MS patients, which demonstrate excellent usability. Acquired data is stored in a citizen-controlled cooperative facility, MIDATA, with its use being well received by tested patients.

5431

E. Boran[2], G. Ramantani[1], N. Krayenbühl[2], M. Schreiber[2], K. König[3], T. Fedele[2], J. Sarnthein[2]

High density ECoG improves detection of high frequency oscillations that predict seizure outcome.

Neuropediatrics, University Children's Hospital, Zurich [1], Neurosurgery, University Hospital Zürich, Zürich[2], Swiss Epilepsy Center, Zurich[3]

Introduction:
Residual intraoperative fast ripples (FRs) are highly specific predictors of seizure outcome in epilepsy surgery. However, a FR is generated by a very small area of tissue and spatial sampling with standard strip electrodes in ECoG might be insufficient and leave clinically relevant information undetected.

Methods:
We analyzed FR rates in the intraoperative ECoG of 23 patients that underwent epilepsy surgery. For 14 patients, we used standard strip electrodes with 10 mm inter-contact spacing and 5 mm contact diameter (standard ECoG). For 9 patients, we used high-density (hd) 4x8 grid electrodes with 4 mm inter-contact spacing and 1.8 mm contact diameter (hd-ECoG). We detected FRs using a previously validated automatic detector (Fedele et al., 2016) and visually inspected events to reject artifacts. We evaluated the performance of hd-ECoG compared to standard ECoG regarding FR detection and seizure outcome prediction.

Results:
Seizure freedom was achieved in 13/23 (56%) patients. Residual FRs predicted the seizure outcome in 16/23 patients (accuracy = 70%). Across all 49 ECoG recordings, FR rates were higher for hd-ECoG than for standard ECoG. In good outcome patients, no residual FRs were detected (specificity = 100%). In poor outcome patients, residual FRs were detected in all cases where hd-ECOG was applied, but only in one case where standard ECoG was applied (NPVstandard ECoG = 46%, NPVhd-ECoG = 100%).

Conclusion:
In our study, higher spatial sampling by hd-ECoG improved FR detection and seizure prediction compared to standard ECoG. Hd-ECoG has the potential to augment the predictive power of FRs in epilepsy surgery.

5432

A. Lutterotti[1], W. Faigle[1], H. Hayward-Koennecke[1], I. Jelcic[1], N. Pfender[1], T. Müller[1], C. Blumer[1], M. Foege[1], S. Schippling[1], M. Sospedra[1], M. Sormani[2], M. Inglese[3], T. Berger[4], R. Martin[1]

Treatment of Clinically Isolated Syndrome and Relapsing Remitting Multiple Sclerosis with RNS60 Administered Intravenously – a Phase IIa Clinical Trial

Neurimmunology and MS Research, Neurology Clinic, University Hospital Zurich[1], Department of Health Sciences, University of Genoa, Genoa, Italy[2], Department of Neurology, Icahn School at Mount Sinai, New York, USA[3], Clinical Department of Neurology, Innsbruck Medical University, Innsbruck, Austria[4]

Introduction:
In the treatment of patients with multiple sclerosis (MS), there is a medical need for therapies with a good balance between safety and efficacy. RNS60 is an electrokinetically altered aqueous fluid. Chemically, RNS60 is composed of saline and oxygen. The processing of RNS60, which involves Taylor-Couette-Poiseuille (TCP) flow in the presence of elevated oxygen levels, is hypothesized to produce charge-stabilized nanostructures (CSN) that exhibit electrical fields. The CSN, by virtue of their size, charge, and stability, are thought to be responsible for the biological effects of RNS60. In cellular and animal studies, RNS60 has demonstrated anti-inflammatory effects by downregulating proinflammatory cytokines, up-regulating anti-inflammatory cytokines and inhibited disease progression by switching the immune response from a Th1 to a Th2 type, suppressing the Th17 response, and altering the ratio of Tregs to T responders via downregulation of nitric oxide (NO) production (1).
Taken together, these data indicate a role of RNS60 as a potent anti-inflammatory agent. Thus, RNS60 may provide significant therapeutic benefit for multiple neuroinflammatory/neurodegenerative diseases including MS.

Methods:
The “Nano Cl iv” trial was an open-label, two-center, phase IIa clinical trial, with a baseline-to-treatment design. The primary objective was to assess the efficacy, safety and *in vivo* mechanisms of action of RNS60 administered intravenously in patients with clinically isolated syndrome (CIS) and relapsing-remitting (RRMS).

Results:
Overall, 36 RRMS and CIS patients were included in the trial and 14 patients fulfilled the eligibility criteria for starting the treatment with RNS60. The primary outcome was the change in the mean number of contrast-enhancing lesions (CELs) during weeks 8 to16 (3 MRIs) compared to the three baseline MRIs (weeks –8 to 0; 3 MRIs). RNS60 had an excellent safety profile in all patients. Complete MRI scans were available for 10 patients, while 1 patient was missing the week 12 and the week 16 scan, because of an early withdrawal from the study. The lesion rate ratio (RR) for the number of CELs during week 8, 12,16 vs week -8,-4,0 including all the available MRI scans was 0.66 (95%CI=0.42-1.06), p=0.08. All the sensitivity analyses gave similar results.

Conclusion:
RNS60 was well tolerated in CIS and RRMS patients and demonstrated efficacy in reducing inflammatory disease activity in a small cohort of CIS and RRMS patients. Further studies are warranted to confirm the efficacy of RNS60 to reduce relapse rate and new MRI lesions in MS patients.

5433

A. Lutterotti[1], T. Ludersdorfer[2], M. Docampo[2], M. Hohmann[2], C. Selles Moreno[2], H. Hayward-Koennecke[2], I. Jelcic[1], N. Pfender[1], T. Müller[2], C. Blumer[1], M. Foege[2], S. Winklhofer[3], R. Stenger[2], M. Kayser[2], U. Schanz[4], M. Sospedra[1], R. Martin[1]

Establish Tolerance in MS with myelin-peptide coupled red blood cells - ETIMSred trial

Neurimmunology and MS Research, Neurology Clinic, University Hospital Zurich[1], Wyss Zurich, University of Zurich / ETH Zurich[2], Department of Neuroradiology, University Hospital Zurich[3], Department of Hematology and Oncology, University Hospital of Zurich[4]

Introduction:
Induction of antigen-specific tolerance can be viewed as the most direct and specific means of correcting an altered and pathogenic immune response, which underlies many organ-specific autoimmune diseases. Compared to unspecific immunomodulatory or immunosuppressive interventions, which are currently used in all autoimmune diseases, antigen-specific therapies have the advantage to solely affect the aspects of the immune system responsible for the pathologic effects, without altering physiological immune responsiveness. We have developed a therapeutic regimen employing autologous blood cells chemically coupled with myelin peptides to induce antigen-specific tolerance in MS. The myelin peptides from three different myelin proteins myelin basic protein (MBP), myelin oligodendrocyte glycoprotein (MOG) and proteolipid protein (PLP) were previously identified as important target antigens in MS. Following a successful first-in-man trial with myelin peptide coupled PBMC in MS patients (1) we have optimized the approach further using red blood cells (RBCs) as tolerogenic carrier cells.

Methods:
To test the safety and tolerability of autologous RBCs coupled with 7 myelin peptides (MBP_{83-99}, MBP_{13-32}, $MBP_{111-129}$, $MBP_{146-170}$, $PLP_{139-154}$, MOG_{1-20} and MOG_{35-55}) in a phase Ib clinical trial in MS patients. Patients received a single infusion of up to $3x10^{11}$ autologous myelin-peptide coupled RBCs.

Results:
Overall, ten relapsing-remitting MS patients were treated in a dose escalation study to receive up to $3x10^{11}$ autologous myelin-peptide coupled RBCs. The trial met its primary endpoint, demonstrating a good tolerability and safety of this novel therapeutic approach. The trial is accompanied by mechanistic studies to assess *in-vivo* immunological effects of the therapy.

Conclusion:
In summary we report the safety and tolerability of a novel therapeutic approach in MS aiming at antigen-specific immune tolerance.

5434

M. Boumasmoud[1], L. Meyer[1], T. Schweizer[1], D. Kuehnert[1], K. Seidl[1], A. Holzmann-Bürgel[1], P. Schreiber[1], S. Kuster[1], R. Kouyos[1], A S. Zinkernagel[1]

Molecular evidence for persistence and adaptation of a vancomycin-resistant Enterococcus faecium ST-203 clone in a central European tertiary care hospital

Division of Infectious Diseases and Hospital Epidemiology, University Hospital Zurich, University of Zurich[1]

Introduction:
Vancomycin-resistant *Enterococcus faecium* (VRE) nosocomial outbreaks are a worldwide problem with increasing prevalence. Despite reinforced epidemiologic surveillance and the adoption of preventive measures, this hospital adapted pathogen is constantly evolving and spreads following complex routes.

Methods:
We collected 66 VRE isolates from patients with either infection or colonization at the University Hospital Zürich between 2014 and 2018. In addition to the routine typing by pulsed-field gel electrophoresis (PFGE) and multilocus sequence typing (MLST), we characterized this collection by whole-genome-sequencing (WGS). Our main aim was to contextualize an ST-203 outbreak which occurred in January-February 2018 (n=18) within the increasing prevalence of VRE detected cases observed during the last 4 years (n=44). We established the phylogenomic relationship of these clinical isolates to unfold transmission events and follow longitudinal dynamics of pathogen adaptation.

Results:
The traditional methods (PFGE and MLST) and the phylogenomic analysis both indicated that many isolates were from multiclonal origin and therefore likely introduced into the hospital by multiple events. However, there were some groups of closely related isolates (clusters) as well. While for some clusters we established an epidemiological link, for others we did not.
In particular, our phylogenomic analysis revealed that the 2018 outbreak isolates belonged to a cluster including ST-203 isolates dating back to 2014. Within this cluster, we identified the specific mutations which arose over time and observed the acquisition of a transposon carrying a phosphotransferase system.

Conclusion:
With the high resolution brought by WGS, we show molecular evidence for persistence of a ST-203 clone over 3 years within our hospital and we report its adaptation over time.

5435

L. Kovtonyuk[1], M. Manz[1]

Determinants of Hematopoietic Stem Cell Aging

Department of Medical Oncology and Hematology[1]

Introduction:
Lifelong continuous blood production is sustained through a stepwise differentiation program by a very limited number of self-renewing Hematopoietic Stem Cells (HSCs) in the bone marrow (BM). Hematopoietic cell development is tightly controlled by both cell intrinsic and extrinsic factors and its dysregulation can lead to aplasia or neoplasia. During ageing, HSCs increase in number, reduce self-renewal capacity on a per cell basis, skew towards myeloid differentiation, and show less efficient bone marrow (BM)–homing ability. We here tested how and to what extend extrinsic and intrinsic factors determine HSC behaviour during aging.

Methods:
CFSE-labelled young (8-12 week old) and aged (>2 year old) HSC-containing lineage negative, c-Kit positive, Sca-1 positive (LKS) mouse BM cell fractions were each transferred into steady state, non-irradiated young and aged WT mice (see methods Takizawa et al., J Exp Med 2011). To test HSCs function based on divisional history, we isolated quiescent and cycling LKS fractions from various combinations and transplanted them into lethally irradiated mice, which were bled monthly to follow long-term donor engraftment and lineage repopulation. To determine aging-associated extrinsic factors, we performed antibody based protein arrays and transcriptome analysis with total BM of young versus aged animals. Candidate factors were further confirmed by ELISA and qPCR. The effects of IL-1 on HSC cycling were investigated using in vivo CFSE assay. To test function of IL-1RI KO HSCs, cells were transplanted into lethally irradiated mice which were bled monthly to follow long-term donor engraftment and lineage repopulation.

Results:
BM analysis at 8 weeks after divisional tracking showed that young HSPCs proliferated faster than old HSPCs, independently of their environment. Moreover, both young and old HSPCs were relatively more dormant in an old versus a young environment. This indicates an increased intrinsic and extrinsic drive towards quiescence during ageing. Quiescent aged HSCs, subsequently transplanted in young or old recipients, favoured myelopoietic differentiation. Similarly, cycling aged HSC isolated from a native aged environment showed myeloid biased repopulation upon subsequent transplantation. In contrast, cycling aged HSCs isolated from a native young environment showed balanced lineage repopulation upon subsequent transplantation (similar to young HSCs that were cycling within a young or an aged environment). Moreover, experimentally aged HSC (serially transplanted HSCs) showed a similar read-out as aged HSCs. Antibody based protein arrays and transcriptome analysis with total BM of young versus aged animals demonstrated that RANTES, MIP-2, IL-1α and IL-1β are upregulated in aged BM at both protein and RNA level. ELISA of peripheral blood (PB) serum and BM lysates indicated that IL-1α is locally produced in BM, but is not upregulated in PB serum. Further, qPCR of various BM cell types of hematopoietic and non-hematopoietic origin indicated that multiple cell types upregulate *Il1α* and *Il1β*. CFSE-dilution and functional HSC read-outs revealed that IL-1α and IL-1β drive young HSC towards proliferation, while this effect is mitigated in aged HSCs, despite the upregulated expression of IL1RI on aged HSCs. Moreover, analysis of aged IL1RI KO mice revealed a reduced aging-associated HSCs phenotype and improved lymphoid lineage repopulation upon transplantation into lethally irradiated mice.

Conclusion:
Our data demonstrate that proliferative history imprints a cell-intrinsic dormancy program on HSCs, which is associated with myeloid-biased differentiation and, at least in natural ageing, with increased IL-1 signalling. Interestingly, this HSC program can in part be “rejuvenated” upon cycling, but not upon dormancy, in young steady-state environments.

5436

F. Caiado[1], L. Kovtonyuk[1], M. Manz[1]

Role of Inflamm-Ageing of the Hematopoietic Sytem on Clonal Hematopoiesis Progression

Department of Medical Oncology and Hematology , UniversityHospital Zürich[1]

Introduction:
Hematopoietic stem cells (HSCs) produce mature blood cells during the lifetime of blood carrying organisms. HSCs are exposed to a continuous ageing process that manifests itself by less efficient blood production, reduced immune function and an elevated risk for clonal evolution and neoplastic HSC transformation. Ageing correlates with proliferative history of HSCs and it correlates with low-level, chronic inflammation. Thus, we hypothesize that HSC ageing and inflammation are biologically closely intertwined processes termed "inflamm-ageing". Clonal Hematopoiesis of indeterminate Potential (CHiP) is defined as the presence of an expanded somatic blood cell clone carrying a mutation in genes that are drivers of hematologic malignancy including DNMT3A and TET2 at a variant allele frequency of at least 2% in the absence of other hematological abnormalities. CHiP has a prevalence of about 10% in the 70-80 year old population and associates with an increased risk of hematological malignancies, cardiovascular disease and with all-cause mortality. Being a premalignant state, therapeutically interfering with CHiP offers a window of hematological malignancy prevention. Thus, it is key to decipher CHiP pathobiology and drivers for progression. Here we hypothesize that hematological inflamm-ageing is a key driver of CHiP and that its therapeutic targeting can prevent progression to malignancy.

Methods:
We will develop a tamoxifen-inducible mouse model containing floxed *Tet2 or Dnmt3A* exons conditional to the stem cell leukemia (*Scl*) stem-cell enhancer. This will allow a HSC-specific deletion of the *Tet2 or Dnmt3A* exons leading to loss-of-function mutant proteins.
To assess the contribution of ageing to DNMT3A / TET2 mutant HSC clonal fitness we will use hematopoietic chimera mouse models in young and old recipients. We will transplant sorted WT Lin-Sca1+ c-kit+ (CD45.1) and HSC-conditional DNMT3A or TET2 mutant LKSs (CD45.2) from adult mice (1 year old) in a 9:1 ratio into lethally irradiated young (2 months old) or old (1.5-2 years old) recipient mice (CD45.1xCD45.2). After three months, the relative frequency of WT (CD45.1) and DNMT3A / TET2 mutant (CD45.2) hematopoietic cells in peripheral blood will be determined periodically. 3-4 months after injection mice will be sacrificed and bone marrow HSC chimerism assessed. WT and DNMT3A / TET2 mutant HSCs will be sorted for molecular and functional characterization.
To determine the influence of exposure to inflammation on DNMT3A / TET2 mutant HSCs clonal fitness we will use hematopoietic chimera mouse models (as outlined above). Chimeric mice will be chronically challenged (up to 6 months) with PBS (control), LPS, polyI:C and pro-cycling inflammatory cytokines: IL-1, IL-6, IFNa, TNFa, TPO; and the relative hematopoietic contribution of WT and DNMT3A / TET2 mutant donor cells will be evaluated in peripheral blood periodically. Upon challenge ending mice will be sacrificed and bone marrow HSC chimerism assessed. WT and DNMT3A / TET2 mutant HSCs will be sorted for molecular and functional characterization.

Results:
Results will clarify if HSC clonal fitness and dominance in DNMT3A / TET2 mutant vs WT are influenced by HSC extrinsic/environmental factors. Results will indicate specific conditions favoring CHiP mutated HSC over WT and whether CHiP HSCs fitness responses are *DNMT3A* or *TET2* mutation specific. Moreover, using the described approaches we expect to establish proof of concept rationale for therapeutic intervention on CHIP carrying HSCs.

Conclusion:
With growing life expectancy in our populations, age-associated health-risks and manifest chronic diseases are becoming a major challenge. Thus, understanding the biologic facets of inflamm-ageing is of fundamental importance. The project here outlined will help to establish the key environmental factors driving progression of CHiP to hematological malignancy and set the basis for the development of therapeutic targeting of this prevalent pre-leukemic condition.

5437

P. Pagella[1], C. Cantu'[2], M. Schwab[3], T. Mitsiadis[1]

The neurite outgrowth inhibitor Nogo-A fine-tunes enamel formation

Institute of Oral Biology, Center of Dental Medicine, Faculty of Medicine, University of Zurich[1], Department of Clinical and Experimental Medicine (IKE), Faculty of Health Sciences, Linköping University, Wallenberg Centre for Molecular Medicine (WCMM), Linköping University, Linköping, Sweden[2], Brain Research Institute, University of Zurich; Department of Health Sciences and Technology, ETH Zurich[3]

Introduction:
Initially discovered as a potent inhibitor of neurite outgrowth, in the last decades Nogo-A emerged as a fundamental actor of nervous system development, physiology, pathology and regeneration. In this context, Nogo-A became a promising target for central nervous system (CNS) regeneration. However, despite the already known widespread expression of Nogo-A in non-neuronal tissues, its role outside the CNS has been poorly investigated. We here investigated the function of Nogo-A during tooth development. Teeth develop as a result of sequential and reciprocal interactions between cells of the oral epithelium and cranial neural crest-derived mesenchymal cells. Differentiation of mesenchymal cells gives rise to the dental pulp and the dentin-producing odontoblasts, whereas the dental epithelium will give rise to the enamel-forming ameloblasts. We here report a new function for Nogo-A as modulator of tooth development via a previously unknown molecular function.

Methods:
We determined Nogo-A expression in teeth by immunohistochemistry and immunofluorescence. Transgenic mouse models were exploited to study the effects of Nogo-A deletion in dental tissues. Morphological alterations were assessed by histology, scanning electron microscopy and transmission electron microscopy. RNA sequencing was performed on teeth isolated from Nogo-A mutant and control littermates. Pulldown assays followed by mass spectrometry and western blot were used to determine the Nogo-A interactome in ameloblasts. Transfections and live imaging were used to study the molecular function of Nogo-A in tooth derived cell lines, as well as in non-dental cell lines.

Results:
We observed that Nogo-A was expressed in both ameloblasts and odontoblasts from early developmental stages. Transmission and scanning electron microscopy analysis revealed that its deletion in a Nogo-A KO transgenic mouse model led to a general disorganization of ameloblasts and the generation of defective enamel. Conditional deletion of Nogo-A in the dental epithelium (K14:Cre;Nogo-A) was sufficient to cause defects in enamel organization and structure, indicating a completely novel, epithelium-specific role for Nogo-A. RNA sequencing analysis showed that, in this context, the loss of Nogo-A induced the deregulation of genes coding for proteins involved in intracellular transport, extracellular matrix remodelling and cell-cell adhesion, processes fundamental for proper enamel formation. Mass spectrometry-based analysis of the ameloblasts-specific interactome of Nogo-A showed a significant enrichment of proteins involved in ribosomal function, as well as proteins involved in exosomal trafficking. We then investigated whether Nogo-A directly modulates the intracellular localization of ribosomes and protein translation in dental and non-dental cell types.

Conclusion:
Taken together, these results indicate a completely novel set of functions for Nogo-A outside the CNS, revealing it as an important regulator of enamel formation, and at the same time uncovering a completely new mechanism of action for this molecule.

5438

M. Sharifshazileh[1], K. Burelo[1], J. Sarnthein[1], G. Indiveri[2], T. Fedele[1]

A Neuromorphic System-on-a-Chip Approach Towards Detecting High-Frequency Oscillations in Human iEEG

Klinik für Neurochirurgie, Universitätsspital Zürich[1], Institute of Neuroinformatics (INI), University of Zurich and ETH Zurich[2]

Introduction:
High Frequency Oscillations (HFO) found in intracranial electroencephalography (iEEG) signals have shown to predict surgical outcome and are therefore, promising bio-markers for epileptogenic zone (EZ). Electrocorticography (ECoG) recordings are part of the surgery procedure. Real-time classification of these signals can provide direct feedback to the surgeon to indicate if the remaining brain areas contain HFO and guide the surgeon towards a better surgical outcome. This application requires a device that can pre-process and classify these signals in real-time. State-of-the-art HFO detectors depend on very stringent requirements on the amplified signal quality which results in large and power-hungry systems, while the classification is off-line with algorithms implemented on conventional digital computers.

Methods:
In this work, we present a low-noise analog frontend interfaced to a spiking neural network (SNN) for spatio-temporal pattern recognition in real-time. The analog frontend extracts predefined spectral features from iEEG signal and translates them to event-triggered spikes using an asynchronous delta modulator. The SNN takes the generated events and indicates the presence of HFO in the provided signal. For training the network, we use a data set comprised of iEEG recordings from 13 patients who underwent resection surgery. HFO markings and surgical outcome data is available.

Results:
The designed frontend has a power consumption of 6.2 µW/channel and the area-on-chip for a single channel is 0.15 square millimeters. These results are obtained from a simulation using standard 0.18µm CMOS technology. The proposed spiking neural network can identify HFO with a 99.48% sensitivity and 55.72% specificity on a test dataset, which is in line with the state-of-the art off-line algorithms.

Conclusion:
Event-based processing techniques can perform real-time biological pattern recognition with extreme power-efficiency. Moreover, employing these schemes relaxes the linearity constraints on neural-recording amplifiers and filters enabling circuit designers to develop portable systems that can aid the medical team during epilepsy surgery.

5439

P. Baumgartner[1], A. Luft[1], S. Wegener[1]

Optic Nerve Sonography to monitor Intracranial pressure afTer large vessel ischemic strokE – The ONSITE Study

Department of Neurology, University Hospital Zurich[1]

Introduction:
Intracranial hypertension (IH) is a life-threatening complication of ischemic or hemorrhagic stroke. It occurs most frequently in large infarcts due to occlusion of the internal carotid artery (ICA) or proximal segment (M1) of the middle cerebral artery (MCA), particularly if the vessel is not successfully recanalized. Mortality in this condition is up to 80% if treated conservatively. Therefore, fast diagnosis of IH is imperative for successful surgical treatment. Since invasive intracranial pressure (ICP) monitoring devices are not always feasible, patients are usually followed based on clinical symptoms. However, medications or comorbidities of stroke complicate clinical IH assessment. Therefore, readily available, non-invasive methods to early detect IH in stroke patients are needed.

Methods:
The goal of this study is to implement optic nerve sonography (ONS) as an easy, non-invasive method to monitor ICP after large-vessel ischemic stroke. ONS utilizes the fact that the optic nerve sheath, which is readily visualized by transorbital ultrasound, is filled with spinal fluid and grows in diameter according to ICP. To perform ONS, the patient is placed in a position 20° supine to horizontal. The ultrasound probe is then placed on the closed eyelid without pressure to avoid any damage to the eye. The optic nerve sheath diameter (ONSD) is then measured 3 mm behind the globe.

Results:
We are conducting a single-center, prospective observer study, where ONSD will be repeatedly assessed in patients with occlusion of ICA and/or the M1 segment of the MCA up to 120 hours after stroke onset. GCS and NIHSS are obtained every 6 hours in clinical routine, and will be used along with neuroimaging (CT/MRI) to confirm IH. Cut-off values for ONSD that best predict the presence of IH will then be determined by a receiver operating characteristic (ROC) curve. Sensitivity, specificity and positive predictive value of this threshold to predict IH after stroke will be calculated. We will present data on intra- and interobserver reliability of the method which we are currently testing in non-stroke patient as well as first data on ONSD in stroke patients.

Conclusion:
ONS has the potential to be an accurate, widely available and easy to learn method to detect IH in stroke patients. If ONSD thresholds can be established to detect IH early after stroke, it could be further tested in a multi-center clinical trial to aid in decision making for hemicraniectomy in stroke patients.

5440

A. Akhmedov[1], F. Montecucco[2], G. Camici[1], A. Schaub Clerigue[1], D. Vdovenko[1], S. Costantino[1], N. Bonetti[1], C. Diaz-Canestro[1], F. Paneni[1], F. Mach[2], T. Lüscher[1]

GDF11 Promotes Increased Sensitivity of the Murine Heart to Ischemic Injury

Center for Molecular Cardiology, University of Zurich, Schlieren[1], Division of Cardiology, Foundation for Medical Researches, University of Geneva, Geneva[2]

Introduction:
Recent studies have implicated a role of TGFβ family members in aging and cardiovascular diseases. Growth Differentiation Factor 11 (GDF11) is a member of TGFβ superfamily with high homology to myostatin/GDF8. Interestingly, in mice its levels decline with age, whereas myostatin and TGFβ1 levels remain unchanged, suggesting involvement of GDF11 in aging. In addition, GDF11 has recently been shown to play a role in cardiac hypertrophy. However, not much is known about its role in the myocardium. The goal of the present study was to investigate whether restoring GDF11 levels of aged mice to the ones observed in young mice by injecting recombinant GDF11 into blood stream would rescue myocardial infarction and provide “youthful” characteristics to the old myocardium.

Hypothesis-Restoring GDF11 levels in aged mice to the ones observed in young mice would improve the myocardial infarction outcome and provide “youthful” characteristics to the old myocardium.

Methods:
12-14-week-old and 22-24-month-old C57BL/6 male mice were injected daily with either recombinant human GDF11 or vehicle for 30 days. Afterwards mice were subjected to 30 min of ischemia (I) followed by 24h of reperfusion (R). Infarct size was assessed morphologically.

Results:
After I/R, both young and aged GDF11-injected mice developed markedly larger infarcts as compared to vehicle-treated group. This was further associated with increased post-ischemic levels of serum cardiac troponin I. In addition, both GDF11-injected groups showed accelerated cardiac cell death after I/R as has been assessed by TUNEL assay on heart cross sections. Of note, both ageing groups showed higher mortality during the GDF11 treatment. Finally, transcription factor Nkx2-5 and its known cofactor Gata4 were both downregulated in GDF11-treated hearts on both mRNA and protein levels further supporting the involvement of Nkx2-5-Gata4 transcriptional interaction in the observed GDF11-mediated cardiac phenotype as assessed by pathway analysis using Ingenuity Pathway Analysis Database as well as by qPCR and Western blotting respectively.

Conclusion:
In summary, present study showed that daily injections of GDF11 promote increased sensitivity of the heart to myocardial infarction. Such GDF11-associated cardiac phenotype is likely to be driven by increased cell death in the injured myocardium together with impaired function of Nkx2-5-Gata4 pathway. Thus, these results do not support proposed role of GDF11 as “rejuvenation” factor for the heart.

5441

A. Akhmedov[1], F. Montecucco[2], S. Costantino[1], A. Schaub Clerigue[1], D. Vdovenko[1], D. Gaul[1], F. Carbone[2], L. Liberale[1], U. Eriksson[3], C. Matter[1], F. Paneni[1], G. Camici[1], F. Mach[2], T. Lüscher[1]

Cardiomyocyte-specific jund regulates infarct size following ischemia/reperfusion cardiac injury by downregulating SIRT3

Center for Molecular Cardiology, University of Zurich, Schlieren[1], Division of Cardiology, Foundation for Medical Researches, University of Geneva, Geneva[2], GZO Regional Health Center, Wetzikon[3]

Introduction:
Myocardial injury during short-term ischemia (I) and reperfusion (R) has become clinically important with the use of primary PCI as a first-line strategy in patients with acute coronary syndrome (ACS). The Jun family of activator protein 1 (AP-1) transcription factors (c-Jun, JunB, JunD) is involved in fundamental biological processes such as proliferation, apoptosis, tumor angiogenesis, and hypertrophy. Its member JunD is specifically expressed in the developing heart and cardiovascular system. Current evidence suggests a complex role for JunD in the adult heart. However, there is little *in vivo* evidence about the role of JunD in the infarcted heart. In the present study we analyzed the role of JunD in the heart using cardiac-specific JunD transgenic mouse line (*cJunDTG*) subjected to I/R.
Hypothesis- Cardiac-specific overexpression of transcription factor JunD contributes to myocardial injury in a mouse model of cardiac ischemia and reperfusion.

Methods:
8-12-week-old *cJunDTG* males and corresponding C57Bl/6 wild-type (WT) controls were subjected to 30 min of I followed by 24h of R. Infarct size was assessed morphologically.

Results:
Infarct size, systemic and local inflammation and production of reactive oxygen species, as well as cytosolic and mitochondrial apoptotic pathways were investigated in adult male mice after myocardial I/R. In wild-type (WT) mice, 30 minutes after ischemia and up to 24 hours following reperfusion, cardiac *JunD* mRNA expression was reduced and *JunB* increased. Cardiac-specific JunD overexpressing mice ($JunD^{Tg/0}$) displayed larger infarcts and left ventricular end systolic volume compared to WT littermates. However, post-ischemic inflammatory or oxidative responses did not differ. JunD overexpression reduced Sirt3 transcription by binding to its promoter, thus leading to mitochondrial dysfunction, myocardial cell death and increased infarct size. On the other hand JunD silencing reduced, while Sirt3 silencing increased infarct size. In myocardial human autopsy specimens, JunD-positive areas within the infarcted left ventricle staining corresponded to undetectable Sirt3 areas in consecutive sections of the same heart.

Conclusion:
Cardiac-specific JunD overexpression increases myocardial infarct size and left ventricular end systolic volume following I/R. These effects are mediated by Sirt3 repression, mitochondrial swelling and increased apoptosis, suggesting that JunD is a key regulator of myocardial I/R injury in mice and potentially in humans. The present data set the stage for further investigation of the potential role of Sirt3 activation as a novel target for the treatment of acute myocardial infarction.

5442

P. Schürch[1], T. Wildschut[1], L. Malinovska[3], V. Lysenko[1], A. Lakkaraju[2], E. Milani[3], A. Aguzzi[2], B. Wollscheid[3], A. Theocharides[1]

Protein clients are differentially affected by mutations in the endoplasmic reticulum chaperone calreticulin

Department of Hematology and Oncology, University Hospital Zürich[1], Institute of Neuropathology, University Hospital Zürich[2], Institute of Molecular Systems Biology ETH Zurich[3]

Introduction:
Calreticulin (CALR) is an endoplasmatic reticulum (ER)-resident chaperone that ensures folding of glycoproteins (GPs) such as the thrombopoietin receptor (TpoR), major histocompatibility complex I (MHC-I) and myeloperoxidase (MPO). *CALR* is frequently mutated in patients with myeloproliferative neoplasms (MPNs). All CALR mutants share a mutant-specific C-terminus with type-1 and type-2 variants covering over 80% of the mutational spectrum of CALR (Klampfl et al., N Engl J Med, 2013). Mutant CALR activates the TpoR and consecutively JAK/STAT signaling through a pathologic protein-protein interaction (Araki et al., Blood, 2016). Furthermore, we have previously shown that MPN patients with homozygous *CALR* mutations develop a maturation defect in MPO (Theocharides et al., Blood, 2016). Therefore, we hypothesize that the protein interactome of CALR and the maturation of further GPs is altered in the presence of CALR mutants. Further, we hypothesized that disease-relevant GPs that are affected by the *CALR* mutations could be detected by their altered structure (e.g. due to misfolding) by using a proteomic-based screen.

Methods:
We first aimed to determine how the maturation of known CALR GP clients is affected by *CALR* mutations. Using CRISPR-Cas9, we generated a CALR knockout in the HL-60 cell line that expresses abundant levels of MPO (HL-60 CALR KO). The expression of MPO and MHC-I on HL-60 CALR KO cells and patients with *CALR* mutations was determined by flow cytometry. To screen for structural changes of GPs in the presence of mutant CALR chaperones, patient-derived neutrophils were subjected to limited proteolysis-coupled mass spectrometry (LiP-MS, Schopper et al., Nat Protoc., 2017).

Results:
The expression of MPO was significantly reduced in HL-60 CALR KO cells resembling the phenotype observed in patients with homozygous *CALR* mutations. In contrast, while MHC-I expression was diminished in HL-60 CALR KO cells, patients with homozygous *CALR* mutations showed normal MHC-I expression. Our preliminary LiP-MS screen revealed 115 GPs with an altered structure in hetero- and homozygous patients. Most GPs that underwent structural changes in heterozygous patients were also identified in homozygous patients. Roughly, two thirds of GPs only changed structure in context of a homozygous *CALR* mutation but not a heterozygous mutation.

Conclusion:
Together the findings from our biased approach with MPO and MHC-I suggest that *CALR* mutations affect the maturation of CALR protein clients in a protein-specific manner. We are currently reconstituting HL-60 CALR KO cells with either wildtype or mutant CALR proteins (type-1 or type-2) to understand how MPO and MHC-I expression are affected by the CALR mutants. The conducted pilot study shows that LiP-MS can be used to detect structural changes in the proteomes of *CALR*-mutated patients. To account for patient-to-patient variability we will measure more samples to identify any disease-relevant GPs affected by mutated CALR. Thus, we will conduct a more comprehensive screen of structural changes of proteins in the proteomes of MPN patients carrying either a type-1 *CALR* mutation or type-2 *CALR* mutation.

5443

D. Hausmann[1], P. Appenzeller[1], D. Kreul[1], C. Caspar[3], A. Nocito[2], M. Klarhöfer[4], B. Kuehn[4], B. Kiefer[4], S. Bensler[1], R. Kubik[1]

Evaluation of an innovative automatized "semi-whole-body" MRI protocol to increase patient comfort and cost-effectiveness of oncologic imaging: initial results

Institute of Radiology. Kantonsspital Baden, Baden[1], Department of Surgery, Kantonsspital Baden, Baden[2], Department of Oncology, Kantonsspital Baden, Baden[3], Siemens Healthcare, Erlangen, Germany[4]

Introduction:
Whole-body (wb) imaging becomes increasingly important in oncologic patients not only for primary cancer staging, but also for assessment of response to therapy. So far, PET/CT is the key method to assess cancer-related changes of metabolism in tumors, which is crucial for response evaluation and to differentiate between benign and malignant lesions. Both CT and administration of radioactive tracer are associated with radiation exposure for patients. Wb MRI including functional techniques (e.g. Diffusion-weighted Imaging (DWI) to evaluate cell density) enables a functional staging and therapy assessment without use of ionizing radiation. Advantages to assess sclerotic bone lesions and organ metastases have been confirmed in recent literature. Limitations of MRI include detection of lesions in organs with high susceptibility and motion like the thorax.

The aims of this study are
- to evaluate the image quality of a "semi-whole-body (thorax/abdomen)" MRI protocol by using an optimized prototypical scanner workflow (DOT)
- to compare lesion detectability between MRI and PET/CT
- to compare patient comfort between PET/CT and MRI using a questionnaire
- to compare duration of image acquisition time between PET/CT and DOT

Methods:
Patients with clinically indicated PET/CT for cancer staging or response assessment and histopathologically confirmed solid tumors (e.g. prostate, breast, gastrointestinal tract, testicles) are included in this IRB-approved prospective study. So far, 20 datasets (10 PET/10 DOT) were independently assessed by two experienced readers. The DOT workflow automatically segments the anatomy and based on this information autoaligns slices and optimizes imaging parameters in a reproducible fashion in order to reduce variability of sequence parameters and to save acquisition time compared to conventional manual sequence planning. Hereby, DOT guarantees reproducible acquisition times that can be used for a more accurate estimation of protocol duration and thus for improved slot scheduling in follow-up examinations.
MRI protocol consisted of non-contrast T1-(coronal T1 Dixon)/T2-weighted (axial T2 haste without fat suppression, coronal STIR) sequences and prototypical ultrafast SMS-epi DWI (including extrapolated b=2000mm/s2). Image quality (IQ), delineation of structures (DoS), artifacts (A) and diagnostic confidence (DC) were rated on Likert-type scales (IQ/DoS/DC: 1 (non-diagnostic)-5 (perfect); A: 1 (no artifacts)-5 (severe artifacts)). Mann-Whitney U-test was performed to compare DC of DOT and PET. Region-based (thorax (th)/abdomen (ab)/lymph nodes (ln)/MSK) lesion detectability of MRI and PET/CT was compared. Patient comfort of PET/CT and MRI was assessed using a questionnaire. Total examination time (tet) was evaluated.

Results:
Ratings for IQ/DoS of DOT (3.8/4.3) were generally high, while A was rated low (2.2). All PET positive lesions were detected by DOT (th=2; ab=0; ln=5+diffuse (2), MSK=3+diffuse (1)) Nevertheless, DC of PET was rated significantly higher by both readers (4.7 vs. 4; $p<0.05$; κ: >0.7). Tet of DOT/PET was 30.7±5.4/92.1±5 minutes. DOT was the preferred method by 8 patients.

Fig. 1

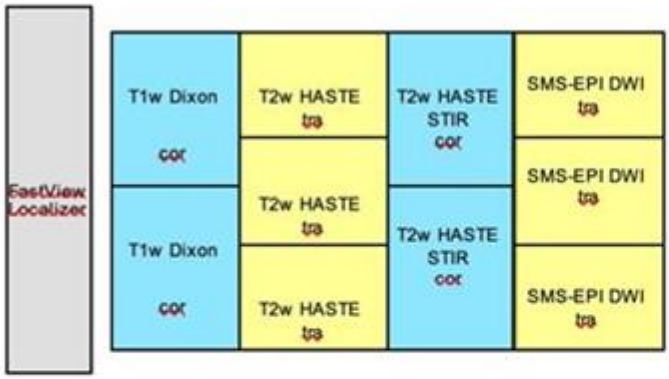

Overview over the DOT workflow. The horizontal direction depicts the time course of the examination, while the vertical direction depicts the head to feet direction of the patient. The grey box symbolizes a moving table localizer scan covering the anatomy from head to the thighs; the yellow and blue boxes symbolize the measurement volumes used for T1, T2 and for the DWI imaging, respectively.

Fig. 2

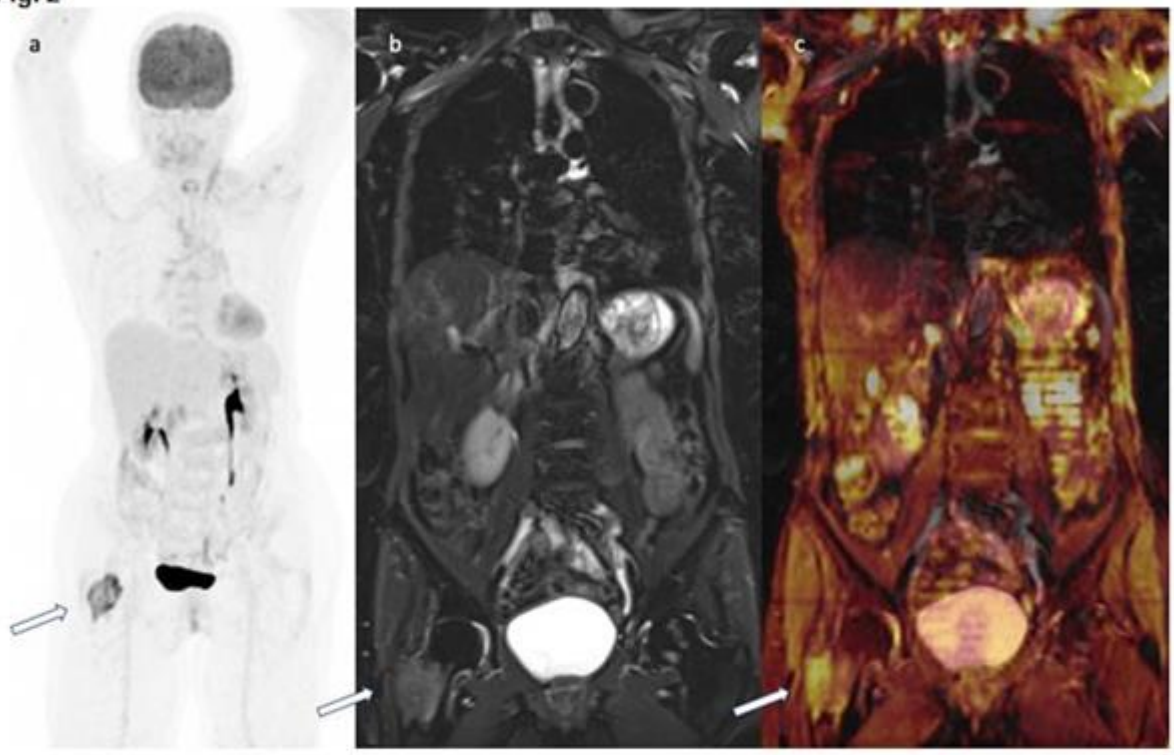

Images of a 76-yo female patient with metastatic breast cancer. 18F-FDG-PET/CT (a) shows increased uptake of a single bone metastasis in the right proximal femur. On coronal STIR (b) and coronal STIR/high b-value fusion (c) the bone metastasis is clearly depicted.

Fig. 3

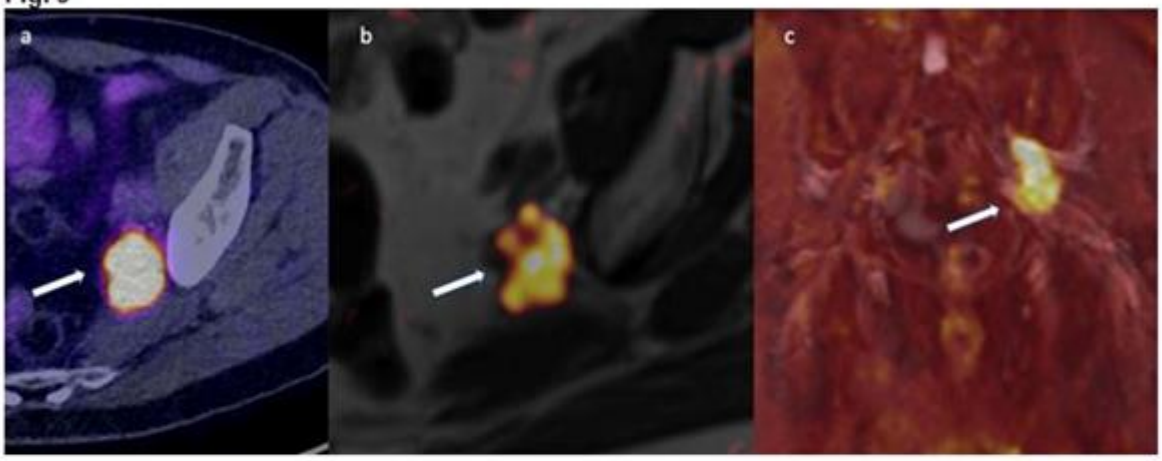

Images of a 76-yo prostate cancer patients with bulky left iliac lymph node metastases. On 68Ga-PSMA-PET/CT significant tracer uptake is confirmed (a). Nodal involvement is visible on axial T2 haste (b)/ and coronal STIR (c)/high b-value fusion.

Fig. 4

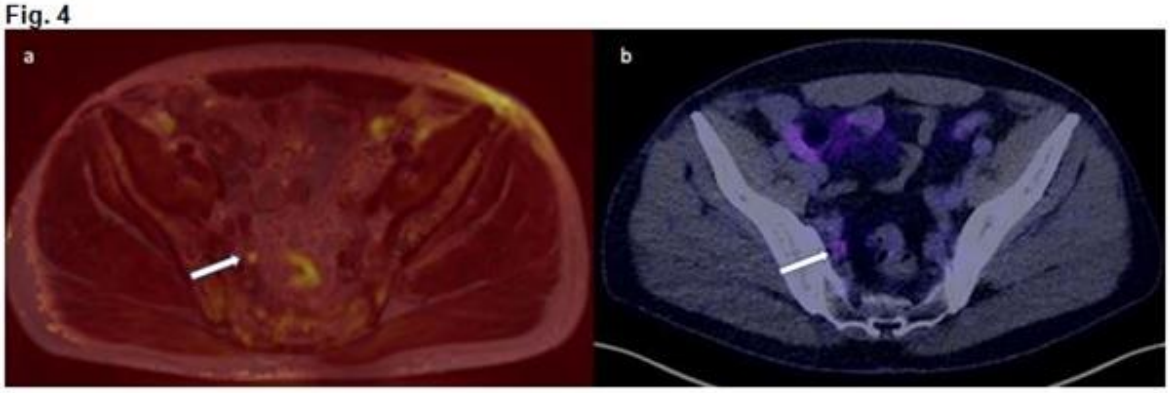

Images of a 74-yo prostate cancer patient with minimal PSA-elevation after radical prostatectomy. Axial T2 haste/high b-value fusion shows a small right iliac internal lymph node with restricted diffusion (a). Single lymph node metastasis was confirmed by 68Ga-PSMA-PET/CT (b).

Conclusion:

By reduction of planning time and hence image acquisition time due to employment of automatic slice alignment as well as increased reproducibility of scan time, DOT may allow a comfortable, time-/cost-effective staging without use of ionizing radiation and contrast media with increased patient comfort, which may be interesting particularly in young patients with multiple follow-up examinations.

5444

M. Emmenegger[1], E. Capodaglio[1], A. Chincisan[1], S. Grathwohl[2], P. Kumari[3], D. Schneider[1], L. Mottier[1], J. Domange[1], J. Grimm[2], R. Riek[3], A. Aguzzi[1]

Identification and characterisation of patients harbouring anti-ApoE4-specific autoantibodies from an unselected hospital-wide patient cohort

Institute of Neuropathology, University Hospital of Zurich[1], Neurimmune Holding AG, Schlieren[2], Department of Chemistry and Applied Biosciences, ETH Zurich[3]

Introduction:
Alzheimer's Disease (AD) is the most common form of dementia affecting around 30% of people over the age of 80 and the fourth leading cause of death in developed countries. Genome-wide association studies (GWAS) have unequivocally pinpointed to the apolipoprotein E (APOE) as the most important susceptibility gene for late-onset AD (LOAD). The ApoE4 isotype is characterised by an arginine instead of a cysteine residue at position 112, which induces a conformational change. While all ApoE isotypes have important and multiple roles in the central nervous system (CNS) lipid metabolism, ApoE-ε4 has been shown to facilitate amyloid beta aggregation, to impair its clearance, and to foster the formation of neurofibrillary tau tangles. Thus, therapeutic approaches have to focus on the selective neutralisation of ApoE4 without affecting the functionality of ApoE-ε2 or ApoE-ε3. Apart from small molecules and gene therapy, the utilisation of human antibodies specifically recognising the ε4 isotype may pose a powerful strategy to offer therapy for people at risk at an early preclinical stage.

Methods:
We have interrogated an unselected patient cohort of 20,000 patients for the presence of autoantibodies against the ε3, ε4, and a lipidated form of the ε4 isotypes of ApoE, aiming to identify patients harbouring anti-ApoE4-specific autoantibodies. Using residual heparin plasma samples provided by the Institute of Clinical Chemistry, a microELISA antibody profiling was carried out in a robotised platform. Medical and experimental data was separately stored in an MS-SQL multi-database system and was correlated and visualised using software packages in Python and R. Cellular material of reactive patients was isolated using Ficoll gradients. ApoE4 isotypes in patients of interest was assessed using an in-house developed ApoE phenotyping approach.

Results:
Testing of so far minimally 13,741 samples per isotype indicates a prevalence of positives of 0.08% for ε3, 0.01% for ε4, and 0.04% for the lipidated form of ε4. We then selected those patients reactive against at least one of the isotypes and tested them against all others. Preliminary data from these secondary screenings suggest that most of the positive patients are pan-ApoE reactive, with few patients that selectively target either only the lipidated form of ApoE-ε4 or bind ε4 (lipidated and non-lipidated) with higher affinity than ε3. So far, the correlation of the medical record with the reactivity spectrum of the patients has not yielded a clear-cut pattern, possibly indicating that the presence of antibodies against ApoE is not associated with a specific disease type.

Conclusion:
While preliminary data indicate the possibility to identify patients harbouring ApoE4-specific antibodies, more sophisticated secondary screenings are needed to validate the findings. Next steps include the elucidation of the isotypes of the interesting patients using a phenotyping approach, the attempt to clone antibodies from the memory B cells of those patients with ApoE-ε4-specific antibodies who signed the general consent, and the characterisation of the antibodies in in vitro and in vivo disease models. The successful realisation of these steps may open up new avenues to help prevent the development of AD in susceptible patient groups at an early presymptomatic stage.

5445

D. Hausmann[1], T. Niemann[1], D. Kreul[1], A. Nocito[2], M. Klarhöfer[3], D. Nickel[3], K. Kiefer[3], S. Bensler[1], R. Kubik[1]

Free-breathing dynamic contrast-enhanced Imaging of the upper abdomen using advanced compressed-sensing reconstruction

Institute of Radiology. Kantonsspital Baden, Baden[1], Department of Surgery, Kantonsspital Baden, Baden[2], Siemens Healthcare, Erlangen, Germany[3]

Introduction:
Motion-induced artifacts are a well-known challenge for dynamic contrast- enhanced abdominal MR imaging. Especially elderly patients and severely ill patients are often unable to adequately perform breath-hold maneuvers with a risk of critically reduced image quality due to motion artifacts and consequently impaired interpretability of the imaging material. Recently fast multiphase contrast-enhanced sequences with artifact reduction by motion-insensitive radial acquisitions were introduced. Long reconstruction times and necessity of an external reconstruction server limited clinical applicability of these approaches for older MR systems. The purpose of this study is to compare the image quality of a prototypical Cartesian compressed-sensing (cs) accelerated free-breathing VIBE (fbVIBE) with clinically acceptable reconstruction time on the standard scanner hardware with that of a conventional breath-hold VIBE (bhVIBE) for dynamic contrast-enhanced imaging of the upper abdomen.

Methods:
So far, 20 datasets (10 fbVIBE/10 bhVIBE) were independently assessed by two experienced readers in this IRB-approved study. All fbVIBE/bhVIBE sequences (temporal resolution: approximately 11/18 seconds) were performed on state-of-the-art 1.5T clinical MRI scanners (MAGNETOM Avanto Fit/Aera, Siemens Healthcare, Erlangen, Germany). Initial cs reconstruction using hard-gating to reduce respiratory motion artifacts was carried out on the scanner during the examination (duration: approximately 8 minutes). Mann-Whitney U-tests were performed to compare image quality (IQ), delineation of structures (DoS), artifacts (A) and diagnostic confidence (DC), which were rated on Likert-type scales (IQ/DoS/DC: 1 (non-diagnostic)-5 (perfect); A: 1 (no artifacts)-5 (severe artifacts)). Interobserver agreement was assessed using Cohen`s Kappa. Motion-state resolved (xd) reconstruction with improved image quality has increased reconstruction times proportional to the number of selected motion states (chosen to be 6, resulting in duration of approximately 45 minutes). Clinically acceptable reconstruction times can only be achieved on GPU supported scanners. Therefore the acquired raw data is stored and selectively reconstructed retrospectively.

Results:
Ratings for IQ/DoS/DC of fbVIBE (3.8±0.6/3.7±0.8/4±0.8; κ:>0.5) and bhVIBE (3.3±0.8/3.4±0.8/3.6±1; κ:>0.8) were moderate to high, while A was rated moderate to low (fb/bhVIBE: 2.5±1/2.8±1.1; κ:>0.4). Mann Whitney U-test showed no significant difference between IQ/DoS/DC of fb/bhVIBE (p=0.19/p=0.46/p=0.34), despite a trend towards superiority of fbVIBE was observed.

Fig. 1

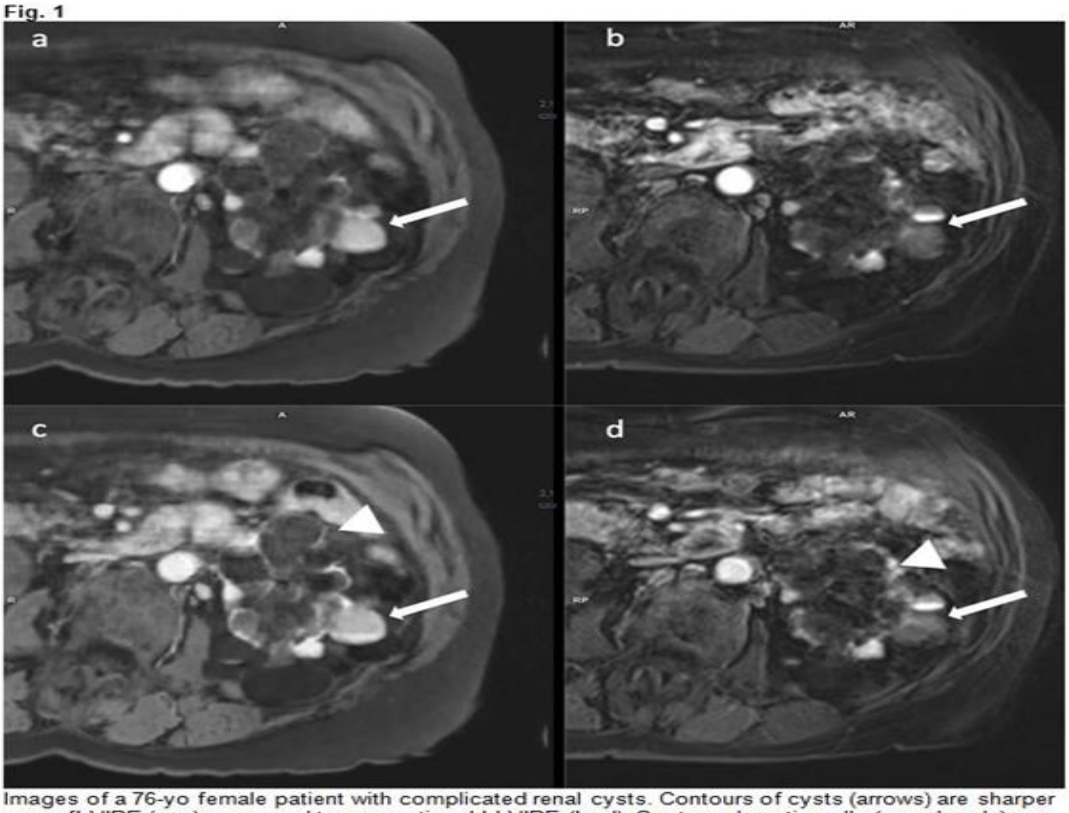

Images of a 76-yo female patient with complicated renal cysts. Contours of cysts (arrows) are sharper on cs fbVIBE (a+c) compared to conventional bhVIBE (b+d). Septa and cystic walls (arrowheads) are easier to assess due to artifact reduction of the cs fb approach.

Fig. 2

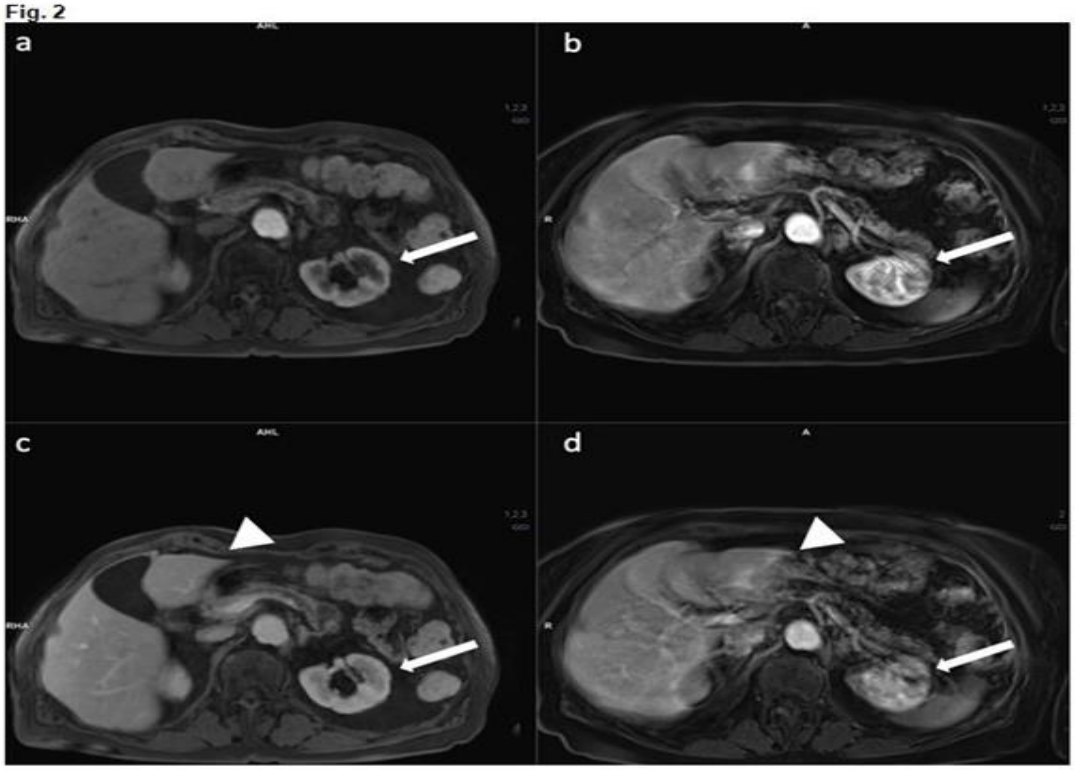

Images of a 85-yo female patient with impaired breath-hold capability. Initial bh VIBE examination (b+d) was non-diagnostic due to severe breathing artifacts. Cs fbVIBE (a+c) was acquired with superior image quality. Clear demarcation of organ borders (e.g. liver (arrowheads) and kidney (arrows) due to artifact reduction is noticable.

Fig. 3

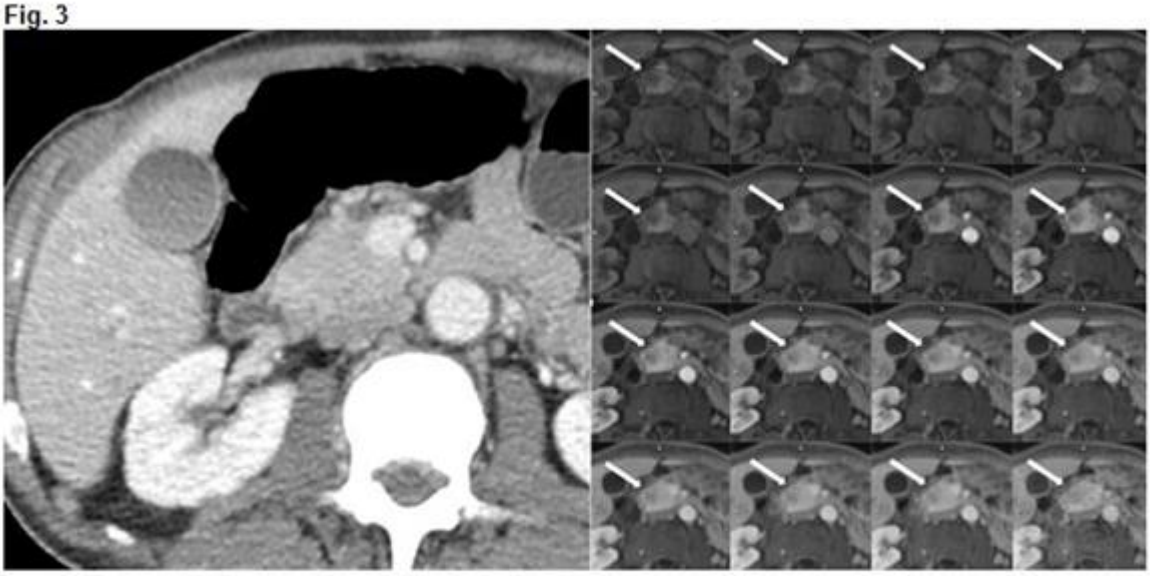

65-yo male patient with metastatic lung and liver lesions of unknown primary. Pancreatic head appears normal on initial CT scan (left). Muliphase free-brathing MR images (right) of the same patient depicting hypovascular adenocarcinoma of the pancreatic head (arrows). No relevant motion artifacts were observed.

Fig. 4

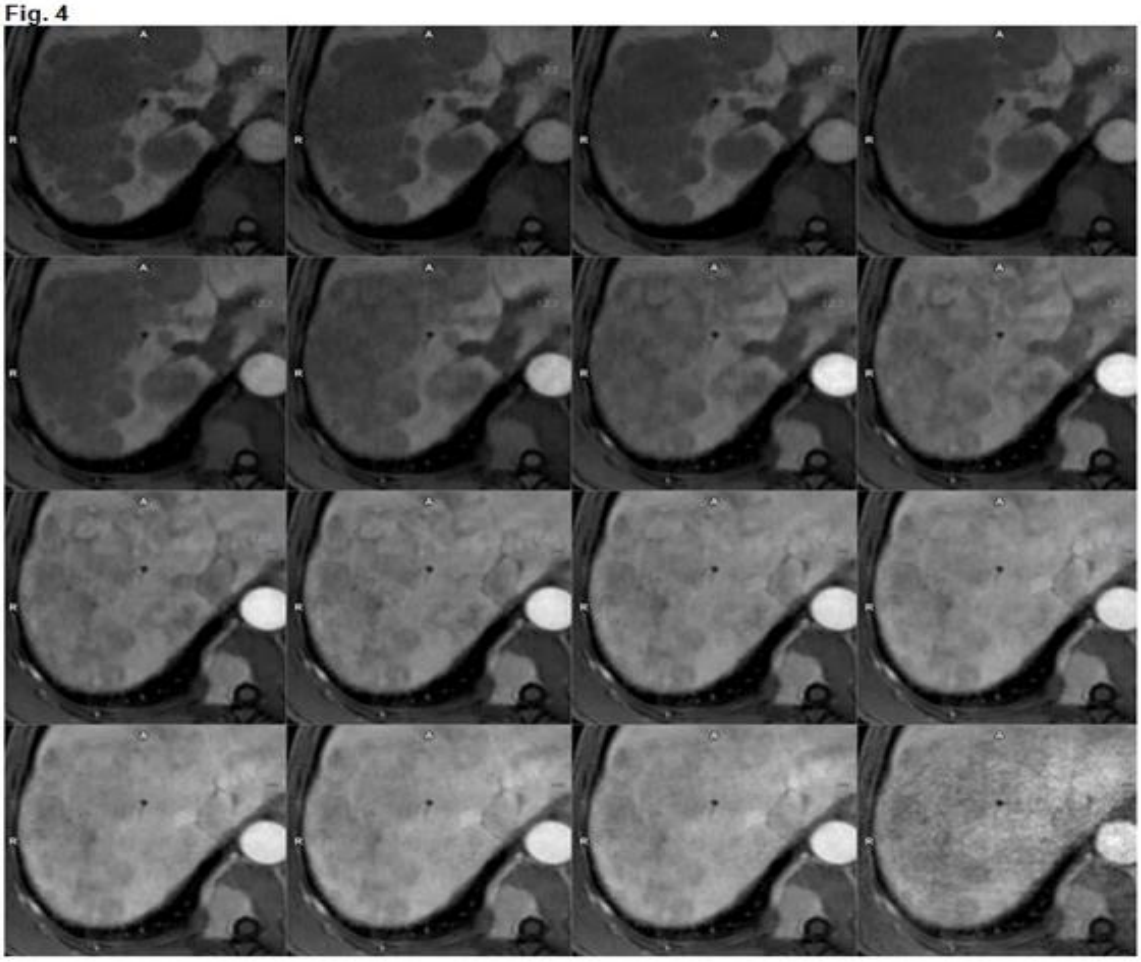

Besides extensive liver metastasis, bone (seen here) and adrenal metastases were detected using the cs free-breathing approach.

Fig. 5

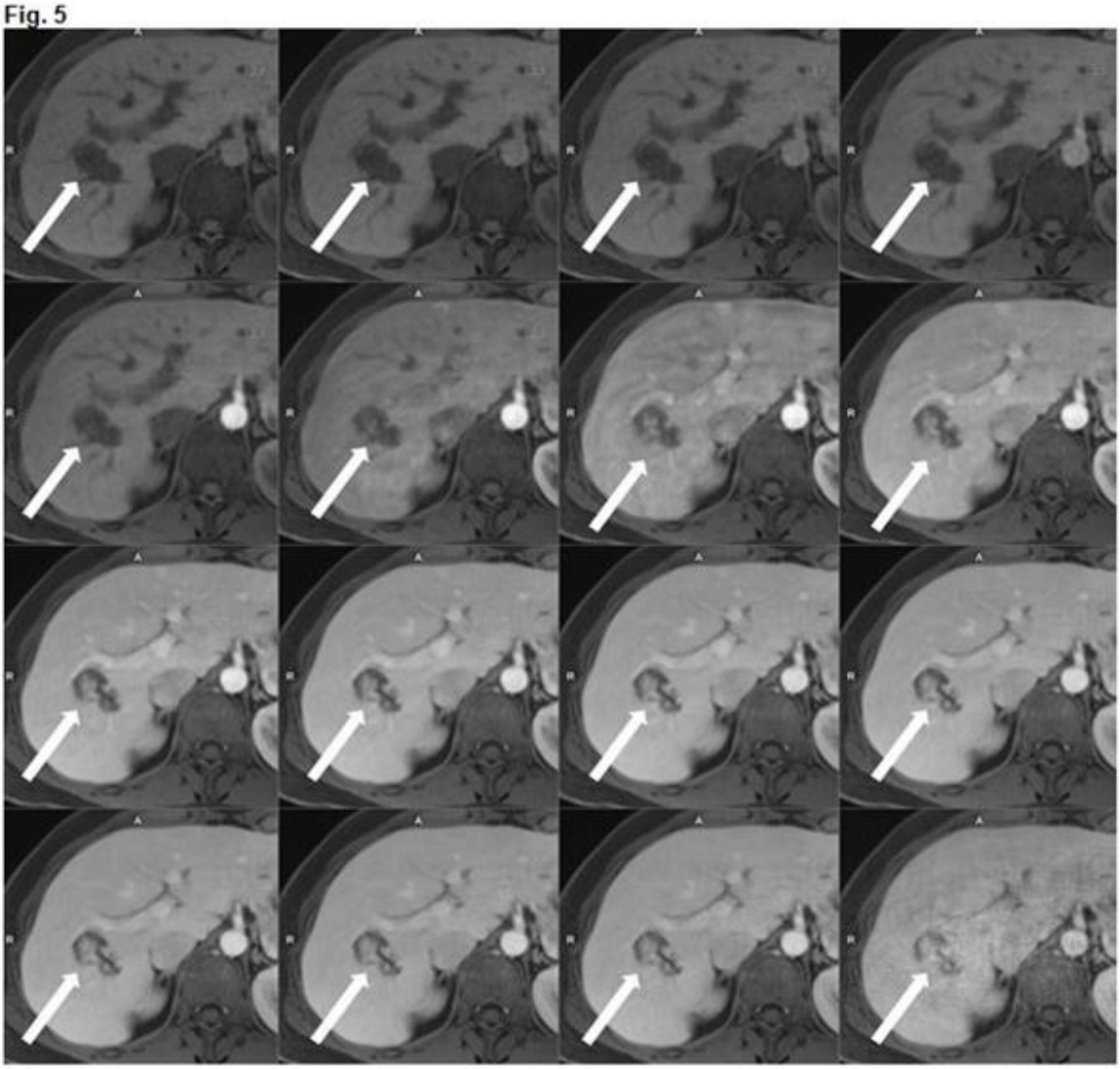

43-yo female patient with a hepatic hemangioma (arrows). Multiphase cs fbVIBE shows peripheral nodular discontinuous enhancement which progresses centripetally on delayed images.

Conclusion:
Fast fbVIBE using cs-reconstruction is technically feasible at a similar image quality compared to bhVIBE. Secondary cs-reconstruction will presumably further improve image quality. fbVIBE may be useful, particularly in elderly and/or severely ill patients with impaired breath-hold capabilities.

5446

M. Emmenegger[1], A. Chincisan[1], R. Müller[1], D. Schneider[1], L. Mottier[1], J. Domange[1], A. Rosati[1], N. Wuillemin[2], D. Bieli[2], T. Sonati[2], A. Barberis[2], L. Saleh[3], S. Hornemann[1], A. Von Eckardstein[3], A. Aguzzi[1]

Antibody profiling in 20,000 unselected patient samples reveals strong enrichment for anti-peanut IgG antibodies in Cystic Fibrosis patients

Institute of Neuropathology, University Hospital of Zurich[1], Mabylon AG, Schlieren[2], Institute of Clinical Chemistry, University Hospital of Zurich[3]

Introduction:
Food allergies are disabling diseases that affect around 4% of children and 1% of adults. The most common food allergen associated with fatal or near-fatal anaphylaxis are peanuts. Apart from strict avoidance of peanut ingredients as the major strategic measure to prevent exposure, availability of epinephrine and antihistamines can help to reduce the symptomaticity. However, peanut allergy remains a potentially life threatening condition for which no cure exists. While many modern interventions attempt to desensitise patients at risk, an unexploited alternative could be to use fully human IgG antibodies with extremely high affinities for the peanut allergens. To detect such antibodies, we have been screening a vast number of hospital patients for the presence of IgGs against Arachis hypogaea 2 (Ara h 2), the major peanut allergen. Antibodies from high-reactive patients can be cloned and safe immunotherapies for allergy patients may be developed. Concomitantly, the interrogation of the full medical record and its correlation with the individual reactivity profile allows deriving insights into the immune profile of anti-peanut antibodies.

Methods:
Using residual heparin plasma samples provided by the Institute of Clinical Chemistry, a microELISA antibody profiling was carried out in a robotised platform. Medical and experimental data was separately stored in an MS-SQL multi-database system and was correlated and visualised using software packages in Python and R. Cellular material of reactive patients was isolated using Ficoll gradients.

Results:
In 22,199 individuals screened, approximately 110 (or 0.5%) patients were identified to be distinctly reactive against natural (n) Ara h 2. We then correlated diagnoses and ICD-10 codes with the reactivity spectrum and found that a high number of positive patients suffer from Cystic Fibrosis (CF), at statistical significance ($p = 4 \times 10^{-241}$), followed by typical comorbidities such as diseases of the gallbladder ($p = 1 \times 10^{-183}$), osteoporosis ($p = 5 \times 10^{-114}$), liver diseases and diseases of the pancreas ($p = 2 \times 10^{-67}$ and $p = 2 \times 10^{-65}$), mucopurulent chronic bronchitis, pneumonia, and transplanted organ and tissue status, all at a significance > 10^{-13} after correction for multiple comparisons. Interestingly, these patients present with anti-n Ara h 2 IgGs but are not known to be allergic against peanuts.

Conclusion:
In a unique endeavour, more than 20,000 patients were screened for the presence of IgG antibodies against Ara h 2, the major peanut allergen. A large and statistically significant proportion of patients presenting with specific antibodies against the allergen suffer from CF but not from peanut allergy. Importantly, in around twelve other campaigns where screens of similar dimensions were carried out using different antigens, no correlation with CF could be made, substantiating the specificity of our finding. Next steps include a validation screen where Ara h 2-reactive patient samples will be tested against a panel of different allergens. Along similar lines, IgE levels against peanuts will be assessed. Moreover, using advanced data mining, we try to subclassify CF patients based on the reactivity profile and diagnoses. Differences may hint towards anti-peanut IgGs as diagnostic or prognostic biomarkers. While this study shows both the potential of an unbiased screening approach and its usage in discovering patients of interest, fully human antibodies from these patients can be cloned and hopefully be employed as safe therapeutics to treat patients with peanut allergy.

5447

S. Forte[1], Z. Wang[2], C. Arboleda[2], L. Lang[2], S. Singer[6], A. Andreas[4], S. Prevrhal[7], C. Leo[5], R. Kubik-Huch[1], M. Stampanoni[3]

Grating-Based X-Ray Phase-Contrast Mammography: From a research setup to a preclinical system

Institut für Radiologie, Kantonsspital Baden, Baden[1], Paul Scherrer Institute, Villigen[2], Institute for Biomedical Engineering, Swiss Federal Institute of Technology [3], Institute for Diagnostic Radiology, University Hospital, Zurich[4], Brustzentrum, Kantonsspital Baden, Baden[5], Pathologie, Kantonsspital Baden, Baden[6], Philips Research, Hamburg[7]

Introduction:
Grating interferometry-based mammography (GIM) is a novel breast imaging technique with the potential of increasing the sensitivity in mammography and to provide complementary information. Unlike standard radiography, simply capable of measuring attenuation, GIM is sensitive to the refraction and scattering of X-rays, resulting in the differential-phase contrast (DPC) and dark-field (DF) signal. The DF signal could possibly discriminate between benign and malignant calcifications.

Methods:
Pre-clinicial study
Method: The ongoing study was approved by the local ethic committee. Biopsies from 49 women with suspicious calcifications were scanned with pre-clinical grating-interferometry system. The R-value (the ratio between the DF signal and the absorption signal) was then computed for individual, manually segmented microcalcifications and the mean value within the biopsy was used as the metric to classify the lesion in comparison with histopathological classification.

Clinical study
Method: Mastectomy samples were imaged with a GIM prototype, a device based on a modified Philips Microdose Mammography System. On that system, four mastectomy specimens were imaged directly after surgical extraction at 38 kVp with a total scanning time of 13.4 s in an uncompressed state. Images were reconstructed with an iterative algorithm. The attenuation and PC signals were fused and processed with a contrast-boosting algorithm. The air kerma was measured with a RaySafe device and used to calculate the mean glandular dose for each sample according to the European Guidelines. The mean glandular dose was 1.74 mGy (range 1.5 - 1.92 mGy) and comparable with commercial mammography.

Results:
Pre-clinicial study
The histopathological workup of the biopsies classified 15 out of 49 lesions as malignant. The corresponding Receiver Operating Characteristic (ROC) curve was generated, using the R-value as the binary classifier to diagnose benign and malignant breast lesion, and the area under the curve (AUC) calculated to be 0.64, indicating a positive diagnostic value.

Clinical study
Mastectomies could be successfully scanned. The majority of the cancers were visible with DF.

Conclusion:
The current results show that the grating-interferometry approach could further discriminate between malignant and benign microcalcifications non-invasively. GIM is capable of retrieving additional X-ray information from mastectomy samples in a clinically compatible setting. Still, the latter has to be further investigated, especially the clinical impact of the additional information. This will be the scope of the ongoing studies, including diagnostic in vivo beast imaging.

5448

I. Jelcic[2], A. Müller[1], T. Pokorny[2], H. Hayward-Koennecke[2], N. Wolfensberger[1], J. Ruder[2], K. Ritter[1], M. Foege[2], A. Lutterotti[2], U. Schanz[1], R. Martin[2]

Safety and Tolerability of Autologous Hematopoietic Stem Cell Transplantation in Multiple Sclerosis Patients at the USZ

Departement of Clinical Oncology and Hematology, University Hospital of Zurich[1], Neuroimmunology and Multiple Sclerosis Research Section, Department of Neurology, University Hospital of Zurich[2]

Introduction:
Based on strong data regarding efficacy and improved safety of autologous hematopoietic stem cell transplantation (aHSCT) in multiple sclerosis (MS), we had applied for its approval early spring 2017. After careful evaluation, the Federal Office of Public Health (FOPH) granted approval in June 2018 with the requirement that patients have to be enrolled into a prospective register study ("aHSCT in MS"). Swiss health insurances are obliged to cover the costs of aHSCT in MS, if aHSCT has been indicated by the interdisciplinary MS stem cell transplantation board at the University Hospital Zurich and if the patient participates in the above mentioned register study. The University Hospital Zurich is currently the only Swiss Center, where MS patients can be included into this registry until June 2024. The register study aims to monitor patients with MS for 5 years after aHSCT for clinical efficacy, safety, tolerability, toxicity and mechanism/s of action of aHSCT in MS.

Methods:
In the context of the "aHSCT in MS" register study, we have performed aHSCT in 10 MS patients in 2018. Hematopoietic stem cells are mobilized using cyclophosphamide and granulocyte-colony stimulating factor (G-CSF), collected via leukapheresis from the peripheral blood and frozen. Conditioning high-dose chemotherapy includes BCNU/Carmustin 300mg/m^2, etoposide 200mg/m^2, cytosine arabinoside 200mg/m^2, melphalane 140mg/m^2, and rabbit anti-thymocyte globulin 7.5 to 10mg/kg (BEAM-ATG protocol). Target doses of hematopoietic stem cells to be re-transfused following high-dose chemotherapy are 3-8x10^6 CD34$^+$ cells / kg body weight. Data for the register study are collected systematically using Redcap. The collection of data and samples was approved by the Cantonal Ethics Committee of Zurich (BASEC-Nr. 2018-01854). We have analyzed demographics, MS disease course and -activity and adverse events in the first 10 patients who received aHSCT for MS.

Results:
Patients had a median age of 42 years (range 29 - 53), median disease duration of 8.3 years (range 1.7 - 16.0) and a median expanded disease status scale (EDSS) score of 4.8 (range 3.0 - 6.5). 3/10 of patients had a replasing-remitting MS (RRMS), 3/10 a secondary progressive MS (SPMS) and 4/10 a primary progressive MS (PPMS). Nearly all patients had either clinical activity (i.e. relapses, 1/10 of patients), radiological activity (3/10) and/or clinical progression (7/10) before aHSCT despite receiving approved highly active immunomodulatory therapy (fingolimod, dimethyl fumarate, rituximab, ocrelizumab, natalizumab). We observed infectious adverse events in all patients (3 mucositis, 1 pharyngitis, 1 upper airway infection, 1 cervical abscess, 2 cystitis, 3 enteritis, 1 symptomatic CMV and HSV reactivation) and severe adverse events in 4/10 of patients (1 pulmonary embolism, 1 hemorrhagic cystitis, 1 episode of mania, 1 CMV enteritis and viremia). Conditioning chemotherapy had to be postponed in 1 patient because of infectious adverse event (cervical abscess) at the insertion site of the dialysis catheter for stem cell collection. We observed mild transient neurological deterioration related to fever after transplantation in 4/10 of patients.

Conclusion:
In 10 MS patients, who have been treated with aHCST at the University Hospital Zurich, we observed a spectrum of adverse events, which is typical and expected after medium-intensity conditioning protocol BEAM-ATG. Systematic collection of data on efficacy, safety and tolerability is of utmost importance for this new treatment option for MS in Switzerland.

5449

C. Pauli[1], H. Hopkins[2], M. Rubin[4], C. Crandori[3], H. Moch[1], L. Cantley[2]

A Precision Medicine Approach to Target KRAS mutant Tumors

Institute for Pathology und Molecularpathology, University Hospital Zürich[1], Englander Institute for Precision Medicine, Weill Cornell Medicine, New York, USA[2], SEngine Precision Medicine, Seattle, USA[3], Department for BioMedical Research (DBMR), University of Bern[4]

Introduction:
RAS proteins regulate signalling pathways that control many cellular responses such as proliferation, survival and differentiation. RAS genes (HRAS, KRAS, and NRAS) represent the most frequently mutated gene family in human cancers and there is tremendous clinical need to find therapies that target RAS driven cancers.
KRAS is the most frequently mutated RAS-family member and occurs in approximately 30% of all human cancers. KRAS is a major driver and mutations occur in approximately 90% of PDAC, 45% CRC and 35% of lung cancers. Despite more than three decades of intensive effort, no effective pharmacological inhibitors of the RAS oncoproteins have reached the clinic, prompting the widely held perception that RAS proteins are 'undruggable'. Using genomics, patient derived tumor organoids and high throughput drug screening we identified a potential novel drug combination to target KRAS altered tumor cells.

Methods:
High throughput combination drug screening was performed on patient derived *in vitro* tumor organoids. Screening results have been validated across an array of different KRAS wt and mutant tumor cell lines and patient derived *in vitro* tumor organoids. The impact of this combination was further assessed using transcriptomics, proteomics and *in vivo* mouse models.

Results:
With a precision medicine platform using multiomics, patient derived tumor organoids and high throughput drug screening we identified a novel synergistic drug combination that effectively kills KRAS mutant tumor cells.
By assessing the impact of this combination across an array of different tumor cell lines and patient derived tumor organoids we observed this synergy was much more pronounced in tumors with KRAS mutations. Using a syngeneic model of KRAS mutant pancreas cancer and patient derived xenograft models we demonstrate that the MEK inhibitor trametinib – thioguanine (purine analogue) combination can be a well tolerated and effective therapeutic strategy in a preclinical murine model.

Conclusion:
Using cutting edge personalized *in vitro* and *in vivo* cancer modeling technologies we identified a novel synergistic drug combination that effectively kills KRAS mutant tumor cells. Based on our *in vivo* data we propose to study the efficacy of this combination in a clinical trial.

5450

T. Karen[1], S. Kleiser[2], D. Ostojic[2], H. Isler[2], S. Guglielmini[2], D. Bassler[1], M. Wolf[2], F. Scholkmann[2]

Cerebral hemodynamic responses in preterm neonates to visual stimulation: Classification according to subgroups and analysis of frontotemporal-occipital functional connectivity

Department of Neonatology, University Hospital Zurich, University of Zurich[1], Biomedical Optics Research Laboratory, Department of Neonatology, University Hospital Zurich, University of Zurich[2]

Introduction:
How neuro-vascular coupling develops in human preterm neonates is still largely understudied.

Methods:
In our study we measured visually (flicker light) evoked hemodynamic responses (HRs) in preterm neonates (n = 25, gestational age: 31.71 ± 3.373 weeks, postnatal age: 25.48 ± 23.94 days) at the visual cortex (VC) and left frontotemporal lobe (FTL) using functional near-infrared spectroscopy (fNIRS) neuroimaging.

Results:
We found that the HR characteristics show a large inter-subject variability and could be classified into three groups according to the changes of oxyhemglobin concentration at the VC (increase (A), decrease (B) or inconclusive (C)). In group A and B, the HRs at the left FTL were correlated with those at the VC indicating a frontotemporal-occipital functional connectivity (fto-FC). Neonates in group A had the largest weight compared to B, and had the lowest baseline total haemoglobin concentration and haematocrit compared to C.

Conclusion:
To the best of our knowledge, this is the first fNIRS study showing that (i) the HRs of preterms need to be classified into subgroups, that (ii) the subgroups differed in weigth and haematocrit at measurement, and that (iii) HRs can be observed also at the FTL during visual stimulation in preterms. These findings add novel insights how the neuro-vascular coupling develops in human preterm neonates.

5451

F. Scholkmann[2], D. Ostojic[2], H. Isler[2], D. Bassler[1], M. Wolf[2], T. Karen[1]

Mathematical modelling of reference ranges for hemoglobin and hematocrit levels in neonates as a function of gestational age and postnatal age

Department of Neonatology, University Hospital Zurich, University of Zurich[1], Biomedical Optics Research Laboratory, Department of Neonatology, University Hospital Zurich, University of Zurich[2]

Introduction:
Hematological values of neonates need to be interpreted taking into account that the reference ranges depend on the age of the neonate.

Methods:
We aimed to derive two general mathematical models for reference ranges for hemoglobin concentration (cHb) and hematocrit (Hct) levels in neonates as a function of gestational age (GA) and postnatal age (PNA) since it is known that GA and PNA are independent factors determining cHb and Hct. For this purpose cHb and Hct values from the data set of Henry and Christensen (Clin. Perinatol., 42 (2015), 483-497) from about 100,000 neonates (GA: 22–42 weeks, PNA: 0–28 days) were used and general models with two quadratic functions was derived.

Results:
The models were successfully validated using the source data and own data.

Conclusion:
To the best of our knowledge, the models we have developed are the first published models to provide reference ranges for cHb and Hct for neonates incorporating the parallel dependence on GA and PNA.

5452

R. Renzel[1], L. Tschaler[1], I. Mothersill[2], L. Imbach[1], R. Poryazova[1]

Sensitivity of Long-Term EEG monitoring as second diagnostic step in the initial diagnosis of epilepsy

Clinic of Neurology, University Hospital Zurich, Zurich[1], Swiss Epilepsy Centre, Zurich[2]

Introduction:
In this retrospective study we aim to evaluate the sensitivity and negative predictive value of Long-Term-EEG (L-EEG) in patients being assessed for epilepsy, who already underwent unspecific standard EEG(s). Secondary endpoints of this study were 1) the correlation of unspecific changes in EEG with epileptiform patterns in L-EEG and 2) the correlation of clinical parameters such as subjective frequency of seizures or epileptogenic lesions in cerebral imaging with epileptiform changes in L-EEG.

Methods:
We retrospectively analyzed clinical and electrophysiologic data of 75 patients, assessed for epilepsy at the University Hospital Zurich, who underwent an L- EEG of at least 48 hrs. between 2010 and 2015. All patient had already undergone S-EEG(s) before L-EEG, which showed no epileptic changes. Furthermore, the association of clinical parameters like frequency of presumptive seizures, abnormalities in standard-EEG, AED intake and cerebral imaging with the final diagnosis were analyzed.

Results:
Out of 75 patients, fourteen (19%) patients were finally diagnosed with epilepsy. In eight of these patients, L-EEGs showed typical ictal/interictal patterns, giving the method a sensitivity of 57%, while the negative predictive value was at 91%. Neither subjective frequency of seizures nor potentially epileptogenic lesions in cerebral imaging were associated with a positive epilepsy diagnosis.

Conclusion:
Also in this preselected cohort of patients, who already underwent a nondiagnostic standard-EEG, the sensitivity of L-EEG remains considerable. Nonetheless, our study also revealed a significant false-negative rate of 43%. With a high negative predictive value of 91% L-EEG appears to be most useful at excluding an epilepsy in this study. A “negative” L-EEG in this context does not exclude epilepsy and thorough evaluation of seizure history and clinical findings remains crucial for a reliable diagnosis.

5453

I. Inci[1], M. Benker[1], N. Citak[1], D. Schneiter[1], C. Caviezel[1], S. Hillinger[1], I. Opitz[1], W. Weder[1]

Extended sleeve lobectomy has same surgical outcome when compared with conventional lobectomy in patients with lung cancer

Universitätsspital Zürich, Department of Thoracic Surgery[1]

Introduction:
No significant data is available to assess whether extended sleeve lobectomy (extended-SL) can be considered comparable to conventional lobectomy (CL) in terms of surgical outcome. The purpose of this study was to compare surgical and oncological outcomes of extended-SL with CL in patients with lung cancer.

Methods:
Between 2000 and 2015, 568 patients who underwent CL *(defined as only one lobe resection without another lobe and/or organ resections; chest wall, diaphragm, pericardium, etc.)* and 187 patients who underwent sleeve lobectomy were analyzed. Sleeve lobectomy was divided into two subgroups; standard-SL (bronchial SL, n=106) and extended-SL (n=81) (*defined as bronchial sleeve resection together with another surgical intervention;* bronchovascular SL, n=40; vascular SL, n=26; atypical bronchoplasty with resection of more than one lobe, n=12; bronchial SL+chest wall resection, n=3).

Results:
Age, gender, BMI, pack/years, and comorbidity did not differ between CL and extended-SL. Extended-SL group had more COPD patients (25.9% vs 12.5%, p=0.001), neoadjuvant treatment (39.5% vs 12.0%, p<0.001), advanced stage NSCLC (53.2% vs 33.1%, p=0.001), and low preopFEV1 (77.2% vs 84.3%, p=0.004) than CL group. The overall surgical mortality (in hospital or 30-days) was 2.6% (n=20). It was 2.8% for CL, 2.8% for extended-SL, and 1.2% bronchial-SL (p=0.4). Postoperative complications occurred in 34.9% of CL and 39.5% of extended-SL group (p=0.4). Pulmonary complication rate was similar between the groups (24.1% for CL, 27.2% for extended-SL, p=0.5). The five-year survival in the CL group was 57.1%, 57.6% for bronchial-SL group, and 56.2% for extended-SL group (p=0.9) (Figure 1). Multivariate analysis showed that TNM stage (p<0.001) and N status (p<0.001) were significant independent negative prognostic factors for survival.

Conclusion:
Extended-SL had comparable outcome to CL although extended-SL had advanced stage, low preopFEV1 and more COPD patients.

5454

D. Kirschenbaum[1], F. Voigt[2], E. Dadgar-Kiani[3], F. Catto[1], F. Helmchen[2], J. Hyung-Lee[4], A. Aguzzi[1]

CRYSTAL & HITS: quantifying Alzheimer's disease pathology in the whole-mount mouse brain

Institute of Neuropathology, UniversityHospital Zurich[1], Brain Research Institute, University of Zurich[2], Bioengineering, Stanford University, CA, USA[3], Neurology, Bioengineering, Neurosurgery, Electrical Engineering (Courtesy), Stanford Universtiy, CA, USA[4]

Introduction:
Histology is based on the slicing and staining of tissue followed by microscopic detection. This did not change in the last centuries. Tissue slicing has been inevitable, because most tissue is non-permissive to light. Thus microscopic information is not accessible beyond a shallow depth. Novel tissue clearing methods address this problem by homogenizing the refractive indices in tissue. This results in transparent samples, allowing for imaging at greater depth without slicing. Recently, multiple approaches for tissue clearing were published. But remaining limitations are that they either take long, quench fluorescence, or are laborious to implement. An additional challenge is the homogeneous introduction of molecular labelling in whole-mount tissue.

Methods:
We developed a method termed CRYSTAL. This method allows the clearing of tissue with unprecedented throughput and ease of-use. Additionally, we developed a methodology for rapid staining of whole-mount tissue, which we termed HITS.

Results:
These methods enabled us to optically clear and label whole-mount mouse brains within a matter of hours. This was followed by rapid light-sheet microscopic acquisition of whole-brain data within minutes. For this a novel custom microscope was used, termed mesoSPIM. We rapidly cleared and stained APP/PS1 transgenic mouse brains. APP/PS1 mice develop β-amyloid plaques (AβP), resembling one of the pathologic hallmarks of Alzheimer’s disease (AD). By quantifying the total amount of AβP and registering this data to a brain atlas, we were able to assess regional differences in AβP loads. Through these methods we were able to test the effect of various therapies targeting cerebral amyloidosis.

Conclusion:
In summary, we present a methodology for high-throughput whole-mount tissue clearing, staining and imaging and show the applicability of this method by testing drugs in a model of Alzheimer’s disease.

Conference Location

University Hospital Zurich
Grosser Hörsaal Ost
Rämistrasse 100
8091 Zürich

Organizer / Contact Address

Gabriela Senti, Prof. MD
Director Research and Education
University Hospital Zurich
Rämistrasse 100
8091 Zürich
dfl@usz.ch

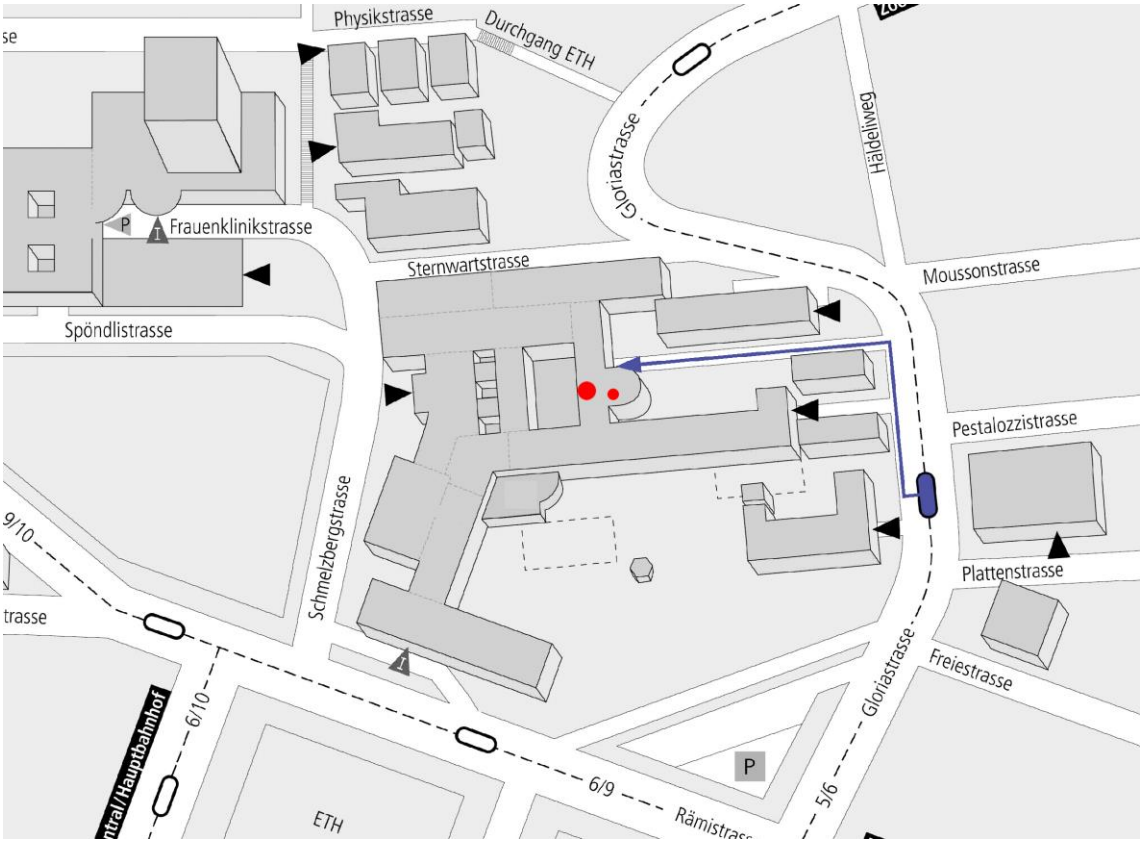

UniversitätsSpital
Zürich